

Development of a Railhead Friction Estimation Tool applying Field Measurements and Machine Learning

Morinoye Olufunmibi FOLORUNSO

A thesis submitted in partial fulfilment of the requirements for the degree of Doctor of Philosophy

The University of Sheffield Faculty of Engineering Department of Mechanical Engineering

Submission Date

May 2024

ACKNOWLEDGEMENTS

I thank God for seeing me through this research and remaining true to His promises.

I truly appreciate the time, effort and encouragement my supervisor, Prof. Roger Lewis put into supporting me over the course of this work. He has played an important role in the successful completion of this work from helping me settle into the university during Covid-19 restrictions to connecting me with external research and conference attendance opportunities and through the numerous brainstorming sessions and corrections.

I also recognise the support of my second supervisor Dr Joseph Lanigan for his pastoral care. He was always available for "rant" sessions without questions. He also helped in signposting me towards necessary resources for this work.

I thank the Rail Safety and Standard Board (RSSB) for sponsoring this research. RSSB also provided me with amazing contacts in the persons of Anup Chalisey and Melissa Frewin, who always went above and beyond to help in acquiring data/information needed for this work. They also provided pastoral support when the need arose, and I appreciate it.

I appreciate my parents Prof. Caleb and Dr Oluronke Folorunso for supporting me emotionally, mentally, financially, and physically during the course of this project. They are the best parents I could ever ask for. I thank my siblings Ms. Mojisola Folorunso for the countless check-ups, encouragement (I have not met anyone prouder of me than my sister) and rant sessions, and Mr Morakinyo Folorunso for the love and support he showed me and the gifts I forced him to buy me.

To my partner, Vladimir Niculescu who endured my repetitive presentation practices, my late-night writing and forcing him to stay up with me, the countless airport and train station pick-ups. I thank him for everything he has done for me and for always being my number 1 fan.

I thank Dr Mike Watson for supporting me with understanding the prediction model and setting up the sensors for the camera box. I appreciate Jamie Booth for assisting me with the machining of parts for the camera box. I thank Tom, Ben, Ruby and Joseph who either helped in training me to use an equipment and/or supported me during field visits. I appreciate the late Richard Kay who was always willing to help me in the Lea Laboratory, especially in moving rail sections. I appreciate the Farmers for being amazing colleagues who never held back on encouraging words and gestures.

I appreciate my PhD girls, Chinwe, Gloria and Sonia who encouraged me to keep going when I felt tired.

ABSTRACT

This research endeavoured to advance the understanding of wheel/rail interface adhesion and subsequently improve adhesion estimation and validation approaches in railway operations. The study comprises of an extensive literature review that established research gaps in wheel/rail adhesion studies, real-world railhead data analysis, and the development of a Neural Network model integrated with a data capturing tool. The literature review established the current understanding of low adhesion, incorporating background studies on wheel/rail interface, low adhesion mechanisms, and techniques for friction measurement and forecast. This aided the selection of appropriate methodology employed in this research. The use of real-world forward-facing images, railhead images, railhead friction and environmental data obtained from Heritage Railway locations in the UK gave this research a unique view into wheel/rail low adhesion mechanisms in the field. The Neural Network model was refined to include these field data, enhancing its accuracy and adaptability. The integration of the camera box (data capture tool designed), validated through testing done on rolling stock at different locations, added practicality to the research. The outcome of this research confirmed the feasibility and versatility of the friction estimation model combined with the camera box for use in the rail industry. It is poised to enhance safety, operational efficiency, and cost-effectiveness in the industry.

LIST OF ABBREVIATIONS

ACCAT- Adhere Controllers Condition Assessment Tool

AI- Artificial Intelligence

AWG- Adhesion Working Group

CoF/µ- Coefficient of friction

EVR- Ecclesbourne Valley Railway

HAROLD- Huddersfield Adhesion and Rolling Contact Laboratory Dynamics

IOT- Internet of Things

IR-InfraRed

LU- London Underground

NN-Neural Network

OTDR- On-Train Data Recorder

PTV- Pendulum Test Value

Raspi- Raspberry Pi

RCF- Rolling Contact Fatigue

RH- Relative Humidity

RSSB- Railway Safety and Standard Board

SPAD- Signal Passed at Danger

ToRFM- Top-of-Rail Friction Modifier

TUoS- The University of Sheffield

UoH- University of Huddersfield

UoS- University of Sheffield

WHR- Wensleydale Heritage Railway

WSP- wheel slip protection

TABLE OF CONTENTS

ACKNOWLEDGEMENTS	
ABSTRACT	iii
LIST OF ABBREVIATIONS	
LIST OF FIGURES	X
LIST OF TABLES	xvii
DECLARATION	xviii
CHAPTER ONE	1
1. INTRODUCTION	2
1.1 AIMS AND OBJECTIVES	3
1.2 NOVEL ASPECTS AND POTENTIAL IMPACT	4
1.3 THESIS LAYOUT	4
CHAPTER TWO	6
2. LITERATURE REVIEW	7
2.1 INTRODUCTION	7
2.2 WHEEL/RAIL INTERFACE CHARACTERISTICS	
2.2.1 CONTACT MECHANICS	
2.2.2 CREEP FORCE	15
2.2.3 METHODS OF FRICTION CONTROL	18
2.3 LOW ADHESION IN THE WHEEL/RAIL INTERFACE	20
2.3.1 CAUSES OF LOW ADHESION	20
2.3.2 LOW ADHESION MECHANISM	21
2.3.3 LAYER CREATION	23
2.3.4 MEASUREMENT TECHNIQUES FOR LOW ADHESION (FRICTION)	25
2.4 METHODS OF LOW ADHESION FORECASTING	31
2.4.1 MODELLING METHODS FOR LOW ADHESION	31
2.4.2 EXISTING METHODS OF FORECASTING LOW ADHESION	38
2.4.3 ADHESION FORECASTING COMPARISON MATRIX	47
2.5 PAPER GRADING TECHNIQUE	47
2.6 SUMMARY	50
CHAPTER THREE	52
3. RESEARCH APPROACH	53
CHAPTER FOUR	56

4.	RAILHEAD DATA GATHERING AND ANALYSIS	57
	4.1 INTRODUCTION	57
	4.2 MEASUREMENT LOCATIONS	58
	4.2.1 BUTTERLEY, Derbyshire (Midland Railway), UK:	58
	4.2.2 WIRKSWORTH & IDRIDGEHAY, Derbyshire, (Ecclesbourne Valley Railway EVR), UK:	
	4.2.3 DARLEY DALE, Derbyshire (Peak Rail), UK:	61
	4.3 METHODOLOGY	61
	4.3.1 EQUIPMENT USED FOR MEASUREMENTS	61
	4.3.2 MEASUREMENT PLANS	65
	4.3.3 MEASUREMENT PROCEDURES	65
	4.4 RESULTS & DISCUSSION	68
	4.4.1 WIRKSWORTH AND IDRIDGEHAY	68
	4.4.2 BUTTERLEY	
	4.4.3 DARLEY DALE	
	4.5 SALISBURY DATA COLLECTION	78
	4.6 GENERAL DISCUSSION	
	4.7 CONCLUSIONS	81
C)	HAPTER FIVE	
5.		
	5.1 INTRODUCTION	83
	5.2 METHODOLOGY	83
	5.2.1 GAUSSIAN PROCESS MODEL	83
	5.2.2 IMAGE PROCESSING	85
	5.2.3 PREDICTION TOOL BUILD WITH GP MODEL	89
	5.3 RESULTS FROM TRAINING AND FIRST STEP VALIDATION THE FRICTION PREDICTION MODEL	90
	5.4 PREDICTION MODEL VALIDATION AND RETRAINING PROCESS	92
	5.4.1 FIRST VALIDATION	92
	5.4.2 FIRST RETRAINING AND REVALIDATION THE FRICTION PREDICTION MODEL	93
	5.4.3 SECOND RETRAINING OF THE FRICTION PREDICTION MODEL WITH LEAF LAYER DATA FROM SALISBURY	
	5.5 CONCLUSIONS	97

CHAPTER SIX	98
6. MODEL SENSITIVITY ANALYSIS	99
6.1 INTRODUCTION	99
6.2 METHODOLOGY	99
6.2.1 RAILHEAD DISTANCE	100
6.2.2 RAILHEAD IMAGE ORIENTATION	101
6.2.3 VIDEO CAPTURE/ FREEZE FRAME IMAGES	102
6.3 RESULTS	111
6.3.1 DRY RAILHEAD CONDITIONS	113
6.3.2 WET RAILHEAD CONDITIONS	113
6.3.3 OXIDISED RAILHEAD CONDITIONS	114
6.3.4 OXIDISED + WET RAILHEAD CONDITIONS	115
6.3.5 OXIDISED + REDUCED WET RAILHEAD CONDITIONS	116
6.4 DISCUSSION	119
6.4.1 DRY RAILHEAD CONDITIONS	120
6.4.2 WET RAILHEAD CONDITIONS	120
6.4.3 OXIDISED RAILHEAD CONDITIONS	122
6.4.4 OXIDISED + WET RAILHEAD CONDITIONS	123
6.4.5 OXIDISED + REDUCED WET RAILHEAD CONDITIONS	123
6.4.6 FREEZE FRAME IMAGES	123
6.5 CONCLUSIONS	124
CHAPTER SEVEN	125
7. ON-TRAIN DATA CAPTURE SENSOR DESIGN	126
7.1 INTRODUCTION	126
7.2 DESIGN PROCESS	127
7.2.1 CAMERA MOUNTED IN FRONT OF TRAIN	127
7.2.2 ADAPT AN EXISTING DESIGN (AIVR CAMERA BOX)	129
7.3 METHODS FOR CAMERA BOX DATA COLLECTION TESTS	135
7.3.1 WENSLEYDALE HERIATGE RAILWAY (WHR) SHORT RUN TEST:	
7.3.2 SCOTRAIL LONG RUN TESTS 30-05	135
7.3.3 WENSLEYDALE HERIATGE RAILWAY (WHR) LONG RUN TESTS	14-07 AND
28-11	136

	7.3.4 WENSLEYDALE HERIATGE RAILWAY (WHR) (SHORT RUNS) WITH LEAF	
	LAYER AND CRYOGENIC CLEANING APPLICATION 28-11	136
	7.4 RESULTS	137
	7.4.1 MONK BRETTON TEST: CAMERA MOUNTED IN FRONT OF TRAIN (26-11	,
	7.4.2 CAMERA BOX V2: FIRST TEST AT WENSLEYDALE HERITAGE RAILWAY (WHR) (14-03-23)	
	7.4.3 SECOND TEST AT SCOTLAND RAIL (30-05-23)	142
	7.4.4 THIRD TEST AT WENSLEYDALE HERITAGE RAILWAYS (WHR) (13&14-0	7-
	23)	143
	7.4.5 FOURTH TEST AT WENSLEYDALE HERITAGE RAILWAYS (WHR) (28-11-	,
	7.5 DISCUSSIONS	
	7.5.1 WHR 14-03-23	
	7.5.2 ScotRail 30-05-23	
	7.5.2 Scotkan 30-05-23	
	7.5.4 WHR 28-11-23	
C		
	HAPTER EIGHT	
8.		
	8.1 INTRODUCTION	
	8.2 OBJECTIVE 1: LITERATURE REVIEW	
	8.3 OBJECTIVE 2: RAILHEAD DATA ANALYSIS	
	8.4 OBJECTIVE 3: PREDICTION MODEL DEVELOPMENT	
	8.4.1 PREDICTION MODEL LIMITATIONS	
	8.5 OBJECTIVE 4: DATA CAPTURE TOOL DEVELOPMENT AND TESTING	
	8.5.1 CAMERA BOX LIMITATIONS	177
	8.6 HOW DOES THE VALIDATED FRICTION PREDICTION MODEL COMPARE TO EXISTING ADHESION FORCAST METHODS?	178
C	HAPTER NINE	183
9.	CONCLUSIONS AND RECOMMENDATIONS	184
	9.1 CONCLUSIONS	
	9.2 RECOMMENDATIONS FOR FUTURE WORK	
	9.3 PUBLICATIONS ARISING FROM THIS WORK	186

	JOURNAL PUBLICATIONS	186
	CONFERENCES AND SEMINAR PRESENTATIONS	186
10.	REFERENCES	187
11.	APPENDICES	192
1	APPENDIX A:	192
	A-1 SAMPLE DATA SHEET AND SPREAD SHEET USED IN COLLATING FIELD D	
	A-2 ADDITIONAL RESULTS FROM ENVIRONMENTAL EFFECTS ANALYSIS IN CHAPTER 4	193
1	APPENDIX B: PREDICTION MODEL CODES	196
	B-1 GAUSSIAN PROCESS	196
	B-2 FORWARD FACING IMAGES	197
	B-2 RAILHEAD IMAGES	200
	B-3 PREDICTOR PROCESS	203
	B-4 PREDICTION MODEL INTERFACE	204
	B-5 IMAGE FEATURES	205
	B-6 GP FITTING_MO	206
1	APPENDIX C: CAMERA BOX	208
	C-1: CAMERA BOX PART DESIGNS	208
	C-2: CAMERA BOX DATA SAMPLE	212
	C-3: STANDARD OPERATING PROCEDURE FOR THE CAMERA BOX	212

LIST OF FIGURES

rigure 1. 1: Carbon jootprints of aifferent modes of transportation in the OK, 2022 [2].	2
Figure 2. 1: Contact stress on the left and right wheel/rail contact [6][6]	8
Figure 2. 2: Contact regions on the wheel/rail interface [6][6]	
Figure 2. 3: Contact between the wheel tread and railhead	
Figure 2. 4: Contact between wheel flange and rail gauge corner	
Figure 2. 5: Pressure distribution across elliptical contact area [10][10]	
Figure 2. 6: Wheel/rail assembly geometric model in ANSYS [10]	
Figure 2. 7: Schematics of the wheel/rail contact [13]	
Figure 2. 8: Coordinate systems used for the section [13]	
Figure 2. 9: The relative position of the wheel and rail profiles [13]	
Figure 2. 10: Depiction of the contact between the rail and train wheel with the	
characteristics given as; v – velocity of the train body, ω - angular velocity of the train	
wheel, P - vertical forces acting on the train wheel, P^{I} – vertical force acting on the rail	
r – radius of the rolling wheel	
Figure 2. 11: Relationship between creepage and creep force [15][15]	
Figure 2. 12: Creep curves for different test conditions [19][19]	
Figure 2. 13: Effects of friction modifiers on CoF [20]	
Figure 2. 14: CoF ranges (adapted from [20] by [25])	
Figure 2. 15: Vehicle-bourne tribometer [34]	
Figure 2. 16: Tribometer train [43]	
Figure 2. 17: Loading measuring wheel [34]	
Figure 2. 18: OnTrak hand operated Tribometer [14]	
Figure 2. 19: Skid resistance slider tribometer [34]	
Figure 2. 20: Braked wheel handheld tribometer [34]	
Figure 2. 21: Static Breakout Friction Tribometer [34]	
Figure 2. 22: Pin-on-Disc [40]	
Figure 2. 23: Twin disc test rig [34]	
Figure 2. 24: Linear Full-Scale-Wheel-On-Rail-Rig [34]	
Figure 2. 25: HAROLD Rig [42]	
Figure 2. 26: Schematic of the tram wheel test rig [29]	
Figure 2. 27: Graphical representation of results from WILAC model[18]	
Figure 2. 28: LILAC system process [42]	
Figure 2. 29: WILAC results compared other railhead conditions	
Figure 2. 30: LILAC results under 60kN load with different rolling speed	
Figure 2. 31: Graphs comparing adhesion coefficient trends for present and previous	
CONTACT model [45]	35
Figure 2. 32: GDOES results for elm leaves under high humidity [31]	
Figure 2. 33: Wheel/rail adhesion coefficient-creepcurve [16][16]	
Figure 2. 34: Sample of adhesion risk index [47]	
Figure 2. 35: Example of adhesion index data from the Met Office:	

Figure 2. 36: Figure showing October layers on Stockholm rail [55]43
Figure 2. 37: Plot showing the relationship between oxide layer thickness and friction
levels per month [55]43
Figure 2. 38: Rail eye sensor [56]44
Figure 2. 39: Paper grading map49
Figure 3. 1: Schematics for methodology55
Figure 4. 1: (a) Aerial view of Track at Butterley, "red line" showing measurement path
[59];,(b) Aerial view of track at Wirksworth, "red line" showing measurement path [60];
(c) Aerial view of track at Idridgehay, "red line" showing measurement path and (d) Aerial
view of track at Darley Dale, "red line" showing measurement path [61]60
Figure 4. 2: (a) Pendulum tribometer schematics diagram, where a is the measurement
scale; b is the pendulum arm pivot (with adjustable height); c is the pendulum arm; d is the
rubber pad; e is carriage handle; f is the levelling screw; g is the Pendulum arm head [62];
(b) Fully labelled diagram of the pendulum tribometer and (c) Conversion of Skid
resistance to CoF measured by the Tribometer Train [34]62
Figure 4. 3: (a) Thickness gauge; (b) Infrared thermometer; (c) Go Pro camera64
Figure 4. 4: Pendulum set in the start position for friction measurement67
Figure 4. 5: Pendulum arm head striking the railhead (left) and pendulum arm caught
before return (right)67
Figure 4. 6: (a) μ against relative humidity with a colour map representing railhead
temperature for Wirksworth on 14-08-2019 and (b) μ against relative humidity with a
colour map representing railhead temperature for Idridgehay on 14-08-201968
Figure 4. 7: (a) Plot of μ against relative humidity with a colour map representing railhead
temperature for Idridgehay on 21-11-2019 and (b) Shaded dry railhead (left) and
artificially wetted railhead (right) at Idridgehay 21-11-201969
Figure 4. 8: (a) μ against relative humidity with a colour map representing railhead
temperature for Wirksworth on 21-11-2019 and (b) Dry railhead (left) and damp railhead
(right) from Wirksworth on 21-11-201970
Figure 4. 9: (a) μ against relative humidity with a colour map representing railhead
temperature for Wirksworth (left) and Idridgehay (right) on 13-11-2020 and (b) Railhead
image with visible oxidisation with μ of 0.33 from Wirksworth on 13-11-202071
Figure 4. 10: (a) μ against relative humidity with a colour map representing railhead
temperature for Wirksworth (left) and Idridgehay (right) on 20-11-2020 and (b) μ against
relative humidity with a colour map representing railhead temperature for Wirksworth
(left) and Idridgehay (right) on 08-12-202071
Figure 4. 11: (a) μ against relative humidity with a colour map representing railhead
temperature for Butterley on 22-10-2019; (b) Dry railhead under shade (left) and damp
railhead under shade (right) at Butterley on 22-10-2019 and (c) μ against relative
humidity with a colour map representing railhead temperature for Butterley on 01-10-
2019

Figure 4. 12: (a) μ against relative humidity with a colour map representing railhead	_
temperature for Darley Dale on 02-10-2019; (b) Corresponding railhead image for the	
Darley Dale \square of 0.13Figure 4. 13: (a) μ against relative humidity with a colour map representing railhead temperature for Darley Dale on 08-10-2019 and (b) Railhead with dew present (left) of the colour map represent the colour map re	
railhead with exposure to the sun (right) at Darley Dale on 08-10-2019	
Figure 4. 14: (a) Ariel image of the crash site at Salisbury Tunnel [71]; (b) Examples of black leaf layer present on the railhead; (c)) μ against relative humidity with a colour	f r
map representing railhead temperature for Salisbury Tunnel Junction 03-11-21	
Figure 4. 15: Salisbury contaminated railhead time series plots showing the 8 individu Pendulum tests recorded before the standardised average was calculated. (a) Friction	
measurements for a dry contaminated railhead. (b) Friction measurements for an	
artificially wetted contaminated railhead. (c) Friction measurements for an artificially	y
wetted contaminated railhead	80
Figure 5. 1: An example forward facing image showing the sub images extracted for further analysis	96
Figure 5. 2: Images from the extremes of the first three principal components for the d	
set. Each pair of rows represents a principal component	
Figure 5. 3: Examples of the different groups of images found by the unsupervised lear	
technique. Columns are separate groups: grassland, trees, rural, urban	_
Figure 5. 4: Railhead Image before (left) and after (right) dimensionality reduction	
Figure 5. 5: Model predictions compared to the actual value at each point, points are	0)
coloured by their leverage. Data on both axes are normalised to a 0-1 scale	90
Figure 5. 6: Results of the leave one out validation (A) and a comparison of the full mo	
to the naïve model for each point (B), with a histogram of the change between the naïve	
and full models. Data on both axes are normalised to a 0-1 scale	
Figure 5. 7: Results of the leave groups out validation for one set of groups (A) and a) 1
comparison of the full model to naïve models for each group (B). Data on both axes are	e
normalised to a 0-1 scale	
Figure 5. 8: 1st Prediction results using Nov-Dec 2020 data with linear points represer the measured friction on the image to the right	nting
Figure 5. 9: An example of a row in the csv file containing the extracted image features	
Figure 5. 10: Retrained regression model plot (left) original regression model plot (rig	
	94
Figure 5. 11: Prediction results using Nov-Dec 2020 from the retrained model data wit	th
linear points representing the measured friction on the image to the right	95
Figure 5. 12: Sample of railhead contamination recorded at the Salisbury 2021 incider	nt.96
Figure 5. 13: Second retrained regression model with the leaf layers image from	
Salisbury	96
Figure 6. 1: Original Image formats used in training the prediction tool	
Figure 6. 2: Selected Rail section used for the sensitivity tests	99

Figure 6. 3: Railhead image taken at a height of 1450mm (L), and the distance used for the
prediction tool training (between 400mm-500mm from the railhead position) (R) 101
Figure 6. 4: Vertical railhead image orientation (L) Horizontal railhead image orientation
(R)102
Figure 6. 5: Example of railhead images for uncleaned state. Horizontal with camera-
railhead distance ≈ 450 mm distance (L) and vertical with camera-railhead distance
≈1450mm (R) (13-04-22)106
Figure 6. 6: Example of railhead images for cleaned with alcohol wipe. Horizontal with
camera-railhead distance ≈ 500 mm (L) and vertical with camera-railhead distance \approx
900mm (R) (13-04-22)
Figure 6. 7: Example of railhead images for cleaned with wire brush. Horizontal with
camera-railhead distance ≈ 1450 mm (L) and vertical with camera-railhead distance \approx
1450mm (R) (13-04-22)106
Figure 6. 8: Example of railhead images for water spray. Horizontal with camera-railhead
distance ≈ 900 mm (L) and vertical with camera-railhead distance ≈ 450 mm (R) (13-04-
22)106 Figure 6. 9: Example of railhead images for previous day wet. Horizontal with camera-
railhead distance ≈ 1450 mm distance (L) and vertical with camera-railhead distance ≈ 1000 mm (R) (14.04.23)
1000mm (R) (14-04-22)
Figure 6. 10: Example of railhead images for 1st water spray. Horizontal with camera-
railhead distance \approx 1450mm distance (L) and vertical with camera-railhead distance \approx
1200mm (R) (14-04-22)
Figure 6. 11: Example of railhead images for 2nd water spray. Horizontal with camera-
railhead distance $pprox$ 1450mm distance (L) and vertical with camera-railhead distance
≈600mm (R) (14-04-22)107
Figure 6. 12: Example of railhead images for 1st appearance of rust. Horizontal with
camera-railhead distance $pprox$ 1450mm distance (L) and vertical with camera-railhead
$distance \approx 900mm \ (R) \ (20-04-22)107$
Figure 6. 13: Example of railhead images for rust1 + water. Horizontal with camera-
railhead distance $pprox$ 1000mm distance (L) and vertical with camera-railhead distance
$\approx 1000 mm (R) (20-04-22)107$
Figure 6. 14: Example of railhead images for rust day2. Horizontal with camera-railhead
distance ≈ 300 mm distance (L) and vertical with camera-railhead distance ≈ 700 mm (R)
(21-04-22)
Figure 6. 15: Example of railhead images for rust day2 + water. Horizontal with camera-
railhead distance ≈ 450 mm distance (L) and vertical with camera-railhead distance \approx
700mm (R) (21-04-22)108
Figure 6. 16: Example of railhead images for rust day2 +2nd water spray. Horizontal with
camera-railhead distance ≈ 450 mm distance (L) and vertical with camera-railhead
distance ≈1000mm (R) (21-04-22)108
Figure 6. 17: Example of railhead images for rust day3. Horizontal with camera-railhead
distance ≈ 450 mm distance (L) and vertical with camera-railhead distance ≈ 900 mm (R)
(26-04-22)

Figure 6. 18: Example of railhead images for rust day3 + water spray. Horizontal	with
camera-railhead distance ≈ 450 mm distance (L) and vertical with camera-railhe	ead
distance ≈450mm (R) (26-04-22)	
Figure 6. 19: Example of railhead images for rust day3 +reduced water spray. How	rizontal
with camera-railhead distance ≈ 400 mm distance (L) and vertical with camera-railhead	
distance ≈ 500mm (R) (26-04-22)	
Figure 6. 20: Example of railhead images for rust day4. Horizontal with camera-r	
distance ≈ 1450 mm distance (L) and vertical with camera-railhead distance ≈ 45	
format (04-05-22)	
Figure 6. 21: Freeze frame images captures from railhead videos for rust day4 (04	
Figure 6. 22: Example of railhead images for rust day5. Horizontal with camera-r	
distance ≈ 450 mm distance (L) and vertical with camera-railhead distance ≈ 100	00mm (R)
(10-05-22)	
Figure 6. 23: Example of railhead images for rust day5 + water spray. Horizontal	with
camera-railhead distance ≈ 1450 mm distance (L) and vertical with camera-railh	1ead
distance ≈1000mm (R) (10-05-22)	110
Figure 6. 24: Example of railhead images for rust day5 + reduced water spray. Ho	rizontal
with camera-railhead distance ≈ 450 mm distance (L) and vertical with camera-railhead	railhead
distance ≈1000mm (R) (10-05-22)	110
Figure 6. 25: Freeze frame images captures from railhead videos for rust day5 (10	-
Figure 6. 26: Freeze frame images captures from railhead videos for rust day5 + v	
spray (10-05-22)	
Figure 6. 27: Freeze frame images captures from railhead videos for rust day5 + v	
spray (10-05-22)	
Figure 6. 28: All sensitivity tests results	
Figure 6. 29: Difference in Ideal image and mean non-ideal image predicted fricti	
Figure 6. 30: Sensitivity test results for Dry Railhead Day 1 & 2	
Figure 6. 31: Sensitivity test results for Wet Railhead Day 1 & 2	
Figure 6. 32: (a) Sensitivity test results for different levels of railhead oxidation	
(b) Increased scale plot for better visualisation of data point	115
Figure 6. 33: Sensitivity test results for different levels of railhead oxidation+ water	
Figure 6. 34: Sensitivity test results for different levels of railhead oxidation+ redu	
water	
Figure 6. 35: Example of railhead image capture in-field	
Figure 6. 36: Image of wet railhead captured in field	
Figure 6. 37: Prediction for wet railhead condition using in field RH (L) and prediction	
laboratory RH (R)	
Figure 6. 38: Example of oxidised railhead image captured infield	
Figure 7. 1: Chart showing the processes considered for the On-board train data c	capture
	40-

Figure 7. 2: Front of Class 153 train highlighting the possibly mounting positions	.128
Figure 7. 3: Google earth image of the track used in Monk Bretton [78] (L) Section of to	rack
with encroaching vegetation (R)	128
Figure 7. 4: Camera set-up mounted on the class 153 train	.129
Figure 7. 5: AIVR Camera box (Source onebigcircle.com)	
Figure 7. 6: Process diagram for the camera box development	
Figure 7. 7: Labelled components image of camera box V1	
Figure 7. 8: Camera box V1 mounted on a class 150 train in Monk Bretton	
Figure 7. 9: Labelled components image of camera box V2	
Figure 7. 10: Google earth image showing the arial view of WHR (Leeming Bar station	
[79]	
Figure 7. 11: Schematics for WHR 28-11-23 short run test, where each pass is a to and	
journey	
Figure 7. 12: Leaf paste circled in red, laid on the railhead section	
Figure 7. 13: Image capture from the GoPro camera set-up (L); Cropped and zoomed in	
image extracted (R)	
Figure 7. 14: Camera mounted on a class 142 train at WHR (14-03-23)	
Figure 7. 15: (a) Plot of all environmental data and the PTV against all data points for	
WHR 14-03-23; (b) COF against all data points for WHR 14-03-23	
Figure 7. 16: Camera box on a class 158 train at Edinburgh Waverley station	
Figure 7. 17: (a) Plot of all environmental data and the PTV against selected data poin	
for ScotRail on 30-05-23; (b) COF against selected data points for ScotRail on 30-05-2.	
Figure 7. 18: Camera box on class 142 train in WHR on 14-07-23	
Figure 7. 19: (a) Plot of all environmental data and the PTV against all data points for	
WHR 13-07-23; (b) COF against all data points for WHR 13-07-23	
Figure 7. 20: (a) Plot of all environmental data and the PTV against all data points; (b	
COF against all data points	
Figure 7. 21: (a) Author installing camera box 1 on the class 142 train; (b) Camera box	
captured in use; (c) Camera box 1 captured in use	
Figure 7. 22: (a) Plot of environmental data and the PTV against data points for came	
box 1 short run; (b) Plot of environmental data and the PTV against data points for	· O
camera box 1 long run; (c) COF against data points camera box 1 short run; (d) COF	
against data points camera box 1 long run	158
Figure 7. 23: (a) Plot of environmental data and the PTV against data points for came	
box 2 short run; (b) Plot of environmental data and the PTV against data points for	· OI
camera box 2 long run; (c) COF against data points camera box 2 short run; (d) COF	
against data points camera box 2 long run	162
Figure 7. 24: Static vs dynamic friction prediction	
Figure 7. 25: Forward facing images of track sections exposed to sun (L) and a shaded	
sections towards the platform (R)	
Figure 7. 26: Class 170 Scotrail train showing camera box position over the railhead	
Figure 7. 27: Forward facing image of a hot spot recorded with air temperature 28.7%	
with a shaded railhead section recording 21.1°C on the railhead IR sensor	

Figure 7. 28: Spots of high railhead temperature with sun exposure for section 3 (L) and	d
section 7 (R)	166
Figure 7. 29: Railhead-air temperature comparison for 13-07-23 tests in WHR	167
Figure 7. 30: (a) Forward facing image in the tunnel exiting Leeming Bar; (b) Forward	
facing image in the tunnel approaching Leeming Bar; (c) Corresponding railhead imag	e
for 'a'; (d) Corresponding railhead image for 'b'	168
Figure 7. 31: Effects of tunnels on railhead friction measured on a Tribometer train	
(adapted from [85] by author)	168
Figure 7. 32: Comparison of Prediction tool and Rivelin Rail (RR) Tribometer Friction fo	or
WHR 28-11-23	169
Figure 7. 33: Comparison of data collected from the camera in the summer 14-07-23 to	1
winter 28-11-23	171

LIST OF TABLES

Table 2. 1: Definition of adhesion levels	20
Table 2. 2: Performance data classification	
Table 2. 3: Adhesion measurement techniques	26
Table 2. 4: Adhesion "forecasting" matrix	
Table 5. 1: Sensor's measurement uncertainty	83
Table 6. 1: Full list of prediction tool sensitivity tests	103
Table 6. 2: Comparison of prediction results from still images and freeze frame	images. 117
Table 7. 1: Design specification for on-train data capture system	126
Table 7. 2: Table of data from WHR 14-03-23	141
Table 7. 3: Table of data from ScotRail 30-05-23	145
Table 7. 4: Table of data from WHR 13-07-23	146
Table 7. 5: Table of data from WHR 14-07-23	147
Table 7. 6: Table of data from WHR (camera box1) 28-11-23	153
Table 7. 7: Table of data from WHR (camera box2) 28-11-23	154
Table 8. 1: Updated adhesion "forecasting" matrix	180

DECLARATION

I, Morinoye Olufunmibi Folorunso, confirm that the Thesis is my own work. I am aware of the University's Guidance on the Use of Unfair Means (www.sheffield.ac.uk/ssid/unfair-means). This work has not previously been presented for an award at this, or any other, university.

CHAPTER ONE

1. INTRODUCTION

According to Department of Transport [1], rail travel is arguably one of the safest forms of public transportation (excluding suicide related fatalities), having recorded 40 non-suicide related fatalities in 2018/19 (which included 25 members of the public who could have been level crossing users or trespassers) compared to the 1784 fatalities recorded for road usage. Travelling by rail is also considered to be a greener mode of transportation as it provides an electricity powered alternative. Figure 1.1 shows the comparison of carbon footprint generated by different modes of transportation, with rail travel accounting for the lowest carbon footprints.

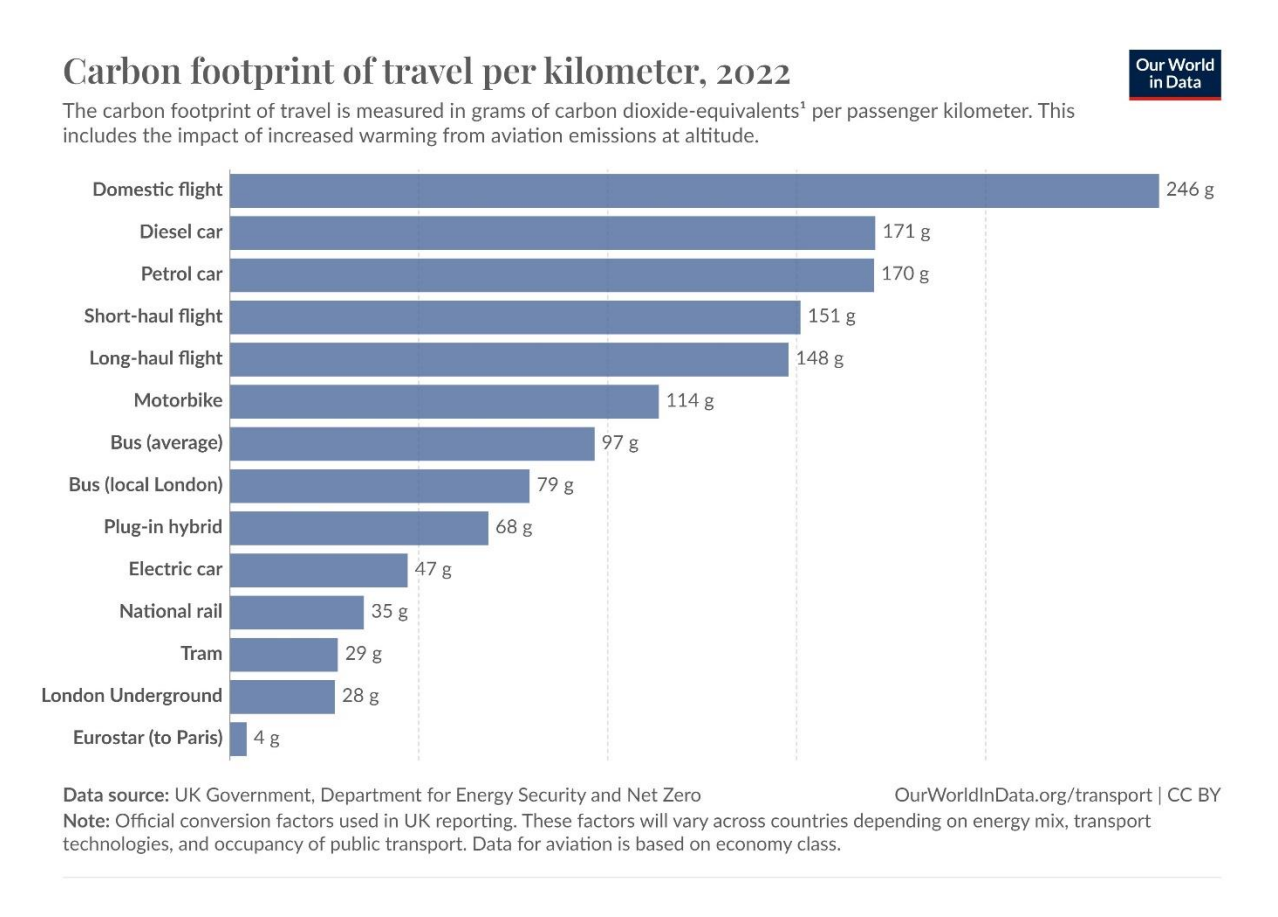


Figure 1. 1: Carbon footprints of different modes of transportation in the UK, 2022 [2]

Low adhesion in the wheel/rail interface has been recognised as one of the major causes of delay in the railway industry. These delays may be caused by braking problems resulting in signals passed at danger (SPADs) or station overruns which are also significant safety concerns, or delays can result from poor traction. The effect of low adhesion is said to cost an estimated £355m annually during autumn where roughly £290 million is the performance impact cost, £0.5 million is safety impact cost and £64 million is spent on cleaning, management and prevention cost [3]. Low adhesion events cause safety concerns and high-cost implication for the railway industry, which is why this research is being done.

The railway industry currently has limited methods of adhesion forecasting with the main validated method being the Met Office Adhesion index. The adhesion index uses a bank of weather data readily available to the met office to predict wind speeds, possible leaf falls and moisture/ice presence from weather forecast. This provides information only related to weather and not the railhead state. It does not give real-time information of railhead conditions which in reality holds more information for adhesion levels, meaning the adhesion index does not have a high temporal resolution.

In order to effectively mitigate low adhesion, there is a need for a more accurate method of adhesion forecasting. Therefore, a method that can estimate railhead adhesion levels in real-time and give the exact location of the probable low adhesion section is required.

This adhesion estimation method will help to cut the costs of low adhesion mitigation and delay related costs whilst improving the safety and confidence of the rail industry. If implemented properly, it will ultimately make the rail system run more safely and efficiently.

1.1 AIMS AND OBJECTIVES

The main aim of the project was to improve the understanding of wheel/rail interface low adhesion mechanisms and to use it to improve adhesion forecasting by employing a novel neural network model. This model was then implemented along sides a data capture system designed specifically for on-train use.

The following objectives were set to aid the completion of the aim stated above:

- Reviewing academic literature and operational information from industry reports
 to establish the current level of understanding of low adhesion; the role of leaf
 layers and wet-rail phenomenon in this including techniques for measuring the
 level of these contaminants on the rail head. Approaches for low adhesion
 forecasting/prediction will also be investigated.
- Analysis of the rail head conditions in a variety of locations at different times to assess levels of contamination and friction levels and gather data for the model.
- Development of the existing Neural Network model for friction prediction in such a way that it incorporates rail head images and enhance it to include other parameters and build-up the data sets used within the model.
- Development of a simple tool for imaging the rail head and track surroundings and for gathering environmental conditions on a railway vehicle.
- Carry out high speed test on the tool in conjunction with the friction prediction tool to validate the output.

1.2 NOVEL ASPECTS AND POTENTIAL IMPACT

A significant aspect of the research involved analysing rail head conditions in various locations at different times to assess relationship between environmental factors and friction variations. This real-world data collection provided valuable insights into the dynamic nature of low adhesion and laid foundation for the development of a neural network for friction prediction. This involved incorporating rail head images, environmental parameters (relative humidity, air, and rail temperature), and additional parameters to improve the model's accuracy and adaptability.

A one-of-a-kind data capture system was developed which is not only useful for this research but can potentially be used by rail industry to capture railhead temperature with exact location output.

In summary, the research contributes unique insights into the understanding of adhesion at the wheel/rail interface using real-world data and provides practical solutions for improving adhesion forecasting in the rail industry. Its impact extends to enhancing railway safety, efficiency, and reliability.

1.3 THESIS LAYOUT

Chapter 2 reviews of past work done on railhead friction which include wheel/rail characteristics, low adhesion in the wheel/rail interface (causes, mechanism, layer creations and measurement techniques), methods of low adhesion forecasting and an introduction to the new friction prediction tool.

Chapter 3 summarises the approach used for each step taken in this research.

Chapter 4 analyses railhead temperature, humidity and friction data obtained from the field visits. This included the methodology used in gathering the data, results obtained from the data, discussion surrounding the implication of the results and trends noticed and a conclusion.

Chapter 5 is outlining the process of the friction prediction tool development, and it justifies the use of the Gaussian process. Validation and retraining of the prediction tool were also discussed in this chapter.

Chapter 6 looks at the robustness of the prediction tool in terms of the types of image formats it can process. Several images captured in-lab were fed into the prediction tool were varied looking at the following parameters: image orientation; static/dynamic image capture; image distance. The predictions resulting from the varied images were analysed and discussed to show how flexible the prediction tool's image processing is.

Chapter 7 details the steps and processes taken in designing the on-train data capture system. It details the methodology used in testing the various designs development and shows the resulting final design with reason. The final design was tested on 4 different occasions, the results are a discussed in this chapter.

Chapter 8 discusses the results and implications of the work done from preceding chapters.

Chapter 9 concludes the thesis with recommendations for future works and publications arising from this research.

CHAPTER TWO

2. LITERATURE REVIEW

2.1 INTRODUCTION

The aim of the literature review was in the first part to give an overview of wheel/rail tribology including the complex contact mechanics and fundamental friction and damage mechanisms. The second part focuses on the problem of low adhesion in the wheel/rail interface, typically seen in Autumn. Causes and mechanisms are outlined as well as ways of predicting the interface conditions. Research gaps are detailed which support the stated aims of the work in the introduction.

A paper grading technique was adapted from [4], it was used to rank the materials used in the literature review based on the relevance to the sections of the literature review they were used as well as in highlighting where gaps exist.

2.2 WHEEL/RAIL INTERFACE CHARACTERISTICS

The contact between the rail and wheels of a train is considered extremely serious/important in terms of the safety and effective operation of the railway network. The contact is expected to carry the weight of the train and transmit the braking and traction forces [5]. The management of the contact mechanics of the wheel/rail interface contributes to keeping operating costs down meaning the contact stresses low for wear reduction and managing friction levels.

The wheel/rail contact is a more complex system when compared to other engineering contact mechanisms. The complexity is mostly caused by the open nature of the system and the dynamic nature of the external (environmental) conditions surrounding the operations.

The contact characteristics such as the position, size and force vary along a distance of a line for each wheel due to the different profiles on each caused by differences in rate of wear on each wheel of the railway vehicle [6].

2.2.1 CONTACT MECHANICS

2.2.1.1 CONTACT LOCATION AND STRESS

The relative position of the contact between the wheel and the rail, which is approximately equal to $1 \, \text{cm}^2$ in area, moves continuously as the train moves along a section of the track. The wheel and rail profile play a key role in determining the exact location of the contact. The location of the contact is also dependent on the degree of curvature of the track as well as the wheel bogie design or position in the train, for example if the wheel on the bogie is the leading or trailing one. On a straight track the wheel tread remains in almost continuous contact with the rail head. The wheel flange will intermittently make contact with the rail gauge as the wheelsets "hunt" or the train enters a curve. Figure 2.1 shows the lead wheelset of the front bogie of the train turning on a right-hand curve and the corresponding contact stress.

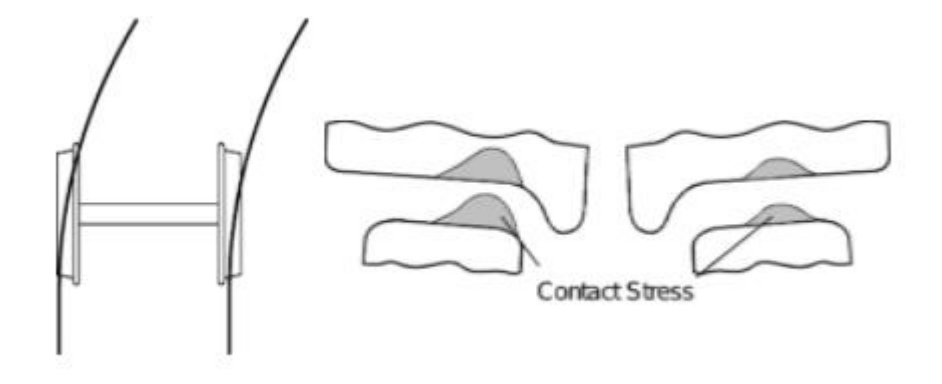


Figure 2. 1: Contact stress on the left and right wheel/rail contact [6]

Figure 2.1 shows the section of the right and left train wheel in contact with the rail gauge. This diagram shows the stress concentrated on the inside (flange) of the rail wheel which carries the major load at the cornering of the train.

The contact stress is responsible for critical issues in the rail operation such as wear and rolling contact fatigue (RCF). RCF crack growth and shakedown limit (which is the load limit below which the material retains its elasticity in a steady state [7]) are determined by contact pressure and friction in the contact. Although, the friction can be controlled with the use of friction modifiers.

The contact stresses experienced by the wheel and rail are dependent on the position of the contact, as seen in Figure 2.2, which gives a more detailed look into the cross-section of the wheel and rail with the three probable regions of contact.

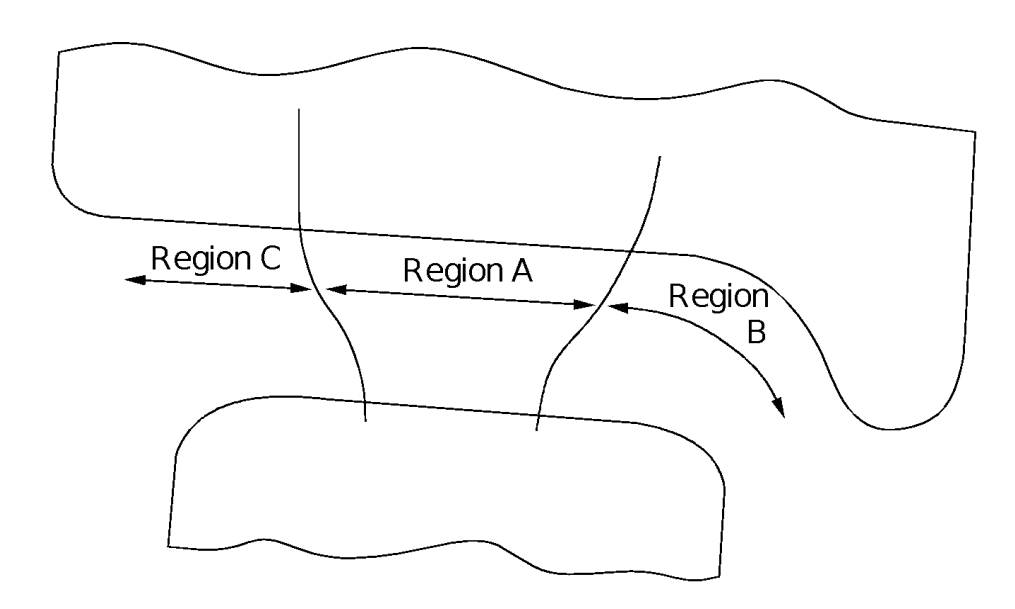


Figure 2. 2: Contact regions on the wheel/rail interface [6]

a) Region A This region represents the contact location between the **wheel tread** and rail head. This most common location of contact as it usually occurs when the train is moving on a length of straight track or curves with a very big radius. This region is known to have the lowest contact stresses as it maintains the highest possible area of contact as seen in Figure 2.3.

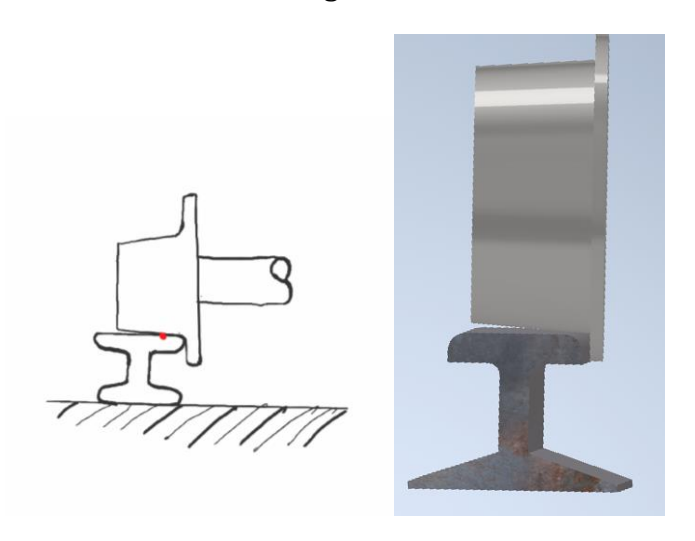


Figure 2. 3: Contact between the wheel tread and railhead

b) Region B: This region represents the contact location between the **wheel flange** and the rail gauge corner. The contact stresses are usually much higher than that of region I because the contact area in the region is much smaller (as seen below in Figure 2.4) than region I's area of contact. This region produces a higher rate of wear.

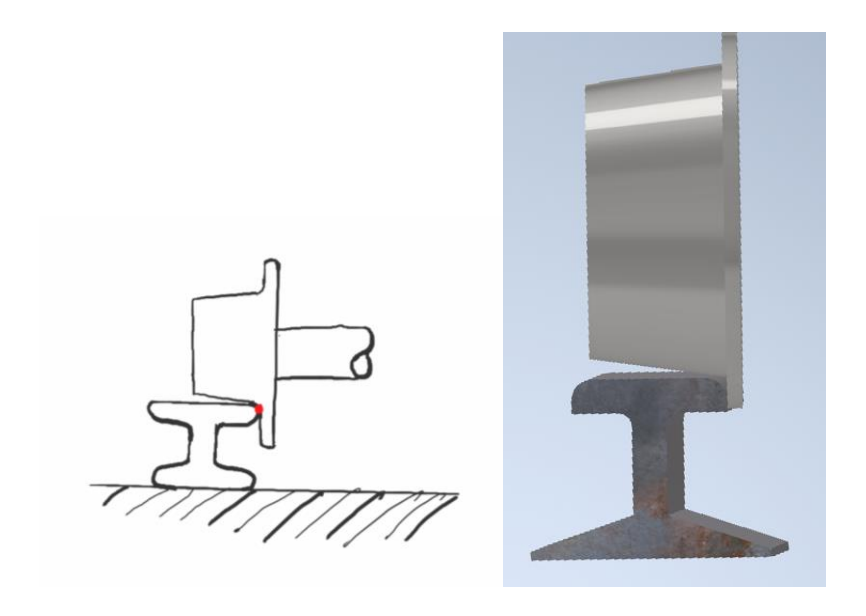


Figure 2. 4: Contact between wheel flange and rail gauge corner

c) Region C: This region represents the contact location between the **field side of wheel and the rail.** The contact location is the least probable to occur of the three regions discussed. In the unlikely case of its occurrence, it will yield high contact

stresses. The high stresses will cause unwanted wear which can result in wrong wheelset steering[6].

The wheel or rail profile shape changes because the contact location is uneven over the profiles of the wheel and rail which is caused by material flow and wear.

2.2.1.2 Contact pressure Solution/Mathematical model for Non-Conforming Elastic Bodies Non-Conforming Elastic Bodies (Circular Contact area)

Hertz [8] analysis is the easiest means of defining the wheel/rail contact geometry and resulting stress. In the Hertz analysis for "solids of revolution", the train wheel and rail can be taken as two perpendicularly positioned cylinders in contact with each other therefore assuming a circular contact to simplify the case. P_0 (maximum contact pressure) is given by Equation 2.1 below:

$$P_0 = \sqrt[3]{\frac{3FE^2}{2\pi^3 R^2 (1 - v^2)^2}} \tag{2.1}$$

where it is assumed that the material for the rail and wheel are the same; F is the normal load, E is the Young's modulus and v is the Poisson ratio.

R is the effective radius given as:

$$\frac{1}{R} = \frac{1}{R_1} + \frac{1}{R_2} \tag{2.2}$$

Such that; R_1 and R_2 are the wheel and rail contact radii [9].

Non-conforming Elastic Bodies (Elliptical Contact area)

Srivastava et al. [10] and Zong [11] stated that a contact area takes on an elliptical shape when two elastic non-conforming bodies are held down against each other. For the elliptical area having a semi major axis 'a' on the x-axis and minor axis 'b' on the y-axis, as seen in Figure 2.5, the contact pressure distribution, P can be given as:

$$P = P_0 \sqrt{\left(1 - \frac{x^2}{a^2} - \frac{y^2}{h^2}\right)} \tag{2.3}$$

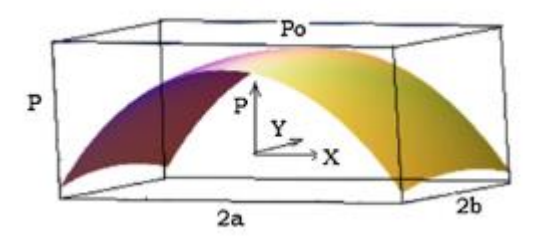


Figure 2. 5: Pressure distribution across elliptical contact area [10]

where 'a', 'b' and ' P_0 ' are given as:

$$a = m \left[\frac{3\pi P(K_1 + K_2)}{4(A+B)} \right]^{\frac{1}{3}}$$
 (2.4)

$$b = n \left[\frac{3\pi P(K_1 + K_2)}{4(A+B)} \right]^{\frac{1}{3}}$$
 (2.5)

$$P_0 = \frac{3F}{2\pi a h} \tag{2.6}$$

where 'A' and 'B' are positive geometric constants used whilst considering the wheel/rail configuration. 'm' and 'n' are tabular functions given by [12] and ' K_1 ' and ' K_2 ' are constants defined by Equations 2.7 and 2.8:

$$K_1 = \frac{1 - v_w^2}{\pi E_w} \tag{2.7}$$

$$K_2 = \frac{1 - v_R^2}{\pi E_W} \tag{2.8}$$

' v_w ' and ' v_R ' are Poisson's ratio for the wheel and rail respectively and ' E_w ' and ' E_R ' are the Young's modulus of elasticity of the wheel and rail materials respectively.

The Hertzian approach Involves the following assumptions:

- The surfaces are non-conforming and continuous (Contact area much lesser that radii of body).
- Effects of strain is negligible due to much smaller contact area than radii of body.
- The surfaces in consideration are frictionless.
- Individual solids can be considered as an elastic half-space.

2.2.1.3 OTHER METHODS OF DETERMINING THE WHEEL/RAIL CONTACT CONDITIONS

Other approaches built on the Hertz theory have been considered by different researchers to analyse the wheel/rail conditions. Below are two other methods used:

FINITE ELEMENT METHOD (ANSYS)

FEM based simulations are tools that have been used to determine the distribution of contact pressure, contact zones, and contact stresses which can be done based on different wheel profiles and configurations of the wheel.

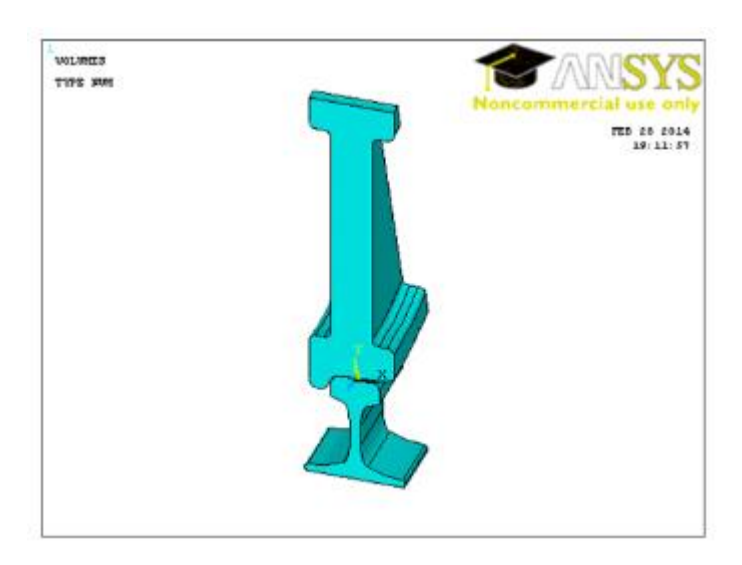


Figure 2. 6: Wheel/rail assembly geometric model in ANSYS [10]

In work by Srivastava et al, the FEM (Ansys) mesh density, with a mesh element size of 1mm, was used around the contact region and has been discovered to have a direct impact on the simulation solution accuracy [10]. A comparison was done using results obtained from the Hertz contact theory method and the Ansys simulation done with a geometrical model seen in Figure 2.6. Similar wheel/rail mechanical properties and contact geometries, such as radius of curvature used in the theoretical method, were used in designing the Ansys model.

The results from the Hertz analytical method showed that there was a decrease in stress as the wheel profile radii increased, its increase consequently increased the ellipse contact area width while the length is decreased. On the other hand, there was a periodical fluctuation between a decrease and increase in the stress results obtained from the FEM simulation. This trend was opined by [10] to be as a result of the near realistic nature of the simulations, where the materials do not have linear limits nor have a half space assumption. The Hertz contact model is based on both assumptions stated above. Therefore, the FEM simulation is a more appropriate method of studying or analysing the wheel/rail contact parameters when available.

NUMERICAL METHODS USING MATLAB

Huang et al. [13] used a simplified schematic diagram of the wheel/rail contact on a straight stretch of track as seen in Figure 2.7, having 'd' as the distance between the centre lines of the parallel running rail cross-sections, W is the axle load and T is the length of the distance between both of the back wheel flanges.

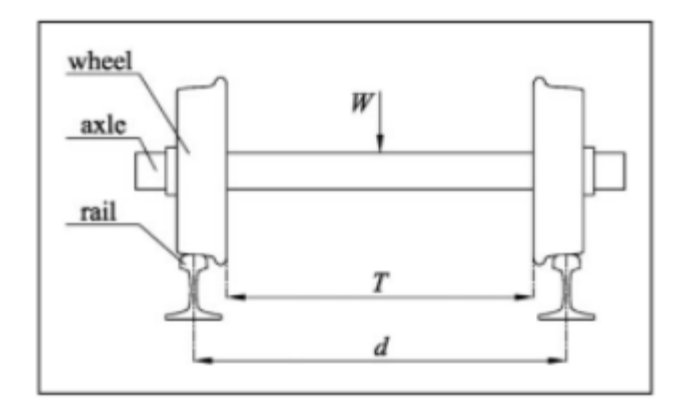


Figure 2. 7: Schematics of the wheel/rail contact [13]

Due to the complexity of finding the centre as a result of the varying relative position of wheel and rail, a method was established by Huang et al. to determine the centre position of the contact points in several contact situations. Using the *x-y* plane coordinate system for the wheel tread section of the "China's National Standard for Passenger Train Wheels and Rails" a wheel/rail cross-section was drawn as seen in Figure 2.8.

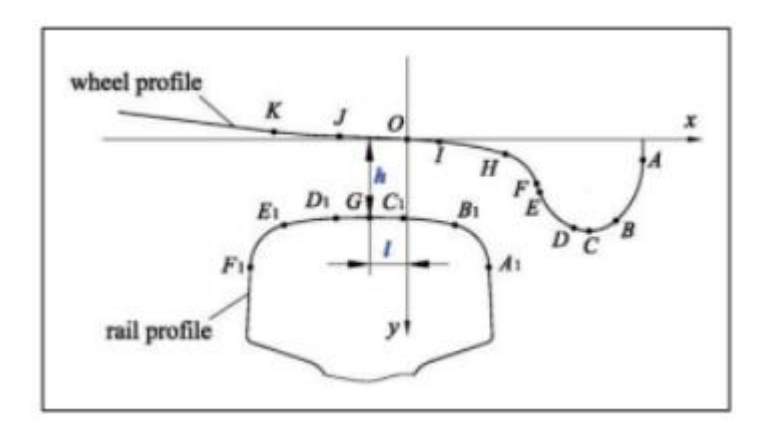


Figure 2. 8: Coordinate systems used for the section [13]

Points A through to K in Figure 2.8 are the partitioning points on the wheel surface profile, with C being the vertex of the wheel flange. While points A_1 through to F_1 are the partitioning points on the rail surface profile and the vertex of the rail profile is G.

It was stated the contact points of any two surfaces could be derived by solving the equations of both profiles simultaneously and if a solution is non-existent, then the surfaces are not in contact, as seen in Figure 2.9. In a case where the equation gives one solution it means there is only one contact point, which is the desired solution but when two or more solutions are produced then the surfaces have become immersed in each other implying there are two or more contact points seen in Figure 2.9. This may be the case when the wheel travels on curved tracks although this two-contact point scenario happens rarely. The equation of profiles 1 and 2 can be given as $y_1 = f_1(x)$ and $y_2 = f_2(x)$ respectively.

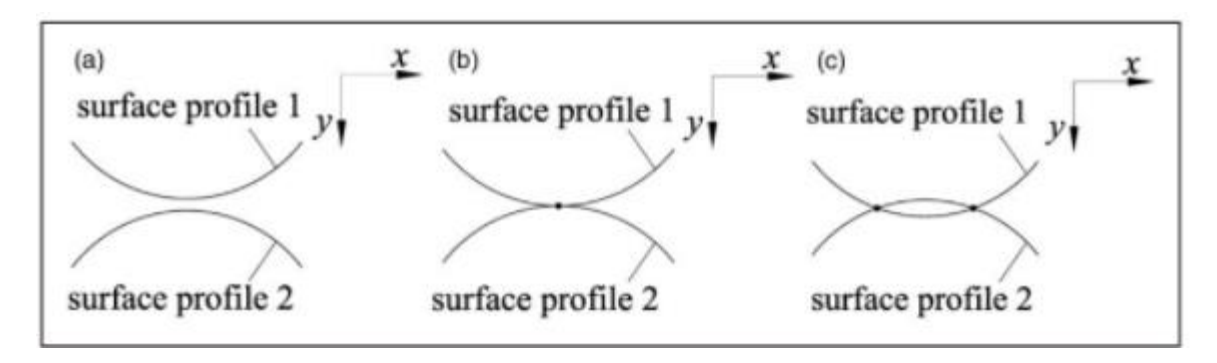


Figure 2. 9: The relative position of the wheel and rail profiles [13]

The complex nature of the wheel/rail contact which consists of arcs and straight lines as seen in Figure 2.8 makes it difficult to find the solutions using analytical methods, hence MATLAB was used to create a numerical method [13].

The wheel profile mathematical equation $y_1 = f_1(x)$ was given as Equation 2.9:

$$y_{1} = \begin{cases} -2.5227 + \frac{1}{8}[x - (-42.2840)], & -60.0 < x \le -42.2840 \\ -220.8243 + \sqrt{220^{2} - [x - (-32)]^{2}}, & -42.2840 < x \le -20.1944 \\ 498.9749 - \sqrt{500^{2} - [x - (-32)]^{2}}, & -20.1944 < x \le 9.5625 \\ 100.3593 - \sqrt{100^{2} - (x - 1.25)^{2}}, & 9.5625 < x \le 29.1531 \\ 17.775 - \sqrt{14^{2} - (x - 25.2466)^{2}}, & 29.1531 < x \le 38.4025 \\ 12.9872 + \frac{x - 38.4025}{39.3543 - 38.4025}(12.9872 + 15.6023), & 38.4025 < x \le 39.3543 \\ 9.4454 + \sqrt{18^{2} - (x - 56.2686)^{2}}, & 39.3543 < x \le 49.4629 \\ 15.0 + \sqrt{12^{2} - (x - 54.0)^{2}}, & 49.4629 < x \le 62.0 \\ 6.0557 + \sqrt{24^{2} - (x - 46.0)^{2}}, & 62.0 < x \le 70.0 \end{cases}$$

$$(2.9)$$

The rail profile's cross-section equation $y_2 = f_2(x)$ was given as Equation 2.10:

$$y_{2} = \begin{cases} -14.8408 + h - \sqrt{13^{2} - [x - l - (-22.4108)]^{2}}, & -35.3946 < x \le -25.3361 \\ -80.1223 + h - \sqrt{80^{2} - [x - l - (-7.3333)]^{2}}, & -25.3361 < x \le -10.0 \end{cases}$$

$$300 + h - \sqrt{300^{2} - (x - l)^{2}}, -10.0 < x \le 10.0$$

$$80.1223 + h - \sqrt{80^{2} - (x - l - 7.3333)^{2}}, \quad 10.0 < x \le 25.3361$$

$$14.8408 + h - \sqrt{13^{2} - (x - l - 22.4108)^{2}}, \quad 25.3361 < x \le 35.3946$$

$$(2.10)$$

SUMMARY

Both FEM and numerical method of wheel/rail contact analysis discussed here have their strengths and weaknesses. One of the key notable points is that neither approach discussed here take into account the contact surface roughness as they both based off the Hertzian contact model with the assumption that contacting surfaces are perfectly smooth. However, in reality, most surfaces are not perfectly smooth; they have irregularities and roughness on various scales. Ignoring surface roughness in the Hertz contact model can lead to several consequences, such as contact area size underestimation and incorrect prediction of stress distribution [9].

The FEM analysis offers a 3-dimensional view of the wheel/rail contact, thereby showing the von Mises stress distribution for the contact in 3 planes. This helps to locate the initiation point for fatigue crack. With FEM stresses can be obtained at every point of the contact, which makes it easier to highlight points of high stress visually. Given these advantages, FEM has shown a trend of inconsistencies in analysis of complex shapes as that presented in the wheel/rail contact, especially in the generation of meshes for such shapes. This method shows promise as with advancement FE packages, complex shapes can be refined better for analysis.

On the other hand, the numerical method covers a simplified analysis of the wheel/contact using mathematical model on MATLAB and does not require 3-dimensional model of the contact to be drawn out. This method considers varying contact profile geometry just like the FEM. This method involves a lot of equation derivations and calculations to obtain contact point coordinates and it is a lengthy process, meaning more errors will be involved. This method also provides a contact stress distribution as in the FEM but does not include a von Mises stress distribution. Due to it been a mathematical model, an error correction factor can be included to improve the accuracy.

2.2.2 CREEP FORCE

As stated earlier the performance of the train is affected greatly by the wheel/rail interactive (friction) forces, hence the performance is also determined by creepage which is influenced by wheel and rail profile. Eadie et al. [14] also opined that parameters such as wheel and rail roughness, Hertzian contact pressure and third body (interfacial layer) shear strength amongst other factors impact the friction force.

Creep takes place when two rigid bodies are under axial compressive loads and can roll over one another [15]. It must be noted that when influenced by gravity, usually referred to as gravity railway (movement of carriages down a slope applying only force of gravity) the wheel/rail components in contact produce elastic deformation, while the contact area grows into an "elliptical contact spot", hence proving the Hertz theory valid [15, 16], consisting of adhesion and creep zones, as seen in Figure 2.10 below.

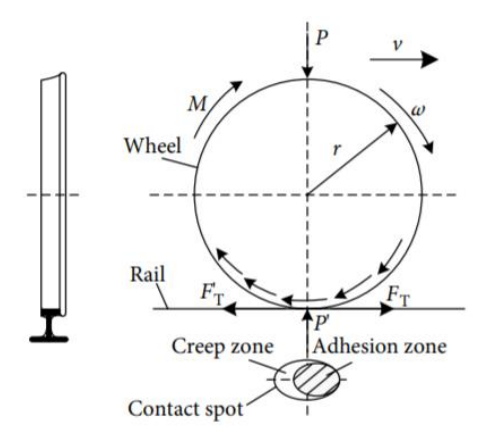


Figure 2. 10: Depiction of the contact between the rail and train wheel with the characteristics given as; v – velocity of the train body, ω - angular velocity of the train wheel, P - vertical forces acting on the train wheel, P^I – vertical force acting on the rail and r – radius of the rolling wheel

The wheel/rail contact has a combination rolling and siding contact as there is usually no pure rolling. The angular velocity and linear velocity are not equal in a combine rolling and sliding contact which brings about creep in the contact. Creep is also referred to as slip.

When a driving torque of magnitude M is applied to the train wheel, a tangential force F_T acting on the wheel contact surface is produced and an opposing tangential force F^{l_T} acting on the rail contact surface, hence producing a forward motion of the wheel.

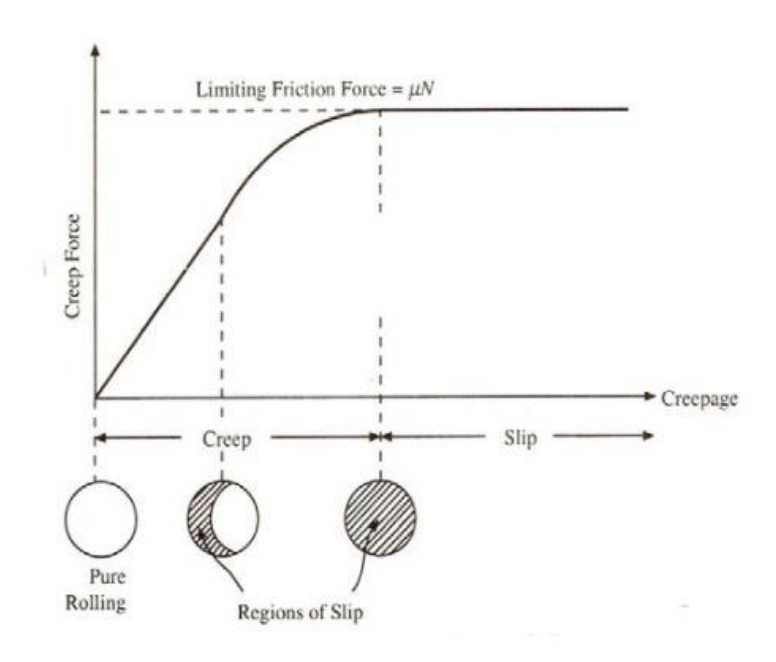


Figure 2. 11: Relationship between creepage and creep force [15]

Monk-Steel et al. [17] define **creepage** as the "relative velocity divided by the rolling velocity". Bhardawaj et al. [15] define **longitudinal creepage** as the "ratio of the

wheel/rail relative speeds and the rolling velocities" while **lateral creepage** is the "change in lateral velocity per wheel forward velocity". **Spin creepage** is also said to be the ratio of the in wheel/rail rotational speed perpendicular to the contact with wheel forward velocity. An increase in the three respective creepage brings about an increase in shear stresses, if the shear stresses are greater than the **creep force** (normal force \times coefficient of friction), wheel slip will occur. Full slip occurs in the contact past the saturation point shown in Figure 2.11 where the limiting friction force (traction force) is reached and remains constant, regardless of slip.

The dependency of wheel/rail friction force on creepage as seen on the creep curve in Figure 2.11 was discussed in [14]. Friction in the wheel/rail interface can be influenced by several factors such as third body (Interfacial layer) shear strength, Hertzian contact pressure and wheel and rail surface roughness among others. The creep curve shows that the creep force which is a function of the **friction coefficient** μ , increases as the creepage (slip) increases moving from a pure rolling zone to a combination of rolling and sliding until the creep force converges at complete slip (pure sliding), where the friction coefficient becomes dominant.

Adhesion as a function of creep or simply the creep curve varies when there are third body materials in the contact, in terms of the curve shape, initial slope and the adhesion levels [18], which is shown in Figure 2.12.

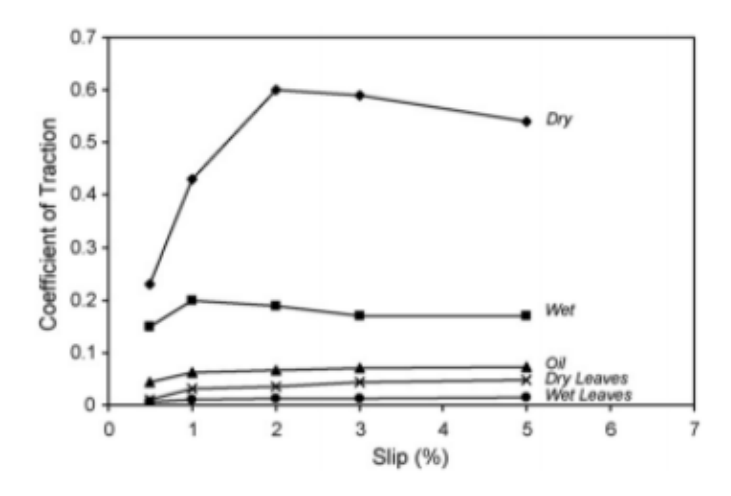


Figure 2. 12: Creep curves for different test conditions [19]

Gallardo-Hernandez & Lewis [19] carried out tests on different rail contamination conditions to assess the adhesion/traction coefficient and slip relationships, as seen in Figure 2.12. As can be seen, contaminants such as water and dry leaves and oil were seen to significantly reduce the adhesion coefficient to below 0.1 with increasing slip when compared to that of the dry railhead surface. The wet surface test also showed a decrease in adhesion coefficient, and it was seen to have a significant drop when compared to the dry surface result.

2.2.3 METHODS OF FRICTION CONTROL

Understanding the adhesion or the friction between the wheel and rail is of utmost importance in understanding many aspects of wheel/rail performance. Wear, corrugation and rolling contact fatigue are some of the damages caused by high traction between the rail and wheel. On the other hand, low friction or adhesion can potentially cause safety issues when there is lowered traction making braking less effective and it may also cause wheel slip conditions which will affect the operation of the train [14].

Therefore, controlling the levels of friction on the wheel/rail interface is of utmost importance in order to maintain safety. This can be done to either reduce friction (adhesion) or increase friction (adhesion).

There are 3 major categories of friction management products:

- Top of rail friction modifiers (ToR-FM).
- Traction enhancers
- Flange lubricants.

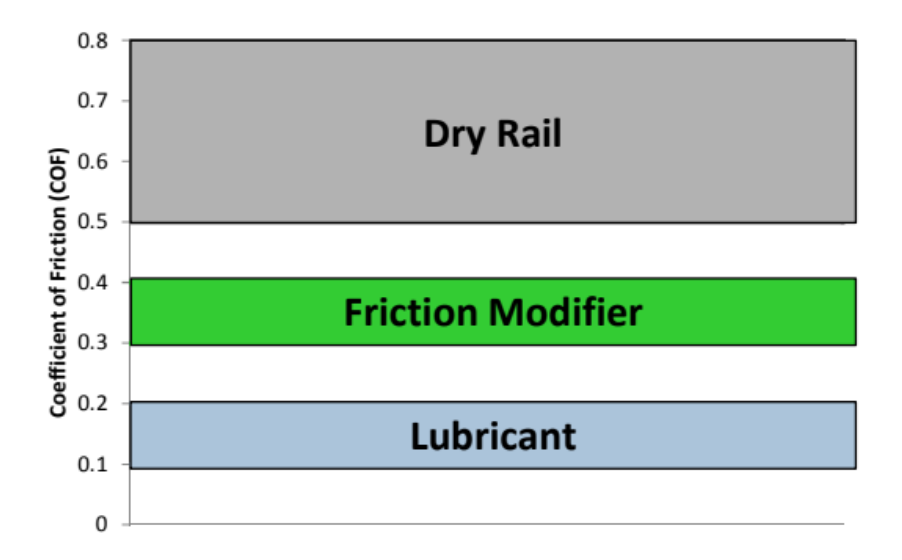


Figure 2. 13: Effects of friction modifiers on CoF [20]

Friction Modifiers

Generally, when discussing methods for friction reduction to reduce damage of energy consumption, controlled lubrication is usually a common thought as a solution. However, lubricants would negatively affect the braking and traction operations of the train and cause damage to the wheel/rail interface. Friction modifier here refers to TOR-FM and Traction enhancers. A friction modifier on the other hand is expected to provide the appropriate intermediate friction coefficient of between 0.3 to 0.4 as seen in Figure 2.13 without the negative effects of a lubricant. Friction modifiers are additives that increases or decreases the frictional properties of a lubricant. These include traction enhancers which increase friction and specially formulated 'TOR' products to be deployed at low adhesion hotspots.

Therefore, Top of Rail Friction Modifiers (TOR-FM) are substances that can only reduce high levels of friction under dry conditions (0.5-0.8) to a moderate level of friction (0.3-0.4). However, a traction enhancer can increase low levels of friction [20].

Generally, friction modifiers are applied to the top of the rail using either a track side, vehicle/train mounted or mobile systems applicator. There are different types of TOR-FM, which are water based-solid suspension and just solid modifiers. Existing products that use water based-solid suspension friction modifiers such as '**KELTRACK**' to deliver the desired level of friction between 0.3 - 0.35 [21]. The water in the mixture evaporates, leaving behind the solid particles which combine with the third body layers on the railhead creating a surface with the required friction level.

The **KELTRACK** TOR-FM has been found by Network Rail to reduce vibration and noise, aid in the control of train on the rail track curvature and reduction of lateral loads [21].

A common form of traction enhancer is sand which is usually applied on the railhead from train mounted applicators and may cause wear due to its abrasiveness, which is why it is only applied when/if wheel slip is detected. It may also interfere with track signal processing by isolating the track circuit. There are new types of traction enhancers in form of sand gels and viscous water-based gels (usually applied using a track side applicator) which reduced the effects of abrasive wear when applied on the railhead and it do not interfere with track signals [5].

Top of Rail Lubricants (ToRL)

Lubricants such as greases are able to decrease the friction level in the wheel/rail contact. They are mainly used to reduce the effect of wear between rail gauge face and the wheel flanges and reduce noise caused by high friction. They can also be used on the top of the rail, and if applied in the right amounts can give intermediate friction. There is a higher risk with these though that they are over-applied which could result in low friction causing braking/traction problems. Unlike friction modifiers, their carry-down distance is shorter than 1600 m. This is because the grease is easily used up along the tracks reducing the length of effectiveness.

ToRL can be classified into 3 categories:

- TOR Oil (oil-based TOR material)
- TOR Grease
- TOR Hybrid (oil and water-based material)

Using grease for top-of-rail friction control in lengths of track with a high rail curvature has benefits of curve noise reduction; force reduction, meaning less RCF and gauge corner cracking; rail and wheel wear reduction [22].

2.3 LOW ADHESION IN THE WHEEL/RAIL INTERFACE

According to the Adhesion Working Group (AWG) [23], adhesion on the railway is simply a measure of slipperiness or grip between the wheel and rail. This is defined by AWG as:

"The measure of adhesion values is approximately equal to the maximum possible rate of deceleration of a given train, when expressed as the percentage of deceleration due to gravity". It is measured as the coefficient of friction and is usually represented by " μ ".

Low adhesion is defined by the "Adhesion Working Group" as a μ value lower than 0.09 [24]. Table 2.1 and Figure 2.14 shows the categories of adhesion levels with the corresponding friction levels that define them.

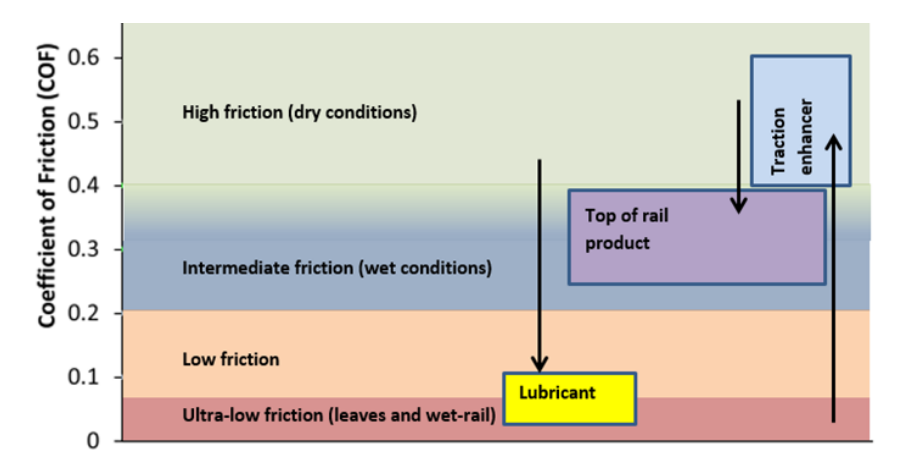


Figure 2. 14: CoF ranges (adapted from [20] by [25])

Table 2. 1: Definition of adhesion levels

Adhesion level	Coefficient of Friction level
Good	Greater than 0.15
Medium	Between 0.1 to 0.15
Poor	Between 0.05 to 0.09
Ultra-low	Less than 0.05

The adhesion levels defined traditionally vary according to the weather conditions, such as having μ between 0.2 to 0.4 under ideal conditions of dry weather and clean uncontaminated railhead. Whereas, in wet weather, a μ value between 0.1 to 0.2 (even with no railhead contaminant present) would be in line with expectations. According to Table 2.1 under both conditions there should not be complications with braking, but poor adhesion levels during full-service braking may occur occasionally. Specifically, during the autumn when fallen leaves blown on the tracks are crushed and mixed with moisture to form a thin film, Teflon like in nature, reducing the adhesion to levels as low as 0.01.

2.3.1 CAUSES OF LOW ADHESION

The main causes of low adhesion stated in the report presented by the RSSB, TUoS and the Met Office [26]were determined as;

- leaf contamination of the rail head during autumn and
- a mixture of low levels of moisture on the railhead, iron oxide and/or wear debris which is referred to as "**Wet Rail Syndrome**". These characteristics are considered as naturally occurring **third body layers** which also exist in dry conditions. Low adhesion can also be experienced in dry conditions, where a thin film of rust (usually a mixture of sub-micron Iron oxide and hydrated Iron oxide particles). This thin film produced can cause low adhesion as it may carry some amount of moisture and contaminant [27, 28].

Some other causes for low adhesion were determined but stated to be less common in occurrence, such as

- improper flange lubrication.
- oil leakage from transitory diesel trains.
- presence of dust, commonly coal dust.
- leakage of hydraulic fluid from track machines.
- settling of contaminant on the track commonly from airborne aviation fuel close to airports and chemical waste close to industrial estates.

With all the possible causes of low adhesion mentioned above, the largest and out of human control cause has been recognised as the leaf contamination especially leaves that are not easily broken down or decomposed. These leaves are usually drawn onto the tracks by trains passing, the leaves settle on the track and are thereafter crushed by the wheels of other passing trains onto the railhead. A hard layer of coating is formed on the railhead with a Teflon texture when the compressed crushed leaves are mixed with moisture commonly dew on the railhead. When dry, this coating can act as an electrical insulator which leads to problems with the operation of track circuits used for train detection for signalling purposes and when wet can act as a lubricant hence causing problems with braking. It must be noted that under heavy water conditions, the crushed leaf layer is softened and broken down by the effect of passing trains and finally washed off then tracks by rain as simulated during the WILAC project [29].

2.3.2 LOW ADHESION MECHANISM

It is common knowledge that lubricants such as grease, fuel and oil reduce the adhesion levels, but moisture, which would not be regarded as a lubricator, is also one of the causes of low adhesion. This occurs when the moisture reduces the shear strength of the third body such as oxides which the creates a slippery layer between the wheel and rail. The implication of this is that dry rusty rail track and dry leaves on the railhead will not cause low adhesion, but once a small amount of moisture is present on the surface, it becomes an active site for low adhesion. The presence of ice is also known to lead to low adhesion, this does not happen because of the slippery nature of ice, but as a result of the melting

process which produces water on the rail head. Fulford [21] made mention that an increased amount of humidity of the surrounding air affects the level adhesion by a small amount, but the major changes are caused by water residue on the rail surface.

The Adhesion Working Group (AWG) carried out an extensive literature research to create a knowledge map of low adhesion and an analysis was done on performance data from a variety of sources [23]. The research done by the group involved a critical assessment on the following factors, highlighted in the T1042 RSSB [24] report that are believed to aid the understanding of underlying causes of low adhesion. The credibility and quality of data was verified whilst inputting in the report.

These performance data were grouped into four areas which were then broken down further into individual parameters as seen in Table 2.2 [24].

Table 2. 2: Performance data classification

S/N	Operational Data	Parameters
1	Regional Environmental Parameters	Regional Air temperature
		Regional Humidity
		Regional Precipitation
		Regional Leaf fall index
2	Local Environmental Parameters	Local Air temperature
		Local Humidity
		Local Precipitation
		Railhead leaf contamination
		Railhead moisture
		Railhead temperature
3	Track Related Parameters	Track gradient
		Rail type
		Track topography
4	Rolling Stock Related Parameters	Brake characteristics
		Drivers report
		Traction characteristics
		Traction or braking demands
		Driving policy

The parameters above play an important role in understanding the mechanisms of low adhesion, as it gives an insight into the conditions surrounding the train and track when low adhesion is experienced.

The two major causes for low adhesion proposed in the report are as follows (albeit other factors may also play a role):

• Leaf layer formed on the railhead, sometimes combined with little moisture. They create a reduced shear strength layer on the railhead. The conclusion was made that this event occurs all through the day as the effects of this leaf fall and precipitation can be experienced all day.

• The interaction between morning dew and contaminants for example iron oxides, this forms a solid lubricant/low adhesion paste on the railhead and is referred to as "Wet-rail" phenomenon. They are known to be the cause of high incident rate during morning peaks. White et al. [30] support this from data gathered from reports of station overruns showing that this occurrence is on the rise in the early hours of the morning and in the night, between the hours of 06:00 - 09:00 and between 20:00 - 22:00 respectively as a result of dew present on the railhead. In research carried out by [29], where water at different levels was added to a full-scale tram test rig to understand how low levels of moisture contributed to the adhesion levels, it was confirmed that the presence of wear debris and iron oxide contributed to lowering of adhesion to "ultra-low" levels in the presence of low moisture. It was stated that this combination formed a third body layer that was visible on inspection. This experiment supports the theory that a combination of low moisture and oxides cause low adhesion.

The summary of the important information that was derived from the research done on the T1042 report as presented by the AWG is as listed below[23, 24]:

- the most effective low adhesion mitigation technique is the use of a "properly functioning on-board sander" and the application of a water jetting on the track for treatment.
- the performance data analysed proposes that an average colder temperature might have a significant effect on the adhesion performance, which may be as result of an increase in leaf fall during autumn.
- railhead contamination becomes a dominant wheel/rail adhesion characteristic, when it is visibly present on the railhead.
- in cases of low moisture level on the railhead, the adhesion level can be notably improved by application of only water.

2.3.3 LAYER CREATION

Leaves, small amount of moisture and oxide layer have been recognised as one of the major causes of low adhesion events in the railway industry:

Leaves + low moisture

Autumn has been recognised as the season where severe low adhesion events have been recorded due to increased number of leaf fall to the surrounding railheads which usually accumulates to the side of the track as well. The accumulated leaves in the track surrounding are swept to the bottom of passing trains by the wind created by the motion of said passing trains. These leaves are then crushed by the wheels of the trains, leaving behind a thin leaf layer on the rail head. The continuous crushing of the leaves by different trains in transit creates a hard, Teflon-like, black leaf film which is capable of completely covering the running length of the railhead. The leaves undergo a chemical reaction with

the rust formed on the railhead which are a form of iron oxides to form the black layer [19, 21, 31].

This black film formed has a somewhat low shear strength which can reduce adhesion by fully obstructing the contact between metals such as the contact between the wheel and rail; it also forms an electrical insulation barrier.

Researchers made note of a thick hard layer of mulched leaves formed on the disc surfaces used in assessing wheel/rail adhesion [19]. It was found that immediately after the test for the wet leaves, the top layer was soft and dark. This layer was easy to remove, leaving behind a harder compacted layer which proved extremely difficult to remove.

In other work it was stated that the mixture of the crushed leaf layer and low moisture (which could be either dew, snow shower or light rain) posed a higher risk in terms of the adhesion levels, as the black layer reduces the adhesion coefficient to about 0.1 while the mixture reduces the adhesion coefficient to less than or equal to 0.05 [21]. These levels of adhesion are much lower than the required operating values for braking and traction which are as high as 0.09 and 0.2 respectively. This shows the significant effect moisture has on the leaf layer in lowering the adhesion.

The composition of this leaf layer was analysed and found to contain basic elements of the leaf just without the water, the basic elements contain a highly polymerised fatty acid that is known to be an effective lubricant. Visible leaf pieces were seen on the black layer found on the railhead which also consisted of a large amount of iron and iron oxides and some water (which have been classified as the non-organic part of the layer leaving the only organic matter as the dead leaf after investigation under an optical microscope). Hence the components of the black layer can be said to be Iron, Iron oxide, Carbon (from the leaf), Hydrogen and Oxygen.

Many other mixtures of material may be responsible for low adhesion on the railhead other than leaves mixtures.

Wet-rail phenomenon

White et al. [30], made note that a number of proposed low adhesion events were omitted from the Network Rail incident data, possibly because there was no visible contamination on the railhead (in this case "contamination" means leaf material) This shows that there are more plausible causes of low adhesion such as wet-rail phenomenon.

White & Lewis [32] stated that the analysis of the slippery black film layer usually present after moist leaves have been crushed on the railhead was found to contain approximately 56% iron oxide. This information implies that wet-rail phenomenon can play a role in the occurrence of low adhesion events if the iron oxides present in both the black film layer and railhead contaminant has an effect on the adhesion levels. Although, it is only considered as wet-rail phenomenon in the absence of leaf contamination, but this shows the contribution oxides have to the railhead adhesion. It has also been noted that the

occurrence of low adhesion outside of the autumn season may be attributed to wet-rail phenomenon, meaning the wet-rail phenomenon can act all year round. The formation of iron oxide on the railhead can be attributed to either contact oxidation caused by high temperature and high forces experienced in the wheel/rail contact or the oxidation from environmental conditions such as high humidity, precipitation among others.

Unlike the black layer caused by the mixture of moisture and leaves, wet-rail phenomenon is difficult to analyse or determine as it is hard to identify.

2.3.4 MEASUREMENT TECHNIQUES FOR LOW ADHESION (FRICTION)

The adhesion levels between the rail track and wheel is almost impossible to measure directly, but the friction coefficient is easily measured from the rail surface [33].

Low adhesion measurements are considered important because it contributes to the safe operation of the railway as well as improved performance. The RSSB [34] catalogue has highlighted some of the reasons as given below:

- Improvement of equipment and procedures used to mitigate the effect of low adhesion which can be brought about by post incident analysis done to determine the causes of previous issues.
- In order to safely operate trains in low adhesion conditions, the industry is required to carry out risk assessments and have mitigation measures in place. Reliable measurement techniques are required to facilitate the successful development of a mitigation technique.
- Existing measurement techniques give the opportunity to simulate low adhesion conditions, which help in giving the train driver the experience needed to successfully handle real life low adhesion conditions if/when the driver encounters such.
- The simulation of low adhesion conditions also helps to test effects of new equipment on safety and performance.

There are several industry recognised methods of measuring friction on the rail head. The major means of carrying out these measurements are with field data or lab tests.

The measurement techniques for low adhesion have been grouped into 3 parts (as seen in Table 2.3), namely:

- Direct measures of low adhesion
- Indirect measures of low adhesion events
- Measures of weather and environmental parameters.

(Information used in this section is obtained from [34], except when stated otherwise.)

Table 2.3: Adhesion measurement techniques

Measurement	Measurement	Description	Advantages	Disadvantages	Sample Data
Technique On-Track Techniques; Vehicle attached Direct					
measures of low adhesion	Vehicle-Bourne Tribometer	The tribometer works on the principle of a brake wheel tribometer where the adhesion levels are determined by applying brakes to the wheel on the tribometer until the wheel starts to slip. It measures the running surface and gauge surface traction with the measuring wheels, which sense the normal force and braking torque exerted [27]. The device provides four measurements which are taken simultaneously; these are the friction on both rails, gauge face and the railhead. (see Figure 2.15)	The vehicle borne tribometer has better accuracy when compared to a portable tribometer. They can be used for simultaneous measurement of both rails and adjustment of its wheel position is possible. A notable length of track can be measured; hence it is a fast method of measurement. The measurement method of using a braked wheel gives the peak adhesion.	It is currently unusable on third and fourth rail electrified lines This method cost more than using a portable tribometer Transportation to problem site is slow [26]	High Speed Tribometer track adhesion profile for low adhesion mitigation 1.
	Tribometer Train	The Tribometer train can measure the longitudinal and vertical forces with normal operation of its suspension. The vertical wheel/rail forces can be included in the low adhesion levels calculation with; the use of a static wheel load and if the static wheel loads cannot be estimated the vertical wheel/rail forces should be determined from the test arrangement. If the speed of measurement is less than 48 km/h (30 mile/h) the use of static load will be enough, this common occurrence in most applications. (see Figure 2.16)	Measurement derived can be built into the railhead treatment train. It is not subject to scaling effect, since it provides a full-scale adhesion measurement for the wheel/rail interface. The peak adhesion level is obtained as well as the adhesion profile.	It requires a train path. It is expensive [26]. The train used for case study on the RSSB manual as at the time of publishing was stated to be obsolete, therefore it is not readily available for use. Results are affected by the flange contact. Transportation to a site is slow due to its size. The wheel/rail forces require serious analysis and data processing.	
	Load Measuring Wheel	This equipment serves as an attachment to either service vehicle or a specially built tribometer. The wheels measure the magnitude of the lateral, vertical and longitudinal force of wheel/rail using a built-in strain gauge. (see Figure 2.17)	system can provide the adhesion profiles. This method is not subject to scaling effects, as it is a full-scale method of measuring the wheel/rail adhesion levels. It is practical in use for test purposes, because it can be mounted on a	considerable amount of analysis and data processing. It is an expensive method which is not readily available and complicated to build. The results from this method are affected by flange contact. The braking stage of the wheel produces heat which must be considered when using the	Day and with 71 MA vertical load and 30 m Radia angle of states. 10
	Strain Gauged Axle	This measurement is relatively recent work and is still being investigated by the RSSB.	It is not subjected to scaling effects because it records force for full scale wheel/rail conditions. Incorporation into a railhead treatment train is possible and it may be suitably fitted onto service trains. Adhesion profile can be obtained.	When using a non-service train, a train path will be required. It is still under development; hence it is not readily available. The wheel/rail forces require serious analysis and data processing, especially in terms of separating forces acting on the rotating assembly. Results are affected by the flange contact.	
		ques; Manually Handled			
	OnTrak HO Tribometer			It is a new tool which means the errors produced while using it are not fully understood. The measurement process can be time consuming depending on the amount repeats required and the number of positions measured on the railhead. The repeatability and precision of the tool have not been tested.	0.40 0.35 0.30 0.25 0.20 0.15 0.10 0.05 0.00 0 20 40 60 80 100 Creep - %

directions[the 97th percentile in both directions[14, 35]. (see Figure 2.18)	levels of the tool can be changed. This makes it easier to understand the state of the railhead		
	Skid Resistance Slider Tribometer	The Pendulum tribometer is a solid example of a skid resistance slider tribometer. This tribometer is best suited for laboratory use as it was designed for use on the road, therefore requiring a flat surface for operation. The pendulum tribometer can be modified or a platform can be fitted over that rail track to carry out measurements on the field [26] The Pendulum tribometer which has a rubber contact pad functions on the energy loss and swinging arm principle. It has an entirely different contact geometry with the contact being in full slip when compared to other tribometers. Albeit, it has few similarities to other portable tribometers, its measurement has been proven to be in agreement with other portable tribometers from comparative tests done [26, 36, 37]. (See Figure 2.19)	It is a portable device, relatively easy to operate and is readily available. it doubles as an ontrack and in-lab measuring method. For a range of contaminants, it provides a notable resolution between the values for skid resistance.	It is not suitable for use in the field, requiring modification for such applications. It is not as easy to use compared to other portable tribometers due to its complex setup. The skid resistance is measured by the pendulum instead of the rolling/sliding peak of adhesion levels. Although a correlation has been confirmed from the comparison.	Calibration of skid resistance against wheel / rail adhesion levels *** *******************************
	Braked Wheel Tribometer	The friction level on the rail is determined using a small, braked wheel. It works on the same principles of most tribometers where a given vertical force (F) is applied on the rail from the wheel and the applied and resulting/reactive force (R) are measured. The coefficient of friction is then given as the ratio of the vertical force and the reaction force i.e., F/R. With the Braked wheel tribometer, an increasing brake torque is applied on the rail surface to produce the required slip [38, 39]. (see Figure 2.20)		S	Compensation for changing conditions 0.25 10.25
	Static Breakout Friction Tribometer	This technique applies a handheld tribometer which provides a coefficient of friction measurement at any angle. The RSSB advises that this method be used only for very coarse assessment of friction conditions. (see Figure 2.21)	It has a short measuring time of 5 seconds. It can be applied on very short rail segments. It is easy to use and accessible.	The results and scaling effects are affected by the lubrication and surface roughness of the slider. It gives a very coarse evaluation of the sliding friction alone. The type of slider used plays an important role in the resolution of results on different types of contaminants. A rubber slider may provide an improved resolution compared to a chromium slider. It is difficult to maintain a steady state because the slider will not be in full contact with the rail at a curve.	Comparison of friction measuring devices Kett tribometer with rubber slider 0.70 0.60 0.60 0.70 0.60 0.70 0.60 0.70 0.60 0.70 0.7
	In-Lab Technique	es			
	Pin-On-Disc	This is a method mainly used for research related to friction and wear, since it is designed in a way it outputs the friction between a rotating disc with a loaded pin rotating against it. The material used for the disc is expected to have identical properties with the track which therefore the use of Rail steel. The same principle applies to the pin material (which is Wheel steel) it has to be identical with the properties of the wheel. (see Figure 2.22)	The introduction of contaminants is easy. It is relatively easy to use with an abundance of tribological contacts [40]. Measurements can be repeated quickly. Test conditions such as the load and environment can be controlled.	The sliding speed is low. The equipment has a maximum sliding speed of 4m/s (9 mile/h). Friction can only be recorded under sliding conditions, restricting the scope of measurement. The rig basically represents the high slip phenomenon observed in very tight curves. This is because the rig mimics the slide component of a partial sliding wheel/rail contact which makes it experience full sliding [41] This method is preferable in the testing of fluid type friction modifiers or solutions for weed killer. Scaling effects are present since the contact area is 8 times less than that of the actual wheel/rail contact. The maximum pressure in a wheel/rail is 10 times larger than the maximum contact pressure of the machine.	

	Twin Disc Test Rig	This method uses two discs, where the top disc has a given diameter and the bottom disc is selected based on the creep percentage required to be generated. A load is applied to the discs till the peak contact pressure is identical to the contact pressure for a wheel/rail contact. (see Figure 2.23)	The introduction of contaminants is easy. Test conditions such as the load and environment can be controlled. Statistical variation of the adhesion can be determined by conducting numerous tests. It is a widely used and available machine for research and laboratory consultancies.	The percentage creep levels can easily be affected by the high rate of wear of the disc. With usage of a crowned disc, the contact pressure can be affected as the disc wears down. Scaling effects are present here as the actual wheel/rail contact is larger than the contact present between the discs. The testing of each percentage creep level requires the usage of a new disc or machined (returned) disc.	0.7 0.6 0.6 0.5 0.5 0.0 0.2 0.1 0.2 0.1 0.2 0.1 0.2 0.2 0.3 0.2 0.3 0.4 0.5 0.5 0.5 0.5 0.5 0.5 0.5 0.5
	Linear Full- Scale-Wheel- On-Rail-Rig	This is a real size depiction of the train wheel on a test rig. It is designed in a way that an angle of attack is produced relative to the wheel when the wheel is rotated during traction and braking. (see Figure 2.24)	Introduction of contaminants to the is easy because of the full-scale nature. Test conditions such as the load and environment can be controlled. Measurement can be repeated in a short time period. It is not affected by scaling effects as the wheel/rail contact is full scale.	The measurement process can be slow as they operate at a low speed of less than 5 mph.	
	Full-scale rig with rail loop	The HAROLD rig was designed by researchers from UoS and UoH. It consists of a Y25 freight bogie with front wheelset positioned on a rolling rail of diameter 2m. Tread brakes are used on the bogie. The braking side is jacked up while the other side is used for the application of contaminants. To test for friction, the brake force is increased gradually till a limit is attained or when the WSP activation vents the pneumatic actuators [42]. (see Figure 2.25)	Introduction of contaminants to the is easy because of the full-scale nature. It has a maximum speed of 200km/h. It is not affected by scaling effects as the wheel/rail contact is full scale. There is precise control over the wheel-rail creep. It has good repeatability for measurements. Test conditions such as the load and environment can be controlled.	Not all the data produced using the rig has been validated. It cannot be used for low adhesion investigations on site because of its size.	0.6 HAROLD, DRY 0.5 m/s 10 m/s 15 m/s 20 m/s 20 m/s 10 kN wheel load 5-20 m/s speed 0.2 0.4 0.6 0.8 1 c _x /-
Indirect measures of low adhesion events	On-Train monitoring Recorder (OTMR)	Data from the OTMR is usually used to investigate accidents. Braking rates distances and time can be determined from the analysis of the speed-time output derived from the OTMR data. The brakes rate can also serve as indicator of the adhesion levels over a stopping distance.	There are no scaling effects, since the data is from an actual train. All trains are required to have OTMR on-board, therefore it is readily available.	Manual download of data. Expertise in data analysis is required. It is a time-consuming process. Data can only be obtained for train acceleration and braking process.	OTMI Speed-time data 100
	Train Management System (TMS)	The Bombardier Mitrac™ is an example of a TMS. The system can transmit real time data from a train (such as the speed profile and slip and slide event) to a central location. This tool provides similar data to the OTMR but also functions as a diagnostic tool.	Provides locations/mapping of slide and slip events. Provides real time data. There are no scaling effects, and it is readily available.	Data can only be obtained for train acceleration and braking process. It is a time-consuming process and experience is required in the associated software.	Total Control
Measures of weather and environmental	Wheel Slip Protect (WSP) Internet of Things; Moisture	Used on service vehicles, it reports the occurrence and location of wheel slide/spin events possibly caused by low adhesion to a central database. The map on the left column is an example of the WSP data display in a control room; the colour coded arrows on the map represent the adhesion conditions at that area. Green represents good levels, yellow and orange represent intermediate levels and Red represents low levels of adhesion. These sensors are planted on the railhead to observe the rail state using electrical	This system provides real time data. The system has no scaling effects, since its data is obtained from an actual train. The LAWSTM is readily available Mapping and statistics data can be obtained from the system.	Data can only be obtained for train acceleration and braking process. It is a time-consuming process and experience is required in the associated software. An indirect assessment of the adhesion is obtained from the LAWSTM via the acceleration/deceleration data, which means further analysis of the data will be required.	AND SECOND COMMENTS OF SECOND CO
parameters.	Sensor Internet of Things; Leaf fall	conductivity readings. Static sensors are used to monitor the amount of leaf fall at a specific area	It can be adapted for onboard train monitoring	It is only currently used for research purposes	

Radar	It uses scientific algorithms to calculate high spatial and temporal measure of rainfall		It is not easily accessible unless a licence is issued	
Satellite Observations	Images gotten from satellites viewing tree canopies from space. It can detect the colour changes in the canopies which may signify when leaves have fallen	Observations are automatic over require locations	Continuous cloud cover may obstruct observation especially during autumn. It does not provide a direct measure of leaf fall	
Leaf Observer Network	This system holds a record of leaf fall from different tree species over a period of two decades in Great Britain. It aids the analysis of amount of tree canopy remaining during autumn and tree species identification	- C	Measurement of leaf fall is influenced by observer bias.	
Great Rain gauge network	It is a location specific tool that measures the amount of moisture present. It is capable of measuring 0.2mm of rainfall or more	measurements of location specific	Observation is not necessarily around the rail network. It does not directly measure the amount of rainfall on the railhead	



Figure 2. 15: Vehicle-bourne tribometer [34]



Figure 2. 16: Tribometer train [43]



Figure 2. 17: Loading measuring wheel [34]

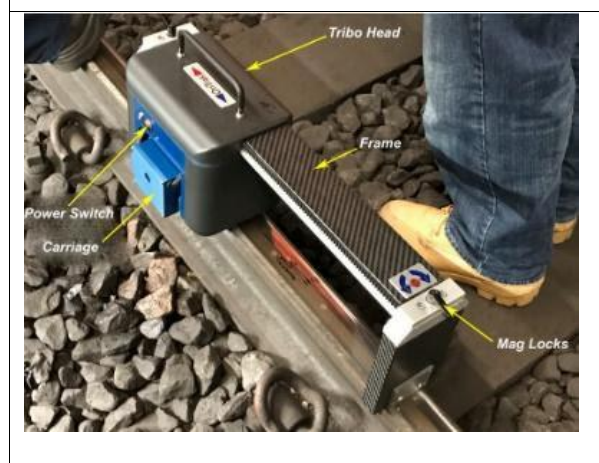


Figure 2. 18: OnTrak hand operated Tribometer [14]



Figure 2. 19: Skid resistance slider tribometer [34]



Figure~2.~20: Braked~wheel~handheld~tribometer~[34]



Figure 2.21: Static Breakout Friction Tribometer [34]

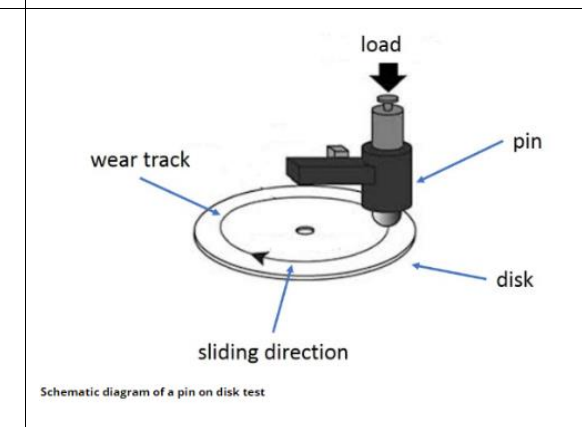


Figure 2. 22: Pin-on-Disc [40]



Figure 2. 23: Twin disc test rig [34]



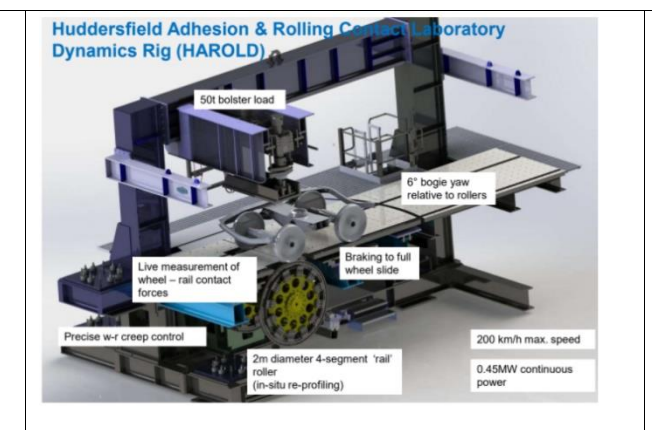


Figure 2. 25: HAROLD Rig [42]

Figure 2. 24: Linear Full-Scale-Wheel-On-Rail-Rig [34]

2.4 METHODS OF LOW ADHESION FORECASTING

2.4.1 MODELLING METHODS FOR LOW ADHESION

Low adhesion modelling creates a link between the wheel/rail contact states and the train operational parameters in a mathematical model form [16]. These models generally look at the creep force relationships under varying conditions, such as wet and dry. A number of these low adhesion modelling methods are discussed below:

2.4.1.1 WATER-INDUCED LOW ADHESION CREEP FORCE (WILAC)

It has been established from various studies that water or moisture contributes to the occurrence of low adhesion between the wheel/rail contact. This prompted the research carried out by [18] which carried out tests using a full-scale tram wheel test rig to develop a model for the creep force which has the capability of predicting the adhesion as a function of the dryness or wetness of the railhead. The full-scale approach was used in the approach because it is easier to introduce contaminants into the system (in this case water).

Adhesion in rolling contact is controlled by two mechanisms in the existence of interfacial fluids which are hydrodynamic lubrication and boundary lubrication. Mixed lubrication is referred to as the area where the adhesion is controlled by the mechanism (transition region). The dominance of the regions is dependent on the fluid viscosity, normal force, contact patch size, the relative velocity between the surfaces and the surface roughness.

Trummer et al. [18] noted that from the maximum adhesion value in dry conditions at low speed was found to be 0.35 and between 0.5 and 0.6 when measured with locomotives with an axle load of 220kN and test rig experiment with axle loads of 44kN and 67kN respectively. When an amount of water was applied to the tests with the other conditions remaining the same the locomotive measured a maximum adhesion of 0.25 and the test rig's result showed a maximum adhesion level in the scale of 0.10 to 0.16 at a speed of 100km/h. The difference noticed in the maximum adhesion value of the dry and wet conditions proves that the presence of low moisture does lower the adhesion level and poses a risk in the safe train operation.

The WILAC model puts more focus on the Wet-rail syndrome which is a mixture of low moisture and iron oxides formed on the railhead, this is done in the absence of oil or grease.

The test carried out by both researchers made use of a test rig as seen in Figure 2.26 which contained a full-scale tram wheel mounted by a swing arm and a roller onto a fixed frame at the University of Pardubice.

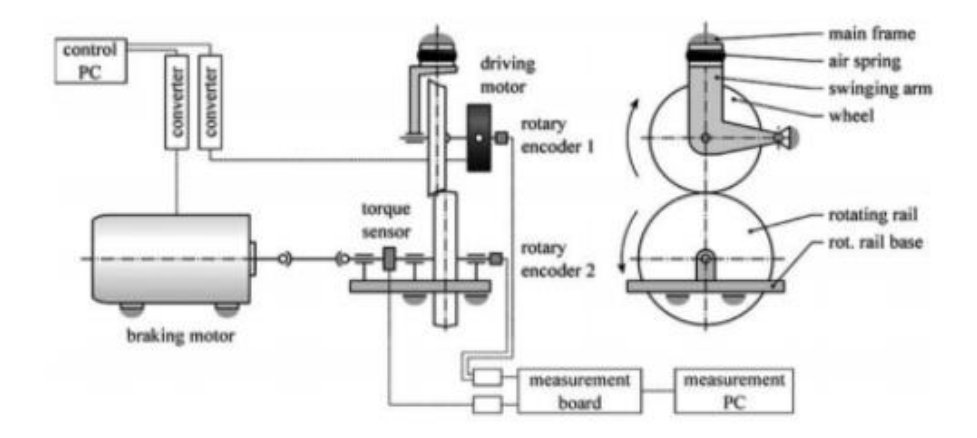


Figure 2. 26: Schematic of the tram wheel test rig [29]

The WILAC model is constructed around the Polach model which was built on theory of boundary lubrication [18].

Trummer et al. [18] approached the test with four conditions in terms of wetness levels of the surface which were:

- Dry with no water added,
- Damp2 at a water flow rate of 25 μl/s,
- Damp1 at a water flow rate of 35 μl/s and,
- Wet at a water flow rate of 350 μl/s.

These conditions simulated were to represent the various levels of moisture caused by rainfall or a light drizzle as well as a typical dry day.

Results showed that under dry conditions the maximum adhesion level was at 0.4 which is as expected for that condition but under wet conditions with a water flow rate of 35 μ l/s the adhesion levels reduced to approximately 0.15 as seen in Figure 2.27 which is categorised as low adhesion.

With a further reduction in the flow rate to 25 μ l/s, as seen in Figure 2.27, the adhesion levels dropped to 0.06 proving that adhesion reduces significantly under the influence of low moisture and wear debris.

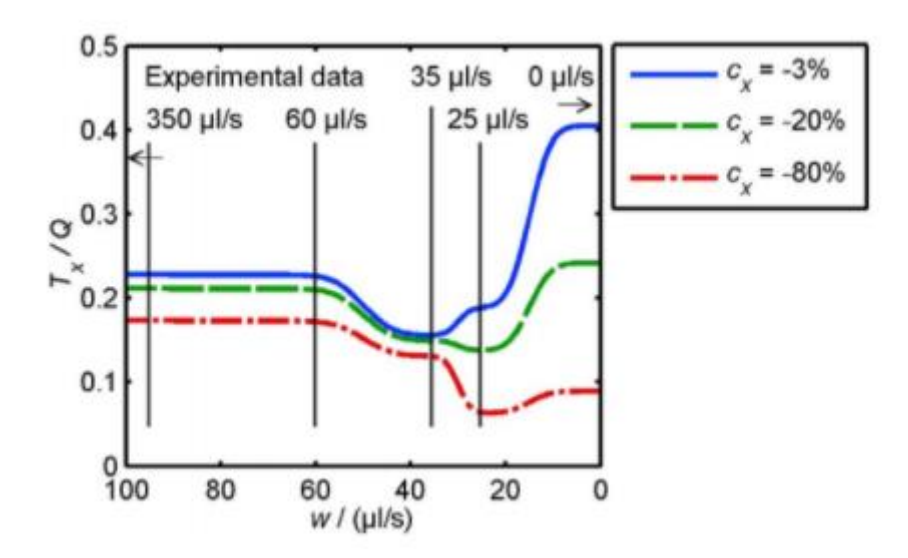


Figure 2. 27: Graphical representation of results from WILAC model[18]

2.4.1.2 LEAF-INDUCED LOW ADHESION MECHANISMS

The Huddersfield Adhesion and Rolling Contact Laboratory Dynamics (HAROLD) rig data was used in this model to simulate the effects of the mixture of leaves and moisture on the railhead. A Polach creep model was used in conjunction with the HAROLD rig to achieve the output. Figure (28) shows the detailed process used to create the LILAC model.

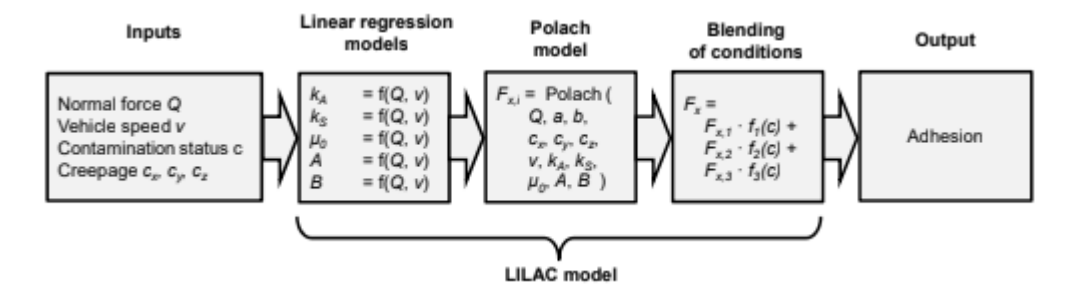


Figure 2. 28: LILAC system process [42]

The creation of the leaf layer is done by firstly wetting the leaf layers followed by slowly rotating the rig as leaves are fed into the designed wheel/rail contact, which is represented by rail loops and a bogie front wheelset. A normal load is applied to press the leaves into the rail surfaces as the roller is rotated. It was noted that the black film layer occurred only after sliding took place.

Results showed that an adhesion level as low as 0.01 was achieved in different braking scenarios for wheel loads reaching 100kN. The results were found to be lower than those obtained from the WILAC model and a control wet one as seen in Figure 2.29. It also showed that the adhesion levels decreased slightly with an increase in the rolling speed, as seen in Figure 2.30.

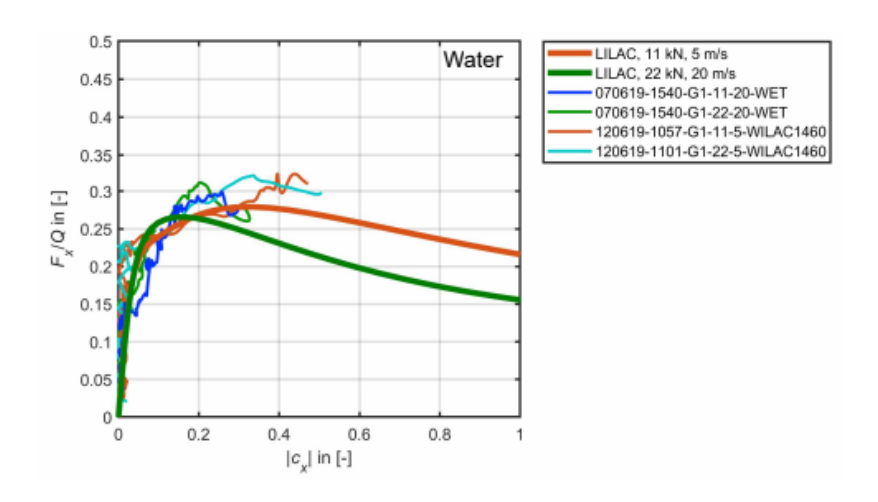


Figure 2. 29: WILAC results compared other railhead conditions.

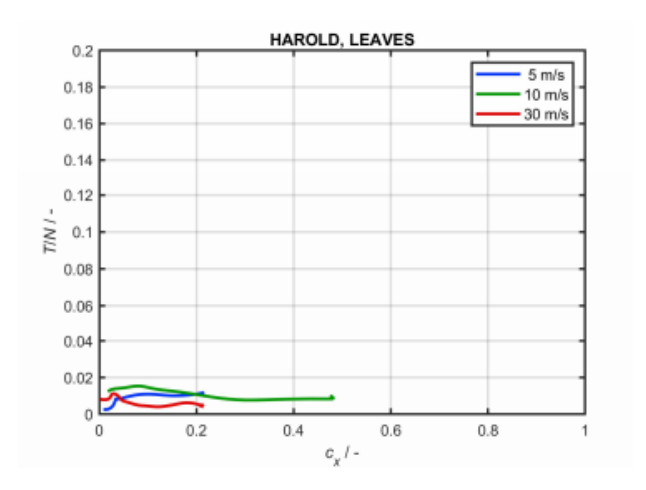


Figure 2. 30: LILAC results under 60kN load with different rolling speed

The LILAC model has the capacity to study the behaviour of trains while in leaf layer related adhesion events if multi-body dynamics models are implemented into it [42].

2.4.1.3 CONTACT MODEL USING MEASURED 3D SURFACES

This model is an improvement on a previous model by Zhu et al. [44] called CONTACT, it involved using measured 3D wheel/rail surfaces to develop a numerical model which could investigate the effect of water or oil contamination on wheel/rail adhesion when in contact with various surface roughness. The CONTACT model only considered the following:

- Normally loaded contact model
- Interfacial fluid model
- Rolling/sliding contact model

Zhu & Olofsson [45] developed the new model which consisted of the above three and additional flash temperature model and local friction coefficient model. The new model

can predict the local contact pressure, global adhesion coefficient, local tangential stress, local flash temperature, local coefficient of friction and plasticity.

It was opined that most contact models done previously had been done based on the assumption that the contact surfaces are perfectly smooth making it easier for the implementation of Hertz theory which is suitable for vehicle dynamic simulation. In order to vary the surface roughness broadly during numerical analysis, a statistical model was employed giving a realistic depiction of the surface topography. The surface topography differs due to wear which is dependent on the wheel/rail contact conditions and the initial surface finishing.

The work done considered the real measured 3D surface samples sectioned out of actual rail and wheel pieces under dry conditions [45]. Their model assumed stationary contact with no spin and a unidirectional creep in the longitudinal direction.

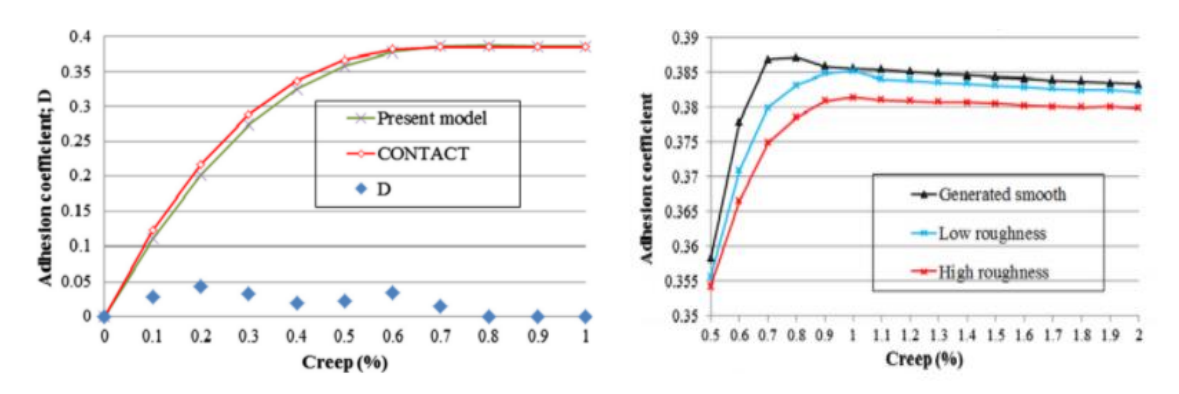


Figure 2. 31: Graphs comparing adhesion coefficient trends for present and previous CONTACT model [45]

The results obtained from the model were firstly compared to that of the previous CONTACT model done by [44] and from the adhesion curves computed seen in Figure 2.31, the previous model had a higher adhesion coefficient than that of the one is discuss, though the difference was little.

The results from the model showed that a surface with high roughness has a lower adhesion coefficient than of low roughness and a smooth surface, although the difference may not be significant as seen in Figure 2.31.

It was noted that an increase in speed reduced the adhesion coefficient as the surface roughness increased.

2.4.1.4 MULTI-LAYER MODEL

This model was proposed by Olofsson [31], it takes into account the effects of crushed leaves on the railhead. It was stated that leaves crushed by passing trains form a slippery (Teflon-like) coating on the railhead which is an "easily sheared" surface layer when it has undergone chemical reaction. This layer is usually visible to the naked human eye as it is black in colour, and they are very difficult to remove.

In the testing used to develop the model carried out by Olofsson, Glow Discharge Optical Emission Spectrometry (GDOES) was used to profile the elemental depth of the surface layers which was employed in analysing the "presumed chemically reacted surface layer" and proving if it does actually exist. A controlled pin-on-disc was used to recreate the wheel/rail contact for the experiment. This experiment was based in Stockholm, Sweden. The test specimens were obtained from rail sections and wheel rolling stock that had been used in local traffic.

The tests were carried out using a maximum contact pressure of 800 MPa and a sliding velocity of 0.1m/s. The tests were run under different conditions for the rail surface, which were:

- clean rail surface tested at 95% relative humidity.
- clean rail surface tested at 40% relative humidity.
- rail surface lubricated with elm leaves.

After the tests were carried out, a pin-on-disc machine was used to measure the frictions on rail surface samples.

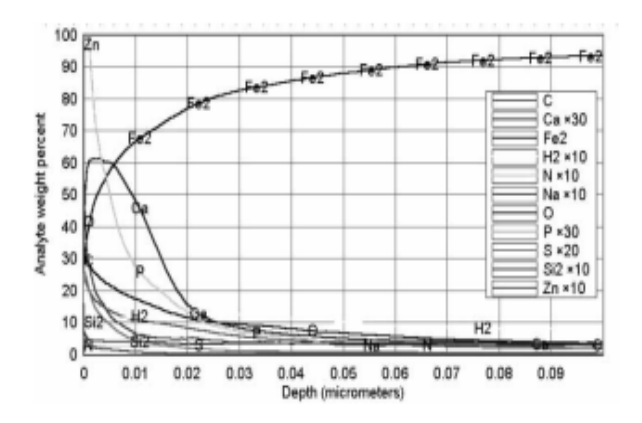


Figure 2. 32: GDOES results for elm leaves under high humidity [31]

The results from this experiment (Figure 2.32) showed that the crushed elm leaves on clean steel and low humidity had formed a chemically reacted layer that contained Phosphorus and Calcium which is in agreement with the initial proposed theory that a chemically reacted layer which acts as an easily sheared surface layer is present. This model was also able to prove that the presence of high humidity on a clean rail surface reduces the adhesion levels, which explains why reports of low adhesion incidences exist without the visible hard black layer on the railhead. This has been explained by Olofsson as the presence of an oxygen layer thick enough to act as an easily sheared surface layer.

2.4.1.5 KERNEL EXTREME LEARNING MACHINE (KELM) & PARTICLE SWARM OPTIMISATION (PSO) - PSO-KELM

This model was developed by [16] proposing a combination of the PSO and KELM used in analysing the traction performance of heavy haul locomotives aiming at analysing adhesion states with real-time operational data. This involves using adjustable creep velocity done by varying output torque of a traction motor, showing the performance of the wheel/rail adhesion force. It was stated that the major challenge of modelling low adhesion is the ability to recreate the actual condition in which the train operates, hence the identification of the model's precision is affected by uncategorised noises, uncertain nonlinear parameters among other factors. The method proposed by Liu et al. [16] is a combination of a network-based method KELM which combines extreme learning machine functions with kernel functions and a swarm intelligence algorithm PSO, this is expected to be adaptable to the changing nature of the environment conditions in terms of the research, improving the identification performance. Although the model parameters need to be adjusted manually for the different operating environments/conditions.

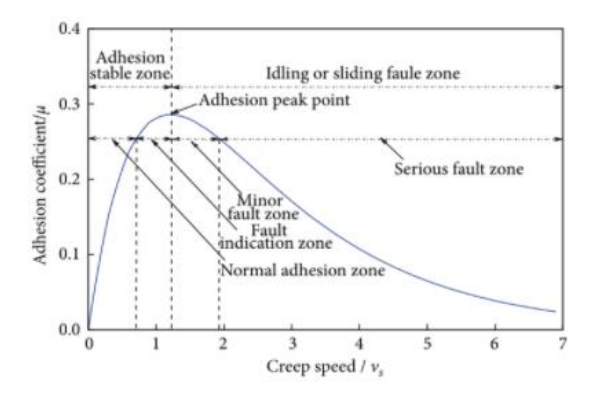


Figure 2. 33: Wheel/rail adhesion coefficient-creepcurve [16]

A new KELM-based wheel /rail adhesion identification model has been designed using PSO to optimise the model parameters [16]. The creep velocity and wheel/rail adhesion coefficients were designated as the inputs for the identification model. The model processes an output of the following wheel/rail adhesion states (as seen in Figure 2.33):

- minor fault
- serious fault
- fault indication
- normal adhesion

The data used for the model was extracted from a RT-LAB Test stand which comprises of a heavy-haul locomotive traction transmission sub-model designed using MATLAB-Simulink and Mechanical sub-model designed using ADAMS-Rail. 3000 data types for

different wheel/rail adhesion states were obtained from the wheelset of a single motor drive by adjusting the torque output of the motor. It was concluded that the proposed KELM-PSO model was able to attain an identification accuracy of 92.60% which is significantly higher than existing methods of using only KELM (87%) or PSO-SVM (85.11%). Therefore, the model was able to effectively identify the wheel/rail adhesion states using optimised real-time data whilst improving the environmental flexibility.

2.4.2 EXISTING METHODS OF FORECASTING LOW ADHESION

Existing Adhesion forecast tools are founded on the principles of scientifically confirmed causes of low adhesion such as moisture on the rail head and leaf contamination on the railhead. These forecasts are usually communicated through a colour coded risk index, alerting operators of the chances of low adhesion events. There are several potential methods of forecasting low adhesion which will also be discussed in this section.

2.4.2.1 LOW ADHESION RISK FORECAST/ ADHESION INDEX (MET OFFICE TOOL)

This is a forecasting technique delivered by the Met Office [46] and is widely used across the rail industry. Extensive weather and climate data are used to "accurately predict low adhesion, leaf-fall and wind throw at high spatial and temporal resolutions for a certain band of lead times. The predictions from the tool are used to prepare mitigation strategies, reducing SPADS, station overrun among others.

The adhesion index approach takes into account the amount of leaf fall, tree density, topography in conjunction with the weather elements such as; temperature, type of rain and humidity levels of a specific area. The leaf fall is processed to a higher resolution to give the different species of trees at the given area or station. It has been shown from the work carried out by several researchers and then compiled by [4] that different species of leaves have different effects on the adhesion level. The knowledge of the precise tree species and the expected time of the leaves shedding around the specific station contributes to the reliability of the adhesion index [47].

The result of data input in the adhesion index system is a colour coded prediction output which is rated from good adhesion levels (that is low risk) to bad adhesion levels (extremely high risk). The colour code assignment is as follows:

- Green (0-2) Low risk, that is good adhesion level.
- Yellow (3-5) Medium risk, that is moderate adhesion level.
- Red (6-8) High risk, that is poor adhesion level.
- Black (9-10) Very high risk, that is extremely poor adhesion level.



Figure 2. 34: Sample of adhesion risk index [47]

Figure 2.34 shows an example of the Met office's adhesion index prediction using just the colour codes.

Generally, the model can predict low moisture levels and leaf-fall on the railway network. These predictions can be done 10 days in advance. It is capable of giving an hourly report of the following parameter:

- Low adhesion risk
- Leaf fall risk
- Traffic volume
- Wind-throw risk [48]

Advantages

- The tool combines both spatial and temporal resolution in its prediction.
- The tool is customised for specific routes; therefore, it will have good precision.
- It implements data on location and time of leaf fall, moisture levels with the weather forecast to give a good quality forecast.

Limitations

- It is not a real time tool but a prediction of events that may take place which will be subject to change.
- Weather forecasts are not 100% accurate meaning the predictions may vary to actual events.

2.4.2.2 OPERATIONAL DATA BASED FORECAST

This method is based on work done by researchers [49] from the University of Huddersfield and the Met Office. The case study of this research was the Birmingham Cross City Line (BCCL). The project was aimed at using operational data to improve the current adhesion forecast method.

The method developed is a combination of weather forecast data and On-Train Data Recorder (OTDR). A motivation for this project is the plan for Automatic Train Operation in the future, which will require ability to plan for and mitigate against low adhesion. The OTDR data was employed to provide better understanding of the where and when the wheel slip protection was activated during traction and various brake steps. The severity of the recorded slip was also recorded. Line side moisture sensors were used to give a high resolution of the observation network showing when the railhead was most likely going to have some moisture at a site situated in close vicinity to a live operational railway.

Weather observation data from the UK Met office was used to compensate for the data (such as frost, dew, rainfall as soon on) that the isolated sensors did not provide.

The dates which had previously recorded the highest WSP activity were selected as the case study days, since it had given a range of when to expect slip to occur. This led to selection of the 13th, 15th, 29th of November and 8th December.

The team used weather data, leaf fall rate and WSP activity in comparison to the predicted adhesion risk forecast. The work done here (see summary in Figure 2.35) validated that the WSP activity is captured well by the adhesion forecasts, but some discrepancies occurred in the timing of occurrence predicted. Meaning there was a mismatch in the forecast and actual occurrence of wheel slip. It was also stated that the train drivers are aware of the forecast and would have been driving carefully, therefore reducing the likelihood of wheel slip occurring.

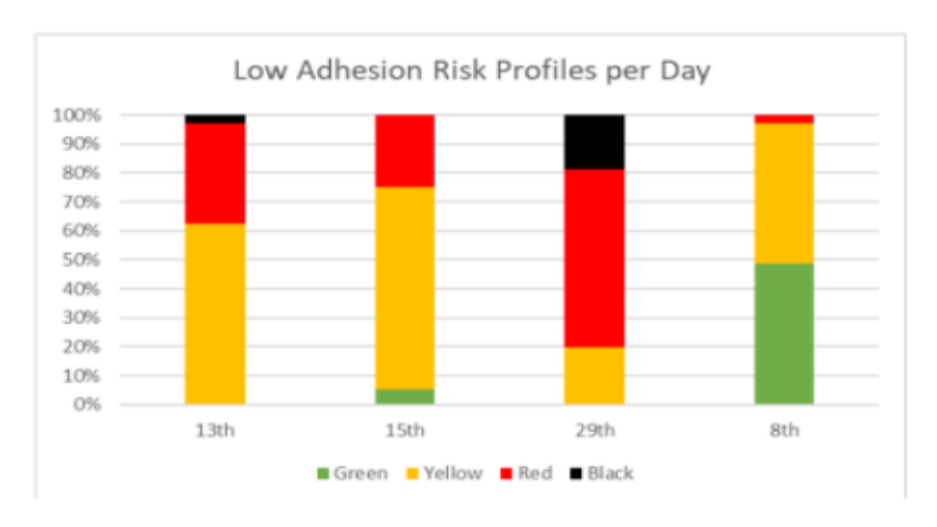


Figure 2. 35: Example of adhesion index data from the Met Office:

Green indicates a region of low adhesion index (High adhesion level).

Yellow indicates a region of moderate adhesion index (Medium adhesion level).

Red indicates a region of high adhesion index (Low adhesion level).

Black indicates a region of very high adhesion index (Exceptionally Low) [50] [49].

Advantages

- The use of line side moisture sensors overcomes some of the limitations related to capturing the spatial variation in the application of standard weather observation sites.
- It included the use of vegetation data along the train route, although it was outdated.
- The research confirms the influence of moisture and leaf containment on the adhesion of the rail and wheel, contributing to WSP activities.

Limitations

- Unavailability of geolocation, although Train Describer and Train Running Under System TOPS (TRUST) data were used to determine the location of each train and the service it operated under.
- Limitation of OTDR data as it was only extracted from a limited number of trains and a short span of days. This means that some wheel slip protection activity may be missed during the study.
- Quality issues with OTDR data such as: a) varying speed calibrations between the train cabs b) unrealistic records c) varying clock times between train cabs.
- The use of OTDR in live operational system is challenging due to the analysis being very resource intensive.
- Outdated vegetation data, this was the network rail vegetation data survey from 2009 to 2011.
- Low adhesion events recorded were reduced because of prior mitigation implemented to the rail head.

2.4.2.3 ADHESION CONTROLLERS CONDITION ASSESSMENT TOOL (ACCAT)

This is a tool utilised by London Underground for the prediction of low adhesion on the railhead for the central and metropolitan lines. The ACCAT tool implements the function of Internet of Things (IOT).

This tool uses railhead moisture sensors which detect electrical resistance as a result of water droplets that get on conductors planted on an insulating circuit board. This device

is incorporated into the ACCAT, essentially the sensors report data on the level of humidity on the railhead to the ACCAT. The tool also has the ability to consider the source of fallen leaves and amount of rainfall as it is implemented into a weather station [51-53].

This tool was specifically designed for use on Automated Train Operation (ATO) and provides a prediction of 3 to 6 hours prior to the incident occurrence.

Advantages

- IOT components for moisture measurements are cheap.
- If properly implemented, it will deliver precise information.

Limitations

- Although individual components are cheap, it is expensive to implement due to the cost data logging equipment, number of sensors needed to achieve desired result and GSM communication.
- It is not widely used despite its availability.
- It is not a real-time source of information; hence it is difficult to implement into decision making.
- Requires internet connection, therefore may not be applicable in remote areas.

2.4.2.4 RAIL SMART ADHESION DIGITAL SOLUTION (ADS)

This tool was developed in collaboration with the Met Office and the RSSB [54]. The digital tool functions by collecting route and railhead conditions information from the train drivers using the ADS app. This information input on the app is made visible for other train drivers following the selected route as an initial input and will give "near-live time" information of the adhesion conditions on the track. The data viewed on the app also aids the train drivers in regulating the trains to best suit the conditions reported. The information is also shared with the rail industry and may be used to plan mitigation against delays and wheel flat causing events (low adhesion).

Advantages

- It is easy to use for both drivers and industry stakeholders.
- It provides a near-real time report.
- It gives access to time series information on adhesion for research and analysis.

Limitations

- It relies on driver information which may be inaccurate.
- The information is not real time, therefore there may be discrepancies.

2.4.2.5 SWEDISH TOOL

Within this tool designed by the weather trends in relation to the adhesion levels history on the Stockholm underground rail system were used to predict adhesion [55]. It was noted that the portion of the underground rail that was exposed to the effect of the environmental condition (that is the portion of the track that is run in open air) experienced more wheel flats, which could be said was caused by low adhesion in the wheel/rail contact [30].

The method used here involved regular friction measurement taken from the "open-air" site and measurements from cut out rail pieces to check the influence of leaves on the track.

These measurements were focused on the months of June, September, October, November (2008) and March (2009).

In the month of October, the leaf layers and black layer were clearly visible as seen in Figure 2.36:

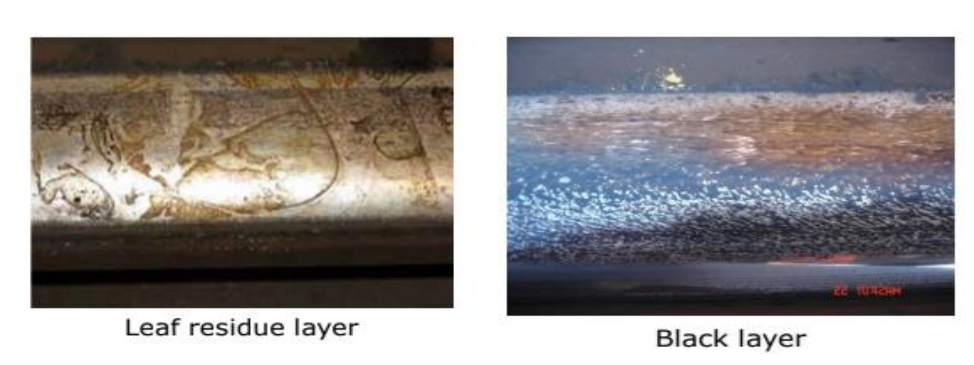


Figure 2. 36: Figure showing October layers on Stockholm rail [55]

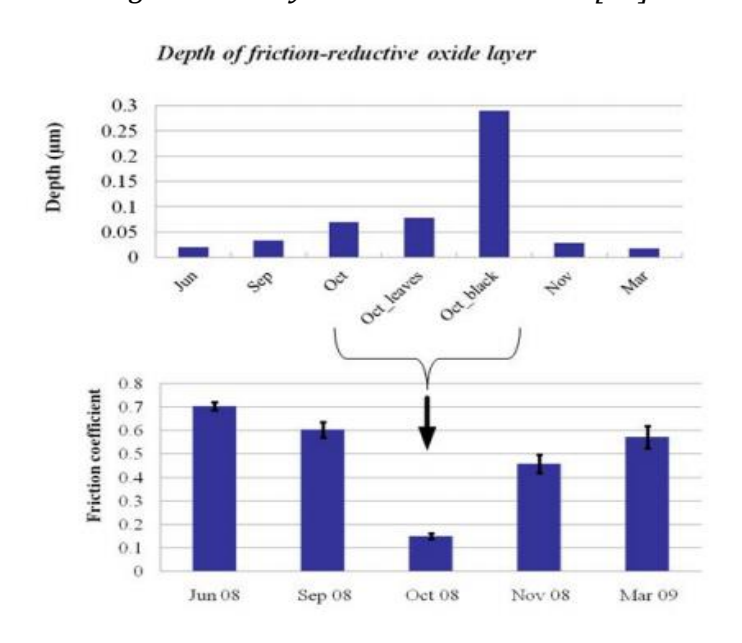


Figure 2. 37: Plot showing the relationship between oxide layer thickness and friction levels per month [55]

An analysis on the thickness of the oxide layer also showed that a thicker layer of oxides brings about a reduced level of friction as this was also found to be more prominent in October as seen in Figure 2.37. This implied that an accurate prediction of the oxide layer thickness can also mean predicting the friction level.

The plot in Figure 2.37 also showed that weather with above average rain and mist, strong winds, frost/ice and decreasing temperatures influence the friction levels.

Advantages

- Provides a good history bank for previous low adhesion events.
- Thickness of oxide layers' prediction can potentially be used to predict adhesion.

Limitations

- There is low accuracy due to persistent climate changes.
- It is not real time.
- It can only be used in region with similar weather conditions/patterns.

2.4.2.6 RAIL EYE SENSOR (OPTICAL SENSOR)

The tool design was based on the need to detect the contaminants such as leaves, moisture and oil on the railhead. This design is intended to be a low friction prediction tool for track sections, it considers factors such as weather, wheel/rail contact conditions and biological pollution which are of benefit to railway operators [55].

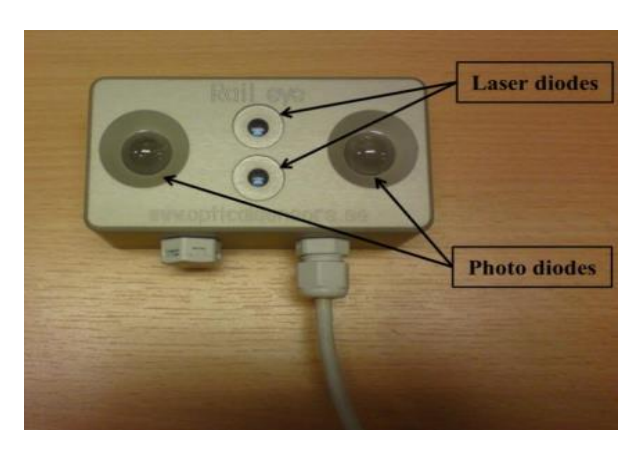


Figure 2. 38: Rail eye sensor [56]

The optical sensor uses infrared spectroscopy to identify low friction conditions on a track. The optical sensor used in Olofsson et al. [56] is called a "Rail eye" sensor and was constructed by Sten Löfving optical sensors in Sweden.

Figure 2.38 shows the sensor design, it has two laser diodes of wavelength 1450nm and 1566nm. The laser diodes provide illumination on surfaces at their stated wavelength, the light reflected off the surfaces is measured by the photodiodes at a sample rate of

15Hz for a vehicle running at 15 ms⁻¹ (the frequency can be adjusted to suit the running speed of the train). The specific type of contamination on the railhead can be classified from the illumination of the rail surface with different wavelengths of light and the recording of the amount of light reflected.

A pendulum test rig was used alongside the rail eye sensor to link the contamination classification derived from the sensors to the friction value. The conclusion of the tests carried by Olofsson et al. [56] was that the rail eye sensor successfully identified different rail surface conditions including a blackish layer, wet rail, blackish + ice layer and dry rail among others tested. The tests were performed whilst manually moving the sensor over the railhead to capture data.

Advantages

- It is capable of providing real-time estimation of adhesion level if successfully implemented, that is when used in conjunction with the friction measurements database, temperature and relative humidity information.
- It can give precise information on the type of contamination present on the railhead, hence making mitigation easier and possibly cost effective.

Limitations

- Certain logistics such as the measuring frequency for a non-uniformly spread layer of leaf contamination are unknown.
- The prototype has not been tested on an actual train; therefore, the viability of the tool has not been confirmed.
- Detection points of the railhead surface can be lost due to the lateral dynamic force which cause the wheel to move laterally on the rail.
- Numerous sensors may be required on the train which increases the amount of data to be processed and consequently making it a lengthy process. The development of a robust processor was suggested by Olofsson et al. [56] for quick processing of signals received from the diodes.

2.4.2.7 PORTERBROOK TARGETED ADHESION MANAGEMENT USING ON-TRAIN DATA

The tool developed here by Porterbrook uses OTDR data and GPS from their train fleets to determine location + causes of lost time and aid adhesion management. The adhesion forecasting tool is still in the rollout stage with no current update. The Porterbrook system can track the position and speed of the trains on their fleet via the use of passenger Wi-Fi available on the trains. This system assists in pin-pointing Lost Time hotspots which can be as a result of low adhesion on the tracks. The Lost Time hotspots data also has the potential for analysing the sub-threshold delay and correlating track works data, adhesion data, earthworks data among other forms of data to narrow down the exact cause of the Lost Time [57].

Advantages

- It has the potential to output real-time data.
- Provides other types of information that maybe useful for rail track management.

Limitations

- It currently can only be used to track data from Porterbrook train on the Sussex route specifically.
- The viability of the system has not been established.
- WSP data is restricted to trains with remote OTDR, and it does not have information related to traction loss events.

2.4.2.8 INTRODUCTION TO THE PREDICTION MODEL.

A friction estimation/prediction tool has been designed in this work based on a regression model, a neural network based and traditional image processing programme, with the aim of estimating the value of friction on the rail tracks in real-time on board a train. This tool will provide better accuracy than existing forecast tools, as it is a real-time data which will be beneficial for the driver (with the tool on board) and successive drivers.

Research reviewed in this literature review revealed that environmental factors such as temperature and relative humidity are important elements in understanding low adhesion mechanisms. Hence, these environmental characteristics need to be included in the prediction model to fully capture their effects on adhesion. It is also important to capture and analyse the railhead state as noted in the Rail Eye Sensor discussed in section 2.4.2.6.

A neural network-based regression model was previously created by a colleague at the University of Sheffield for RSSB funded project CF-UOS-02. The model uses machine learning (a regression model) to determine the relationship between the track surrounding characteristics and the railhead data. Machine learning was chosen as it can recognise patterns which would normally be difficult to recognise by conventional means such as simple statistical models. These patterns can be seen in the relationship between the mathematical data of temperature to non-mathematical data of the railhead images.

This work will look at training and optimising the prediction model and implementing the model into an on-train data capture system..

The prediction model will require an input of the railhead images and/or forwardt facing images and sensor data which include relative humidity, rail temperature, air temperature, layer thickness, dew point and surroundings data. The railhead images will be processed using traditional image processing techniques, infrared spectroscopy (optical sensor) will not be utilised in this work but rather regular coloured images to

make it easier for the prediction model classify and identify railhead states using the colours seen on the railhead images. The forward facing images will be processed using a pretrained convolutional neural network (CNN), which can then identify and classify the amount of tree cover, type of terrain and colour of railhead layer. A regression model (Gaussian) is used to analyse the collated sensor data and the processed images to predict the probable level of adhesion on the rail track.

An input of numerous data collected over a specified period of time during autumn will be used to develop the tool.

2.4.3 ADHESION FORECASTING COMPARISON MATRIX

Table 4 shows a matrix drawn to provide a visual representation of the key characteristics of the existing methods of adhesion forecasting. It aids in understanding the features lacking and features that work well in existing tools.

Table 2. 4: Adhesion "forecasting" matrix

Туре	Tool	Spatial Resolution			Temporal Resolution			Confidence	Use
		Metres	Stations	Routes	Real time	Hours	Days		
Rail/lineside information based	UoS m/c learning tool (NN tool)	Х			X			ТВС	Validation in process
	Rail eye Sensor	Х			х			Low-Medium	Only used at test phase (not on a real train)
Weather forecast + train performance based	MetOffice Adhesion Index	X	Х	х		х	X	High – used over many years, verification process in place	Widespread use in UK
	Swedish Tool		X				х		Still in design phase
	Operational data based forecast tool			Х			X	In process	for validation and improvement of met tool
Train performance based	ADS App by (3Squared)			x		х		Information unavailable	Information unavailable
	Porterbrook			X			X	TBC	Validation in process
Rail/lineside information based + weather based	ACCAT	х		X		X		Medium-High	Used by London Underground on the central line and metropolitan line

2.5 PAPER GRADING TECHNIQUE

The paper grading method adapted from Ishizaka et al. [4] was used in this work. This literature review has been written using information from several sources which include and not limited to published journals, papers, technical reports, chapters in textbook and conference proceedings. These materials/references were graded in order to show their relevance to this research and also show possible knowledge gaps and areas for improvement in this research. They were graded using Boolean values of Yes/No, where yes is 1 point and No is 0 Point. The scoring system is not a grade of the quality of the materials/references.

A paper grading map (see Figure 2.39) was created to give/aid the visual understanding of the relevance of these materials to sections in this review. The review was split into four primary sections for the purpose of the grading; these sections are:

- Wheel/rail low adhesion
- Railhead measurement
- Low Adhesion forecasting techniques
- Wheel/Rail Interface friction modelling.

These primary sections have been split further into secondary sections as seen on the map to give a more precise look at the relevancy.

The following criteria below were used to evaluate the materials:

- Is it a peer reviewed publication?
- Actualisation of theory (full/scale testing)
- Weight of conclusions (are the conclusions sound?)
- Data backed theory (are the theories supported by data?)
- Full scale test backed theory.
- Small scale test backed theory.
- Field validation (has the method or data been validated in the field?)

Each source assessed is represented by their numbers in the list of references. The highest possible scores for a material using the above criteria and the Boolean points are 7. The scores have been grouped into a category of three; 0-2 (C), 3-4 (B), 5-7 (A).

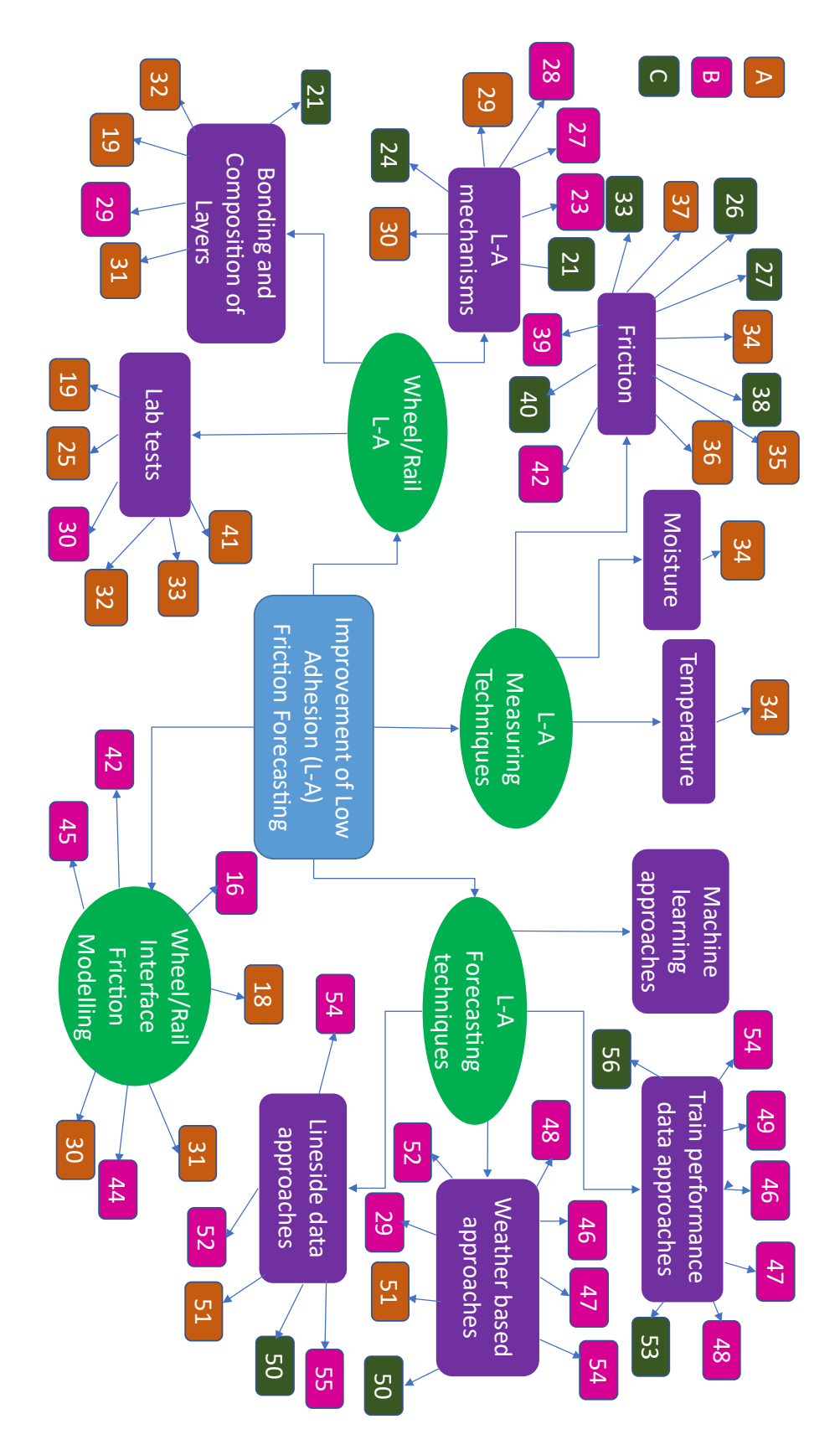


Figure 2. 39: Paper grading map

2.6 SUMMARY

Several causes of low adhesion in the railway industry have been recognised such as the wet-rail phenomenon and leaves on the rail. Although this has been recognised as part of the culprit of low adhesion events, the exact details of how it occurs is still very much under study. There are not many literatures available for adhesion mechanisms as it is a topic that is still under study. It is expected that the measurements taken during the rail track site visit will give an additional perspective into what conditions are needed for low adhesion to occur.

Work has shown that different types of contaminants have varying effects on the adhesion level [19]. This is really important in understanding low adhesion mechanism and will play a role in identifying railhead states for friction prediction.

In this study, numerous friction measure methods were assessed and discussed. A common issue that was identified was the size and/or precision of the equipment, it was found that most of them with good precision (that is near real-life conditions) were big in size. Hence, such methods are not easily mobile and would be difficult to transport them to an active site for investigation. While the smaller (portable) tools commonly had scaling problems which negatively affected the precision and accuracy of the readings. Some other methods involved indirect measurement but involved extra skills to read the data such as analytical skills and time consuming. A new tool called the On-trak Hand Operated (HO) Tribometer, which was recently acquired by the university which has the potential to combine the precision and accuracy of full-scale measurements rig, the portability of the smaller tool and the robustness of some of the indirect methods. The precision and accuracy of this tool has not been validated yet as it is a very new tool, and it is intended to validate it through the course of this research. This is also an aspect of work lacking records shown in the paper grading in Figure 2.39.

A considerable amount of work has been done by other researchers to create mathematical models for different possible scenarios of low adhesion events to help understand the conditions in which low adhesion occurs. Some of these models such as the WILAC showed that there is a relationship between the presence of high humidity on the railhead and low temperature in creating a suitable condition for the occurrence of low adhesion. These models have given an understanding from field and laboratory tests as to how low adhesion takes place and it will aid in the forecasting of low adhesion.

The forecasting tools identified in this review either do not have the ability to do real-time or do not provide accurate information or do not take into consideration the performance of the train or use streamlined information, as it is also seen to be lacking on the paper grading analysis. None of them employ the use of machine learning process which have the capability to revolutionise the process of predicting friction on the wheel/rail interface. These factors affect the reliability of the tools and means there is a gap that needs to be filled as all the tools discussed do not derive their information from on-board a train with weather information. The Neural network tool which uses machine

learning can potentially do both meaning it can bridge the gap between accuracy of forecast and availability of on-board real time data with an inclusion of analysing the trackside vegetation to possibly forecast leaves fall just like the Met Office tool does.

CHAPTER THREE

3. RESEARCH APPROACH

From the literature review carried out, it was established that there is a major gap that needs to be researched further in the railhead friction prediction aspect of the rail industry. In this work, different properties of the railhead will be considered to aid the understanding of low adhesion occurrence and how it can best be predicted.

Previous work done by researchers in this field have shown that ultra-low friction is mainly brought about by leaf layers which present a reduced shear strength layer and the "wet-rail" phenomenon, which occurs when small amounts of moisture and oxides mix to form a solid lubricant/low adhesion paste on the railhead. Although these have been established as causes of low adhesion, the conditions in which they occur has not been fully understood yet. Therefore, further work needs to be carried out to understand the mechanism of low adhesion.

The approaches used in this work were:

1. Friction and Environmental data collection:

The work described here was done to further understand railhead adhesion (friction) mechanism and ultimately use the information to predict railhead friction. In order to get an understanding of actual in-service railhead friction variation, fiction values had to be collected from the field.

Based on the literature reviewed on railhead friction measurement methods, the pendulum tribometer was selected for use in this work because of its portability and ease of transportation. Its measurements have been calibrated against the BR research trib. train, hence giving a conversion factor with some confidence. Environmental data that have been established in the literature review to be linked to the occurrence of low adhesion was collected alongside the friction measurements.

Environmental data collected included:

- Air and railhead temperature,
- Relative humidity,
- Dew point and
- Contaminant layer thickness.

Relationships between the friction and environmental data (temperatures and relative humidity) were analysed on graphical plot to show and aid the understanding of the effects they have on the railhead friction. It also showed if they were significant variables in the prediction of railhead friction.

Railhead and forward-facing images were captured from a handheld camera to record the railhead state (such as leaf layer presence or moisture presence among other possibilities), at the time of measurements. The friction, images and environmental data were used collectively in understanding low adhesion mechanisms and looking at the viability of such data for friction prediction.

2. Prediction tool model:

After establishing the dependence of railhead friction on the railhead temperature, air temperature and relative humidity, it was important to link the images showing the railhead state to the other variables. The leading causes of low adhesion on the railhead which were identified in section 2.2.1 as the presence leaf layers and wet-rail phenomenon can be recognised from the railhead images, hence the importance.

The relationships shown between the railhead friction and environmental data were expected to be non-linear due to nature of variations/unpredictability faced in a non-control environment in field. Also, the images are a non-mathematical variable that cannot be integrated into a simple statistical model.

Given the complexity of the types of variables being worked with, a Gaussian Regression Model (GP Model) was deemed to be best suited in modelling the railhead friction prediction tool. The other models considered were linear models and a supervised neural network (SNN) model. The linear models were not considered, as the relationship between the data being analysed in this work is not linear. A GP model was selected over the SNN model because these are more established in processing smaller data sets, as were available for this work, whereas the SNNs are known to encounter problems while processing small data but does well with large datasets [58].

The GP model was the best fit for creating the prediction tool, as it can flexibly accommodate large variables having non-mathematical functions, large amount of data and random variables. Figure 3.1 shows the summary of the variable inputs for the model, the data processes and the expected output from the model, basically how the proposed railhead prediction tool will work.

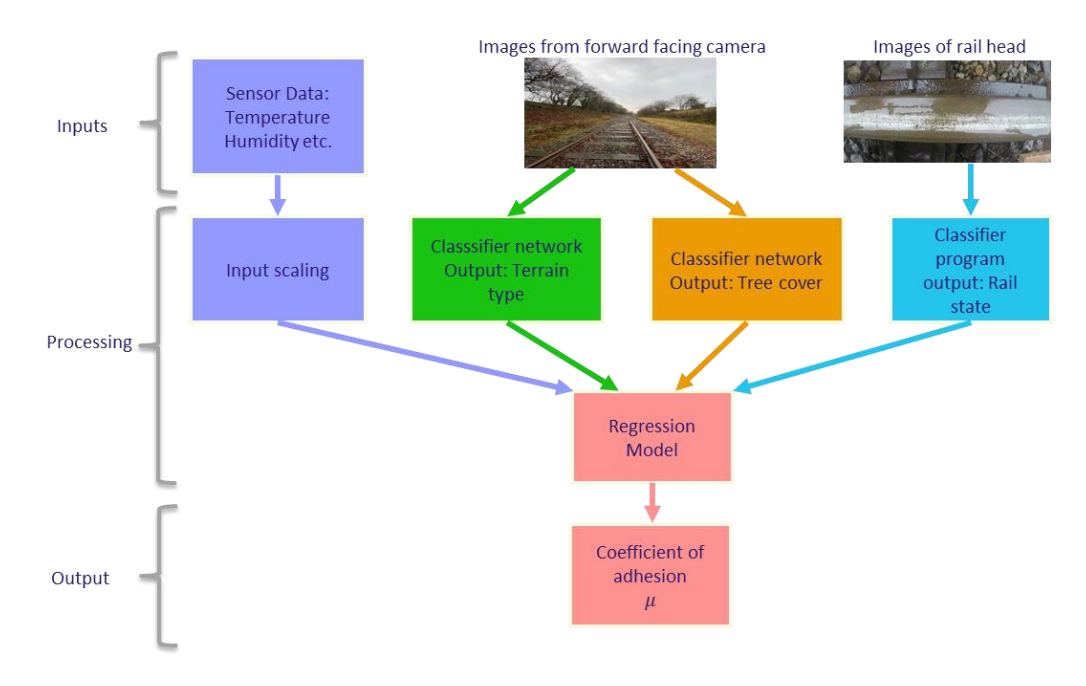


Figure 3. 1: Schematics for methodology

3. Model Sensitivity Analysis:

Sensitivity tests were carried in a laboratory for the prediction tool to show its limitations and capacity. Here orientation and distances of camera to railhead were varied to show how predictions reacts to changes in the image characteristics. It also informed the most suitable way to capture the railhead images for the on-train design.

4. On-Train Data Capture:

The final step was to tie all the information garnered from the previous approaches and create an innovative system capable of capturing the data stated as important in understanding and forecasting railhead friction in approaches 1 and 2. While applying the most appropriate railhead image capture format established from approach 3. These all aided the creation of data capture system used on-board selected rolling stocks, predicting railhead friction from a dynamic open-system.

CHAPTER FOUR

4. RAILHEAD DATA GATHERING AND ANALYSIS

4.1 INTRODUCTION

The aim of this section was to study/analyse the railhead condition in various locations at different given times and days, assessing the levels of friction and contamination on railhead.

This determined the parameters that influences the friction mechanism, therefore providing information on the form of data required to predict friction in the friction prediction model.

The data collected was also to be used to validate the friction prediction model proposed in this work.

The environmental conditions, as suggested by the RSSB GM/GN2642 manual [34], were recorded to analyse their influence on the adhesion levels. The environmental conditions recorded were:

- Weather elements such as relative humidity, air temperature, rainfall level and sunny, dry, mist or fog
- Railhead contamination thickness and
- Contaminant properties (Swabs or LIBS)

Other information that was recorded and/or considered in accordance with the RSSB manual [34] was:

- Track information.
- Moisture level of the track.
- Site features, such as vegetation around track, proximity to factories, local lakes, roads or airport.
- Railhead and forward-facing images.

The locations selected for the first set of track measurement were on the Ecclesbourne Valley Rail (EVR), Midlands Railway and Peak Rail network. The locations used to obtain data are outlined in Section 4.2.

4.2 MEASUREMENT LOCATIONS

The train stations in the UK listed below were the locations of the measurements:

- Butterley, Derbyshire (Midland Railway)
- Wirksworth and Idridgehay, Derbyshire (EVR)
- Darley Dale, Derbyshire (Peak Rail)

They were selected because they were accessible, and they are less busy rail tracks improving the safety factor of working line side and on track.

4.2.1 BUTTERLEY, Derbyshire (Midland Railway), UK:

Data was collected from this site on 4 different dates: 05-09-2019; 01-10-2019; 22-01-2019; 14-11-2019.

The track side and path of measurements depicted by the red line (seen in Figure 4.1a) had a sparse tree coverage at the time of the visits. The trees were at about a 7m distance from both sides of the track and the only effect they had on some of the track sections was shading caused by the overhead angle of the sun.

At the time of the visits there was no visible sign of the leaves near the track. A section of the track is located across a very low traffic road which minimises the effects of contaminants on the railhead.

4.2.2 WIRKSWORTH & IDRIDGEHAY, Derbyshire, (Ecclesbourne Valley Railway EVR), UK:

Data was collected from these sites on the following dates: 14-08-2019; 28-08-2019; 16-10-2019; 13-11-2020; 20-11-2020; 25-11-2020; 01-12-2020; 08-12-2020.

The track side has a dense tree coverage in the summertime and early autumn, the trees lost most of their leaves by the end of November, hence a sparse tree coverage into the winter (as shown in Figures 4.1b and 4.1c). The path of measurements is depicted by the red line.









Figure 4. 1: (a) Aerial view of Track at Butterley, "red line" showing measurement path [59];,(b) Aerial view of track at Wirksworth, "red line" showing measurement path [60]; (c) Aerial view of track at Idridgehay, "red line" showing measurement path and (d) Aerial view of track at Darley Dale, "red line" showing measurement path [61]

The track sections that were measured were not located near the road (seen in Figure 4.1b). The rail tracks were still in use in 2019 (date of track visit), which meant the railhead was relatively clean with little oxidation. However, visits in 2020 (during the COVID-19 pandemic) meant the track was less used than normal and had a visible layer of oxides on the railhead. The EVR lines were not operational during the lockdown, they only had a few operational trains in a 9-month period, used to 'warm up' the trains and for routine maintenance checks.

4.2.3 DARLEY DALE, Derbyshire (Peak Rail), UK:

Data was collected from this site on the following dates: 02-10-2019 and 08-11-2019.

The track side had sparse tree coverage at the time of the visits, the trees hung over very little of the track. There was tree shadow being cast over a section of tracks resulting in protection from the sun, and likely less heat exposure during the day. The path of measurements on the track (depicted by the red line) is located alongside a low traffic road, seen in Figure 4.1d.

4.3 METHODOLOGY

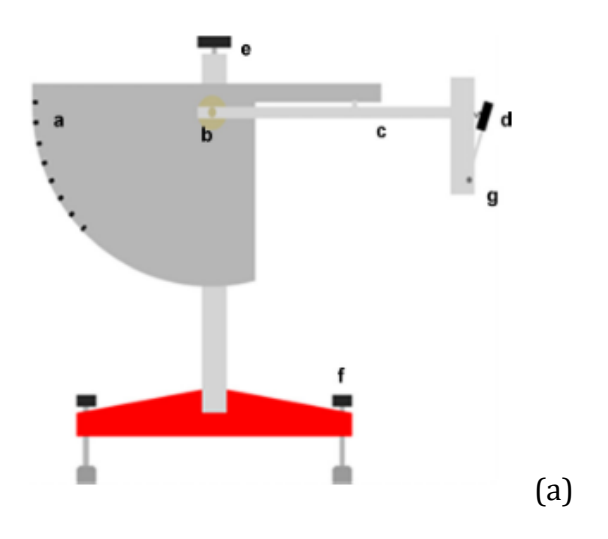
The approach used for the field work has been categorised into:

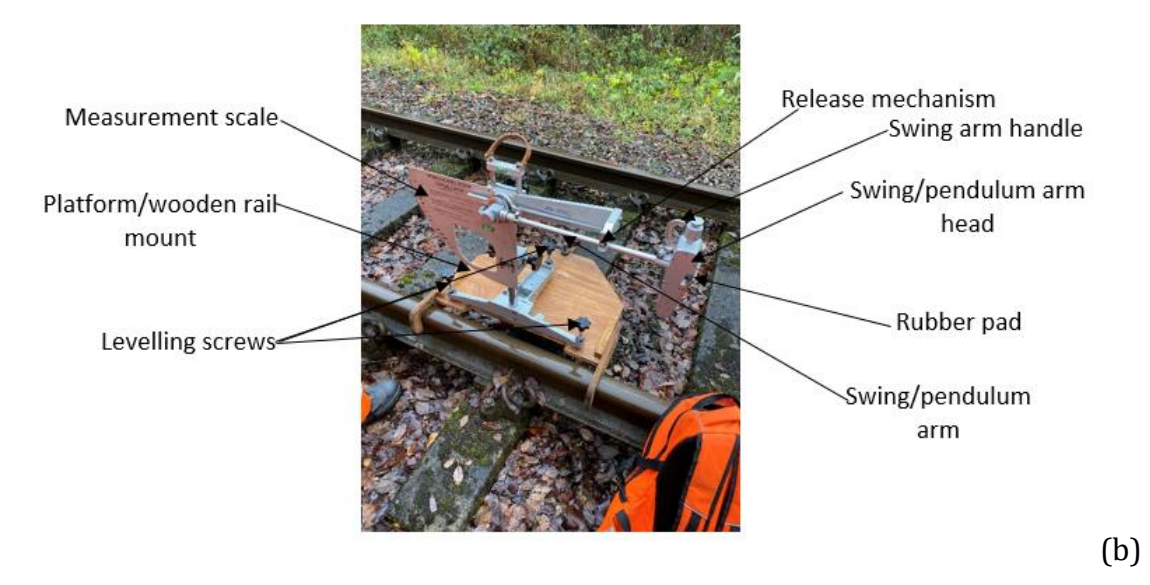
- Equipment used for measurements,
- Measurement plans and
- Measurement procedures.

4.3.1 EQUIPMENT USED FOR MEASUREMENTS

PENDULUM TRIBOMETER

The pendulum tribometer (see Figure 4.2b) is a portable friction measurement tool and is classified as a skid resistance slider tribometer. This pendulum tribometer was originally created as a "Slip resistance meter/Pendulum tribometer" which functioned as a measurement tool for slip resistance levels on different type of floors/pedestrian surfaces and was used in slip incidents report [37, 62]. Lewis et al. successfully modified a pendulum tribometer to a tool for measuring railhead friction as the tool functions on a similar principle on which the Charpy impact test functions, which is an energy loss principle [37]. The friction reading is taken when the rubber pad (d) on the swing/pendulum arm head strikes the test material in the case the railhead, the contact produces friction consequently producing an energy loss (Pendulum test value) which is measured on the scale (a), as seen in Figure 4.2a.





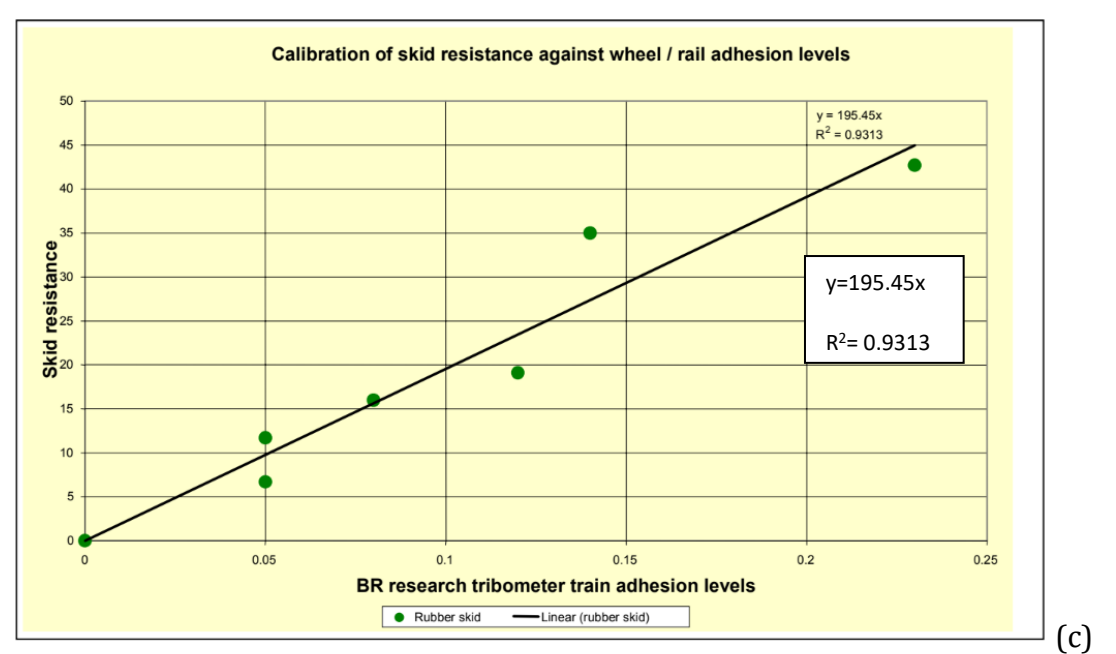


Figure 4. 2: (a) Pendulum tribometer schematics diagram, where a is the measurement scale; b is the pendulum arm pivot (with adjustable height); c is the pendulum arm; d is the rubber pad; e is carriage handle; f is the levelling screw; g is the Pendulum arm head [62]; (b) Fully labelled diagram of the pendulum tribometer and (c) Conversion of Skid resistance to CoF measured by the Tribometer Train [34]

The choice of rubber slider used on the pendulum tribometer was the 96-rubber slider (Four-s rubber). It was selected because of its hardness, which produced friction levels similar to other existing test methods. The length of contact between the rubber pad and the test surface (railhead), which is 127mm, was used to derive a formula used to convert the Pendulum test value (PTV) to the friction coefficient, μ [37]. The equation given as;

$$\left(\frac{110}{PTV} - \frac{1}{3}\right)^{-1}$$
 (4.1)

Equation 4.1 was not used for conversion as the pendulum tribometer does not give an accurate representation of the wheel/rail interface contact pressure as it uses a rubber pad to strike a section of the railhead, as discussed in the literature review. However, RSSB guidance on low adhesion friction measurements [34] reports work comparing the friction values obtained from a pendulum tribometer and the British Railway Research (BRR) Trib. Train at the same point on track at different conditions. The comparison graph shows a linear trend line fit (see Figure 4.2c), and this showed a 93% confidence level from the R^2value. This can be used to convert between pendulum measurements and wheel/rail contact friction.

Hence, $x = \frac{y}{195.45}$ was used for the conversion of PTV to CoF

where: *x* is the CoF, and *y* is the PTV.

Giving the final equation in this form:

$$\mu = \frac{PTV}{195.45} \tag{4.2}$$

The pendulum tribometer is used alongside a platform, that is a wooden rail mount pictured in Figure 4.4, which was designed to attach the pendulum tribometer to the rail and to keep it in a stable position while carrying out the tests. The platform is a three-point structure as seen in Figure 4.4, two of the points or slots in the case are placed on the track while the third point which is at the rear rests on the sleeper or ground. The third point can be adjusted with a screw to match the height of the rail [62].

THICKNESS GAUGE

Eddy current thickness gauge- A FN-Evo Paint gauge (see Figure 4.3a) was used to measure the thickness of contaminant layer on the railhead, as the name implies. The tool uses a ferromagnetic probe to measure contaminants or coatings found at the top of a steel/ferrous base material. The calibration of the tool is done by checking the zero reading on the manufacturer supplied ferromagnetic base plate. According to the RSSB [34] in the presence of a black film (leaf layer) on the measuring surface, an average reading of $42\text{-}44~\mu\text{m}$ is expected. Measurements were taken 5 times on different spots in very close proximity to each other on each measurement points on the track to account for thickness variation and to ensure repeatability of the measurement.







Figure 4. 3: (a) Thickness gauge; (b) Infrared thermometer; (c) Go Pro camera

INFRA-RED THERMOMETER

A RS-8662 dual laser thermometer (see Figure 4.3b) was used to take the railhead temperature, air temperature, dewpoint and relative humidity level.

CAMERA

A Go-Pro Hero4 and Go-Pro Hero8 (see Figure 4.3c) was used to take railhead and forward-facing images.

4.3.2 MEASUREMENT PLANS

The same measurement plans were used at each location because similar sets of data were collected with the same equipment.

At each location a target minimum of 8 data points was set for the visit, in order to give broad picture of the railhead condition along the track.

The following precautionary measures were taken at all locations before and while using the pendulum tribometer [34, 63]

- 1. All necessary Personal Protective Equipment were worn while working with on the rail track.
- 2. Social distancing between colleagues was observed on the track side to prevent spread of COVID-19.
- 3. Commonly touched on the equipment was cleaned regularly to also help prevent the spread of COVID-19
- 4. The manual for the Stanley Morgan Pendulum tribometer was consulted for proper set up and use of the equipment.
- 5. It was ensured the pendulum counter was set to zero before every measurement was taken.
- 6. Whilst using the pendulum tribometer to take friction readings, all forms of interference with the swing/pendulum arm and the balance of the stand was avoided.
- 7. The rubber slider was cleaned before the start of measurement to prevent contamination.
- 8. The peak displacement value was monitored on the return swing to ensure the value was not altered.
- 9. It was ensured that the swing/pendulum arm head mechanism was firmly clamped after lowering or raising it, to keep it in a safe position.

4.3.3 MEASUREMENT PROCEDURES

The following procedures below were followed when using the pendulum tribometer to take friction readings according to the RSSB (2008) [34] and BS 7976-2:2002+A1:2013 [63] guidelines.

PRE-FRICTION MEASUREMENT STEP

- 1. The Pendulum tribometer was visually inspected for damages or abnormalities before assembling it in accordance with the user manual.
- 2. The Infrared thermometer was used to measure and record the relative humidity, railhead and air temperature. This step was done before carrying out any test on the railhead, because the presence of foreign objects (tribometer and mount) on the rail surface would alter the original railhead temperature.
- 3. The thickness gauge was used to measure the thickness of contaminants, if there was any present.
- 4. The track information was recorded and adapted front facing images were taken.
- 5. The wooden mount was placed on the rail, using the three points and it was secured with a rear screw to the sleepers.
- 6. The pendulum tribometer was set on the wooden mount, over the railhead.
- 7. The swing/pendulum arm head was clamped securely in the spring-loaded release mechanism.
- 8. The Go Pro camera was clamped on the pendulum frame to take the railhead image. After the image was taken, the GoPro was detached as it will be an obstruction for the swing/pendulum arm movement.
- 9. With the release mechanism engaged by the swing/pendulum arm, the base of the pendulum tribometer was set to level using the three levelling screws and the spirit level found on the base frame.
- 10. The fittings of each part of the pendulum tribometer were checked by swinging the pendulum arm for any loose fits or potential damages.
- 11. The rubber slider was checked for wear and damages.
- 12. The zero setting was checked and adjusted if needed.
- 13. The contact length between the rubber pad and the railhead was set to approximately 127mm [36, 37]

FRICTION MEASUREMENT STEP

- 1. It is expected that a reference measurement should be made on an emery paper to check the calibration of the tool (the slider rubber pad specifically). This was not implemented in the track testing because the emery paper was unavailable during testing time.
- 2. The swing/pendulum arm was placed in the release mechanism and the pointer was brought to its starting position see Figure 4.4



Figure 4. 4: Pendulum set in the start position for friction measurement

3. The swing/pendulum arm was released striking over the railhead position of interest, and it was caught on return before the slider struck the railhead, see Figure 4.5.



Figure 4. 5: Pendulum arm head striking the railhead (left) and pendulum arm caught before return (right)

- 4. The swing/pendulum arm handle was lifted to ensure the slider pad would not touch the railhead when returning to its release position, hence not altering the reading taken previously.
- 5. The reading was recorded on data sheet designed specifically for these data collection (data sheet shown in appendix A-1).

- 6. Steps 3-5 were repeated 7 more times on the same position on the railhead to ensure repeatability of the readings. (BS 7976-2:2002+A1:2013 recommended recording the friction measurements 8 times per points [63])
- 7. The whole process of the pre-friction measurement and friction measurement steps was repeated for each selected point on the track.

4.4 RESULTS & DISCUSSION

The railhead temperature (°C), Relative Humidity (%), and railhead friction (μ/mu) recorded from each site were collated for each measurement point (per day) to help understand their relationships. The μ data was plotted on the y-axis as the dependent variable while the RH was plotted on the x-axis and railhead temperature was represented on a colour map as independent variables, enabling visualization of effects of RH and railhead temperature on μ .

Not all the data plots from Butterley, Wirksworth and Idridgehay have not been included individually, to avoid repetition. The omitted graphs have been included in Appendix A-2.

4.4.1 WIRKSWORTH AND IDRIDGEHAY

RESULTS

Figures 4.6a through to 4.6j are plots of the resulting measurements and railhead images taken at Wirksworth and Idridgehay. These figures generally show the effects of high relative humidity in conjunction with railhead temperature on the railhead μ . The independent effect the relative humidity can have on the railhead μ can also be seen.

Figure 4.6a shows a temperature range between 15.6°C – 16.9°C and a RH ranging between 88.5% - 97% with μ ranging between 0.09 – 0.16 for Wirksworth. Data on the same date from Idridgehay shown in Figure 4.6b, shows a slightly higher temperature range of 17.25°C – 19.0°C and RH of 97% - 100% with μ ranging between 0.08-0.17 for a wet day.

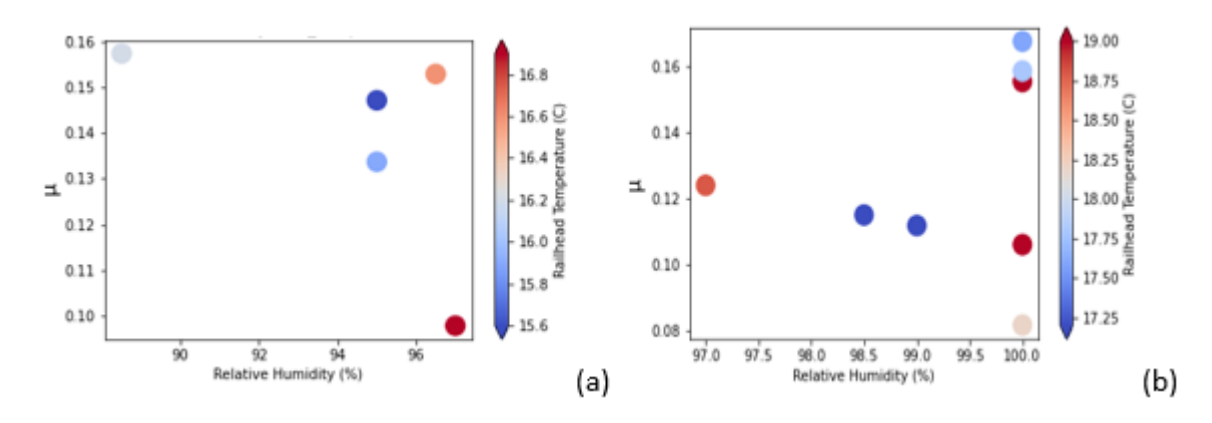


Figure 4. 6: (a) μ against relative humidity with a colour map representing railhead temperature for Wirksworth on 14-08-2019 and (b) μ against relative humidity with a colour map representing railhead temperature for Idridgehay on 14-08-2019

Figure 4.7a is a plot of the data from Idridgehay of artificially wetted railhead and the natural railhead state, while Figure 4.7b shows railhead image samples of both railhead conditions. The μ ranged from 0.11 – 0.33 with railhead temperatures of 4.2°C – 5.0°C and RH ranges of 71% - 79%.

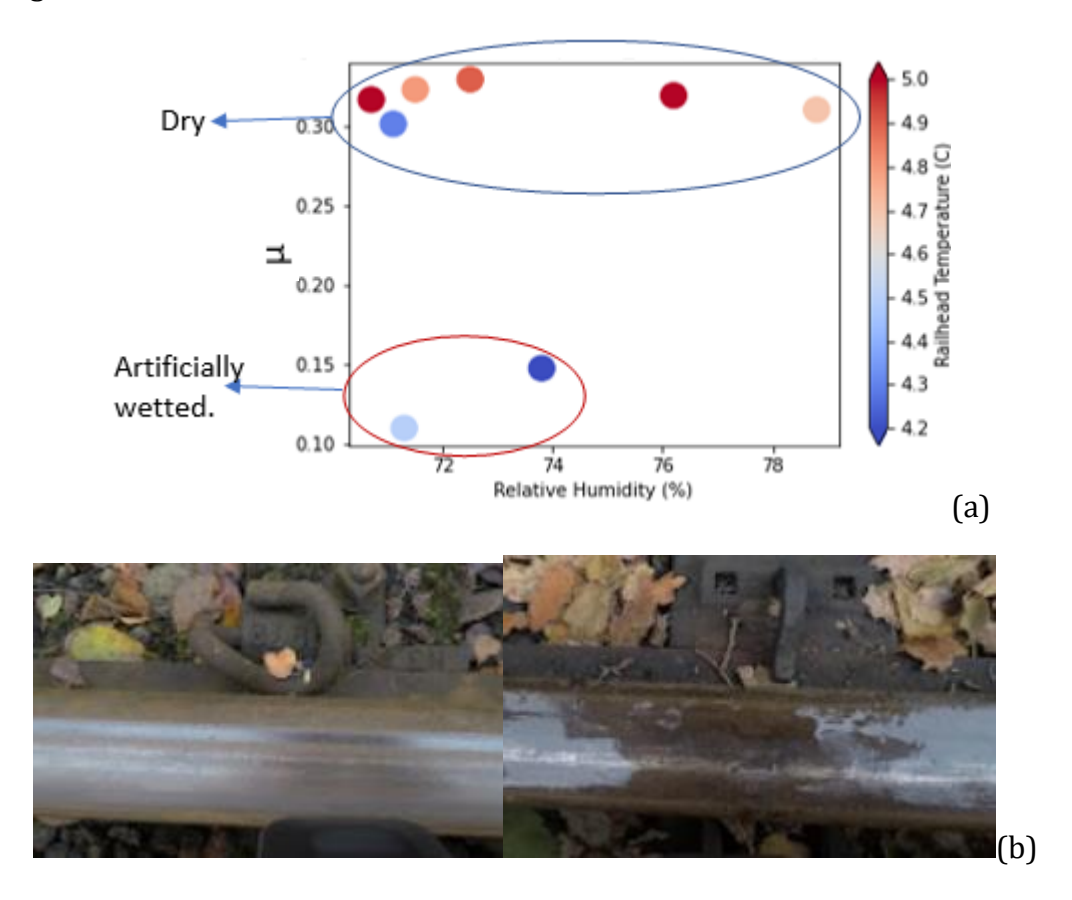


Figure 4. 7: (a) Plot of μ against relative humidity with a colour map representing railhead temperature for Idridgehay on 21-11-2019 and (b) Shaded dry railhead (left) and artificially wetted railhead (right) at Idridgehay 21-11-2019

Wirksworth data collected on the same day is shown in Figure 4.8a with railhead temperatures ranging from 1.7° C to 4.0° C and Influence of RH between 53.5% to 71% resulting in a μ of 0.12 – 0.33. Figure 4.8b shows image samples of the railhead state: under dry conditions (left) and in a damp condition (right) highlighted in the plot shown in Figure 4.8a.

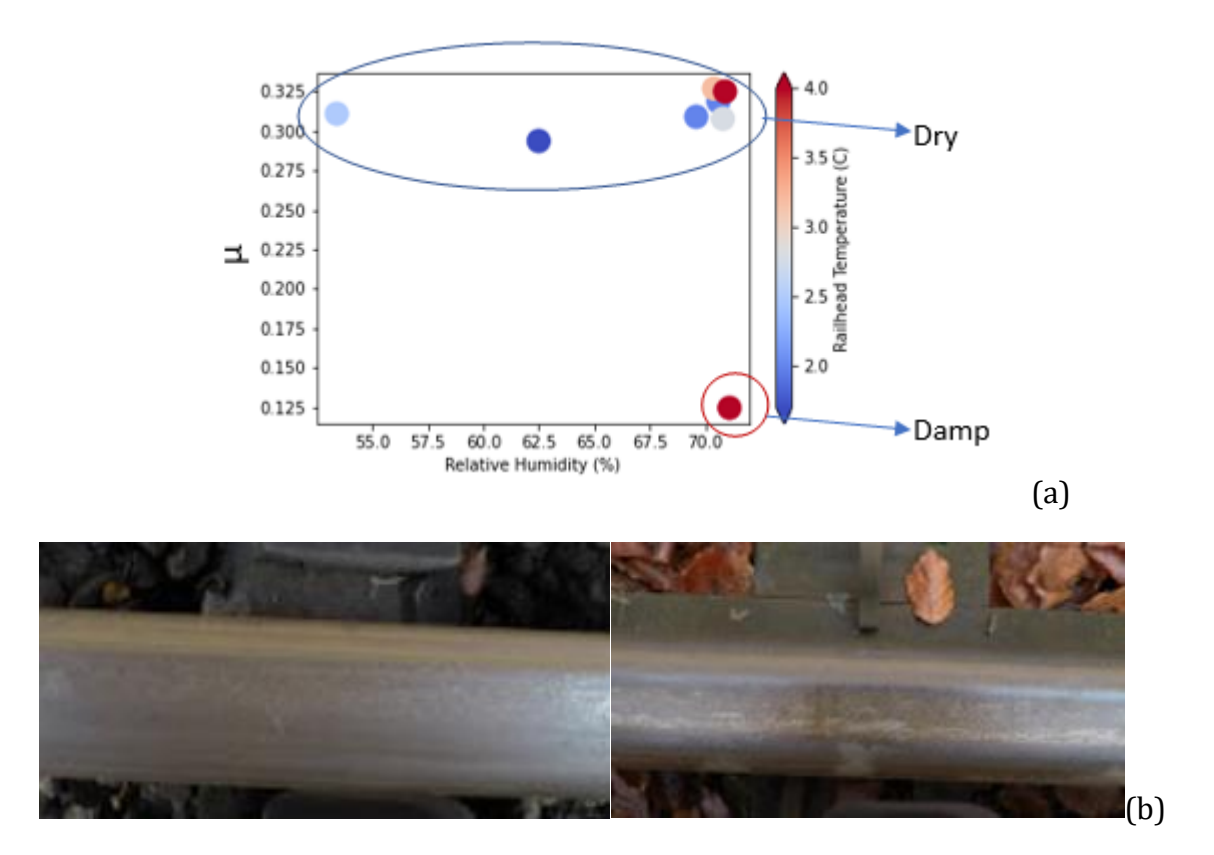


Figure 4. 8: (a) μ against relative humidity with a colour map representing railhead temperature for Wirksworth on 21-11-2019 and (b) Dry railhead (left) and damp railhead (right) from Wirksworth on 21-11-2019

Figure 4.9a presents data collected on the same day from both sites with an upward progression of environmental conditions with RH ranging from 60% to 78% and 69% to 80% with railhead temperatures of 3.6°C – 9.4°C and 7.8°C – 10.9°C for Wirksworth and Idridgehay respectively. The state of the railhead showing visible oxidation present at the time of data collection can be seen in Figure 4.9b.

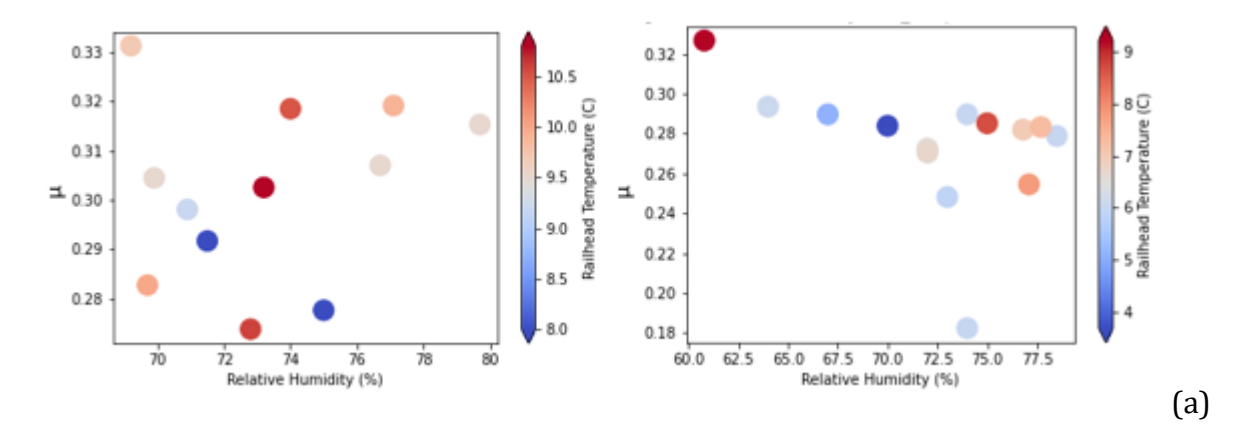




Figure 4. 9: (a) μ against relative humidity with a colour map representing railhead temperature for Wirksworth (left) and Idridgehay (right) on 13-11-2020 and (b) Railhead image with visible oxidisation with μ of 0.33 from Wirksworth on 13-11-2020

Table 4.1 summarises the data obtained from both locations on 20-11-20 and 08-12-20 represented on Figures 4.10a and 4.10b. It shows the minimum and maximum values for μ , RH and railhead temperature for each site.

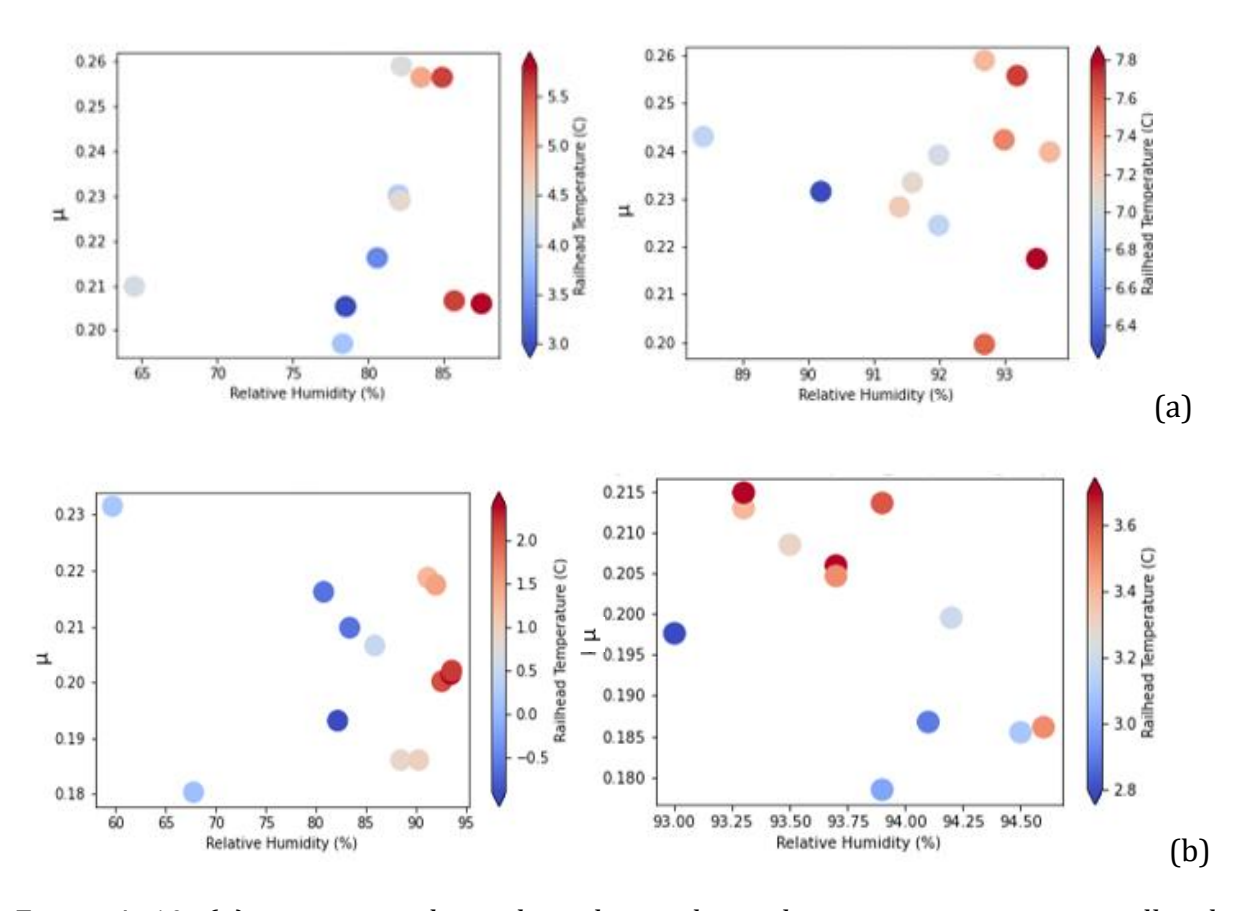


Figure 4. 10: (a) μ against relative humidity with a colour map representing railhead temperature for Wirksworth (left) and Idridgehay (right) on 20-11-2020 and (b) μ against relative humidity with a colour map representing railhead temperature for Wirksworth (left) and Idridgehay (right) on 08-12-2020

Table 4. 1: Data from Wirksworth and Idridgehay on 20-11-20 and 08-12-20

Date	Location	μ (Min-Max)	RH/% (Min- Max)	Railhead temp/C (Min- Max)
20/11/2020	Wirksworth	0.197	64.5	3.0
		0.259	87.5	5.8
20/11/2020	Idridgehay	0.199	88.4	6.3
		0.259	93.7	7.8
08/12/2020	Wirksworth	0.180	59.7	-0.9
		0.232	93.6	2.4
08/12/2020	Idridgehay	0.178	93.0	3.8
		0.215	94.6	3.7

DISCUSSION

On 14-08-19 in Wirksworth, there was a small temperature range on the high side between 15.6°C – 16.9°C and a high RH ranging between 88.5% - 97% with weather conditions of heavy rainfall and wind, shown in Figure 4.6a. At this temperature the μ values recorded were lower than expected and this was due to the high RH levels caused by the rainfall and the moisture deposited on the railhead. The lowest μ of 0.097 was recorded at the highest temperature and highest RH, 16.9°C and 97% respectively.

The μ trend at Idridgehay on 14-08-19, seen in Figure 4.6b, was like that of Wirksworth as they are located 3.7 miles apart with similar weather conditions. The lowest μ recorded was 0.081 under light rainfall with 100% RH and railhead temperature of 18.2 °C. This μ value is very close to the ultra-low friction region. In-lab tests carried out in [64] on a ball-on-disc apparatus supported that a low amount of moisture (such as light rainfall) brought about a significant drop in μ , while flooding conditions did not cause any noticeable drop in the μ values.

Data presented in Figure 4.7a where two sections of the railhead were artificially wetted at Idridgehay on 21-11-2019 resulting in a lower μ of approximately 0.11 and 0.15 compared to the recorded range of 0.30 - 0.33 on the dry railhead in overcast conditions, shown in Figure 4.7b.

While at Wirksworth on the same day a μ of range 0.29 - 0.33 was recorded (shown in Figure 4.8a) because the railhead was dry with overcast conditions, but a section of the rail which was damp had a μ of approximately 0.12, shown on Figure 4.8b. The cause of

dampness at that point may be as result of its closeness to a field (vegetation) where condensate from the plants may been dispersed by wind. In locomotive tests conducted at the Vuz Velim test track which had a section alongside a farmland, a drop in traction force was noted on that section citing moisture or visible leaf fall as the cause [65]. Both the wet phenomenon (referring to when there is visible moisture on the railhead) and damp phenomenon (referring to when there a moderate moisture coverage on the railhead which may be visible or felt by touch) show the effect moisture presence on the railhead has on lowering the μ .

The unused rail tracks caused by the Covid-19 lockdown, resulted in some parts of the railhead having slight oxidation which will have influenced the PTV readings and the μ values.

On 13-11-20 in Wirksworth (Figure 4.9a), it was sunny and dry, hence the μ values recorded were in the intermediate range of μ between 0.258 - 0.327. A lower μ of 0.183 was recorded on the same day, although not ultra-low but it was significantly lower than the range recorded for the weather conditions. This can be attributed to some visible oxidisation of the railhead at that point of measurement as seen in Figure 4.9b. Similar results were recorded in Idridgehay, shown on the right-hand of Figure 4.9a, without the oxidised railhead μ data noted at Wirksworth.

From Table 4.1, on 20-11-20, the lowest μ ranges were recorded at a combination of low temperatures between 3°C - 3.9°C and RH of 78.5% - 80.6% at Wirksworth. The μ levels recorded were in the intermediate range corresponding with expected wet conditions.

At Idridgehay a higher RH of 93.7% was recorded with a corresponding μ of approximately 0.24 within the intermediate μ range likely due to the temperature of 7.3°C not being low enough.

Data collected on 08-12-20 showed μ values ranging between 0.180 - 0.219 and 0.178 - 0.214 for Wirksworth and Idridgehay respectively. The μ values are similar to the expected values for wet railhead between the low and intermediate range for μ with high RH levels reaching 94.6% at Idridgehay and 93.6% at Wirksworth.

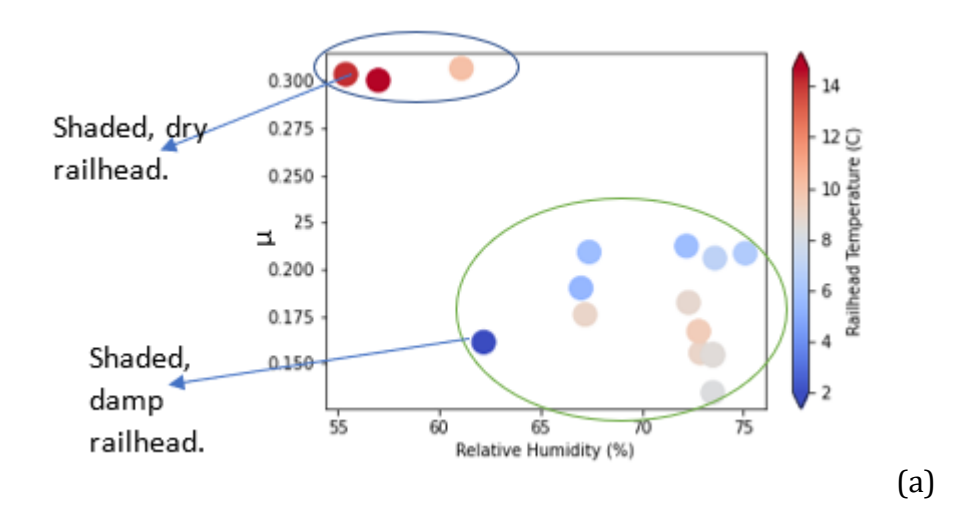
The temperatures recorded at Wirksworth ranged between -0.9°C to 2.4°C with the lowest μ of 0.18 occurring at a temperature 0.1°C and a RH of 67.3% under raining conditions. Similar trends were noted as Idridgehay as the temperature reduced, and the RH increase the μ decreased as seen in the plot in Figure 4.10b right-hand side. This suggests that lower temperatures also contribute to the occurrence of low adhesion. These results were recorded without physical contamination meaning the presence of contaminants will further increase the risk of low adhesion occurring. Research done on simulating ice formation on a railhead using a pin-on-disc tribometer showed that in the absence of ice/snow on the disc surface with a temperature range of temperature of 3°C to -15°C, had low temperature embrittlement acting which was the main cause of wear and increased friction. When an ice layer formed with the further temperature reduction

to - 25°C, the ice layer condensed forming a layer of moisture on the surface which caused the friction to drop, hence reducing wear [66]. The researchers also stated that with the addition of snow crystals to the pin-on-disc test with an increasing temperature from - 25°C to 3°C, the wear and friction levels reduced as the snow melted creating a lubricating layer of water. This again proves the importance of high humidity and the presence of moisture on the railhead in the creation of low adhesion in agreement with lab tests carried out by [64, 67], while the effect of snow/ice becomes dominant when it melts which can occur in reality by heat produced between the wheel/rail interface.

4.4.2 BUTTERLEY

RESULTS

Figures 4.11a through to 4.11c show the resulting measurement plots and railhead images from Butterley and the independent effects of high humidity on the railhead friction are highlighted.





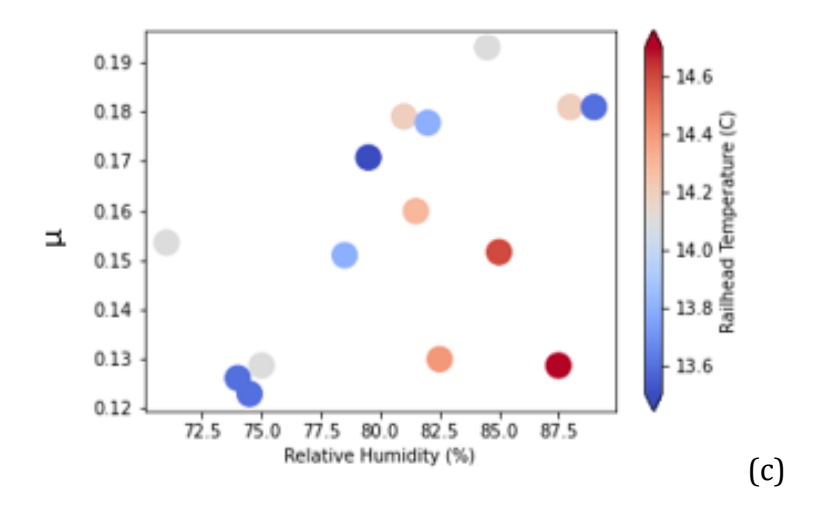


Figure 4. 11: (a) μ against relative humidity with a colour map representing railhead temperature for Butterley on 22-10-2019; (b) Dry railhead under shade (left) and damp railhead under shade (right) at Butterley on 22-10-2019 and (c) μ against relative humidity with a colour map representing railhead temperature for Butterley on 01-10-2019

Figure 4.11a shows that a noticeable cluster of lower μ values between 0.12-0.15 were seen on 22-10-2019, around the region of high RH 72% -7 6% and lower temperatures for late October 5°C-10°C compared to μ of 0.30-0.32 recorded in the region of higher temperature 10°C-16°C and lower RH 54%-62% where the railhead was visibly, dry shown in Figure 4.10b.

Figure 4.11c shows data collected 01-10-19, temperatures were in the range of 13.5°C – 15°C combined with high RH of 70% - 90% due to drizzle at the time the measurements were taken.

DISCUSSION

Work done by researchers on a Mini-traction machine showed that there was a considerable decrease noticed in the μ to between 0.1 – 0.15 with the rough specimen used when submerged in water of 5°C compared the a μ of approximately 0.20 for water at 20°C [68]. Although this experiment does not give a representation of the field conditions, it supports the occurrence of lower μ under reduced temperature. Lower μ was recorded in a shaded and damp section of the track. It was noticed that there was a temperature drop in the region (comprised of four data points circled in black) of the lowest μ which is the right conditions for dew formation where warmer temperatures allow for moisture to be held in the air and a drop in the temperature (as seen on the graph in Figure 4.11a) releases the moisture as dew [69]. This accounts for the higher RH reading in that region. While the higher μ values were recorded on a dry section of the track.

A μ of 0.16 on the plot was recorded at a medium RH of 62.2% and lower temperature of 2°C, has shown that even at low temperatures the RH must be high before any significant drop in the μ value is recorded. At this point the moisture content on the railhead had reduced supported by the RH value recorded.

Although the temperatures recorded (13.5°C – 15°C) with high RH (70% - 90%) on 01-10-19 (seen in Figure 4.11c) are not classified as low, the data from the plot shows that if the temperature were to have dropped further (on some points of the track) the friction would potentially have reduced. The data shows the μ reducing as the railhead temperature reduces with the high RH in the presence of moisture.

The second lowest temperature recorded on the same date was 13.6° C with a RH of 74.5% which accounted for the lowest μ of 0.125 recorded. This shows that low adhesion can occur in warmer temperatures and with different railhead contaminants under the right conditions, especially high RH on the railhead.

4.4.3 DARLEY DALE

RESULTS

Figure 4.12a shows μ readings measuring within a temperature range of 9°C - 16°C with low RH. A standout μ of 0.13 compared to range 0.22 – 0.38 was recorded, shown circled on the image, the railhead image for the standout reading can be seen in Figure 4.12b showing significant rust contamination.

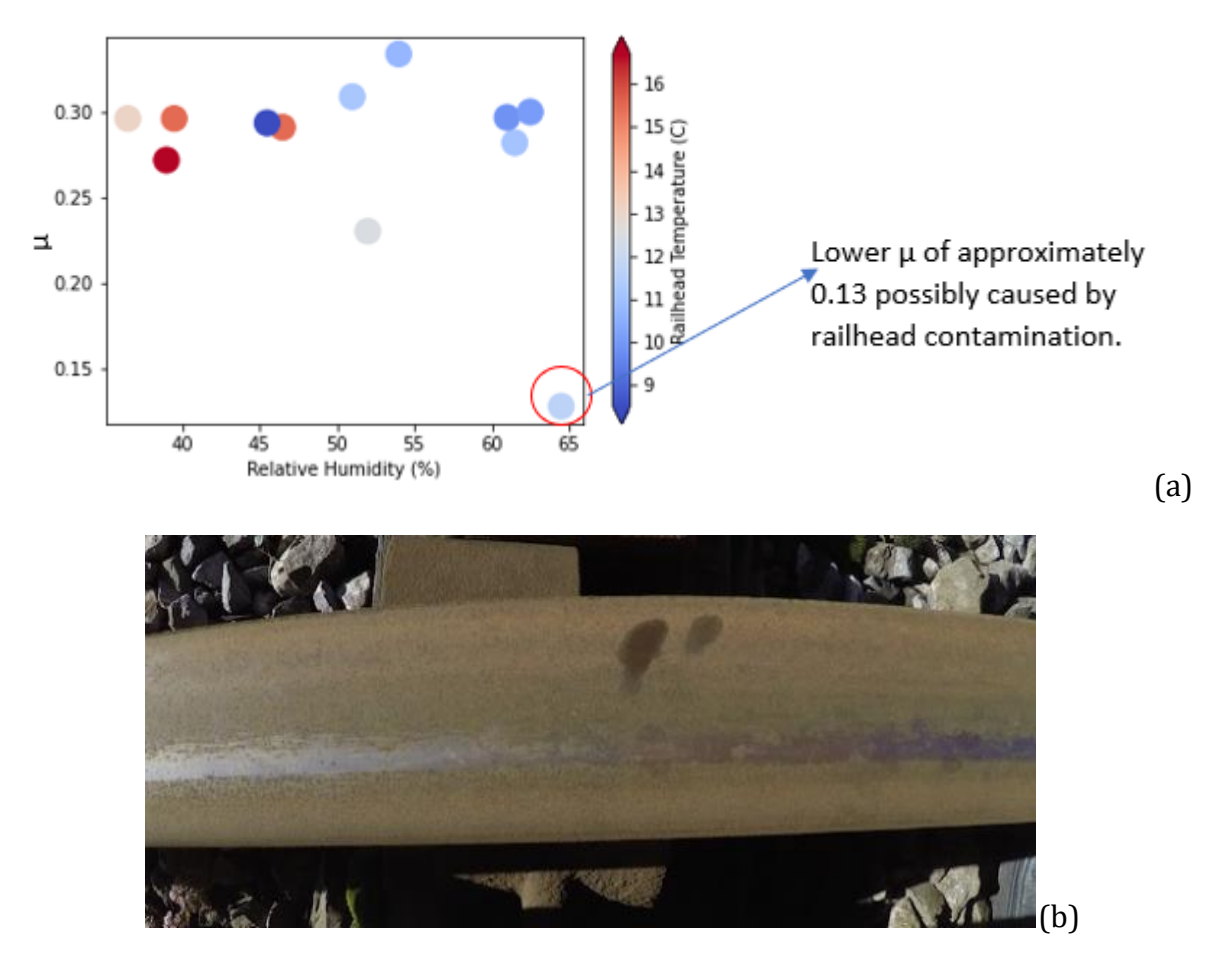


Figure 4. 12: (a) μ against relative humidity with a colour map representing railhead temperature for Darley Dale on 02-10-2019; (b) Corresponding railhead image for the Darley Dale \square of 0.13

Measurements taken under shaded and sunny conditions were recorded in Figure 4.13a at a temperature range of 7.5°C – 18.5°C and RH range of 50%-68%. Dry railhead conditions yielded a μ of 0.28 – 0.35, a sample of the dry sunny railhead can be seen in the right-hand image of Figure 4.13b. A low μ of 0.13 was recorded under shaded conditions with dew present as seen in Figure 4.13b (left).

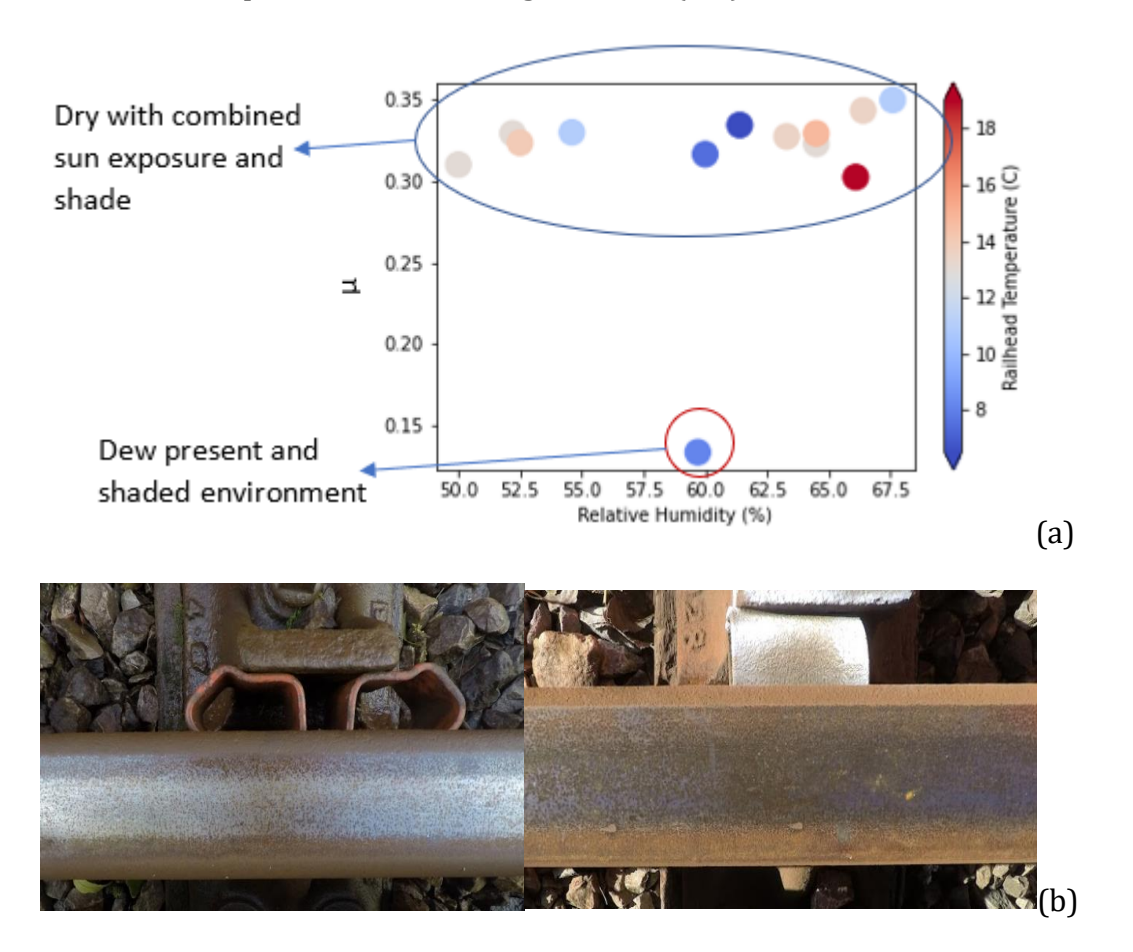


Figure 4. 13: (a) μ against relative humidity with a colour map representing railhead temperature for Darley Dale on 08-10-2019 and (b) Railhead with dew present (left) and railhead with exposure to the sun (right) at Darley Dale on 08-10-2019

DISCUSSION

The highest RH recorded on 02-10-2019 at Darley Dale of 64.5% with a temperature of 11.7°C produced the lowest μ of approximately 0.13, shown in Figure 4.12a. Ideally, it is expected that the μ values should all be in the intermediate region as the railhead conditions were dry with a combination of sunny and shade effects, but the lower μ reading stood out which was possibly caused by contamination of the railhead at that point, which is very likely as a patch of grease was noticed on the railhead shown in Figure 4.12b. The temperature variation was caused by the transition to shady environment from sunny environment. Shade and track orientation causes a drop in railhead temperature [70].

On 08-10-2019, similar trends were noted as on the previous visit with similar weather conditions. Although a lower μ of 0.13 was recorded within the medium RH range of 59.7

and railhead temperature of 8.7°C (see Figure 4.13a). The presence of dew due to the drop in the temperature (this can promote the "wet-rail" phenomenon) on the rail section explains the drop in μ as the presence of moisture contributes to the reduced friction value on the railhead if mixed with oxides, which were clearly present here shown in Figure 4.13b [30].

4.5 SALISBURY DATA COLLECTION

Following the train crash in Salisbury Tunnel Junction, UK on 31 October 2021 when a South Western passenger train travelling from London Waterloo to Honiton crashed into another passenger train operated by Great Western travelling from Portsmouth Harbour to Bristol Temple Meads, an opportunity arose to test/measure the railhead at the site of the collision for low adhesion [71].





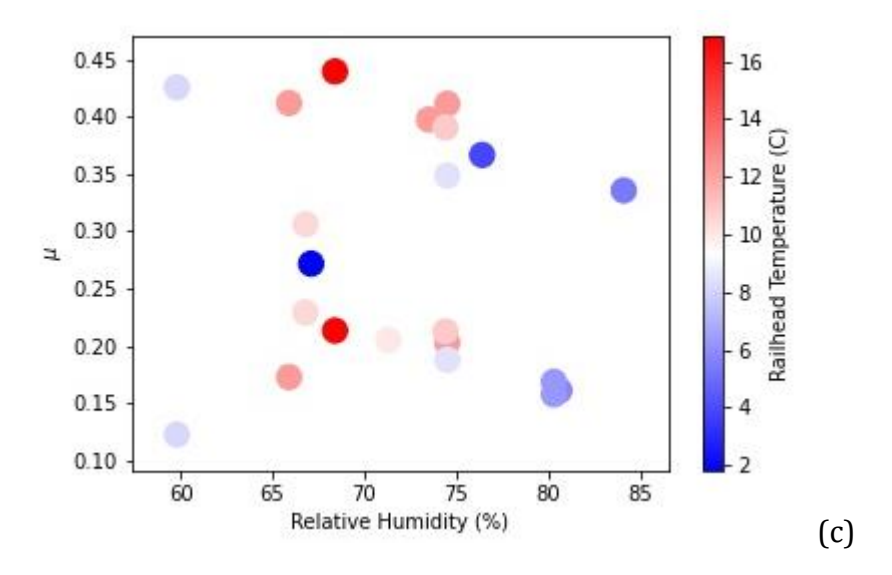


Figure 4. 14: (a) Ariel image of the crash site at Salisbury Tunnel [71]; (b) Examples of black leaf layer present on the railhead; (c)) μ against relative humidity with a colour map representing railhead temperature for Salisbury Tunnel Junction 03-11-21

The site of the collision (see Figure 4.14a) appears to have a dense leaf coverage over the rail tracks and leaf contamination/low adhesion becomes a suspect for the derailment and crash. A colleague at the university named Tom Butcher went down to the crash site on 3-11-21 to collect friction measurement using the Pendulum tribometer, environmental data and railhead images. The images collected (see Figure 4.14b for example) clearly showed that railhead was contaminated with black leaf layer and this was confirmed to cause of the crash by the Rail Accident Investigation Branch (RAIB) [71].

The data collected was analysed and plot as seen in Figure 4.14c to understand how and why the low adhesion occurred. Given the fact that the information data collected happened 3 days after the incident, the environment was not the same as the actual day and the railhead condition may have also changed over that period.

The pendulum measurements were taken across 2 railhead conditions (natural state and artificially wet). All the μ measured for the artificially wet section was significantly lower at 0.12 - 0.34 than the natural state at 0.23 – 0.72 which appeared to be dry. Before the averages of the pendulum reading were calculated, the lowest μ recorded on the wetted rail section was 0.037 which falls in the category of ultra-low friction. This gives an indication of the possible μ that was experienced on the day of the incident.

The Salisbury data set highlighted the occasional poor repeatability experienced in using the pendulum tribometer to measure contaminated railhead friction (see figures 4.15 (a-c)).

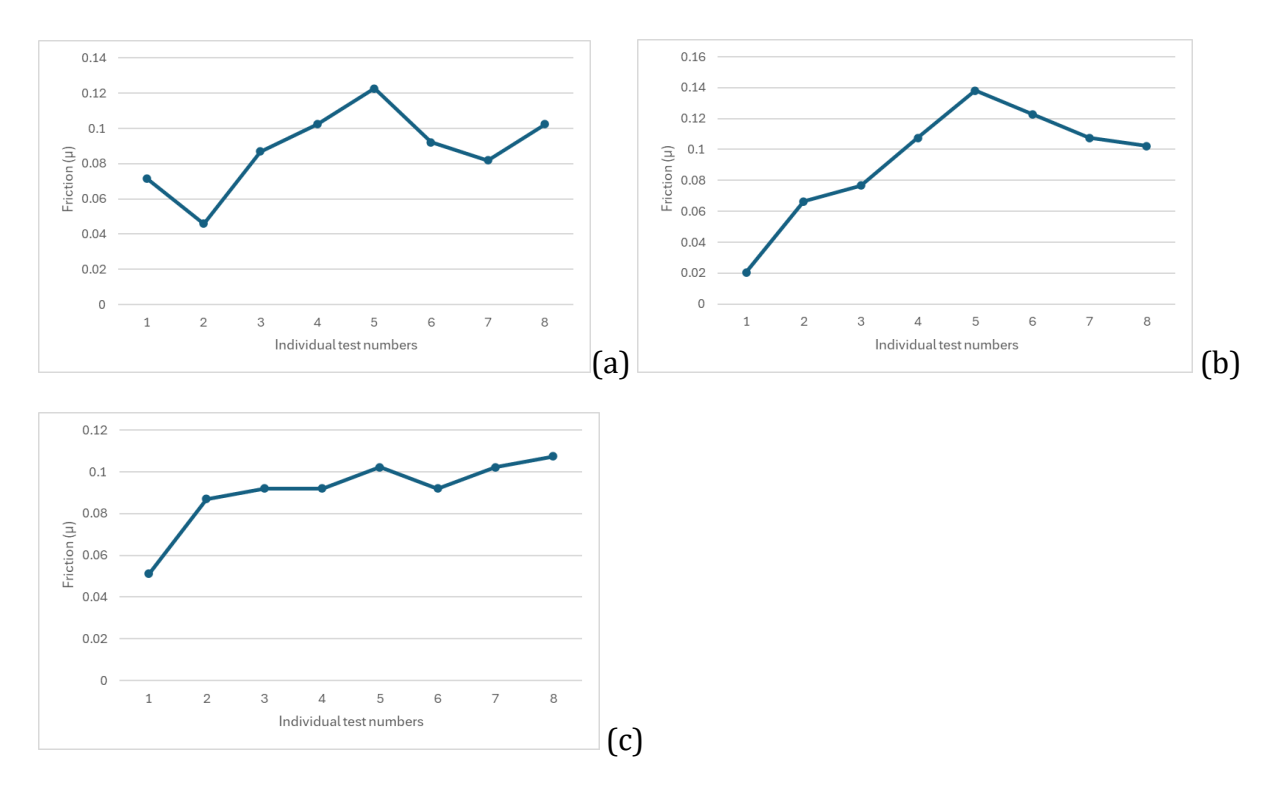


Figure 4. 15: Salisbury contaminated railhead time series plots showing the 8 individual Pendulum tests recorded before the standardised average was calculated. (a) Friction measurements for a dry contaminated railhead. (b) Friction measurements for an artificially wetted contaminated railhead. (c) Friction measurements for an artificially wetted contaminated railhead.

Before the averages of the 8 pendulum friction readings were calculated, the individual frictions measured at the beginning is seen to convey the lowest and possibly the actual friction values of the rail head, especially for the wet railhead conditions shown in Figures 4.15 (b) and (c). The subsequent friction measurements are seen to increase because the pendulum tribometer's rubber pad wipes off the contaminants and/or moisture on the railhead, hence altering the railhead conditions and consequently the friction value.

4.6 GENERAL DISCUSSION

These results have shown that relative humidity is an important factor in understanding low adhesion on the railhead as seen from the data presented in this work. The variation in the RH data makes the results unique, which is usually not considered in in-lab or controlled environment testing. Further work should be considered for including variations of RH levels for in-lab friction tests.

The RH and temperature were effectively taking at every point of friction measurement because the pendulum tribometer is portable and can be moved easily from point to point. Compared to in-lab test methods, where the railhead temperature is independent of real weather elements. On the contrary, for on-field measurement techniques where the railhead conditions are dependent on the weather element, but the exact measurements of weather elements for a corresponding friction reading cannot be

determined because the exact point of measurements on the railhead is not easy to determine.

From the analysis done we can infer that the railhead friction is dependent on the relative humidity, air and railhead temperature. Therefore, this informs that those 3 parameters are key variables that should be considered in the prediction of railhead friction.

4.7 CONCLUSIONS

- These data sets have successfully linked on-field weather elements to friction data, with the use of the British railway research train conversion factor. This shows that a friction predication tool can be design using the variables presented.
- This data provides a better understanding of the variations that occur in the railhead friction because of the open system nature of the wheel/rail interface showing the unpredictable changes in environmental conditions.
- At 75% RH and above low adhesion will be highly likely especially with the presence of moisture on the railhead, even with warmer temperatures.
- A significant drop in the railhead temperature leading to a rise in RH is seen to be accompanied by a decrease in the adhesion level. This can be attributed to the formation of dew (light moisture) on the railhead.
- Data collected from the Salisbury tunnel incident was very important in understanding the effects of the black leaf layers in combination with environmental effects. This will be very useful in creating a robust friction prediction tool.

CHAPTER FIVE

5. DEVELOPMENT OF FRICTION PREDICTION TOOL

5.1 INTRODUCTION

From Chapter 4, it was established that railhead friction is dependent on the railhead temperature, air temperature and relative humidity. In order, to design a railhead friction prediction software these variables are key to understanding adhesion and building an accurate model. From the resulting plots in section 3.4, it is obvious that the relationship between the variables is non-linear. Alongside these variables, railhead images will be included for contaminant identification and possible differentiation between wet-rail phenomenon at different temperature. It is therefore important to use a method that will account for these characteristics in building the prediction model.

Table 5.1 shows the measurement uncertainties of the measurement equipment used in building the prediction model, which are the same as the equipment used in the analysis done in Chapter 4.

Table 5. 1: Sensor's measurement uncertainty

S/N	Sensor Instrument	Condition Measured	Measurement Uncertainty
1	RS-88662 IR Thermometer	Air and Rail Temperature	±3.5°C at -50°C - 20°C ±1.5°C at 20°C - 260°C
2	RS-88662 IR Thermometer	Relative Humidity	±1%
3	Eddy current thickness gauge	Layer thickness	±(2μm+3%)

The sensors used in training the prediction model had a measurement uncertainty of $\pm 3.5^{\circ}$ C for the temperature range between -50° C -20° C which is not a large variation. The results generated by the model will be impacted negatively by a sensor having higher uncertainty.

5.2 METHODOLOGY

5.2.1 GAUSSIAN PROCESS MODEL

In order to establish a relationship between non-linearly related parameters such as friction, relative humidity and temperature with non-mathematical parameters in this case images, an appropriate statistical model has to be chosen. The relation of a set of

independent parameters to one or several dependent variables is done by a statistical model. For any statistical model the complexity of the model and dimensionality of the input space need to be balanced by the amount of data available for training [72]. More complex models, or models of high dimensional data require more training data. The most appropriate type of model will depend on the complexity of the relations present, how much data is available and what other information is required with the prediction.

The Gaussian regression model is the most appropriate for the prediction operation because of its flexibility in representing a large variety of models having non-mathematical functions, large amount of data and random variables.

Given a finite set of input of $x = [x^{(1)}, ..., x^{(n)}]^{\mathsf{T}}$ with corresponding function represented by a group of random variables $y = [y^{(1)}, ..., y^{(n)}]^{\mathsf{T}}$; the Gaussian function can be used to define the jointly distributed random variables (y) as: $\wp(y|x) \sim \exp\left(-\frac{1}{2}y^{\mathsf{T}} \Sigma^{-1}y\right)$ (5.1)

Having a matrix Σ presented by C the covariance function, where 'cov' stands for the covariance operator [73]:

$$\Sigma_{pq} = cov(y^{(p)}, y^{(q)}) = C(x^{(p)}, x^{(q)})$$
(5.2)

This concept is further explained in the work done by Brahim-Belhouari and Bermak [73]. The Gaussian process model framework used in this work is a pre-existing module on Scikit learn which is a python package.

For image processing tasks, the size of the input is extremely large, for example, a one mega-pixel image with three colour channels requires a vector with three million elements to uniquely represent an input. In addition, the relations between individual pixel values and dependent variables of interest are often extremely complex, meaning that models need to be flexible, with many trainable parameters, to achieve good accuracy.

For these tasks Convoluted Neural Networks (CNN) are typically used, these leverage the structure of image data by filtering the input image, first producing maps of primitive features such as edges, then progressively higher order features such as simple shapes or objects. The result of this filtering is then fed into a further 'fully connected' network which is used to classify the input image. The network is trained by automatically adjusting the filter values and the weights in the fully connected network based on their derivative of the error, which can be found using the chain rule of calculus [74].

As the number of parameters in the filter kernels is high and many are needed to represent complex shapes, this process requires an enormous amount of data to avoid spurious correlations. This data requirement is a direct result of the high input dimensionality and the complexity of model, not a specific feature of neural networks. The resulting model consists of two distinct parts: a filtering network which takes an input image and produces "ratings" for each of a set of high-level features and a fully

connected network which links these features to image classes or other variables of interest. The model used is attached in Appendix B-1.

5.2.2 IMAGE PROCESSING

As stated in the chapter four, forward facing and railhead images were collected from a GoPro camera. The images collected have numerous features which may contain some noise, image processing was required to reduce the image features to only reflect relevant features for the friction prediction. The image processing techniques used for the forward-facing images varied from that of the railhead images due to the amount of data available.

FORWARD FACING IMAGES PROCESSING

The forward-facing images being processed are the ones collected from the field work described in chapter 4. The images were complex, containing many different objects and situations. As such traditional image processing would be impossible, while manual labelling would be too time consuming to scale to a full network system. Neural networks offer an attractive solution, but the small number of images makes directly training a network impossible. Instead, these images were augmented with a large set (\sim 20,000) of visually similar forward-facing images scraped from various UK sources on the internet. The images used were open source, therefore there is no ethical violation or copyright infringement, in addition these set of forward-facing images were not included in the final package produced in this research. The resulting set provides a representative sample of images from UK networks and can be used to train a dimensionality reduction model which retains relevant distinguishing information from the images, while discarding information common to all images.

An example image from the augmented set is shown in Figure 5.1. Many parts of these images are common for every image, these areas are removed by cropping the image into two sub-images as shown. The sub images were then resized to the correct input size for a pre-trained CNN.

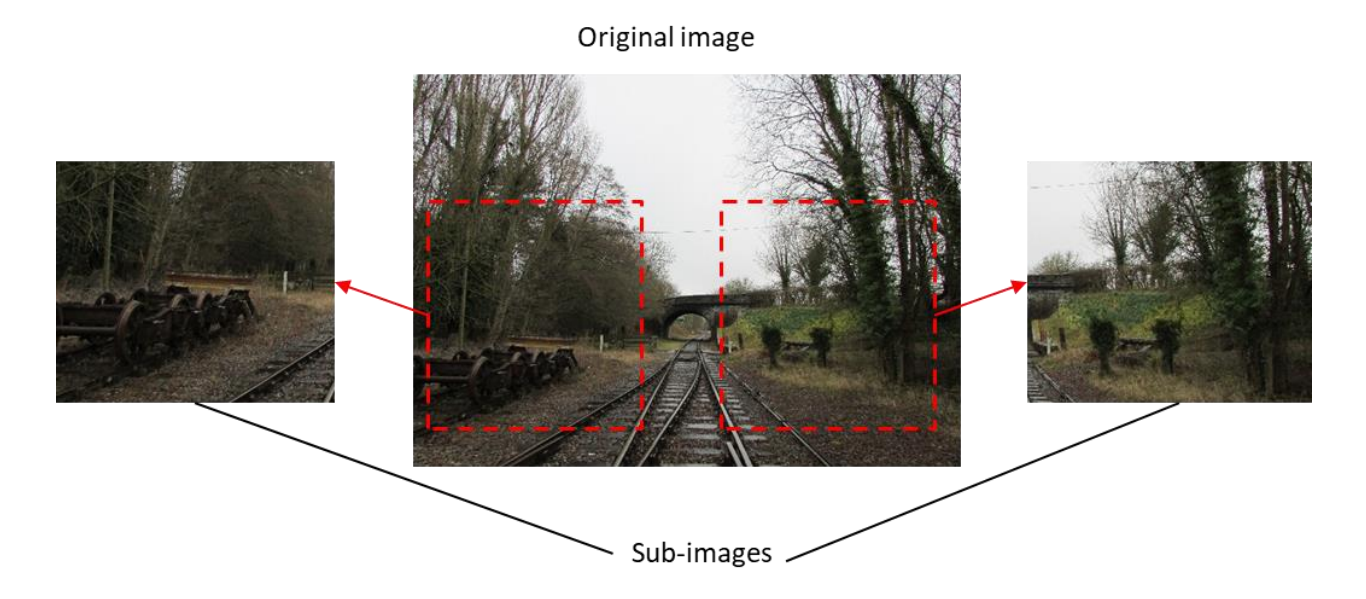


Figure 5. 1: An example forward facing image showing the sub images extracted for further analysis

These sub-images are passed through a CNN that has previously been trained on a large, labelled data set. In this study MobileNet V2 (which is a readily available open-source CNN) was used as it is suitable for high-speed use on low-cost devices. This network reduces the dimensionality of the data from millions of brightness values to a 2048 element feature vector. The feature vector consists of features which have been trained to be useful for common image classification tasks. These are high level features, many of which relate to familiar concepts (e.g. a human face).

Within this vector many features are irrelevant for our task or strongly correlated to each other. To further reduce the dimensionality, a Principal Components Analysis (PCA) was carried out on the feature vectors. The PCA simplifies the large data set into smaller set whilst preserving important patterns and trends. This finds orthogonal, linear combinations of parameters which contain the most variation for the data presented [75]. Examples from the extremes of the first three principal components are shown in Figure 5.2. The values for the first 600 principal components were retained, these contained 90% of the total variation in the image data. These components are high level, abstract representations of the data and are unlikely to be summarised well by a description.

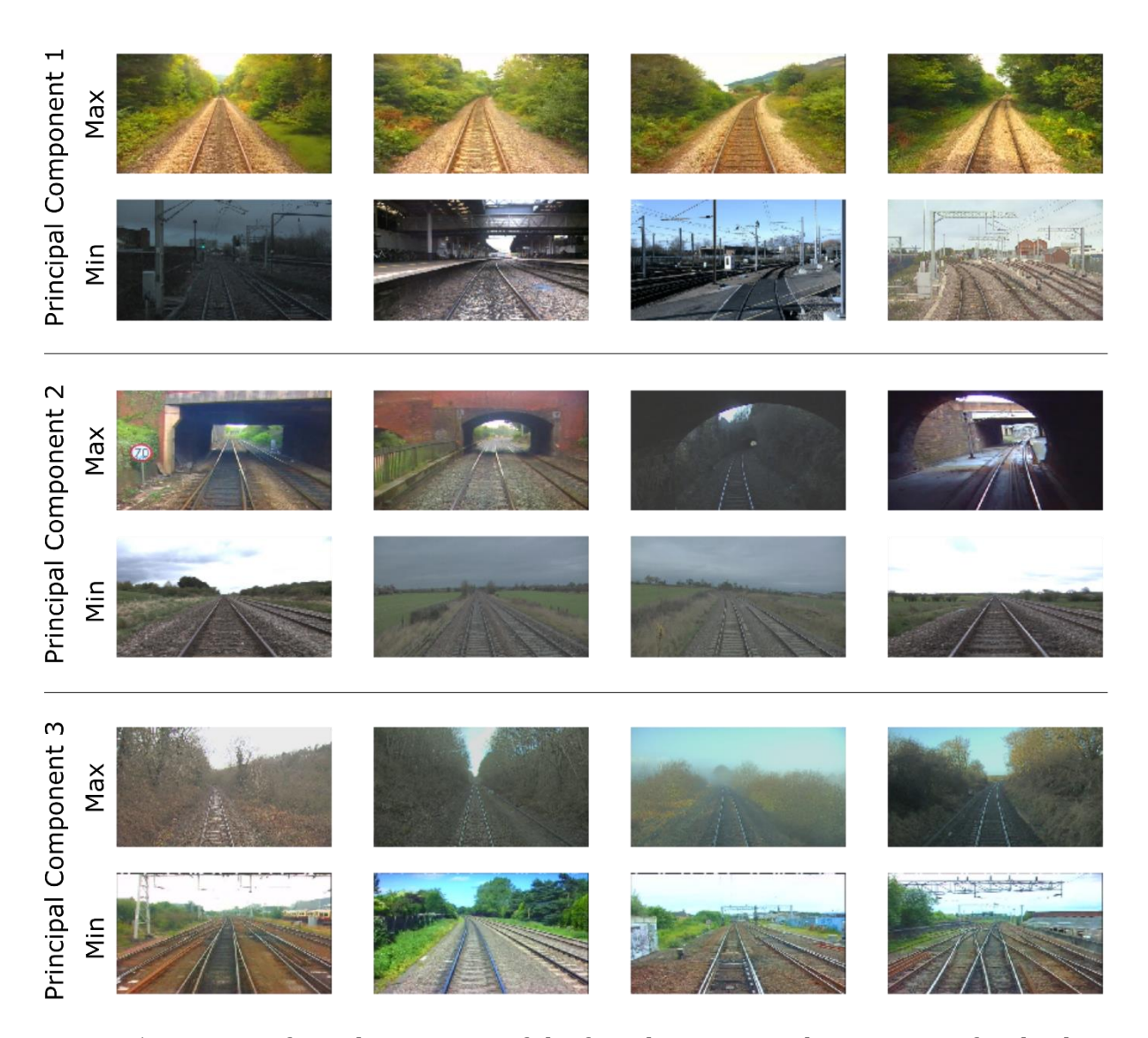


Figure 5. 2: Images from the extremes of the first three principal components for the data set. Each pair of rows represents a principal component

With this lower dimensionality and a large number of images an unsupervised classification tool can be used. This splits the data into groups which are similar to each other. There are many methods of completing this task, here we have used a self-organising map (a type of neural network). The results of this classification are shown in Figure 5.3.

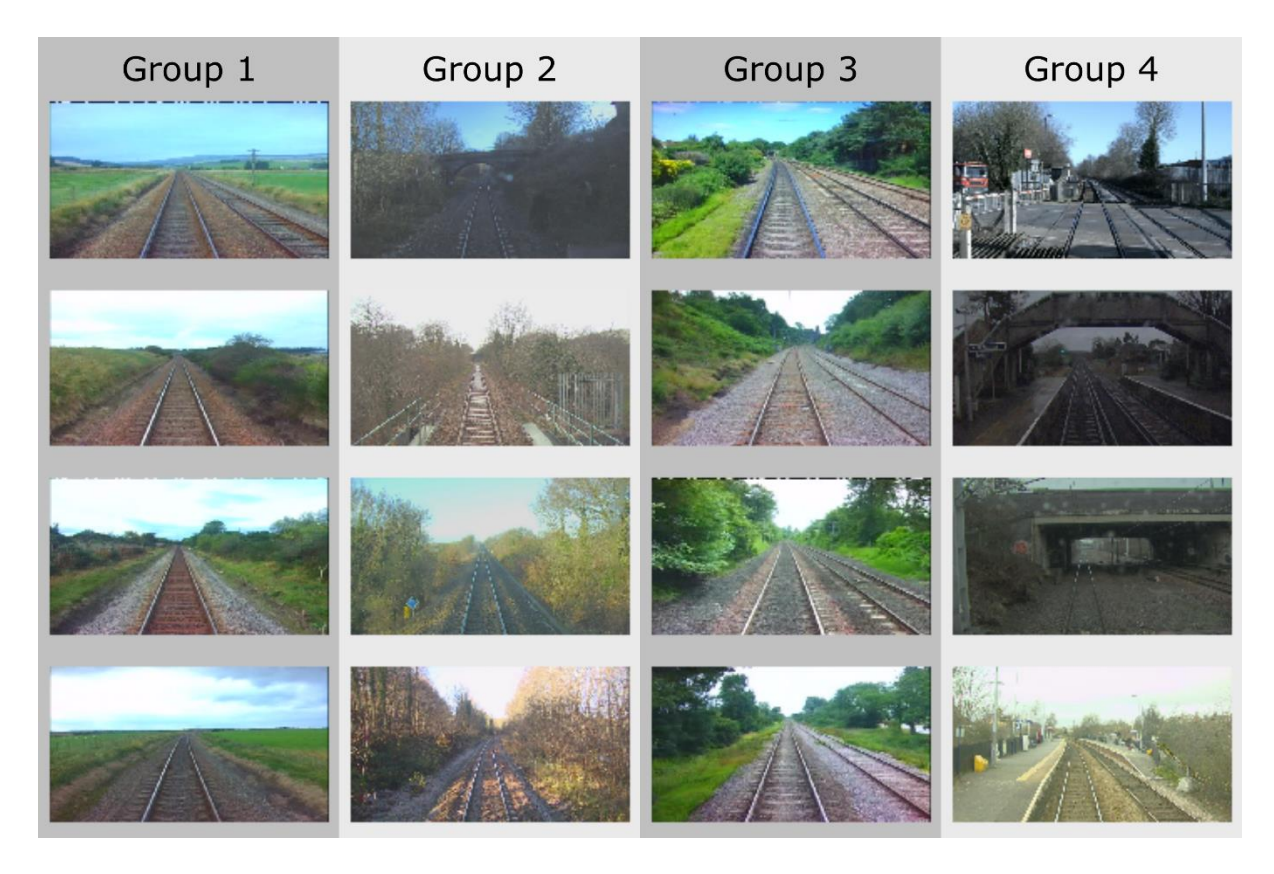


Figure 5. 3: Examples of the different groups of images found by the unsupervised learning technique. Columns are separate groups: grassland, trees, rural, urban

The result of this process is a pair of coordinates, which place a railhead image on the map. The groups presented in this map have been made from a representative sample of forward-facing images. The codes used are attached in Appendix B-2.

RAILHEAD IMAGES PROCESSING

Similarly, to the forward-facing images railhead images were collected along with associated environmental and friction data as described in Chapter 4. Unlike the forward-facing images there is no large source of representative railhead images. In addition, pretrained networks are typically trained on images which are very different from the railhead images and are unlikely to be useful. However, the dimensionality of the images must still be reduced before the images can be used (See Figure 5.4). To achieve this, features were extracted from the images using traditional image processing techniques. The traditional image processing techniques and tool kit used included an Edge detector for identifying the boundaries of the railhead in the image, Numpy for indexing operations to modify the pixel values of the image, SciKit-image that works alongside Numpy which was used for feature extractions and Pandas for reading the image file, directories from .csv [76].



Figure 5. 4: Railhead Image before (left) and after (right) dimensionality reduction

Before feature extraction, the images were normalised and the rail was located in the image, the rail was then cropped out for further processing. The features were chosen as features likely to be correlated with the friction present. These were: the number of black pixels in the image, the number of orange pixels in the image, the average colour of the railhead and the sum of the first derivatives in the along-rail and across-rail directions. The first derivatives are higher when many strong edges are present, such as when the rail is rough. These features could then be used directly in the prediction tool. The codes used are attached in Appendix B-3.

5.2.3 PREDICTION TOOL BUILD WITH GP MODEL

The forward-facing image map positions, railhead image features and sensor measurements from data collected between August 2019 to February 2020 were combined in a model to predict the railhead friction. A Gaussian process regression model was selected as it is flexible enough to accurately capture the relations which are likely to be present, and data efficient enough to be fitted well using a data set of this size. In addition, these models also provide an estimate of the error of the prediction given [77]. The predictor model code is attached in Appendix B-4. This mitigates the risk of incorrect estimation/prediction in new scenarios. Before fitting, all data have been linearly scaled to a unit scale, meaning that the highest value is scaled to 1 and the lowest value is scaled to 0.

The Gaussian process is defined by a kernel function. This encodes the joint variability of the model's parameters. This can be used to set prior information about how the data relate to each other, how much noise is present in the data and any underlying structure. The model consists of a summation of a constant kernel, a white noise kernel and a nonlinear kernel. Multiple non-linear kernels were fitted and the one producing the highest marginal likelihood (rational quadratic) was chosen. The constant kernel is set to 0.5 while the further hyper-parameters of the model are set by optimisation during the fitting process. The optimisation aimed to achieve the maximum log marginal likelihood for the data given the model and a Gaussian error function.

5.3 RESULTS FROM TRAINING AND FIRST STEP VALIDATION THE FRICTION PREDICTION MODEL

The first version of the prediction tool using the data from the Heritage railways (2019) discussed in Chapter 4 got the fit shown in Figure 5.5. The overall log likelihood of the model is 176.5 and the R² value for the model, with this data is 0.97. In order to validate the system, data were left out of the fitting process and the prediction of the naïve model compared to the actual value at the left-out points. The first step in the validation process was to leave a single point of data out at a time. The prediction of the naïve model at the left-out point can both be compared to the true value at that point as shown in Figure 5.6A and the prediction of the full model as shown on in Figure 5.6B.

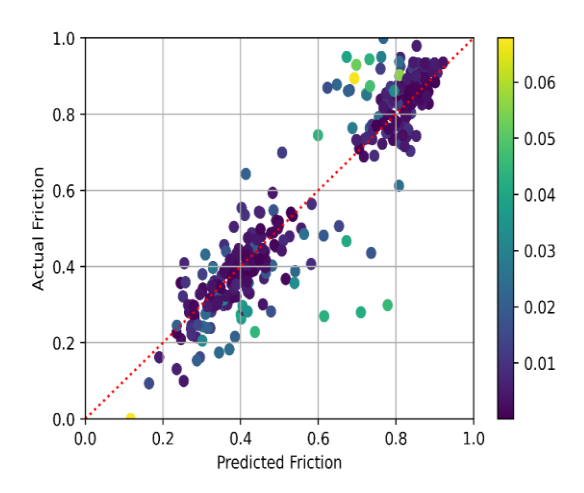


Figure 5. 5: Model predictions compared to the actual value at each point, points are coloured by their leverage. Data on both axes are normalised to a 0-1 scale

These results show naïve models are still able to explain 96% of the variation in the data (coefficient of determination = 0.96). Additionally, the average change in prediction between the full model and the naïve models is only 3% of the measurement range. This shows that, in general, the model is not over-fitted to the data, and that trends fitted by the model are likely to be real.

This process was extended to leaving groups of twelve points out. The models fitted leaving groups of twelve points out are compared to the true value at the left-out points in Figure 5.7A, this plot is for one set of groups which include the whole data set. These values are again compared to the result from the full model in Figure 5.7B. This process has been repeated for all possible groups of twelve points.

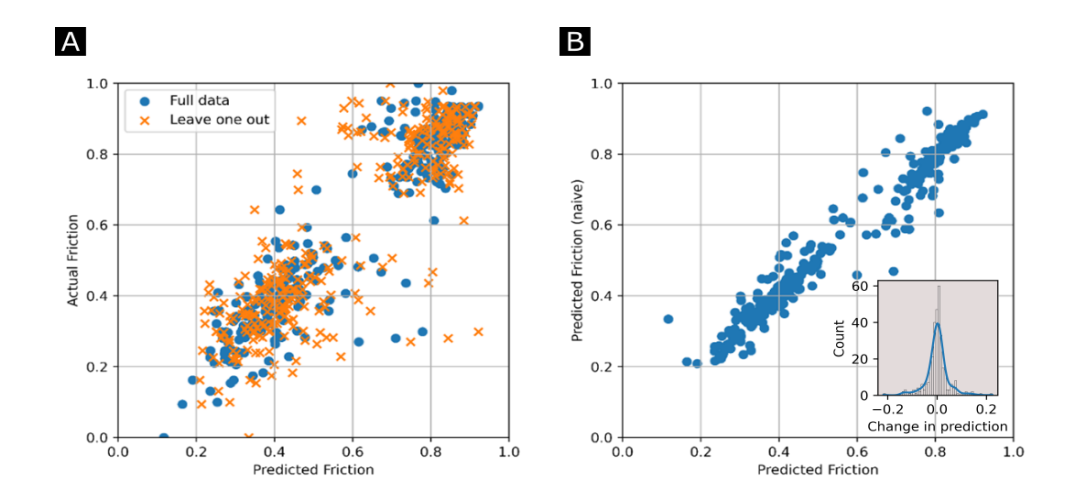


Figure 5. 6: Results of the leave one out validation (A) and a comparison of the full model to the naïve model for each point (B), with a histogram of the change between the naïve and full models. Data on both axes are normalised to a 0-1 scale

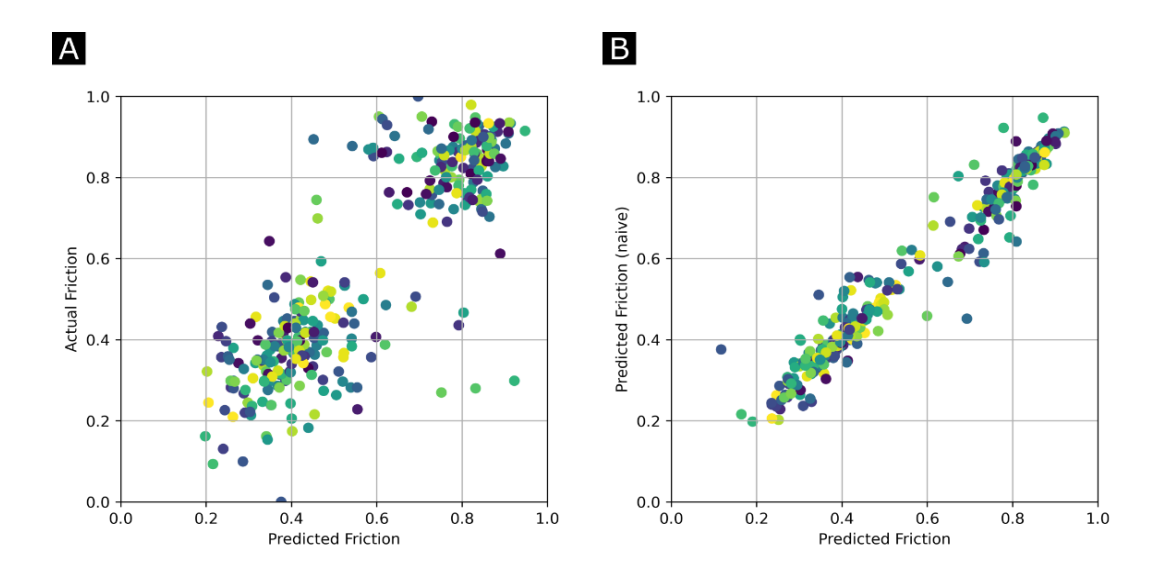


Figure 5. 7: Results of the leave groups out validation for one set of groups (A) and a comparison of the full model to naïve models for each group (B). Data on both axes are normalised to a 0-1 scale

As seen in Figures 5.6 and 5.7 for the leave one out validation, the mean change in prediction between the full model and the naive models was only 3% of the measurement range. The mean coefficient of determination for the left-out points was 0.96.

While it is clear from Figure 5.6 and Figure 5.7A that several points are over leveraged, and not predicted well when left out, the majority of the points are not. In collecting these data, we have aimed to collect from locations and in conditions likely to cause low adhesion, as such much of the data are from low adhesion conditions and are well predicted when left out of the fitting process.

5.4 PREDICTION MODEL VALIDATION AND RETRAINING PROCESS 5.4.1 FIRST VALIDATION

Given the predictions and first step validation from the model was done by inputting data it had been previously trained on, it was important to test its accuracy on a new set of data to see what type of prediction it will give.

Hence, a second validation was carried out. This was simply done by running images of already measured railhead friction through the tool and comparing the predicted friction to the measured friction for the corresponding image.

Data collected from Wirksworth and Idridgehay on the Ecclesbourne Valley Railways (one of the Heritage Railways) between **November to December 2020** described in chapter 4 was used because the tool had not been trained on those data set.

The images and corresponding environmental data were run through the model, and it gave the predictions in terms of the Pendulum Test Value (PTV) shown in Figure 5.8. The plot was created using the established friction measurements that was taken in the field against the predicted friction to give a simple visual representation of the deviations in predicted data.

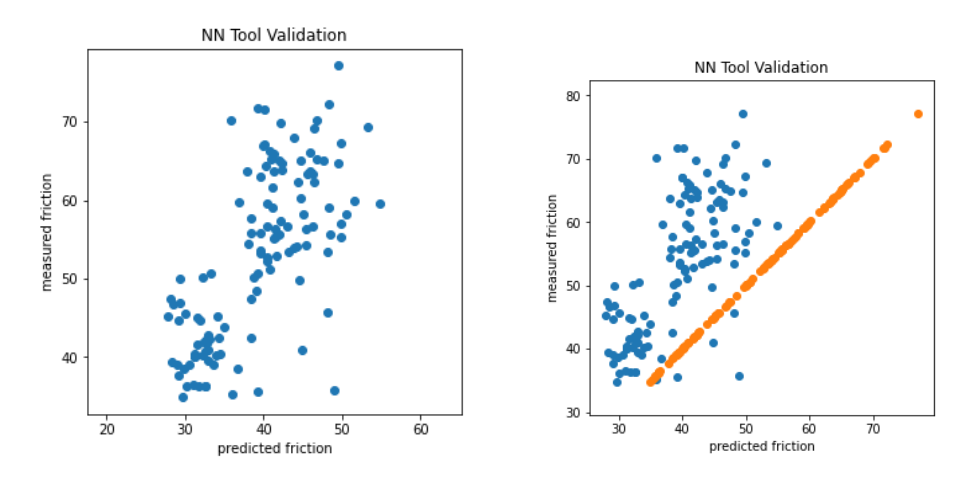


Figure 5. 8: 1st Prediction results using Nov-Dec 2020 data with linear points representing the measured friction on the image to the right

From the first view of the plot in Figure 5.8 it was seen that the model was under predicting the friction values for the Nov - Dec 2020 data set. The railhead images were referred back to understand what could have caused the underprediction, it was then noticed that the railhead conditions captured during the latter field visit were not representative of what that the prediction tool had been trained on based on the former field visit between Aug 2019 - Feb 2020. This may have been as result of the lack of train operation over the railhead during the latter data collection, creating a different railhead condition.

Asides for the railhead condition factor, the poor repeatability of results from the pendulum test rig, may have given wide variations in the measured data and making it harder to get a precise friction prediction.

Another contributing factor could have been the lack of robust data for the training of the model, which is evident in absence of certain types of railhead conditions data. To solve this problem, the NN tool has to be continuously trained to adapt to the various types railhead conditions..

5.4.2 FIRST RETRAINING AND REVALIDATION THE FRICTION PREDICTION MODEL

The first attempt of the model validation showed that was under predicting the friction due to the absence of similar data sample in data bank used to train. In order to improve the robustness of the tool, additional images and corresponding data will be used to retrain the model. In this case, the additional data will be that of Nov - Dec 2020 since it was confirm that it represented different railhead states in comparison to the original images the model was trained on.

The following steps were taken to retrain the model:

- 1. The original .csv data sheet used to train the model was updated to include the new dataset.
- 2. The image file names were included in the data sheet with their file directory, so the program can locate them for the feature extraction process. The image format is preferably ".jpg".
- 3. The IMAGEFEATURES.ipnyb files (see Appendix B-5) was located in the prediction model folder.
- 4. The image file directory in the python script was confirmed to ensure it matches the csv file, a name and location for the extracted csv file was assigned for it to be stored. IMAGEFEATURES.ipnyb was run to extract the image features, see Figure 5.9.

	date	time	air_temp	humidity	dew_point	rh_temp	layer_thick	friction	is_raining	mean_brightness	black	orange	edge_v	edge_h	color
Ī	0 43691	0.5	15.0	88.5	13.1	16.2	4.0	30.75	True	170.346052	0.0	0.002096	0.011879	0.0144	0.061112

Figure 5. 9: An example of a row in the csv file containing the extracted image features.

- 5. The image features properties were stored in a new csv file as assigned by the user. The csv file was then imported to the Gpfitting_MO.ipynb (regression model for the prediction, see Appendix B-6) which were the retraining takes place.
- 6. The GPfitting_MO with updated Image analysis file was run, this generated an updated .pkl file. That is the model has been retrained.

7. The pkl file generated will be updated in the "predictor" folder, which generates the prediction.

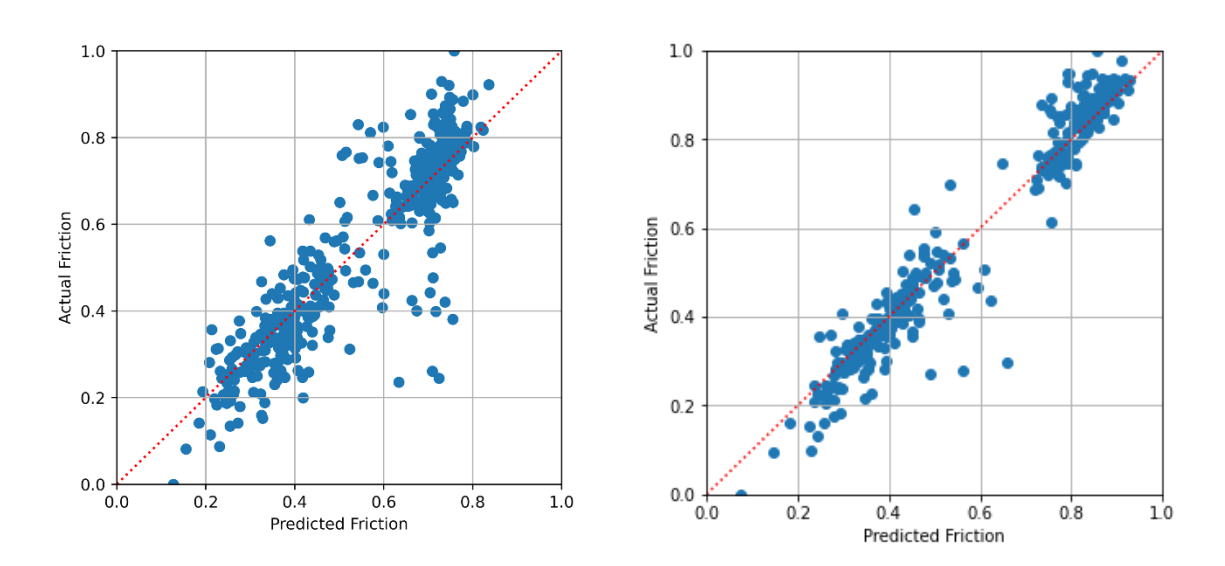


Figure 5. 10: Retrained regression model plot (left) original regression model plot (right)

The regression model fitting obtained after the retraining and before the retraining is shown in Figure 5.10. The plot is presented in form of a normalized data on a scale of 0-1. When the original model with an overall log-likelihood of 176.5 was compared to the retrained model with an overall log-likelihood of 257.46 it shows an improved fit for model. And from visual inspection of the plot an increase in the data cluster around the linear line representing more data with accurate prediction.

The retrained model can now be employed to re-predict the friction for the same Nov – Dec 2020 data set. The re-validation will show the effects of retraining the prediction model as well as the importance of having robust bank for the model.

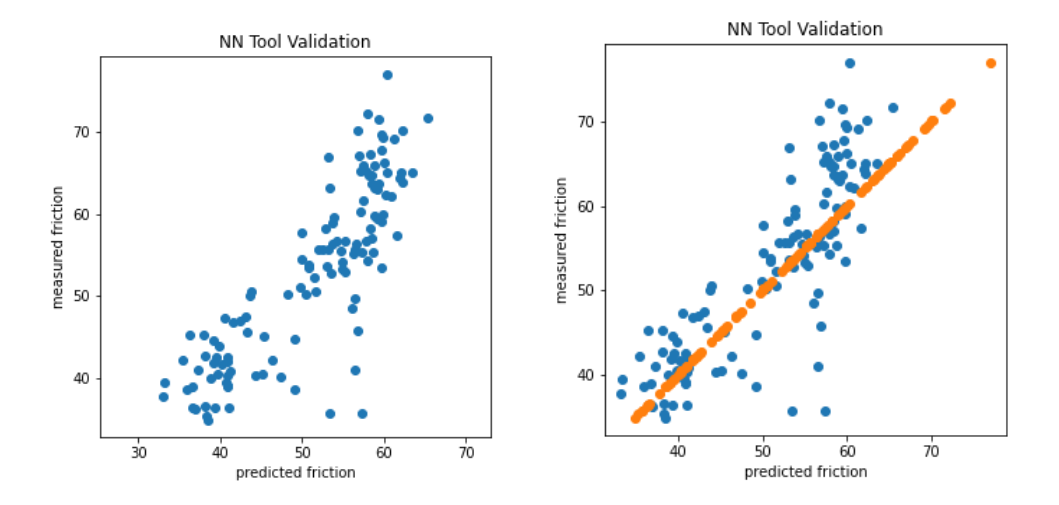


Figure 5. 11: Prediction results using Nov-Dec 2020 from the retrained model data with linear points representing the measured friction on the image to the right

From Figure 5.11 the data correlates better with the linear line compared to the original prediction in Figure 5.8. There are some noticeable outliers on the plot which can traced backed to the original data sheet which was a result of anomalies in the pendulum tribometer measurements. With continuous training of the model the predictions will keep nearing a perfectly linear result, albeit may never be $R^2 = 1$ or in fact close to 1 due to nature of model requiring a very large data set to function effectively and the poor repeatability of the pendulum tribometer result.

5.4.3 SECOND RETRAINING OF THE FRICTION PREDICTION MODEL WITH LEAF LAYER DATA FROM SALISBURY

It is important to include a variety of data for training of the prediction tool especially from in-field situation, to increase the robustness of the tool. The images (see Figure 5.12) collected at the scene of the collision showed heavily contaminated railhead with leaves and debris. Which was later determined to have caused low adhesion which caused a two passenger train collision [71].





Figure 5. 12: Sample of railhead contamination recorded at the Salisbury 2021 incident

Including such images/data in the data bank of the friction prediction model like this is of extreme importance in the implementation of the friction prediction tool as it can help to prevent such accidents.

Friction measurements were also collected at the site alongside the images and environmental data as stated in section 4.5; therefore, it was possible to retrain it with this key data. The same steps highlighted in previous section were followed and a new pkl file was generated.

The 2nd retrained data had an overall log-likelihood of 298.69, giving an improved fit for the dataset.

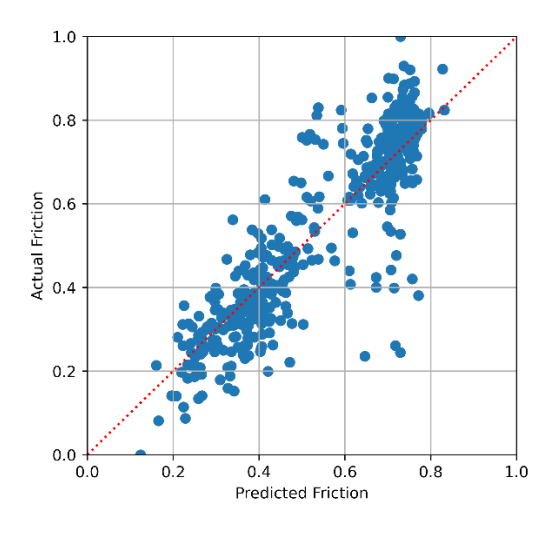


Figure 5. 13: Second retrained regression model with the leaf layers image from Salisbury

The plot shown in Figure 5.13 has a denser concentration of data point around the linear line showing the retrained prediction precision is increasing. Hence, the model should be

able to recognise leaf layer images and make a prediction, although the prediction may not be very accurate as the model needs to be trained on a larger set of leaf layer images to improve the confidence in the model for that type of data.

5.5 CONCLUSIONS

- The Prediction model tool is fully capable of been trained to give accurate friction.
- The prediction model has to be retrained as many times as possible to hold a sufficient variation of railhead conditions data to increase the confidence in its prediction and robustness of the tool's use.
- The retraining process is a continuous one and it is very dependent on the access to rail tracks to ensure different railhead conditions and friction data are collected to increase the model's data bank.
- The Pendulum tribometer is not the ideal friction measurement tool due to its poor repeatability noticed during the validation.
- Model itself is doing what it is supposed to do shown in the increase of the log likelihood through the retraining process increasing the model's fit for the data.
 Further testing should be done to determine how flexible it is to changes in the image format, basically an Image sensitivity test.
- In summary the more the training with a wide variety of data the better the reliability of the prediction output.

CHAPTER SIX

6. MODEL SENSITIVITY ANALYSIS

6.1 INTRODUCTION

The aim of model sensitivity analysis was to test the ability of the friction prediction model to process images under different conditions. The conditions being tested were:

- Railhead distance (from the camera)
- Railhead image orientation (vertically or horizontally placed)
- Lighting



Figure 6. 1: Original Image formats used in training the prediction tool

The model was trained using a set-type of images (as described in section 5.2.2.2), as shown by the examples in Figure 6.1, which were taken in very controlled conditions to ensure consistency of orientation and distance from the camera to the railhead and the resolution was good as the images have been taken statically. As the step is made to take images on the move from a train where some of these factors may change, it is important to know what effect changing them has on the friction predictions if any.

6.2 METHODOLOGY

Tests were undertaken on seven separate days in laboratory conditions. The railhead used for the tests, shown in Figure 6.2, was shiny in appearance and had been previously used for tests on the Full Scale Linear-Tribometer hence the striations (wear scar) visible in the image.

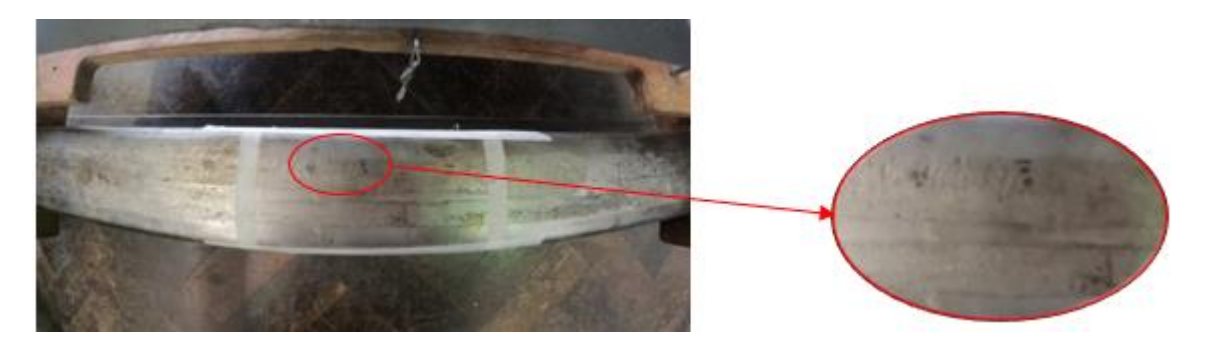


Figure 6. 2: Selected Rail section used for the sensitivity tests

The tests involved capturing input information for the friction prediction tool such as the railhead images with relative humidity, railhead and air temperatures under the stated conditions and recording corresponding friction measurements using the pendulum tribometer. The images and sensor data were processed by the model to give friction predictions. The resulting friction predictions were compared to the friction values recorded from the pendulum tribometer (converted using the BRR trib. train conversion factor [34]) to determine the correlation.

Alongside this, different railhead conditions were simulated in the laboratory to determine if the prediction tool has been trained to recognise images depicting such conditions. These conditions included either a combination of or simply:

- dry railhead,
- clean (shiny) railhead,
- wet railhead (achieved by spraying water on the railhead with a spray bottle),
- reduced wetness on railhead (achieved by lightly wiping the wet railhead with a piece of blue roll),
- oxidisation/rust (achieved by leaving the sprayed water over a period on the railhead).

It should be noted that as the tool may not have been trained for the specific rail conditions used in these laboratory tests, the tool predictions were not necessarily expected to match the measured values. The critical aspect though was how the predictions changed as lighting, railhead distance and image orientation changed.

Table 6.1 contains details of all the sensitivity tests carried out with corresponding images shown in Figures 6.5 – 6.27.

6.2.1 RAILHEAD DISTANCE

The railhead distance (distance between railhead and camera) was varied to determine if the prediction tool can accurately identify the railhead portion in an image from surrounding "clutter", see Figure 6.3. It will also aid in identifying the errors that may be encountered because of camera positioning on the train. This was done simply by moving the camera closer or further away from the railhead and capturing the images. The friction was recorded using the pendulum after the images were taken, for the railhead state, and then compared to the friction predictions from the variations of images captured.



Figure 6. 3: Railhead image taken at a height of 1450mm (L), and the distance used for the prediction tool training (between 400mm-500mm from the railhead position) (R)

Images captured in a horizontal orientation with approximately 400mm distance to the railhead were expected to give accurate results provided they were similar to previously trained data.

Each image captured has a pixel count of 5184 by 3888, the predictor tool scales the image down to 250 by 1250 to create the focus on the railhead for further processing. With the predictor tool being trained using images at approximately 450mm away from the railhead, the image scaling focused on a "rectangle" cropped out of the centre of the image which is where the railhead should be. So, in the case of Figure 6.3 (L) about 40% of the railhead portion of the image will be present in the reduced scale image and 60% will be noise from surrounding features (this increase for vertical oriented images), which can either be the floor or the pendulum tribometer and its platform, while Figure 6.3 (R) will have at least 90% of the railhead in the scaled down image window.

Varying these distances will show if the image scaling factor is applicable for the different image formats.

6.2.2 RAILHEAD IMAGE ORIENTATION

As stated in the introduction the prediction tool was trained using set parameters such as the **horizontal** orientation in the railhead images. Images were taken in the vertical orientation to see if that will affect the prediction given (see Figure 6.4 for examples of the railhead image orientation). These images were taken along with the railhead distance images under the same railhead conditions (see Section 6.2.1).



Figure 6. 4: Vertical railhead image orientation (L) Horizontal railhead image orientation (R)

The term 'non-traditional' railhead images will be used to refer to any railhead image format that differs from the original format used to train the prediction tool as shown in Figure 6.1.

Note that all 'non-traditional' horizontal and vertical orientations images included below have been cropped to fit into the pages. Hence the distance of the railhead cannot be judged using the images below, but the prediction tool has been fed with the raw (uncropped) images (refer to Figure 6.3 for clearer view of the distances).

6.2.3 VIDEO CAPTURE/FREEZE FRAME IMAGES

Later in the testing, video capturing of the railhead was included in the tests, with the aim of examining if/how well the prediction tool would process the freeze frame images from video capture resolutions. These images were not taken at high speed. They were in fact captured in a slow pan over the railhead using the GoPro camera while handheld. Therefore, this test will not account for variations experienced on a train in motion at either slow or high speed. The videos were taken in a horizontal and vertical orientation.

Table 6. 1: Full list of prediction tool sensitivity tests

Test Date	Test No.	Railhead state/Preparation	Air Temp, °C	Relative Humidity, %	Dew point, °C	Rail Temp, °C	Railhead Image	Average measured μ (from 8 repeats)	Image orientation capture
13-04-	1	Unclean railhead, dry (that is the original state of the railhead)		46.1	9.7	25.5	Figure 6.5	0.209	Horizontal Vertical
		Cleaned with alcohol wipes.	23.7	41.5	9.7	25.7	Figure 6.6	0.254	Horizontal Vertical
		Cleaned with a wire brush.	23.9	41.4	9.9	25.7	Figure 6.7	0.283	Horizontal Vertical
		Sprayed with water to simulate moisture presence and start the process of rusting.	24.1	40.2	9.7	24.9	Figure 6.8	0.084	Horizontal Vertical
14-04- 22	2	Results from previous (day1)	21.3	41.9	7.7	24.7	Figure 6.9	0.314	Horizontal Vertical

		wetting (dry state)							
		First spray of water	21.8	40.2	7.7	25.2	Figure 6.10	0.098	Horizontal Vertical
		Second spray of water	22.3	39	7.5	25.3	Figure 6.11	0.104	Horizontal Vertical
20-04-	3	Rust day1 (1st appearance of oxidisation)	22	58.2	13.2	25.7	Figure 6.12	0.338	Horizontal Vertical
		Rust day1 and water	23.1	57.4	14	26.1	Figure 6.13	0.170	Horizontal Vertical
21-04-	4	Rust day2	21.8	53.6	12.1	26.2	Figure 6.14	0.365	Horizontal Vertical
		Rust day2 and water	23.1	52.7	12.7	26.1	Figure 6.15	0.235	Horizontal Vertical
		Rust day2 and reduced water	23.5	50.4	12.5	26.7	Figure 6.16	0.221	Horizontal Vertical

26-04- 22	5	Rust day3	20.4	42.9	7.3	23.8	Figure 6.17	0.340	Horizontal Vertical
		Rust day3 and water	21	42.6	7.9	23	Figure 6.18	0.217	Horizontal Vertical
		Rust day3 and reduced water	21.3	42.1	7.6	22.8	Figure 6.19	0.208	Horizontal Vertical
04-05- 22	6	Rust day4	21.9	65.9	15.1	25.5	Figure 6.20	0.459	Horizontal Vertical
10-05- 22	7	Rust day5	23.7	58.2	14.9	26.7	Figure 6.22	0.423	Horizontal Vertical
		Rust day5 and water	24.5	56.5	15.2	26.4	Figure 6.23	0.236	Horizontal Vertical
		Rust day5 and reduced water	25.1	56.5	15.9	27.4	Figure 6.24	0.222	Horizontal Vertical
	6&7	Freeze frame images					Figure 6.21 & 25-27		



Figure 6. 5: Example of railhead images for uncleaned state. Horizontal with camerarailhead distance ≈ 450 mm distance (L) and vertical with camera-railhead distance ≈ 1450 mm (R) (13-04-22)



Figure 6. 6: Example of railhead images for cleaned with alcohol wipe. Horizontal with camera-railhead distance ≈ 500 mm (L) and vertical with camera-railhead distance ≈ 900 mm (R) (13-04-22)



Figure 6. 7: Example of railhead images for cleaned with wire brush. Horizontal with camera-railhead distance \approx 1450mm (L) and vertical with camera-railhead distance \approx 1450mm (R) (13-04-22)



Figure 6. 8: Example of railhead images for water spray. Horizontal with camera-



Figure 6. 9: Example of railhead images for previous day wet. Horizontal with camera-



Figure 6. 10: Example of railhead images for 1st water spray. Horizontal with camera-railhead distance \approx 1450mm distance (L) and vertical with

railhead distance ≈ 900 mm (L) and vertical with camera-railhead distance ≈ 450 mm (R) (13-04-22)

railhead distance ≈ 1450 mm distance (L) and vertical with camera-railhead distance ≈ 1000 mm (R) (14-04-22)

camera-railhead distance \approx 1200mm (R) (14-04-22)



Figure 6. 11: Example of railhead images for 2nd water spray. Horizontal with camerarailhead distance \approx 1450mm distance (L) and vertical with camera-railhead distance \approx 600mm (R) (14-04-22)



Figure 6. 12: Example of railhead images for 1st appearance of rust. Horizontal with camera-railhead distance \approx 1450mm distance (L) and vertical with camera-railhead distance \approx 900mm (R) (20-04-22)



Figure 6. 13: Example of railhead images for rust1 + water. Horizontal with camera-railhead distance \approx 1000mm distance (L) and vertical with camera-railhead distance \approx 1000mm (R) (20-04-22)



Figure 6. 14: Example of railhead images for rust day2. Horizontal with camera-railhead distance ≈ 300 mm distance (L) and vertical with camera-railhead distance ≈ 700 mm (R) (21-04-22)



Figure 6. 15: Example of railhead images for rust day2 + water. Horizontal with camerarailhead distance \approx 450mm distance (L) and vertical with camera-railhead distance \approx 700mm (R) (21-04-22)



Figure 6. 16: Example of railhead images for rust day2 +2nd water spray. Horizontal with camera-railhead distance ≈ 450 mm distance (L) and vertical with camera-railhead distance ≈ 1000 mm (R) (21-04-22)







Figure 6. 19: Example of railhead images for rust day3 +reduced water spray. Horizontal with camera-railhead

Figure 6. 17: Example of railhead images for rust day3. Horizontal with camera-railhead distance ≈ 450 mm distance (L) and vertical with camera-railhead distance ≈ 900 mm (R) (26-04-22)

Figure 6. 18: Example of railhead images for rust day3 + water spray. Horizontal with camera-railhead distance \approx 450mm distance (L) and vertical with camera-railhead distance \approx 450mm (R) (26-04-22)

distance \approx 400mm distance (L) and vertical with camera-railhead distance \approx 500mm (R) (26-04-22)



Figure 6. 20: Example of railhead images for rust day4. Horizontal with camera-railhead distance ≈ 1450 mm distance (L) and vertical with camera-railhead distance ≈ 450 mm (R) format (04-05-22)



Figure 6. 21: Freeze frame images captures from railhead videos for rust day4 (04-05-22)



Figure 6. 22: Example of railhead images for rust day5. Horizontal with camera-railhead distance ≈ 450 mm distance (L) and vertical with camera-railhead distance ≈ 1000 mm (R) (10-05-22)



Figure 6. 23: Example of railhead images for rust day5 + water spray. Horizontal with camera-railhead distance \approx 1450mm distance (L) and vertical with camera-railhead distance \approx 1000mm (R) (10-05-22)



Figure 6. 24: Example of railhead images for rust day5 + reduced water spray. Horizontal with camera-railhead distance ≈ 450 mm distance (L) and vertical with camera-railhead distance ≈ 1000 mm (R) (10-05-22)

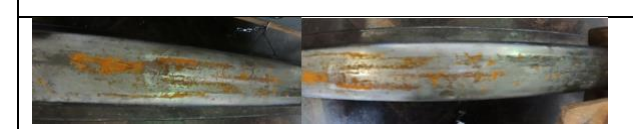


Figure 6. 25: Freeze frame images captures from railhead videos for rust day5 (10-05-22)



Figure 6. 26: Freeze frame images captures from railhead videos for rust day5 + water spray (10-05-22)



Figure 6. 27: Freeze frame images captures from railhead videos for rust day5 + water spray (10-05-22)

6.3 RESULTS

The data collected from the tests for all image formats used, for each railhead condition was processed using to the AI tool to make a friction prediction and then compared to the measured friction. Each railhead condition captured had images taken in the horizontal and vertical orientation with camera-railhead distance varied for both orientations.

The results were then classified into similar railhead conditions in order to easily identify what type of conditions the prediction has been trained on and which type has to be considered for future training.

For the purpose of the results graphs in this section and following discussion, the camerarailhead distances have been summarised as:

- Very close ≤ 350mm
- Close 351mm 650mm
- Midway 651mm 1000mm
- Far > 1000mm

The distance and orientation of the data points have been highlighted on the graphs using the following keys:

Distance Orientation	Very close	Close	Midway	Far
Horizontal				
Vertical	0	0	0	0

The ideal form of image used in the prediction tool is the horizontal-close image (\square) .

Figure 6.28 shows the predicted versus measured friction for all the tests carried out. It clearly shows the areas where the prediction tool values are accurately clustered around the line indicating actual = predicted, whereas the points farther away from the linear line indicated inaccurate predictions. The railhead conditions with insufficient training will be narrowed down in the results subsections.

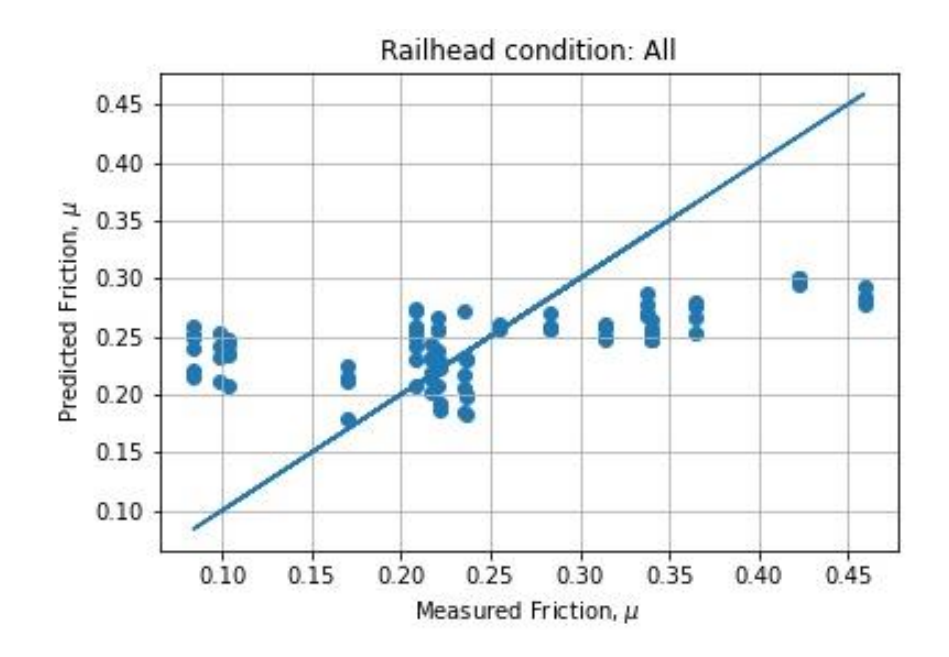


Figure 6. 28: All sensitivity tests results

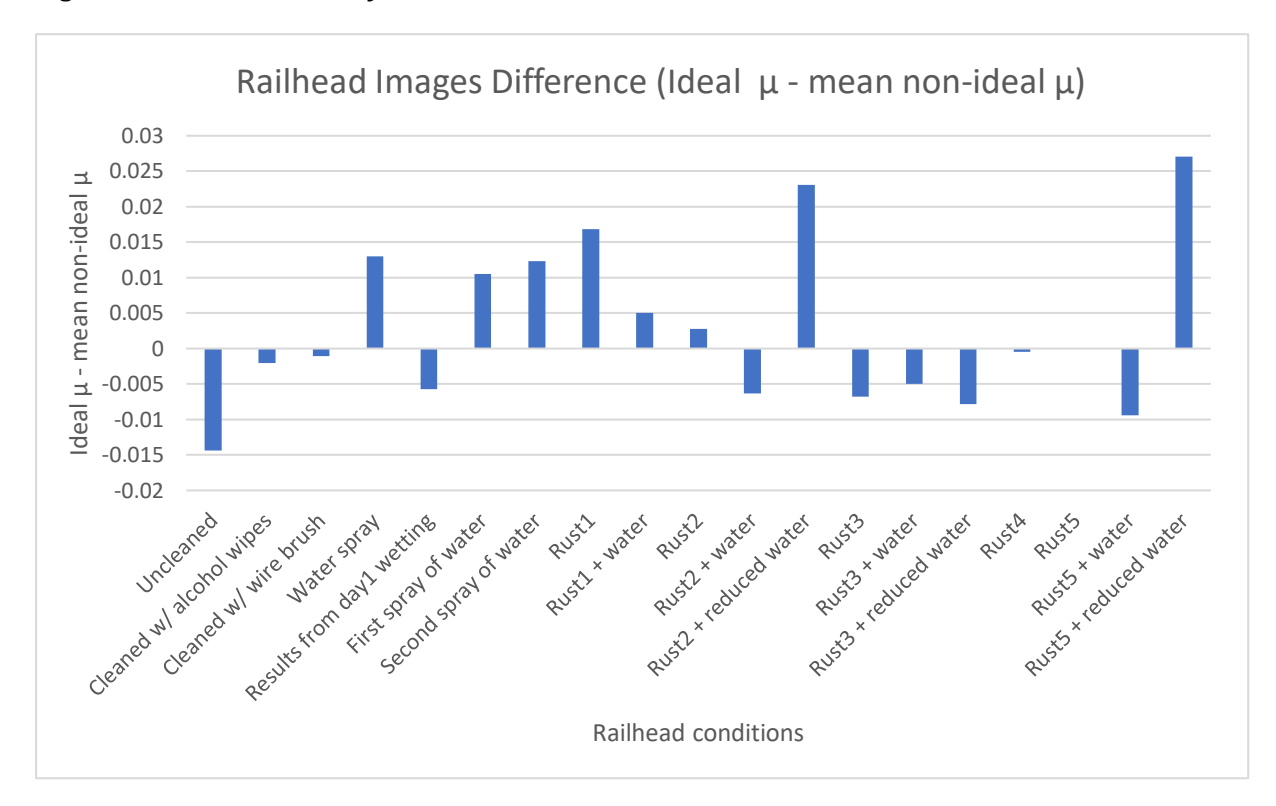


Figure 6. 29: Difference in Ideal image and mean non-ideal image predicted frictions

In order to quantify the spread between data collected for the same conditions, the prediction from the ideal form of railhead image marked as has been compared to the mean value of the other variations of railhead image capture. This summary of this analysis is shown in Figure 6.29. The difference shows if most of the non-ideal image predicted data is under predicting (positive) or over predicting (negative) when compared to the ideal image, therefore giving a statistical insight into the variations. Generally, the closer the variation is to 0, the lower the spread in the data.

6.3.1 DRY RAILHEAD CONDITIONS

Four dry railhead states were tested on day 1 and 2 (see Table 6.1) and images were taken in the formats stated in the methodology.

The plot in Figure 6.30 shows the comparison of the predicted railhead friction to the measured friction, with an actual = predicted line to judge the accuracy of the tool.

The results recorded from the day 1 cleaned (with alcohol wipes) railhead had near accurate predictions while the other 3 conditions were not very accurate.

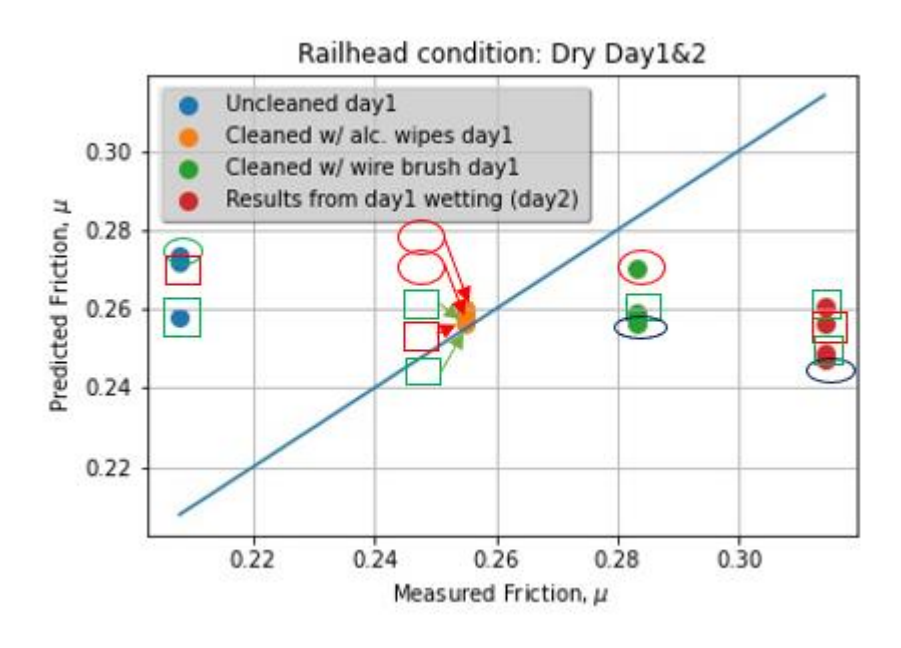


Figure 6. 30: Sensitivity test results for Dry Railhead Day 1 & 2

In general, the horizontal-close image yielded results closer to the measured friction which is as expected with exception of day 1 wire brushed condition where the prediction of the vertical-far image of 0.271 was closer to the measured friction of 0.283 while the horizontal-close images had predictions closer to 0.26. As stated earlier the prediction tool has not been trained on these data sets, but the tool analyses the railhead by categorising the colours. So, in a situation of farther camera-railhead distances, the model's reduced scale image may include the rail foot and/or surrounding sections such as a floor in the case here. The floor in the image is brown (see Figure 6.4 for reference) and the tool will process it as a state such as oxidisation. This is expected to be a recurring factor where predictions look more accurate for images taken at a further distance from the railhead.

6.3.2 WET RAILHEAD CONDITIONS

Three different wet railhead conditions were tested on day 1 and 2 shown in Table 6.1.

The plot in Figure 6.31 shows the comparison of the predicted railhead friction to the measured friction, with an actual = predicted line to judge the accuracy of the tool. From first glance all the results for this railhead condition were over predicted by the tool. This

can partly be attributed to the presentation of moisture on the railhead as not being representative of what appears in the field captured images where generally the rail was very wet.

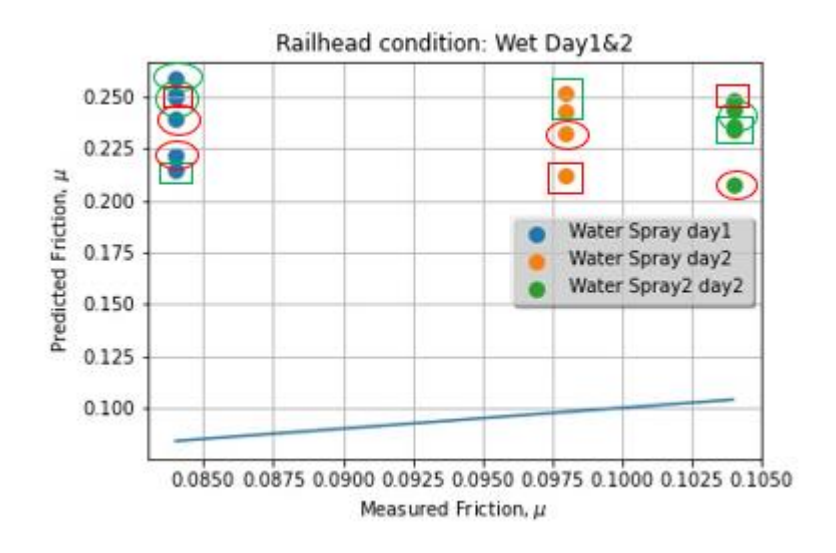


Figure 6. 31: Sensitivity test results for Wet Railhead Day 1 & 2

Looking at Figure 6.31, images taken with same orientation and a close camera-railhead distance (that is green squares or ovals), but with repeats have yielded similar predictions. Whereas the inclusion of varied images has significantly increased the differences from the mean value in comparison to that of the dry railhead conditions, they have image differences in ranging from 0.0105 to 0.0129.

This once again is a common characteristic, more noticeable variations in the predicted friction are noticed when the distance or orientation is changed due to the alteration occurring in the reduced scale image position.

6.3.3 OXIDISED RAILHEAD CONDITIONS

The last spray of water on the railhead done on days 1 and 2 were left on to encourage occurrence of oxidisation to vary the railhead conditions. The first appearance of oxidisation was recorded on the third day of testing seen in Figure 6.12.

Following the appearance of the first sign of oxidisation, the process of leaving water on the railhead was continued to produce more rust as shown in Table 6.1 and in Figures 6.14, 6.17, 6.20 & 6.22. The results showing the comparison of the predicted railhead friction to the measured friction from the 5 oxidisation states recorded over five test day is shown in Figure 6.32.

The results on Figure 6.32 (a) and (b) show the prediction tool under predicted the friction for all 5 railhead conditions. The reasons may also be attributed to the presentation of oxidisation on the railhead being different to how it actually appeared in the field where the original measurements were carried out.

The images taken in similar orientations and distances once again produced very similar results for these tests. The highest range recorded on rust day3 for horizontal-close images was 0.005, with an image difference mean value for the test day at -0.00676. Showing an over prediction in the mean variation compared to the ideal image. Although it has lower spread in comparison to the wet results, the different image orientations have played a significant role in the variation noticed.

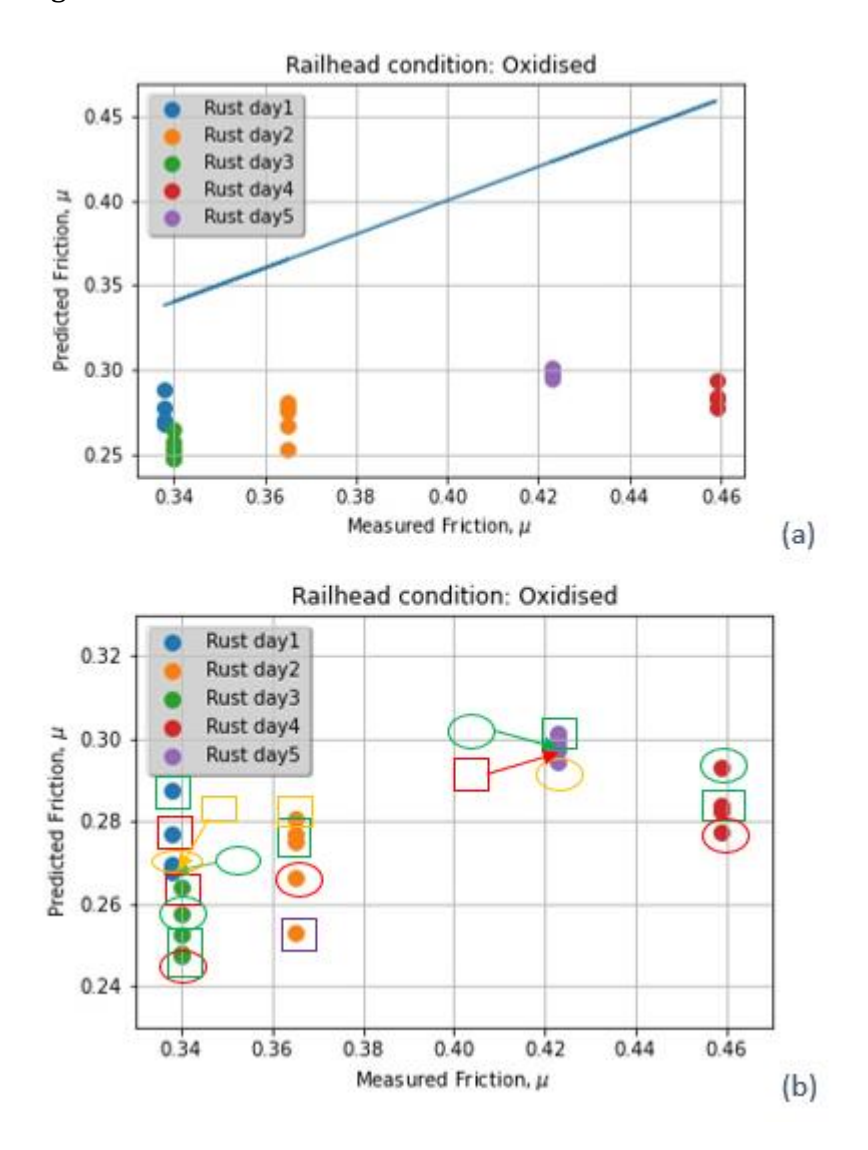


Figure 6. 32: (a) Sensitivity test results for different levels of railhead oxidation (b) Increased scale plot for better visualisation of data point

The same is true for all dry oxidised test, with "rust day5" having a near zero variation at 6.7×10^{-5} .

6.3.4 OXIDISED + WET RAILHEAD CONDITIONS

After recording the data set for the oxidised conditions, water was sprayed on the railhead to simulate moisture on the railhead (as stated in Table 6.1).

The images collected from this railhead condition are shown in Figures 6.13, 6.15, 6.18 & 6.23 were plot shown in Figure 6.33. This was done to show the comparison of the predicted railhead friction to the measured friction with an actual = predicted line to help judge the accuracy.

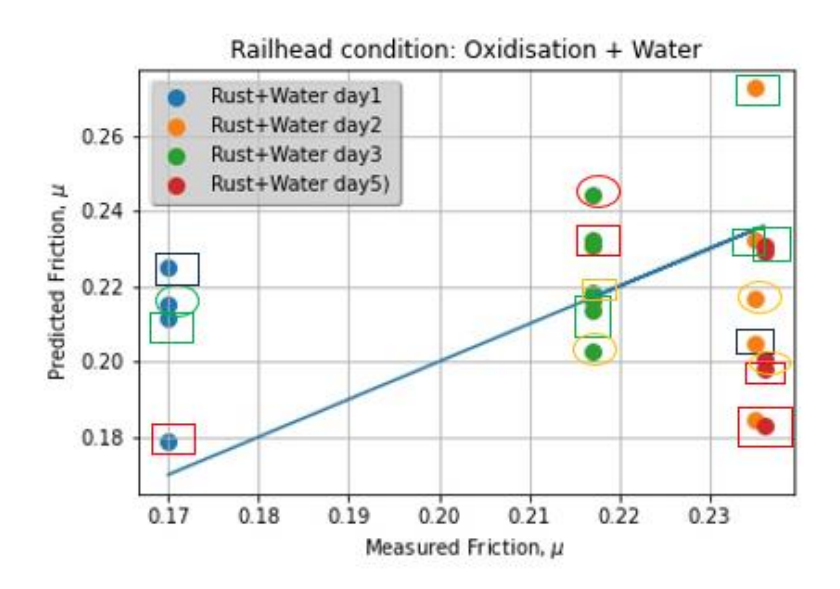


Figure 6. 33: Sensitivity test results for different levels of railhead oxidation+ water

The results shown in Figure 6.33 have a mix of under prediction and more of over prediction for the different test days. At the same time the tool made 3 accurate predictions as seen for Rust+water "day2", "day3" and "day5", although with differences to mean non-ideal image prediction of -0.00635, -0.00496 and -0.0094 respectively. The variation noticed in the prediction on those days were because of the non-traditional images and once again the misrepresentation of those conditions recreated in the laboratory. The results once again showed a majority of horizontal-close image gave predictions closer to the measured friction whereas the prediction for "rust+water day1" had a similar scenario as that of dry railhead conditions for the same reasons explained for those tests.

6.3.5 OXIDISED + REDUCED WET RAILHEAD CONDITIONS

This dataset was collected on the same test days as section 6.3.4 except Rust day1. The difference is that the water spray on the railhead was lightly wiped off to try to simulate a more realistic wet-rail appearance as seen in Figures 6.16, 6.19 & 6.24.

Figure 6.34 shows the comparison of the predicted railhead friction to the measured friction with an actual = predicted line from the 3 oxidised+reduced wet railhead states recorded over 3 test days.

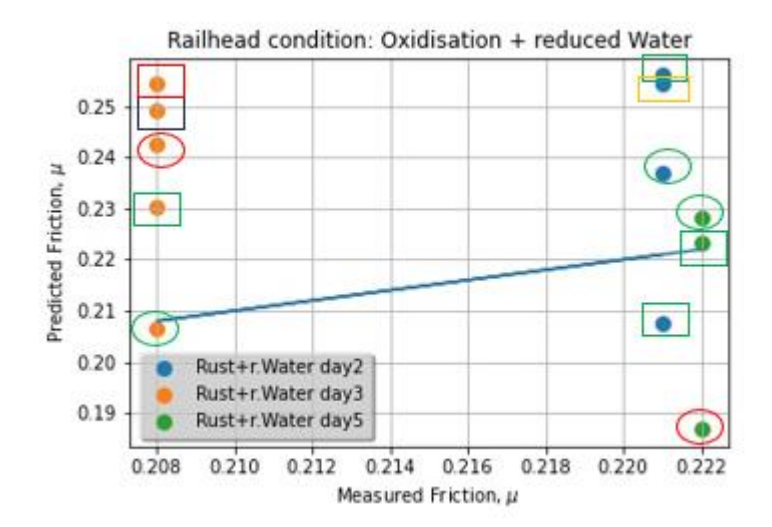


Figure 6. 34: Sensitivity test results for different levels of railhead oxidation+ reduced water

The results are similar to that of the "oxidised+wet railhead" condition and the variation can be accounted for by similar reasons.

6.3.6 Freeze Frame images.

The freeze frame images captured from videos taken on the last 2 days of testing, showed that taking such images from videos is viable, but only at handheld speed. The video was slow enough to allow paused clips in the video to show undistorted images with good enough resolution for the to the tool to process.

The images extracted from each video were more than the still images captured which it makes tricky to present in graphical form. The results have been present in a tabular form with the prediction from still images and video freeze frame images in separate column.

The difference in the freeze frame prediction and the image prediction was captured in the third column of table 6.2 by subtracting the video freeze frame prediction from the average of the image prediction in the second the column for each condition, showing how the prediction of the freeze frame images varied to that of the already used still image capture.

Table 6. 2: Comparison of prediction results from still images and freeze frame images.

Railhead Condition	Video Freeze Frame Image Predictions	Images Friction Predictions	Difference (Image- Freeze frame) Predictions
Rust Day4	0.290	0.284	-0.006
	0.294	0.282	-0.010
	0.295	0.277	-0.011

	0.302	0.293	-0.018
	0.297		-0.013
	0.295		-0.011
	0.294		-0.010
	0.296		-0.012
	0.296		-0.012
	0.297		-0.013
	0.295		-0.011
	0.293		-0.009
	0.294		-0.010
Rust Day5	0.286	0.301	0.012
	0.286	0.298	0.012
	0.258	0.300	0.040
	0.256	0.294	0.042
	0.283	0.297	0.015
	0.286		0.012
	0.290		0.008
	0.295		0.003
	0.295		0.003
	0.298		0
	0.297		0.001
	0.297		0.001
	0.297		0.001
Rust Day5 + water	0.244	0.201	-0.036
- Water	0.240	0.229	-0.032
	0.229	0.198	-0.021

0.225	0.183	-0.017
0.226	0.231	-0.018
0.229		-0.021
0.229		-0.021
0.241		-0.033
0.240		-0.032
0.243		-0.035
0.243		-0.035
0.242		-0.034
0.238		-0.030
0.239		-0.031
0.236		-0.028

6.4 DISCUSSION

Generally, looking at the tool's sensitivity to changes in the image formats, it can be seen for each set of predictions for different railhead state there is a change to the values predicted for the railhead orientation, distance, and image quality this is more noticeable in Figures 6.30, 6.31, 6.33 and 6.34. The variation noticed in the results grows wider when camera distance to the railhead is taken further away, the data points usually farthest from the actual = predicted line on the point often falls in the "red zone" category which signifies the farthest camera-railhead distance. This is because the amount of noise in the image increases hence making it difficult for the tool to correctly identify the railhead section in the image. Although, as explained in the results section, the noise may also provide false predictions that may look accurate depending on the colours in the railhead surrounding.

Therefore, the prediction tool can process data from 'non-traditional' image formats from a close distance to the railhead with some variation to the original horizontal format but may not be accurate depending on the circumstance.

The predictions for wet rail scenarios had a wider data spread when analysed on the image difference chart in Figure 6.29, with Rust day2 + reduced water having the highest difference at 0.0231 in image variation with under predictions compared to the ideal image prediction. This is mainly due to bad correlation of the laboratory environment to the field environment used to train the prediction as well as the unrealistic appearance

of moisture on the railhead. This created several uncertainties around the predictions for wet railheads.

6.4.1 DRY RAILHEAD CONDITIONS

The results (Figure 6.30) from the dry railhead states show accurate prediction for railhead samples cleaned with alcohol wipes (Figure 6.6) with some under prediction variation noted for the non-traditional image formats. The uncleaned original railhead as seen in Figure 6.5 produced over predicted friction while the railhead cleaned with wire brush and the day2 railhead state from day1 wetting were showing under predicted friction from the tool.

Referring back to images in Figures 6.5-6.7 & 6.9 and the images used to train and retrain the prediction tool (see Figure 6.35 for example), the images in Figure 6 are not similar to any of the training images, hence the prediction tool cannot accurately identify and give a friction value for these set of railhead states. Also, railheads in service usually do not appear this shiny with wear scars and the tool has been trained on field/in-service railhead images to give an accurate prediction for real-time train activity. The spread shown in each set of prediction (see Figure 6.29) also confirms the tool's sensitivity to image formats used for prediction. The differences found in ideal – mean non-ideal image prediction were found to be closer to 0 at -0.00204, -0.00105 & -0.00571 for "cleaned with alcohol wipes", "cleaned with wire brush" and "results from day1 wetting" railhead conditions respectively. This implies the tool has good repeatability for this type of railhead conditions disregarding the accuracy levels.



Figure 6. 35: Example of railhead image capture in-field

6.4.2 WET RAILHEAD CONDITIONS

The wet condition without oxidisation yielded some interesting result, due to high over prediction of the tool as seen in Figure 6.31. The measure friction ranged between from 0.08 to 0.104 while the predicted friction ranged from 0.19 to 0.27. Merely looking at the wet rail images simulated in the laboratory, they do not depict a realistic wet rail image seen in the field. It is fairly difficult to create the appearance of dew, light or heavy rainfall by spraying water (uniform-like moisture distribution as seen in Figure 6.36) on the railhead surface in the laboratory, so a difference in predicted friction was expected, but not to this extent.



Figure 6. 36: Image of wet railhead captured in field

In addition to the difference in wet rail image presentation, the relative humidity for simulated moisture on the railhead measured in-lab did not depict the real values measured in the field. From field data obtained earlier in this work, relative humidity for moisture on the railhead is usually greater than 70%, but the relative humidity measured in-lab is a function of the laboratory environment as opposed to the railhead state being simulated. The highest relative humidity recorded in the laboratory throughout the testing period, as seen in Table 6.1, was 57.4% and 65.9% in a wet and dry instance respectively. This shows that the prediction is sensitive to changes in environmental conditions and depends on accurate environmental information. These factors also contribute largely to the wide variation in the wet railhead data collected, where the ideal – mean non-ideal image of 0.0129, 0.0105 & 0.0123 for "water spray day1", "water spray1 day2 and "water spray2 day2" railhead condition respectively were noted for the predictions. There was an under prediction in the data set compared to the ideal image prediction.

Figure 6.37 shows comparison of results for the images processed for wet railhead conditions, but with relative humidity expected for infield scenarios. The image on the left shows lower predicted frictions with the increase in relative humidity representing in field environment, although not "spot-on" accurate, but closer to the measured versus measured line. Whereas the relative humidity recorded in the laboratory (shown on the right) has its prediction further away from the measured versus measured line.

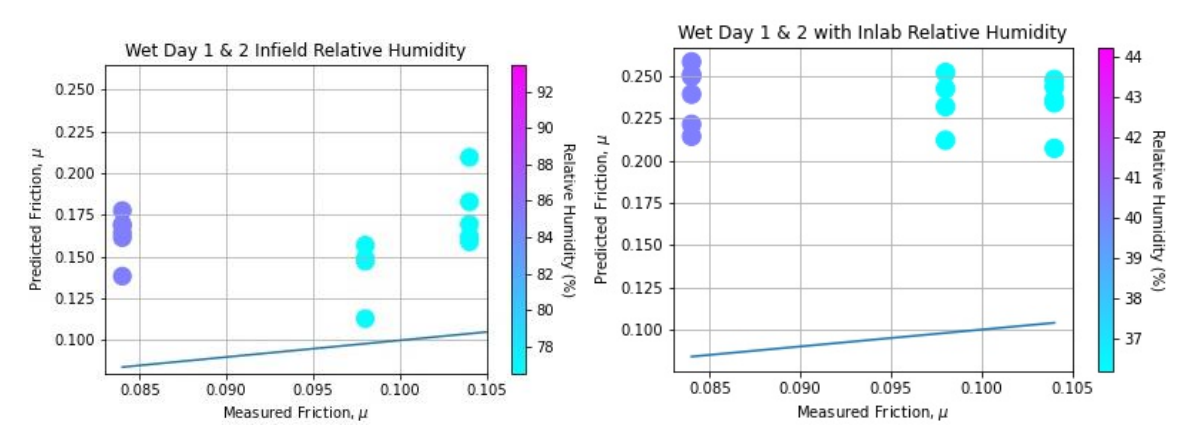


Figure 6. 37: Prediction for wet railhead condition using in field RH (L) and prediction for laboratory RH (R)

This furthermore emphasises the prediction tool's sensitivity to changes in environmental factors in the prediction of friction. The relative humidity difference will be a factor in the other wet railhead conditions considered in this sensitivity test.

6.4.3 OXIDISED RAILHEAD CONDITIONS

Looking at Figure 6.33 for the results of all the scenarios of rust appearance on the railhead, measured friction values were high on the pendulum tribometer (from 0.33 to 0.46) and the model under predicted friction values of 0.20 to 0.28.

The predictions for the traditional images (datapoints) were closer to the actual = predicted line than the non-traditional image. Although all the results where under predictions with a good variance, showing the predictions from the model were close to mean predictions (see Figure 6.29)



Figure 6. 38: Example of oxidised railhead image captured infield

These results once again highlight missing railhead conditions used to the train the prediction tool. Looking at the oxidised railhead image from the field measurement in Figure 4.12 (also see Figure 6.38) compared to the laboratory simulated oxidised state in Figure 6.12, 6.14, 6.17, 6.20 & 6.22 one can argue that the appearance of the oxidisation is not uniform, unlike what an actual oxidised field railhead looks like. Most importantly the colours are more concentrated and sharper than an in-field oxidised railhead. Therefore, the under-prediction experienced in the oxidised railhead condition is as result of the images being alien to the prediction tool.

The environmental conditions recorded in the laboratory were also higher on average to what was recorded while collecting data to train the prediction tool. This highlights the importance of the continuous training of the prediction tool to include a robust dataset, covering a vast range of railhead condition and environmental conditions.

The variations noticed here are not widespread (see Figure 6.29), this indicates good repeatability of the prediction tool because for each railhead condition only 1 image was categorised as "Far" with exception of "Rust day3" having 2 images. In addition, the far

images may have produced false predictions because of the noise around the railhead section. But generally, images with similar orientation and distances produce very similar predictions especially noticed on horizontal-close images (which were taken multiple times), re-indicating the tool's good repeatability for each image format.

6.4.4 OXIDISED + WET RAILHEAD CONDITIONS

The prediction tool mostly over predicted the friction for the oxidised+wet railhead condition as seen Figure 6.33. When water was introduced to the later oxidised railhead (i.e., day2, 3 & 5), the vibrant orange colour became deeper and looked more like a realistically presented oxidised wet railhead, therefore producing accurate predictions for these scenarios. While day1 which was just splotch of oxidisation on the railhead which still look unreal, was over-predicted.

For each day of results, a wide spread of data with image differences 0.00499, -0.00635, -0.00496 & -0.00939 (as shown in Figure 6.29) in the predicted results can be noticed. The difference noted for day1 showed and under prediction when compared to the ideal image while the rest of the days showed over predictions with the negative differences. This shows the effects of the non-traditional images especially varied distances as stated earlier as seen the plot. The increased noise and unfamiliar railhead conditions increases the variables in getting an inaccurate prediction.

Figure 6.33 rust + water day1 results (shown in blue) appears to be contrary to the expectation. In this case, the horizontal (far) images were giving closer predictions to the measured friction. What has happened here is due to farther distance of the camera to the railhead, the railhead image quality is reduced and also not positioned in the centre hence the scaled images have included parts of the brown flooring which have has been processed and given a prediction.

6.4.5 OXIDISED + REDUCED WET RAILHEAD CONDITIONS

This railhead state had 1 prediction in each test day in close accuracy range, although the other result varied widely mostly across the over predicted zone and 1 under prediction each for day 3 & 5. The variation in the results is due to the same reasons as the oxidised+wet states.

6.4.6 FREEZE FRAME IMAGES

There are variations in each of the freeze frame images which simply because the sections of the railhead been analyse is changing with each image as well as the orientation. These are one of the reasons it is difficult make a comparison to still image results for the same railhead. The predictions from the freeze frame images were subtracted from the mean predictions of the still images (seen on table 6.3) to show how far off or close they were to the original prediction. The calculated difference showed the dynamic nature of the freeze frame images compared to the still images as the difference values varied along the images.

Using video capture with a Go Pro Hero camera at train running will not be viable for image capture as the images will be too blurry and of low resolution, so the tool will not be able to process them. This method is only useful when the videos are captured at slow walking pace as this the only time the images extracted will be viable for predictions.

6.5 CONCLUSIONS

- Laboratory tests were useful in testing the sensitivity of the prediction tool, showing the variations for different predictions under different railhead condition. The tests helped to highlight uncertainty that results from the noise in images.
- These tests have helped to highlight the type of railhead states missing from the trained dataset such as shiny railhead. Therefore, indicating what type of new data, the prediction tools need to be trained on.
- The tests have shown that the prediction tool has good repeatability for multiple images taken in similar orientation and distance regardless of the correlation to the measured friction.
- The prediction tool gave incorrect predictions for some of the railhead conditions that were simulated in the laboratory because they were not representation of the field data it had been trained on. It also confirmed that the tool correctly takes the environmental conditions into account when making predictions.
- Further in-field training is required to increase the robustness of the prediction tool. As it has been established that the environmental conditions in the laboratory to imitate or correctly depict that of the field.

CHAPTER SEVEN

7. ON-TRAIN DATA CAPTURE SENSOR DESIGN

7.1 INTRODUCTION

After establishing the sensitivity of the prediction tool to camera-railhead distance and railhead orientation, as detailed in Chapter 6, a system had to be put in place to capture images alongside environmental data from a moving train to trial dynamic data capture to feed into the model.

The proposed system was required to capture railhead images at a very close distance between 350-400mm as well as forward facing images, it needed to have sensors for measurement of relative humidity, railhead and air temperature integrated into it. It also needed to record all the data on the same interface.

A design specification was developed for the data capture system which is shown in Table 7.1. These characteristics were selected based on the preferred functionality for the proposed data capture system. Features like operational and recorded temperature ranges were estimated based on UK historical weather data [78] and data recorded manually that was analysed in Chapter 4. The materials used for manufacture had to be up to the British Standards, for example BS 4929 & BS 4320 (for Steel), BS EN 755-2:2016 & BS 485-2:2016 (for Aluminium) and BS 857 (for laminated glass).

Table 7. 1: Design specification for on-train data capture system

Category	Features
Functionality	Capture forward facing and railhead images
	House and protect sensor from external and environmental
	factor
	Easily attachable to and removable from the train
	Located outside on the train
	Capture relative humidity railhead and air temperature
	Record location of data capture
	Portable
	Should be able to last 12 hours on DC supply
Performance	Forward camera: High definition (HD)
	Railhead camera: minimum 2MP and lens focal length
	50mm
	Temperature ranges recorded -10°C to 45°C
	Operating temperature ranges -10°C to 50°C
	DC power supply of 17 000 to 20 000 mAh
	Net weight: ≤ 7kg
	GPS sensitivity: minimum -90dBm
Material	Widely available material like Steel and/or Aluminium
requirement	Robust material to prevent damage to internal components
	in case of fall
	Laminated toughened glass for window openings
Legal	Approved by network rail to be attached on a train body
	Must fit necessary British Standards (will not be approved
	by Network Rail if it does not)

7.2 DESIGN PROCESS

Three methods for the data capture design were considered for this work while two of them were finally explored. The following methods were considered for the on-board train data capture:

- camera mounted somewhere on the front of the train,
- adapt an existing design/system used to capture images or videos. Typically, an enclosure that can hold sensors for additional data collection.
- and design a brand-new system.

Figure 7.1 shows a summary of the methods considered.

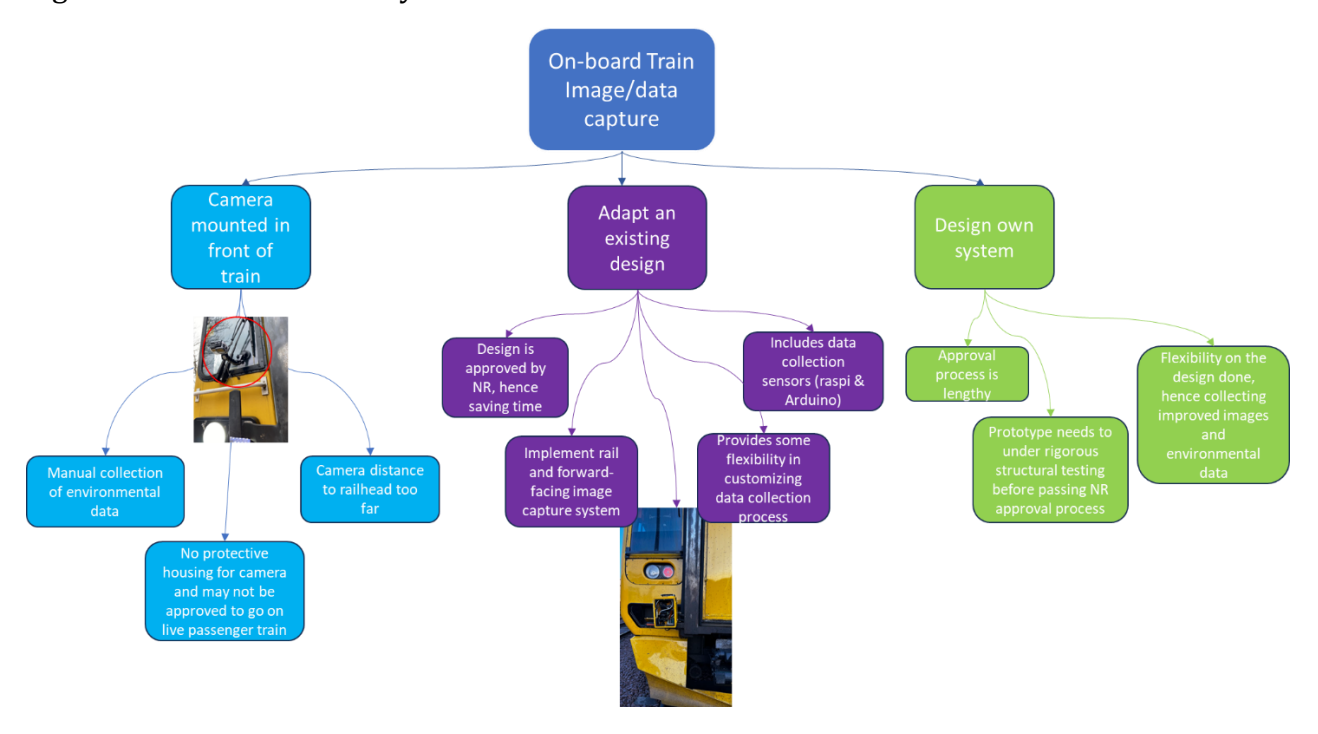


Figure 7. 1: Chart showing the processes considered for the On-board train data capture

The first two methods were trialled (the second was selected) while the third method was not explored because of numerous constraints, some highlighted in Figure 7.1. Designing a brand-new system is time consuming as it would have been required to undergo structural testing (after the lengthy prototype design process) to make sure it was safe and strong enough to be mounted/placed on an in-service train. It would also have had to be approved by Network Rail after establishing it was safe to be used by the designer. The time needed for this was not available for this project, nor was there budget available.

The details of the trials carried out are shown in the following sub-sections.

7.2.1 CAMERA MOUNTED IN FRONT OF TRAIN

A rudimentary design was created for a front of train mountable system to go on a Northern Trains Class 153. The design simply contained a GoPro Hero 8, a suction mount, an extension arm and a flexible light weight steel wire with lock clutches (for security/safety purposes). The aim of this design was to capture the railhead images only (as a start) with the environmental data collected manually.

Two points on the front of the train were considered for the mounting of any type of data capture system. These two points were the lamp bracket holder and handlebar, both circled in red in Figure 7.2.

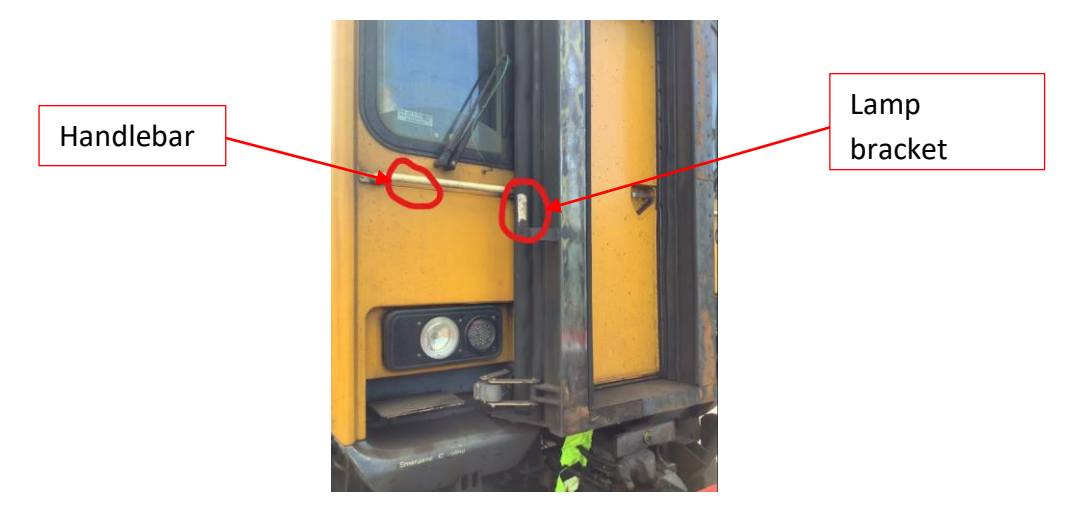


Figure 7. 2: Front of Class 153 train highlighting the possibly mounting positions

The first opportunity to collect data arose on the Monk Bretton freight branch line route on 2^{nd} April 2022 through a Northern Trains driver training session. I was allowed to mount the camera system on the front of a Class 153 train.

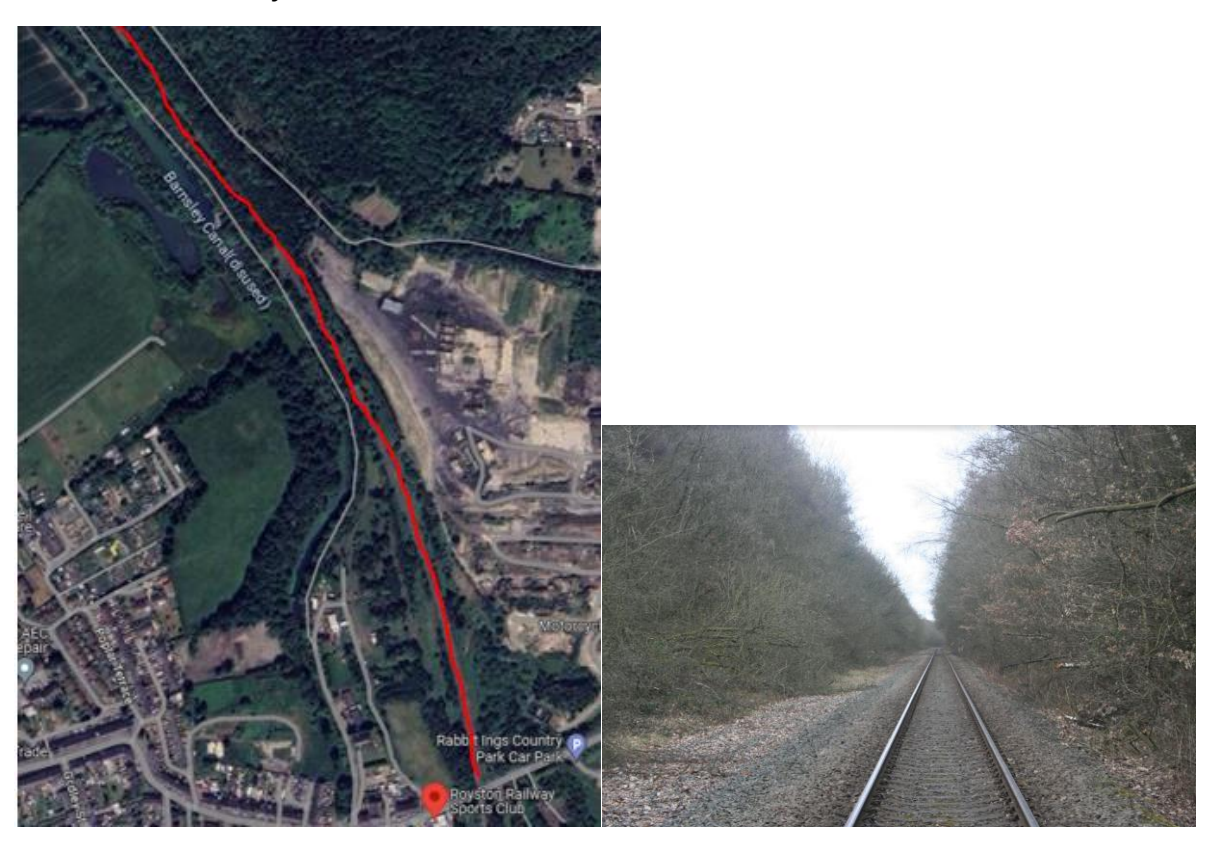


Figure 7. 3: Google earth image of the track used in Monk Bretton [79] (L) Section of track with encroaching vegetation (R)

Figure 7.3 (left) shows the track route used in Monk Bretton highlighted in red where some sections of the rail track had dense vegetation coverage over it, as shown in the image on the right.

A GoPro supplied suction cup was used to mount an extended arm holding the camera pointing downwards towards the railhead, in an attempt to capture images from a moving train. The full set-up was secured to the handlebar using a light-weight steel wire to keep it attached to the body of the train in the event of the suction cup failing and the camera set-up falling off. This would help prevent damage to the set-up and potential incidents caused by debris on the track. The full set-up is shown in Figure 7.4.

The trial process involved using the GoPro camera to record videos over the length of the journey and then manually capture freeze frame images from the videos. An example of freeze frame images extracted from the video captured at Monk Bretton is seen in Figure 7.11 (L).

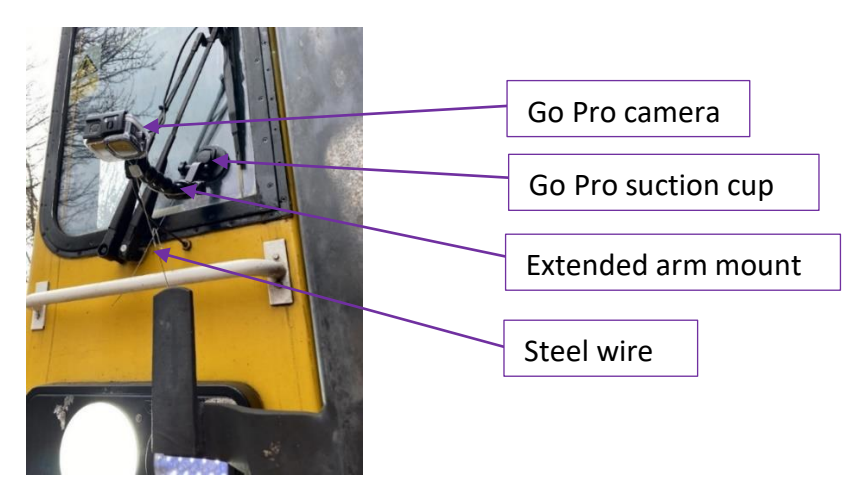


Figure 7. 4: Camera set-up mounted on the class 153 train

7.2.2 ADAPT AN EXISTING DESIGN (AIVR CAMERA BOX)

In the search for a working alternative to the first design, I was put in contact with the software company "One Big Circle" who had been working on different data collection projects from trains. The company had created a 'camera box' (see Figure 7.5) collaboratively with Network Rail that held their data collection instruments. The design had been approved by Network Rail for use on-board a wide range of trains in the UK for data collection and satisfied relevant British Standards. The camera box body was made of aluminium with joints and flanges made from steel.

This camera box offered a great starting point for my design. My design was not intended as a competitor product to the existing camera box utilised by One Big Circle. The camera box is simply a vessel to be used with different components for different purposes.

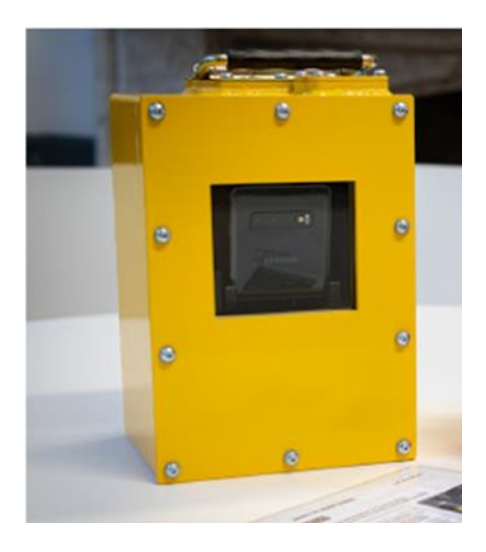


Figure 7. 5: AIVR Camera box (Source onebigcircle.com)

This camera box was ideal to hold the equipment needed for data capture to feed the prediction tool with on-board train railhead data. The main components required were:

- A forward-facing camera: A webcam was used to capture the forward-facing images because it has a USB connection which needs no further modification to work with the microcontroller and it can capture high-definition images (1920x1080 pixels)
- **Railhead camera**: A Raspberry Pi camera module and lens was used. Once again for ease of connectivity and to zoom in close to the railhead from the lamp bracket position.
- **GPS sensors**: The GPS sensor used to record the location of each data capture point was the E-1612-UB module. It is low power, high performance and ultra-high sensitivity at -160 dBm. It consumes a maximum 40mA with a maximum power supply voltage of 3.6V and can operate in temperature range -40°C to 85°C. This was ideal for the expected temperature ranges (-10°C to 50°C) and power source of the camera box.
- Relative humidity and Air temperature sensor: An HTM2500LF Temperature and Relative Humidity Module was used based on it being non-contact and rugged. It had a low power consumption with a maximum of 1.2mA, operates on a maximum supply voltage (peak) of 12V, temperature of -45°C to 85°C and relative humidity of 0% to 100%. It can record relative humidities from 1% to 99% with an accuracy of ±3% and a temperature measuring range of -45°C to 85°C. This sensor was an analogue sensor meaning it can only be operated with a microcontroller that can process analogue inputs such as an Arduino uno.
- Railhead temperature sensor: An Infrared (IR) thermometer was selected to measure and record the railhead temperature. The IR thermometer was pointed at the railhead in order to capture its temperature. An Optris CS LT IR thermometer was used because it has a 15:1 optical resolution (up to 800mm range) measuring from -40°C to 1030°C with an accuracy of ±1.5°C. This thermometer can be applied either as a digital or analog input. It was used as an analog input in this set-up in order to link it with the air temperature sensor.

- **Power bank**: Power source choice for the camera box was a battery pack (power bank) because it is portable, rechargeable and does not need to be continuously connected to an AC source. The power bank used here is V75 USB battery pack with two 5V/2A (3A max) USB output slots. It has a capacity of 19 200mAh, 71 Wh and output operating temperature ranges from -15°C to 65°C. The power bank will power the camera box's component for at least 24 hours on a single charge which sufficient for the purpose of this project.
- **Single board computer (SBC)**: A Raspberry Pi 4 (Raspi) model B was used to collate the data from each source: (UART: GPS, USB: Web cam and environmental sensors, MIPI CSI: rail head camera). This data was saved as a csv file on the computer's SD card. The computer had an operating voltage of 5V allowing it to be powered directly by the power bank, its operating temperature range is 0°C to 40°C.
- **Microcontroller:** An Arduino Uno Rev 3 SMD was used to interface with the analog environmental sensors as the SBC did not have an onboard analog to digital converter. This was connected to and powered by the raspberry pi by a USB port, using the Arduino's onboard UART to USB chip. It had an operating temperature range of -40°C to 85°C.

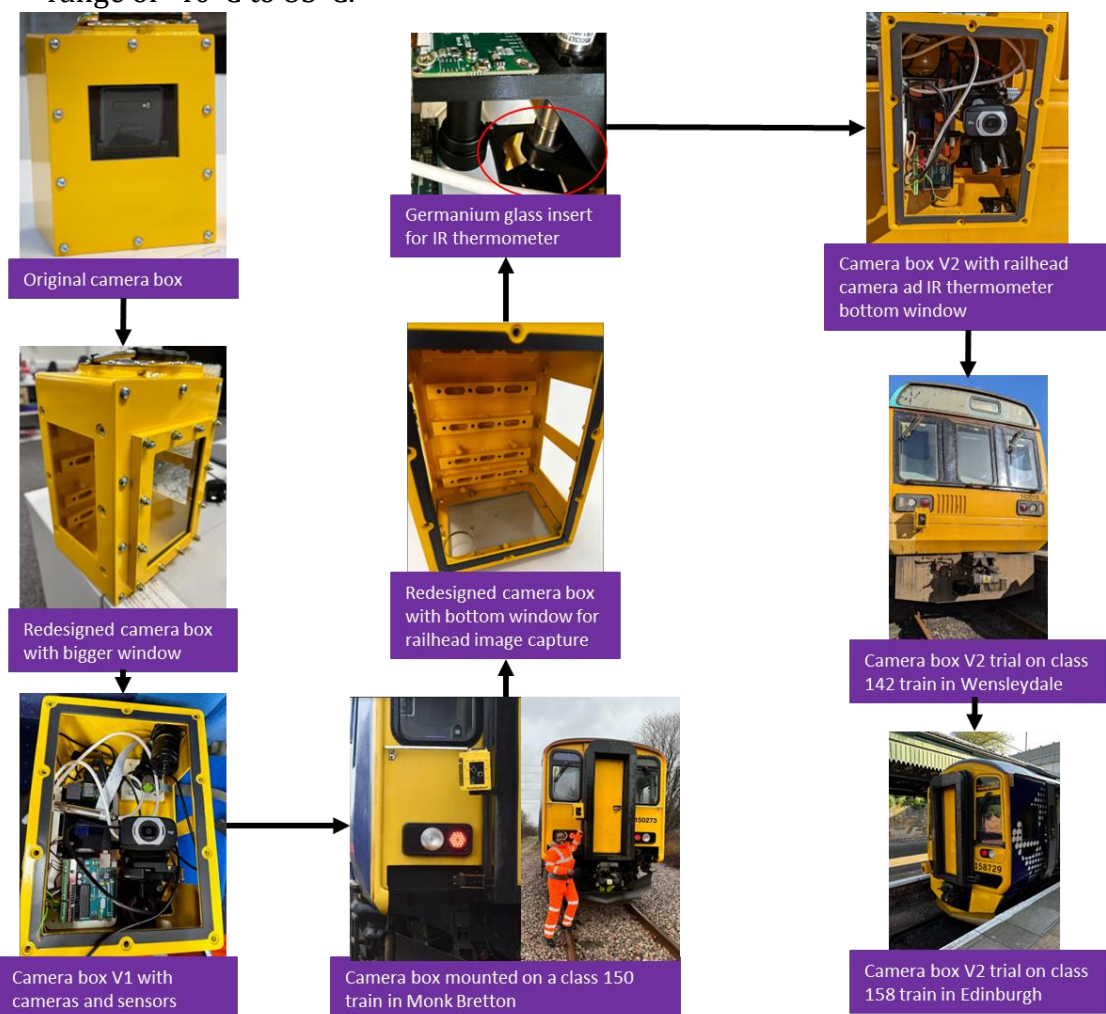


Figure 7. 6: Process diagram for the camera box development

A. CAMERA BOX COMPONENTS FOR VERSION 1 (V1) DESIGN.

The original designs available from Network Rail had a small window of 65×50 mm which was determined to be too small to face/angle a camera from inside the box towards the railhead. The window size was increased to 151×100 mm, giving more area for the camera to be tilted and capture the railhead. This is shown on the process chart in Figure 7.6, process 1 to 2.

The redesigned camera box (Figure 7.7) received was fitted with multiple components to achieve uniform data collection from the train. These components and their functions are listed below:

- 1. 1 Railhead Camera: 12MP Raspi HQ camera module coupled (with adjustable back focus range of 12.5-22.4mm) with a C-Mount 50mm Focal Length lens.
- 2. 1 Forward facing camera.
- 3. 2 Tripods to support and adjust both cameras.
- 4. 1 GPS module.
- 5. 1 Temperature and relative humidity analog sensor: for air temperature and relative humidity of the environment
- 6. 1 Infrared thermometer: to record the railhead temperature.
- 7. 2 Microcontrollers: Raspberry Pi model 4B and Arduino Uno
- 8. 3D printed parts for attachment to inner brackets and also for support (see Appendix C-1 for images)

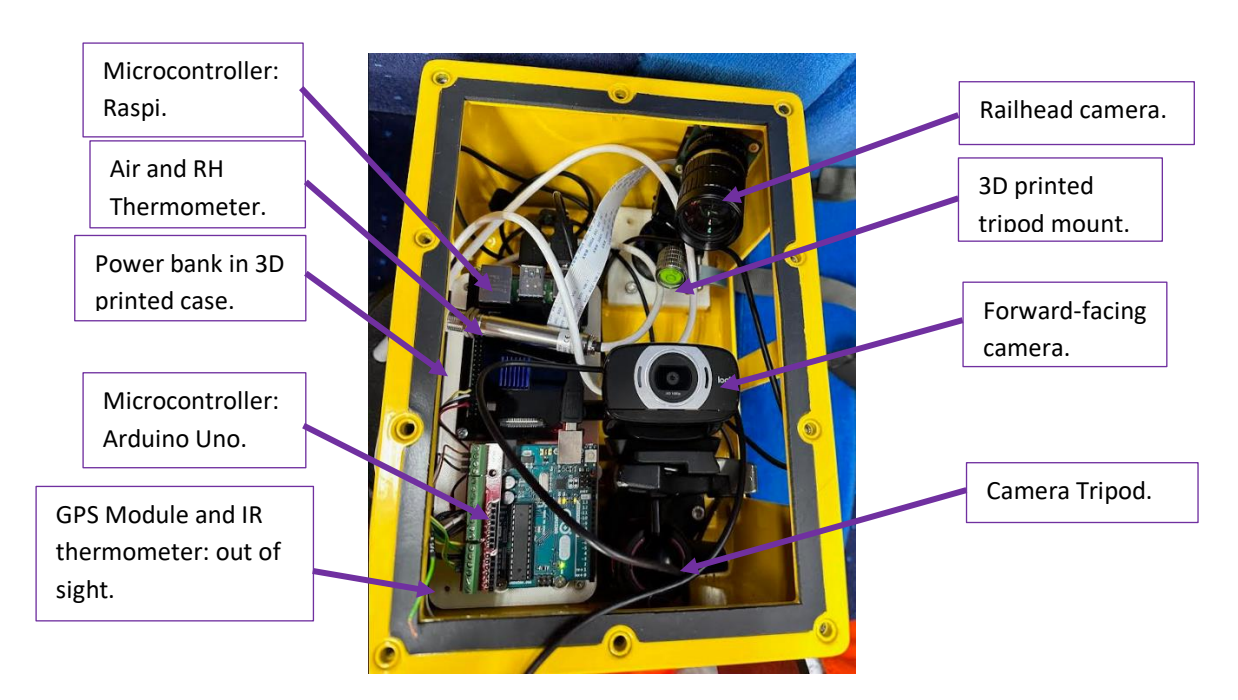


Figure 7. 7: Labelled components image of camera box V1

The modified camera box and the fitted instrumentation was taken out to Monk Bretton for testing (see Figure 7.8). However, some problems were found with the design, hence no results were recorded. The problems with the design were:

• Railhead camera: It was difficult to focus the lens (basically the image was out of focus and too zoomed in and the camera was also not pointing at the railhead the

- way it was intended) so the railhead camera needed replacing with one with a lower focal length and it needed to be repositioned in the camera box.
- IR thermometer: This did not work because it was not in the range of the railhead. The IR thermometer was positioned behind the camera box window which was out of the 800mm range, and it was not pointing at the railhead.
- Microcontroller: An error was made in the data save thread and as a result the data did not save and as a result there were empty result folders. This was rectified in V2.



Figure 7. 8: Camera box V1 mounted on a class 150 train in Monk Bretton

B. CAMERA BOX COMPONENTS FOR VERSION 2 (V2) DESIGN.

The camera box was redesigned again to accommodate a downward facing (railhead) camera and IR thermometer, as shown in Figure 7.9. This was simply done by cutting a 145x97mm rectangular hole at the bottom of the camera box and replacing it with a 175x125mm transparent Perspex window so the camera could capture the railhead. A 38mm diameter hole was also cut into the Perspex window to allow a Germanium window to be placed there, allowing the infrared to pass through and measure the railhead temperature. The engineering drawing for the V2 design can be seen in Appendix C-1.

A 3D printed side panel was created with a slot to accommodate the air and RH thermometer whilst exposing outside to record accurate temperatures (see Appendix C-1)

The railhead camera and lens were also changed. The camera was replaced with an Arducam pivariety colour global shutter camera module with 2MP with 2.8 focal length and the lens was replaced with a narrow angle S-mount 12MP lens with a focal length of 50mm.

The standard operating procedure for camera box V2 has been outlined in Appendix C-3.

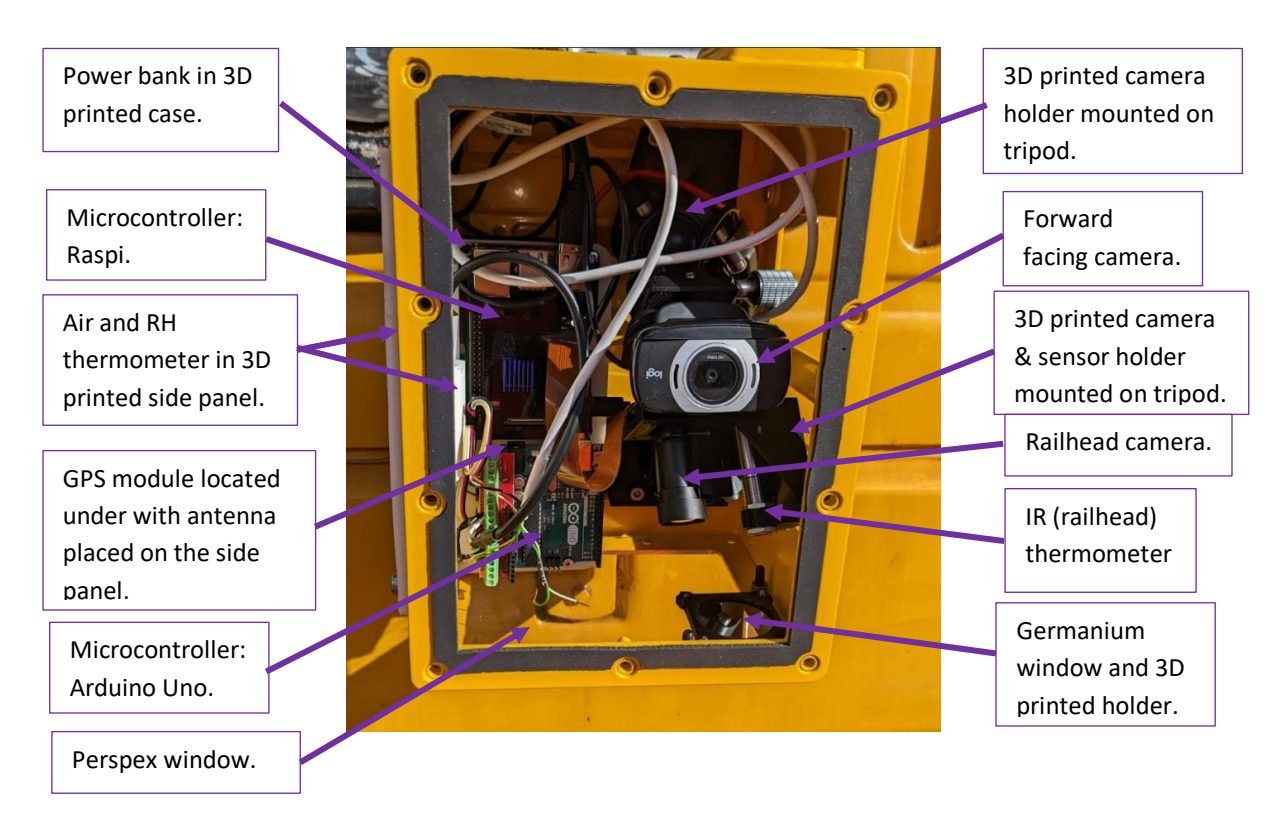


Figure 7. 9: Labelled components image of camera box V2

The Raspberry Pi runs software written in Python. During normal use the Python software opens separate processes for each of the sensor channels. These processes are coordinated by a separate control process. At the start of a data collection cycle the control process signals to each of the other processes to collect data and waits for the responses. Each process then collects data and responds to the control thread, the data is captured every 2 seconds. The responses are then concatenated into a single line of the output csv file (sample shown in Appendix C-2) and confirmation written to the terminal. This structure allows the control process to dynamically monitor the other processes and attempt to restart them if errors are encountered, due to, for example, electromagnetic interference.

Before normal operation can begin the railhead camera and rail head temperature sensor must be aligned to the rail, the camera must also be focused on the correct distance. The Raspi automatically connects to a mobile phone though the phone's Wi-Fi hotspot. This connection is used with the rasp controller app to view the camera outputs allowing the camera to be aligned and focused. The app also allows execution of SSH commands which can be used to run the Python software. The software initially provides a text interface to allow the user to view the output of any sensor process. This interface can be used to align the rail head temperature sensor, by placing a hot object (for example, a cup of tea) on the rail. Prior to this both temperature sensors and relative humidity readings had been compared to an IR thermometer to confirm the accuracy of the sensor's measurements.

7.3 METHODS FOR CAMERA BOX DATA COLLECTION TESTS

7.3.1 WENSLEYDALE HERIATGE RAILWAY (WHR) SHORT RUN TESTS 14-03 AND 13-07

WHR is a heritage railway, as the name implies, which is located in North Yorkshire. The main location for the short run tests was the Leeming Bar station, which is used sparingly, mostly during the holidays and also acts as a depot for trains. Figure 7.10 shows an overhead view of Leeming bar station and indicates the approximate length of track used for the short run test, marked in red.



Figure 7. 10: Google earth image showing the arial view of WHR (Leeming Bar station) [80]

These were tests carried out in the depot over a short distance and at low speed. The details of the tests are given below:

- Train used: Class 142
- Train Speed: max 10 mph.
- Number of runs: 10.
- Length of track used: approximately 260m.
- Data collection rate: 1 per 2 seconds.

7.3.2 SCOTRAIL LONG RUN TESTS 30-05

This test was carried out from Edinburgh Haymarket depot, through Edinburgh Waverley and ended at Perth Station. The test details are given below:

- Train used: Class 158
- Train Speed: max 75mph
- Length of data collection: 5 hour 10 minutes

• Data collection rate: 1 per 2 seconds.

7.3.3 WENSLEYDALE HERIATGE RAILWAY (WHR) LONG RUN TESTS 14-07 AND 28-11

These were tests that included train journeys from one station to another. Two long run tests were done on separate occasions, the first one from Leeming Bar station, through Bedale to Leyburn station (return journey) and Leeming Bar to Bedale station (return journey on cryogenic cleaning train) on 14-07-23 and 28-11-23 respectively. The specifics of the tests were as follows:

- Train used: Class 142.
- Train Speed: max 30 mph.
- Number of runs: 2 (return journey).
- Distance covered: Approximately 1.6 miles and 11.5 miles for Leeming Bar to Bedale and Leeming Bar to Leyburn respectively.
- Data collection rate: 1 per 2 seconds.

7.3.4 WENSLEYDALE HERIATGE RAILWAY (WHR) (SHORT RUNS) WITH LEAF LAYER AND CRYOGENIC CLEANING APPLICATION 28-11

A cryogenic cleaning of railhead test was taking place in WHR, where railhead contaminants are blasted clean by dry ice [81]. Black leaf layers (dried Sycamore) were created for application on the railhead (see description below) Two camera boxes were used on a modified Class 142 train in an attempt to capture the before and after cleaning effects. The modified Class 142 train (which was still a passenger train) was equipped with a cryogenic cleaning system on board. The first camera box was attached to the front end over the right railhead while second camera box was attached to the rear end over the left railhead. Figure 7.11 shows a summary of the tests conducted.

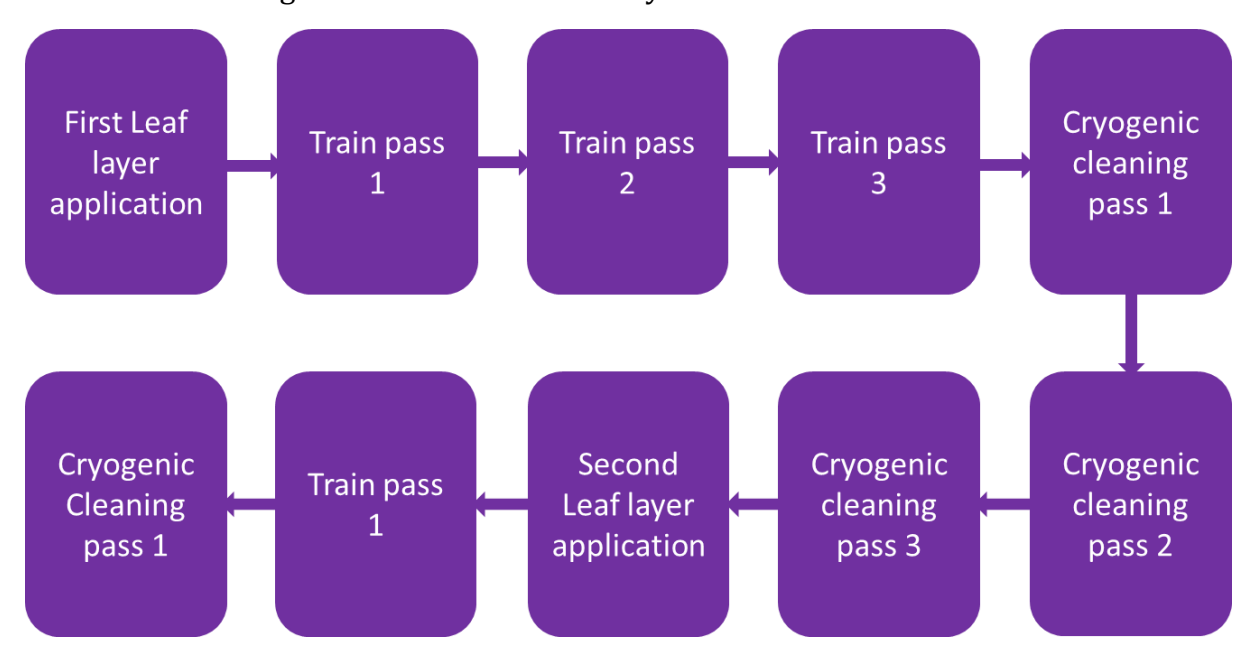


Figure 7. 11: Schematics for WHR 28-11-23 short run test, where each pass is a to and fro journey

Leaf layer application: The railhead was scraped with a sanding star attached to a drill to remove oxides from the surface. The Class 142 then had one pass over the track section

to condition it before application of the leaf layer. Leaf paste created using the method stated in [82]. was applied on 2m sections of the rail parallel to each other (Figure 7.12) and left to settle on the railhead for 10 minutes to promote bonding between the leaf material and rail.

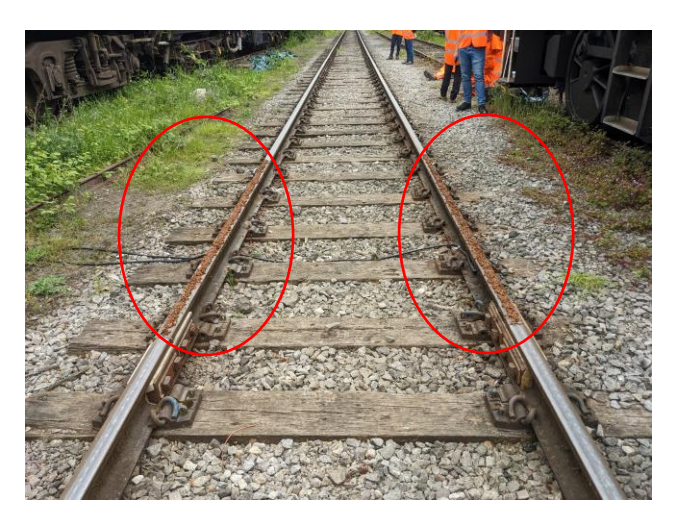


Figure 7. 12: Leaf paste circled in red, laid on the railhead section

Black leaf layer creation: The Class 142 train passed over the leaf paste twice (equivalent to 8 axle passes) at 10 mph to create a black leaf layer. The train was at a constant speed, so minimal slip was applied to the layers. The cryogenic cleaning took place after the black leaf layer was created. In addition, railhead friction was measured using a Rivelin Rail tribometer [83] to create a benchmark for comparison to the prediction tool's results.

7.4 RESULTS

The friction predictions are initially presented in terms of the Pendulum Test Values (PTV) and are later converted into the CoF/μ using the BRR conversion factor discussed in previous Chapters 4, and 6. The true measured temperatures and relative humidity values and predicted PTV were plotted on the y-axis against the data points on the x-axis. While on a different graph the predicted CoF (converted PTV) was plotted on its own on the y-axis (to show appropriate scale) against the data points on the x-axis.

7.4.1 MONK BRETTON TEST: CAMERA MOUNTED IN FRONT OF TRAIN (26-11-21)

The first major problem noticed during image capture with the GoPro system was the resolution of the railhead in the image. The railhead was located too far away from the camera, and as such it only covered approximately 10% of the image (see Figure 7.13 (L)). The image was cropped and zoomed in to try to focus on the railhead (Figure 7.13 (R), but the image resolution was also too low at 306x496 for the prediction tool to process.



Figure 7. 13: Image capture from the GoPro camera set-up (L); Cropped and zoomed in image extracted (R)

Another problem highlighted in this design was that the exact environmental data of the rail section was unavailable as the exact frame of the video did not have corresponding data. The camera set-up is also affected by the vibrations from the train movement, the extension arm used to support the camera is flexible and moved out of position with prolonged exposure to the vibrations. Therefore, with all these problems highlighted this method was deemed unsuitable for data collection.

7.4.2 CAMERA BOX V2: FIRST TEST AT WENSLEYDALE HERITAGE RAILWAY (WHR) (14-03-23)

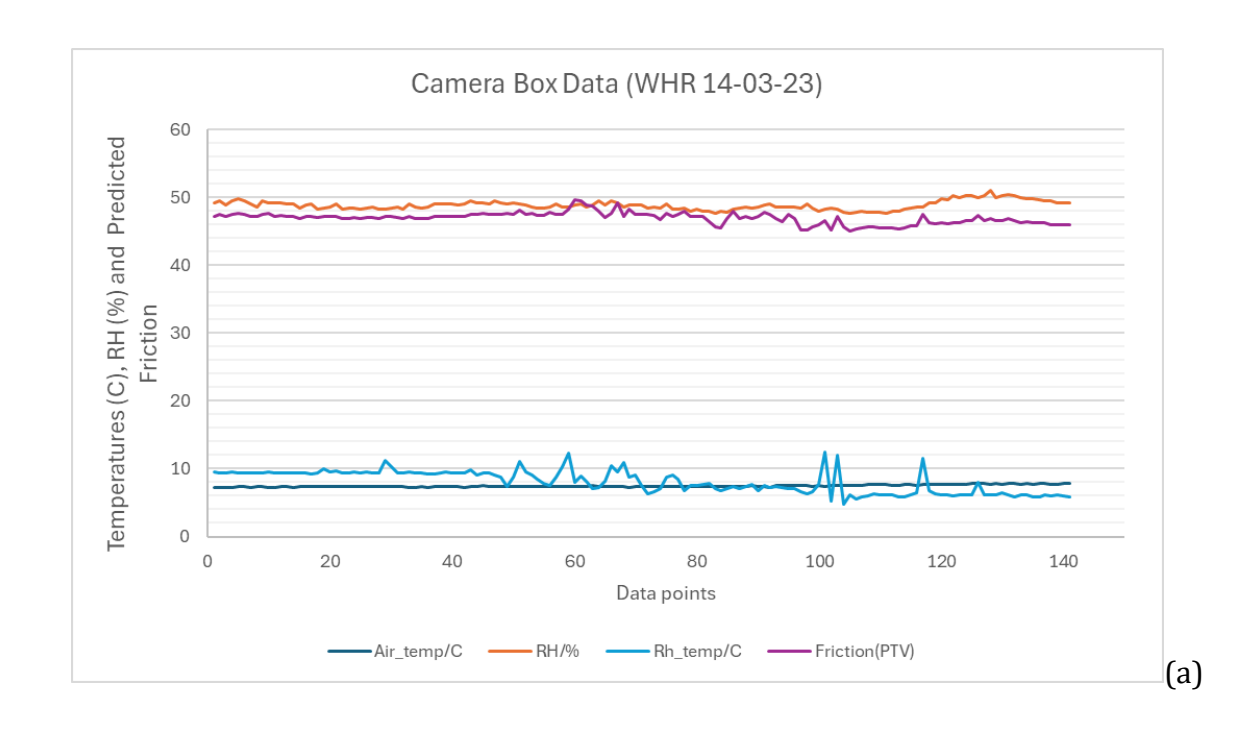
A total of 141 data points were collected on the first successful trial of camera box V2 at the WHR. The camera box was placed on a Class 142 train (see Figure 7.14), and it was driven over a short stretch (\approx 260m) of track.

The image on the right in Figure 7.14 shows a white mug holding hot water, this was used to adjust the IR thermometer's 'field of vision'. The hot water was higher temperature compared to the surroundings. It was placed on the railhead and the thermometer was adjusted until it started to read the warmer temperature from the hot water thus reading the temperature of the railhead region.

Table 7.2 shows an example data set extracted from the trial including the images and friction predictions for the points shown. Figure 7.15a and b show plots of all data collected and the friction predictions.



Figure 7. 14: Camera mounted on a class 142 train at WHR (14-03-23)



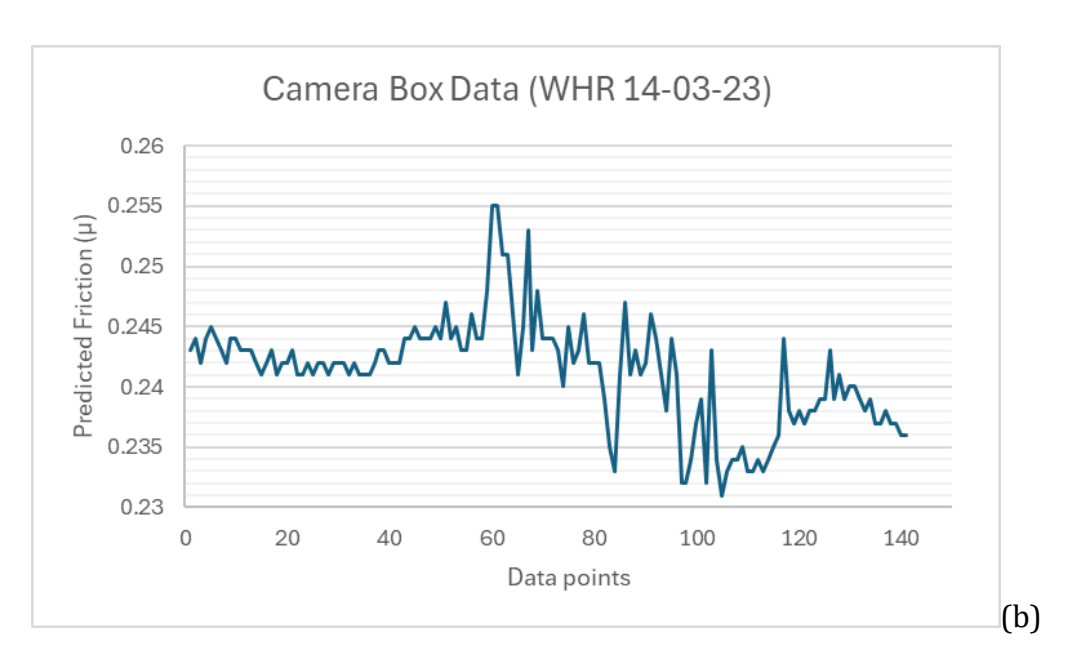


Figure 7. 15: (a) Plot of all environmental data and the PTV against all data points for WHR 14-03-23; (b) COF against all data points for WHR 14-03-23

One of the very noticeable things in result plotted in Figure 7.15 (a) are peaks in the railhead temperature resulting from sections of railhead being exposed to the sun (discussed further in section 7.5.1). Figure 7.15 (b) shows the friction predicted from the prediction model, the friction also has similar peaks to that of the railhead temperature.

Table 7. 2: Table of data from WHR 14-03-23

S/N	Forward facing Image	Railhead Image	Air Temp/°C	Rh Temp/°C	Rh/%	Predicted Friction	Predicted Friction
1			7.2	9.3	49.0	(PTV) 47.1	(μ) 0.242
2			7.7	6.1	50.0	46.3	0.238
3			7.6	7.7	48.4	46.8	0.241
4			7.3	10.5	49.4	47.7	0.245

7.4.3 SECOND TEST AT SCOTRAIL (30-05-23)

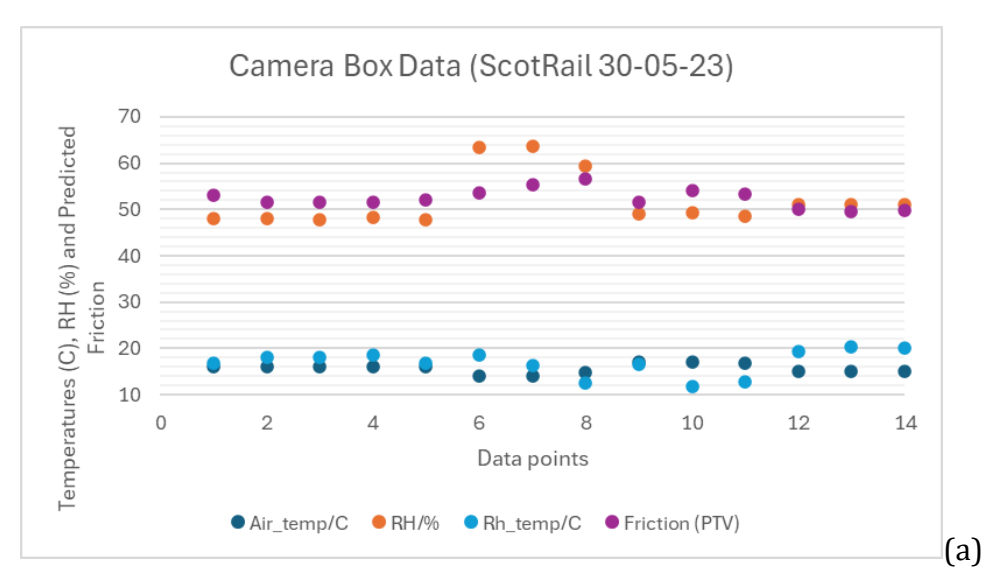
An opportunity arose to trial the camera box V2 on a Class 158 Scotrail train with the aim of testing the feasibility of using the system on a passenger train in service.

The trial started at Edinburgh Haymarket depot, where the camera box was placed on a lamp bracket at the front of a Class 158 (see Figure 7.16) at around 05:20. During the installation it was noticed the railhead facing camera was partially capturing the railhead, due to the lamp bracket being positioned slightly off-set from the railhead.



Figure 7. 16: Camera box on a class 158 train at Edinburgh Waverley station

The railhead images were still collected, with some of them capturing just the rail side/ballast while the rest captured a portion of the railhead. Some of the images containing portions of the railhead (selected from different locations) was then further processed and used to make friction predictions. The data collection was stopped at 10:30 in Perth station. After 5 hours 10 minutes of operation and 6860 data collected the SD card was full. Although over 6000 images were collected, only 14 were processed and plotted (see Figure 7.17 (a) and (b)) due to most of the images being unsuitable for predictions.



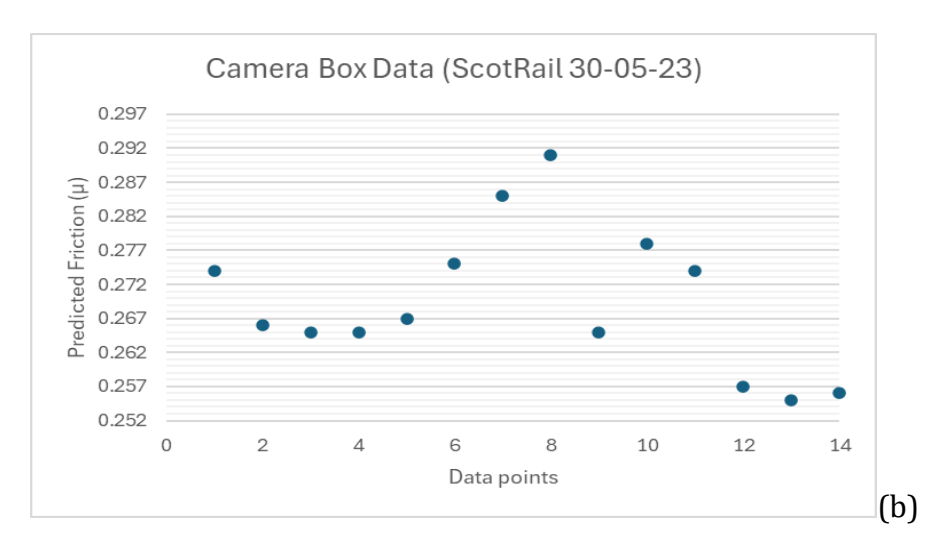


Figure 7. 17: (a) Plot of all environmental data and the PTV against selected data points for ScotRail on 30-05-23; (b) COF against selected data points for ScotRail on 30-05-23

Table 7.3 shows examples of the railhead images captured and used to create the predictions.

The friction predictions for the usable data collated from different locations ranged between 0.254 to 0.291 for relatively warmer air temperatures recorded of 14° C to 17° C.

7.4.4 THIRD TEST AT WENSLEYDALE HERITAGE RAILWAYS (WHR) (13&14-07-23)

The ScotRail trial exposed one of the shortcomings of using the camera box, which was the position of the lamp bracket is a limitation for using it on most train types like the Class 170. A train like the Class 170 or 198 have their lamp bracket positioned closer to the centre of the train which offsets the camera box's railhead camera from the railhead location. The camera box is well positioned on the Class 142 used at the WHR and also some Class 15Xs.

Given this information, more tests were carried out at WHR during the summer of 2023. The trial carried out on 13-07-23 was in the Leeming Bar depot using about a 260m length of rail to collect data. Whereas on 14-07-23 a full journey on a passenger carrying Class 142 train (see Figure 7.18) travelling from Leeming Bar station to Leyburn station and back to Leeming Bar station.

A total of 357 data points were collected on 13-07-23 and 2677 data points were collected 14-07-23.



Figure 7. 18: Camera box on class 142 train in WHR on 14-07-23

Table 7. 3: Table of data from ScotRail 30-05-23

S/N	Forward facing Image	Railhead Image	Air	Rh	Rh/%	Predicted	Predicted
			Temp/°C	Temp/°C		Friction	Friction
						(PTV)	(μ)
1			17.0	11.8	49.4	54.0	0.278
2			14.8	12.5	59.5	56.5	0.291
3			16.8	12.8	48.5	53.4	0.274
4			20.4	15.0	51.0	49.5	0.255

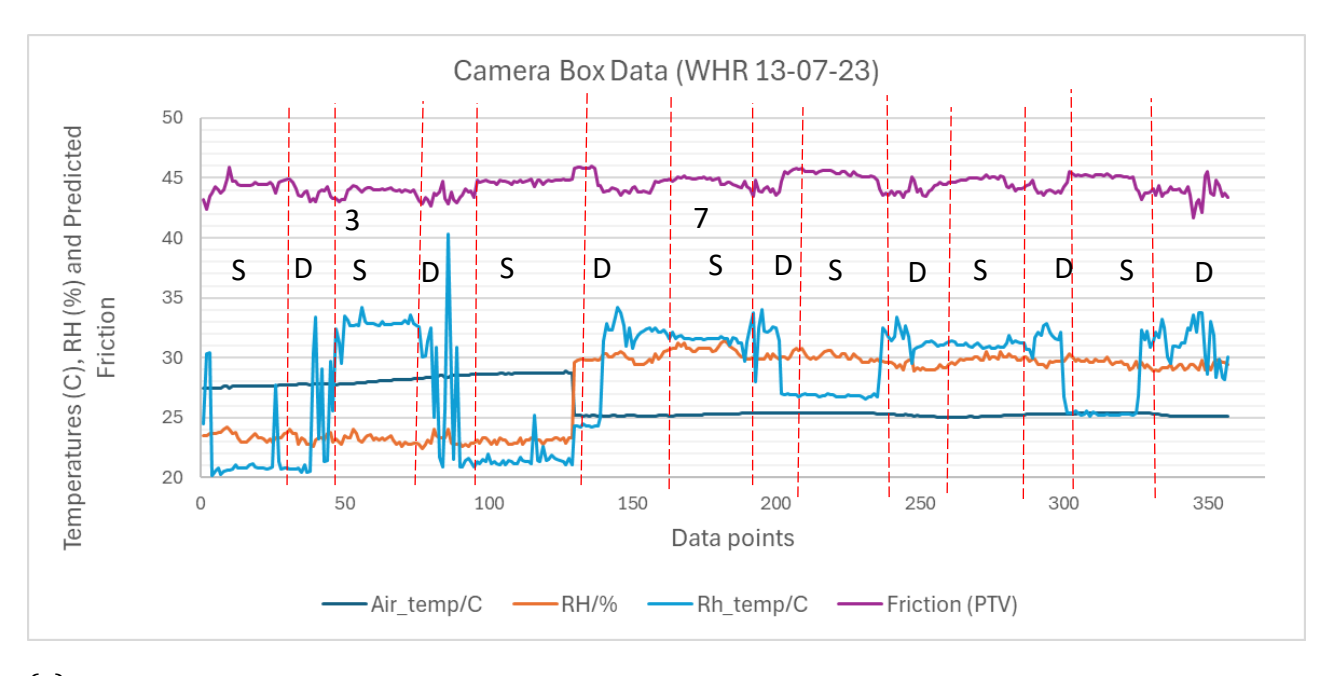
Table 7. 4: Table of data from WHR 13-07-23

S/N	Forward facing Image	Railhead Image	Air	Rh	Rh/%	Predicted	Predicted
			Temp/°C	Temp/°C		Friction (PTV)	Friction (μ)
1			28.6	22.0	23.1	44.7	0.230
2			28.4	31.4	23.1	43.2	0.222
3			27.7	20.5	22.8	43.0	0.221
4			25.1	32.5	29.9	43.7	0.225

Table 7. 5: Table of data from WHR 14-07-23

S/N	Forward facing Image	Railhead Image	Air	Rh	Rh/%	Predicted	Predicted
			Temp/°C	Temp/°C		Friction (PTV)	Friction
1			21.6	20.7	46.8	51.2	(μ) 0.263
2			18.1	21.8	61.1	53.0	0.272
3			18.8	23.9	59.7	53.4	0.274
4			19.2	22.8	59.4	53.6	0.276

Figures 7.19 & 7.20 (a) and (b) show the plots of all the environmental data collected and friction predictions while Tables 7.4 and 7.5 show examples of the camera box output with railhead images and corresponding forward-facing images for 13-07-23 and 14-07-23 respectively.



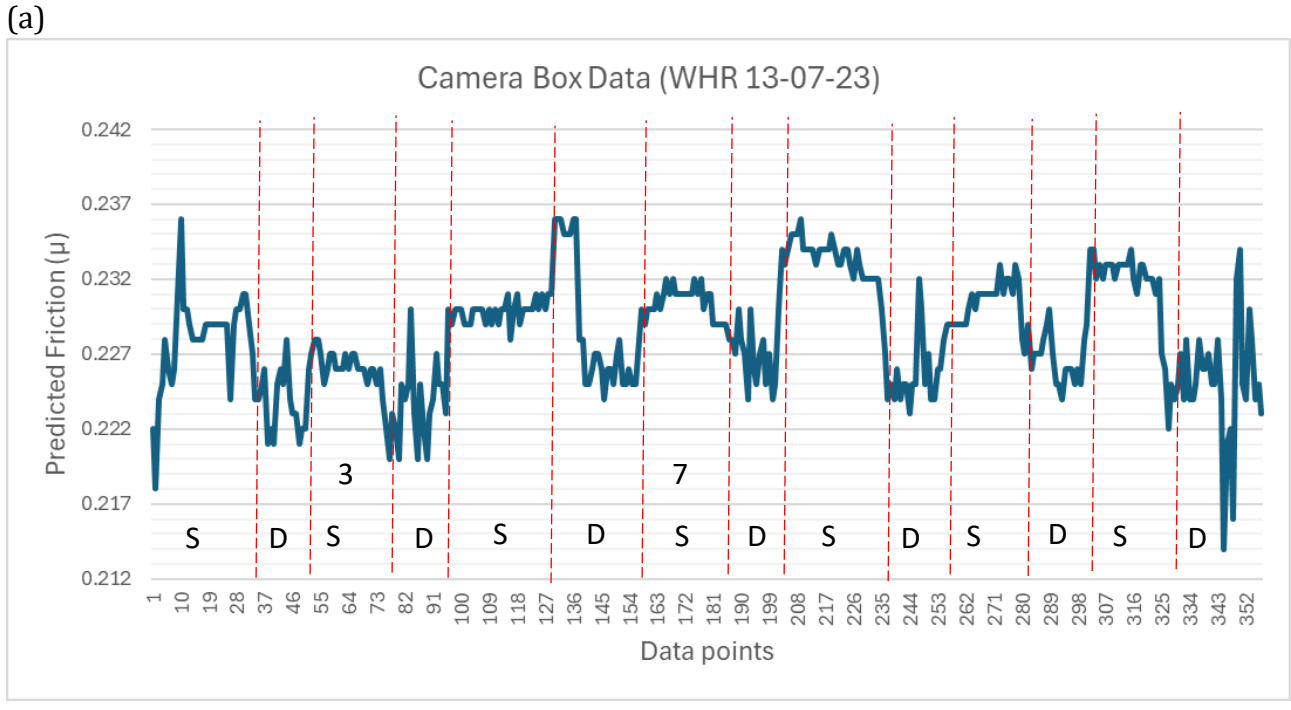


Figure 7. 19: (a) Plot of all environmental data and the PTV against all data points for WHR 13-07-23; (b) COF against all data points for WHR 13-07-23

(b)

The results plotted in Figure 7.19 (a) and (b) show a combination of stationary and moving data points. The plot has been sectioned into static and dynamic showing the repetitive runs done, using 'S' for Static and 'D' for Dynamic.

Tests carried out between the first sections were done on the first half of the track (labelled 1 in Figure 7.10) which can be seen in Figure 7.19 (b) with similarities in the static and dynamic friction predicted while testing done from sections 6 to 13 were on the second half of the short-run track (labelled 2 in Figure 7.10) showing slightly higher friction. Regardless of the section of the tracks, friction values predicted were in a reasonable range for a dry railhead [24] at 0.214 and 0.236 which is also similar to data collected in previous testing. The temperatures recorded here were warmer than what was recorded during past testing at the same location, with railhead temperature between 20.2°C – 40.3°C and air temperatures ranging from 25°C to 28.7°C, typical of summer temperatures.

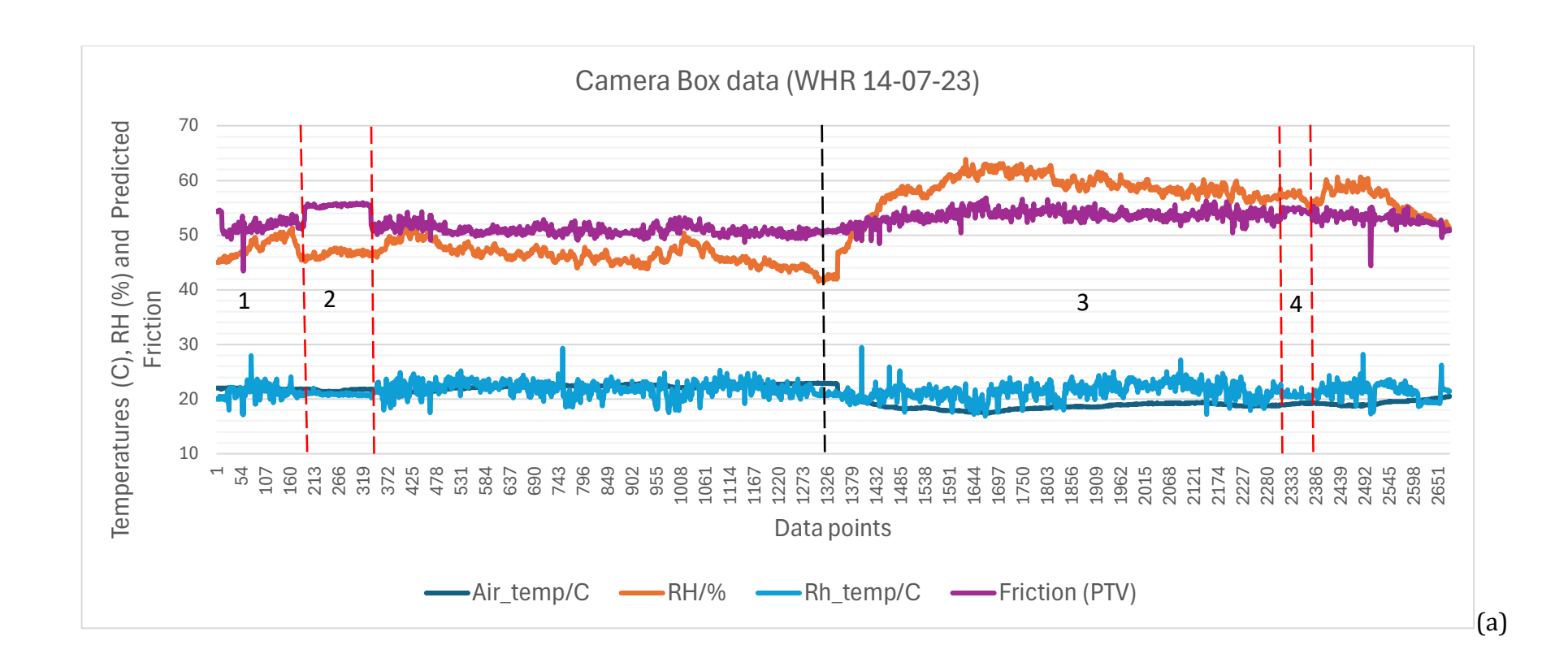
Results recorded from the long run from Leeming Bar to Leyburn and return (shown in Figure 7.20 (a) and (b), show the data recorded over the return trip. The results were sectioned into 4 parts namely:

- 1. Forwards trip from Leeming Bar to Leyburn.
- 2. Sub section showing 5 minutes stop at Bedale station.
- 3. Return trip from Leyburn to Leeming Bar.
- 4. Sub section showing 2 minutes stop at Bedale station.

The data from the GPS module was used in determining the location of the stops seen in the plot. This gave location output in form of degrees and minutes, given as:

- Latitude 54 degrees 17.3339 minutes
- Longitude 001 degrees 35.2286 minutes

A GPS conversion website [84] was used to convert the location, which yielded 54.2890100°, -001.5875400° and with a simple Google Maps search of the GPS points showed the location as Bedale station (54°17'20.4"N 1°35'15.1"W). The friction recorded at the stations where the train was at a stop was as expected with a very short range between 0.283 to 0.287.



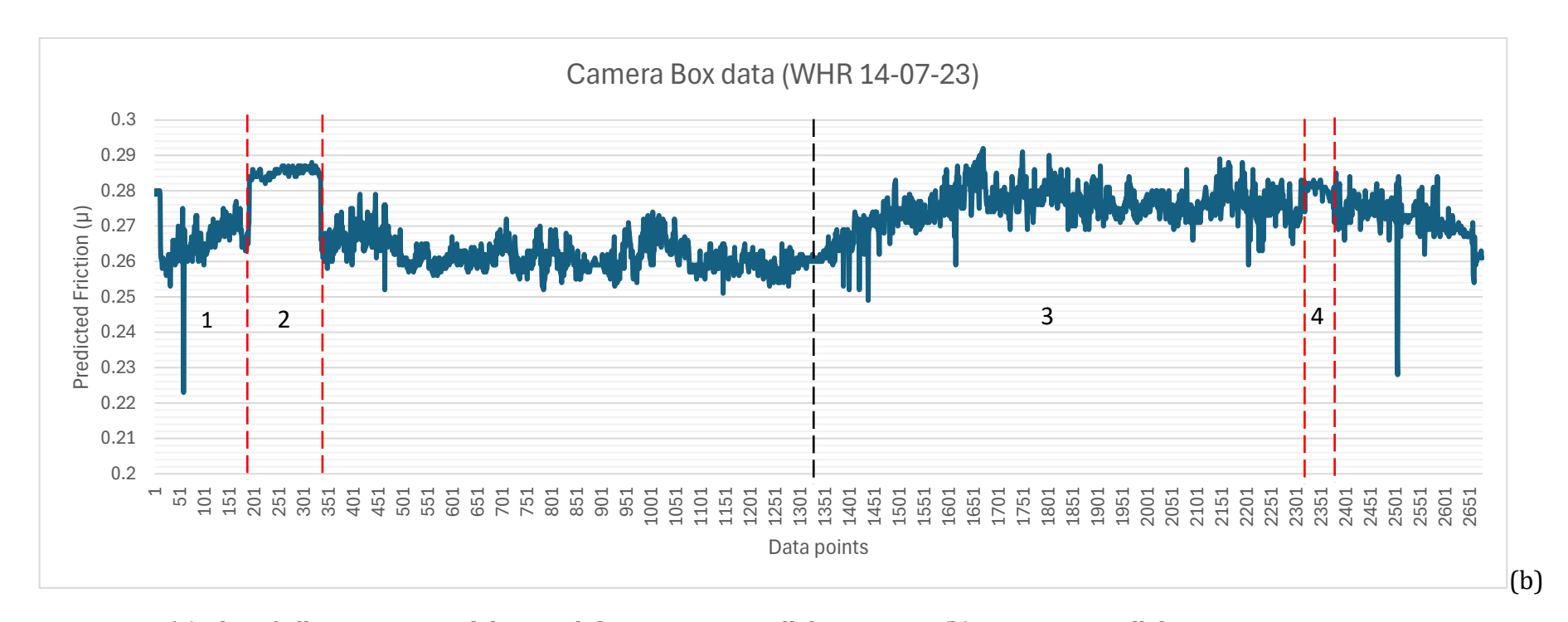


Figure 7. 20: (a) Plot of all environmental data and the PTV against all data points; (b) COF against all data points

7.4.5 FOURTH TEST AT WENSLEYDALE HERITAGE RAILWAYS (WHR) (28-11-23)

For the fourth and final test in this project, two camera boxes were deployed on the University of Sheffield cryogenic cleaning train [81]. The first box (camera box 1) was placed at the front end of the Class 142 and the second box (camera box 2) was placed at the rear end of the train as shown in Figure 7.21 (a) to (c). This was done to capture the before and after images and friction predictions of the railhead used for testing in WHR.

Camera box 1 collected a total of 1228 data points with 991 of them being good for processing while camera box 2 had a total of 971 of which all were usable. Figures 7.22 & 7.23 (a) to (d) show the plot of (camera box 1), (camera box 2) environmental data collected and friction predictions for camera box 1 and box 2 respectively. Both of the datasets were broken into a short run which involved the cryogenic cleaning described in Section 7.3 and a long run return journey from Leeming Bar to Bedale.







Figure 7. 21: (a) Author installing camera box 1 on the class 142 train; (b) Camera box 2 captured in use; (c) Camera box 1 captured in use.

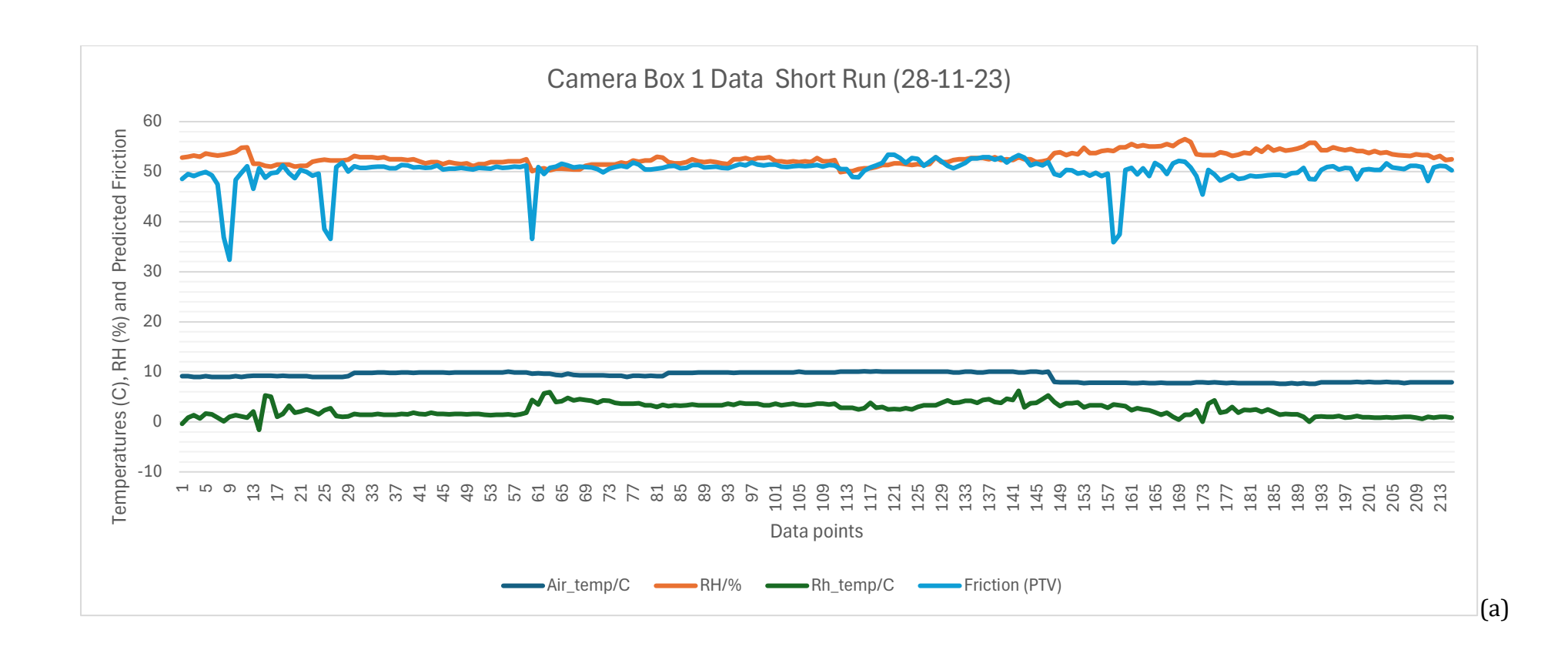
Tables 7.6 and 7.7 show 4 samples each of data collected from camera boxes 1 and 2 respectively.

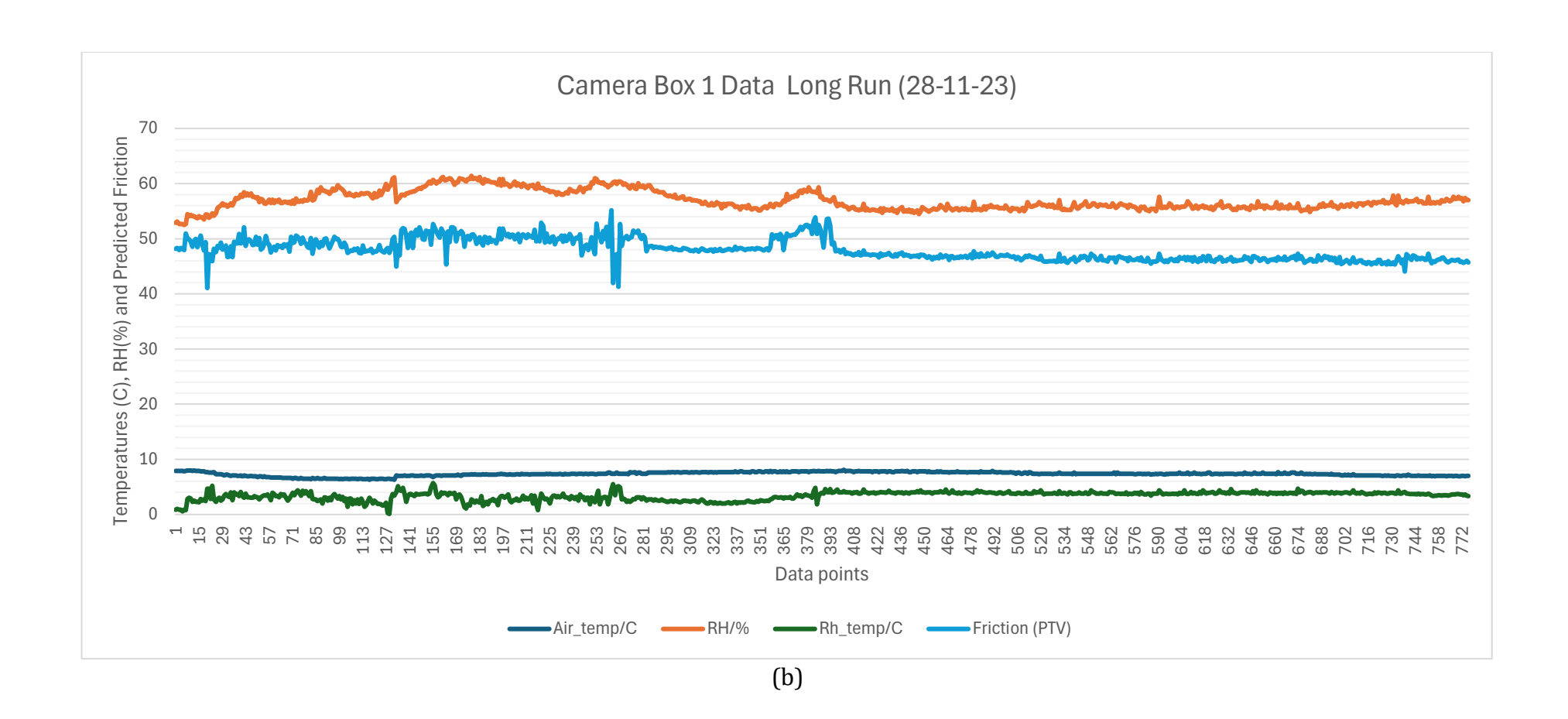
Table 7. 6: Table of data from WHR (camera box1) 28-11-23

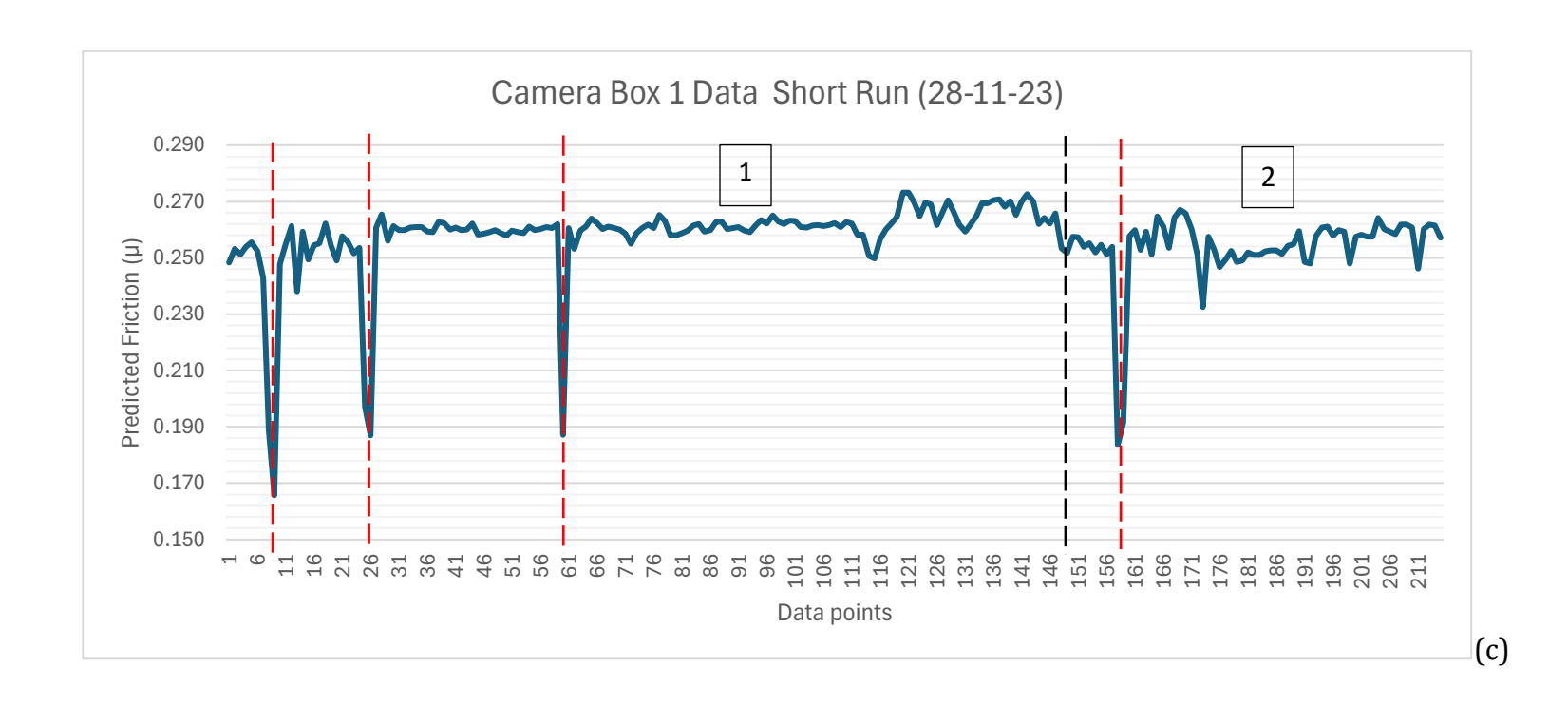
S/N	Forward facing Image	Railhead Image	Air	Rh	Rh/%	Predicted	Predicted
			Temp/°C	Temp/°C		Friction (PTV)	Friction (μ) 0.172
1			9.3	4.1	50.6	33.6	0.172
2			7.6	2.8	59.7	37.0	0.189
3			7.1	3.1	60.4	37.3	0.191
4			9.1	0.8	54.9	51.1	0.261

Table 7. 7: Table of data from WHR (camera box2) 28-11-23

S/N	Forward facing Image	Railhead Image	Air Temp/ºC	Rh Temp/ºC	Rh/%	Predicted Friction (PTV)	Predicted Friction (μ)
1			8.0	2.9	57.3	31.1	0.159
2			7.9	2.5	54.7	34.7	0.178
3			8.3	3.4	53.3	33.7	0.173
4			7.3	3.6	52.6	47.4	0.241







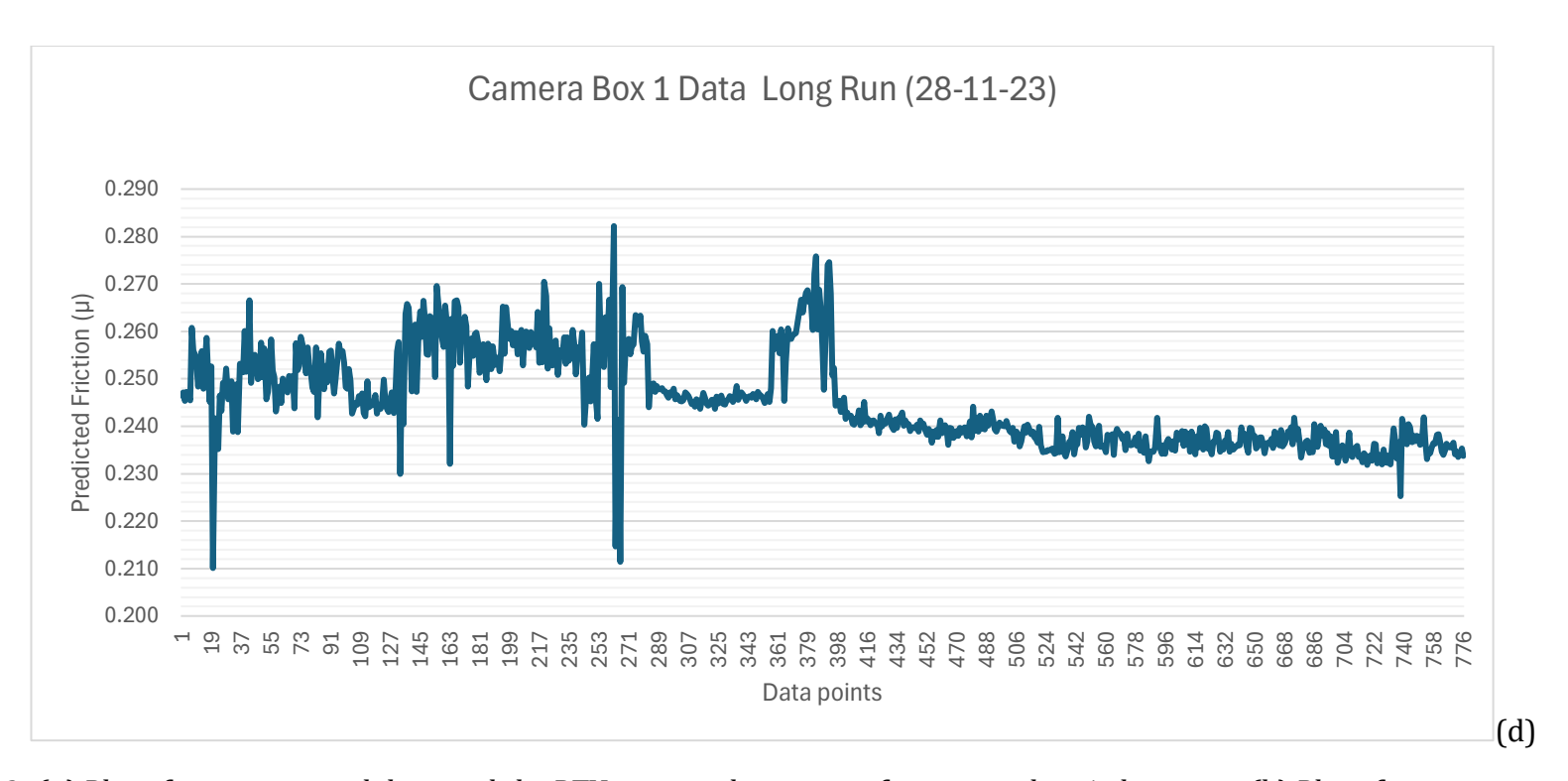
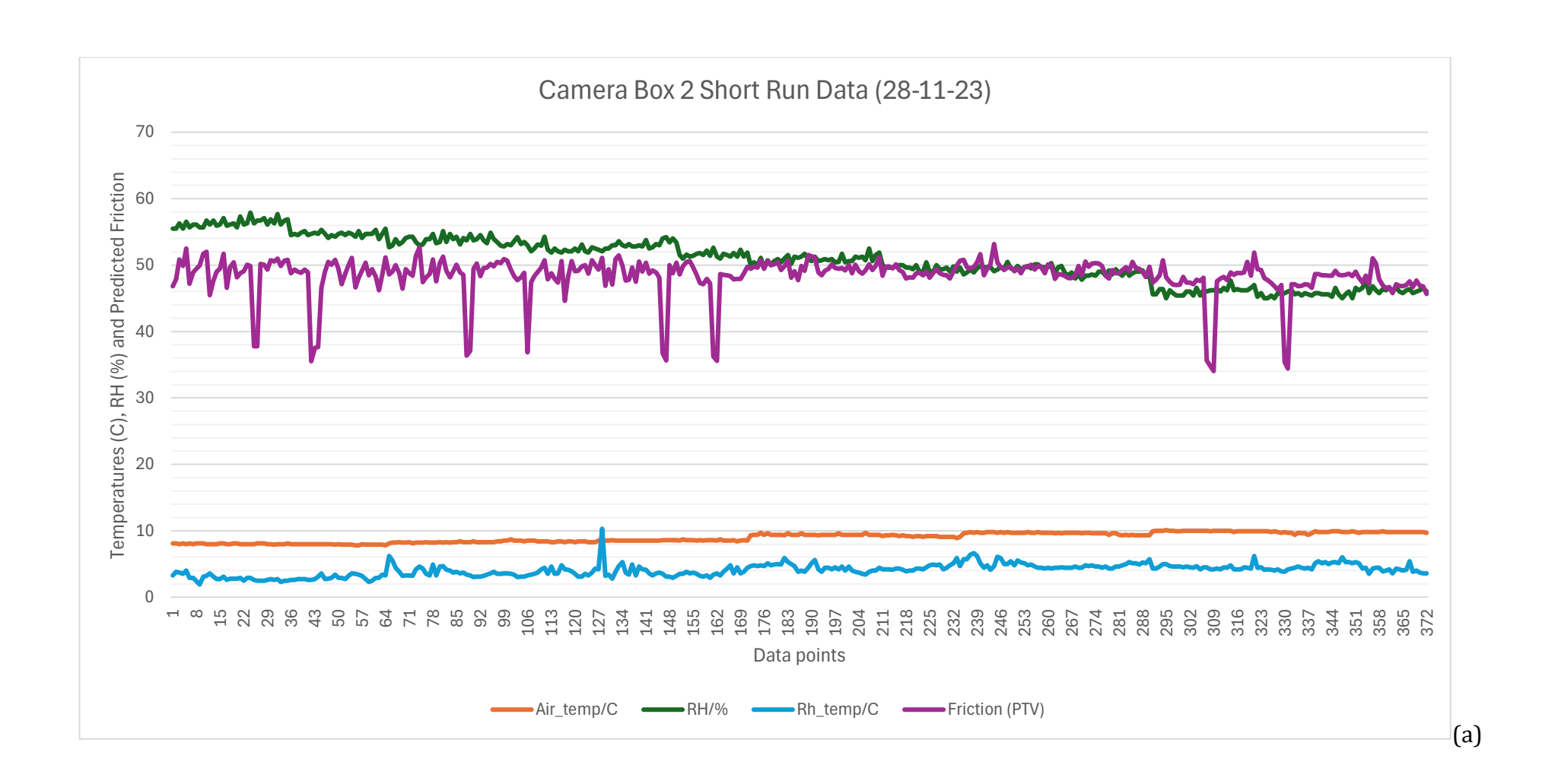
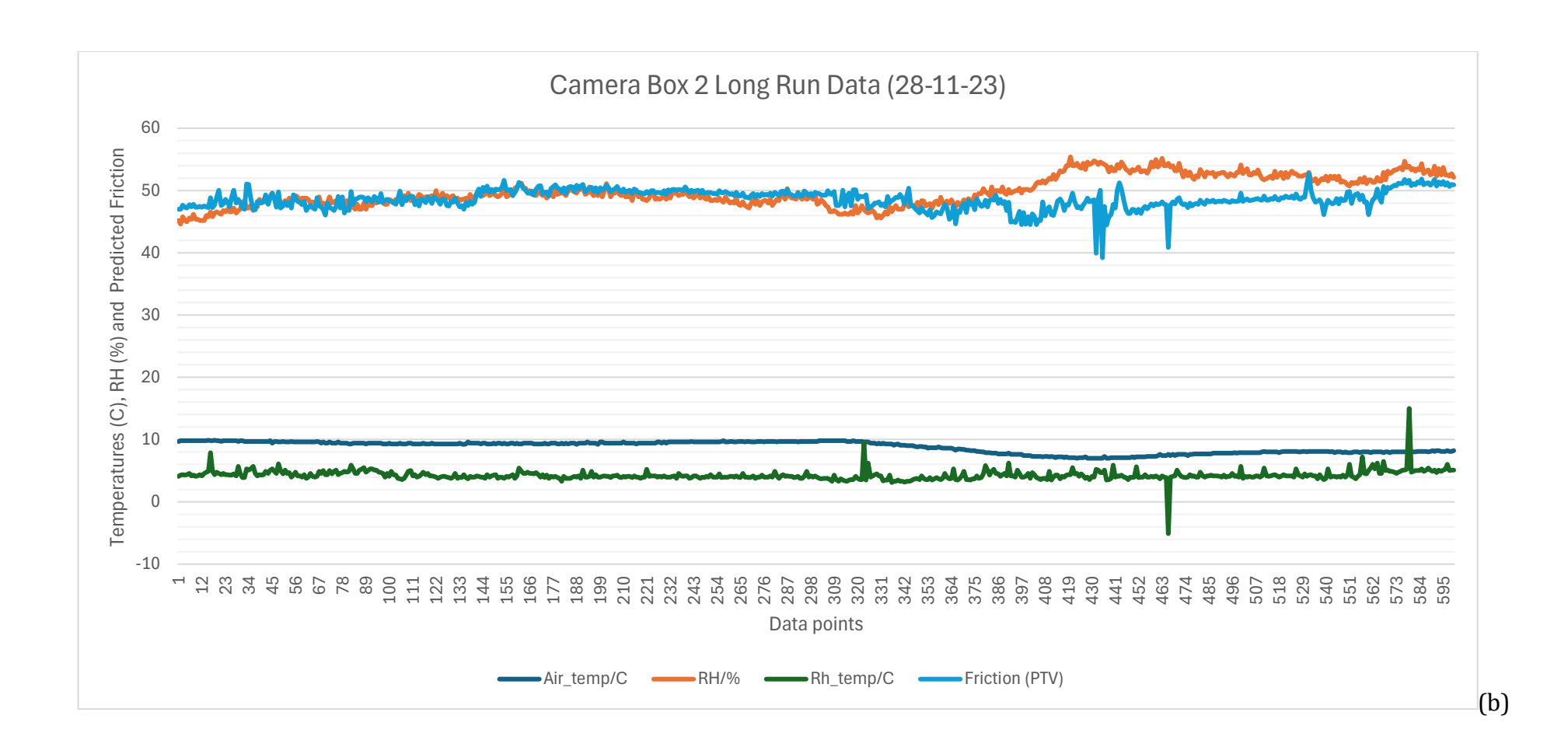
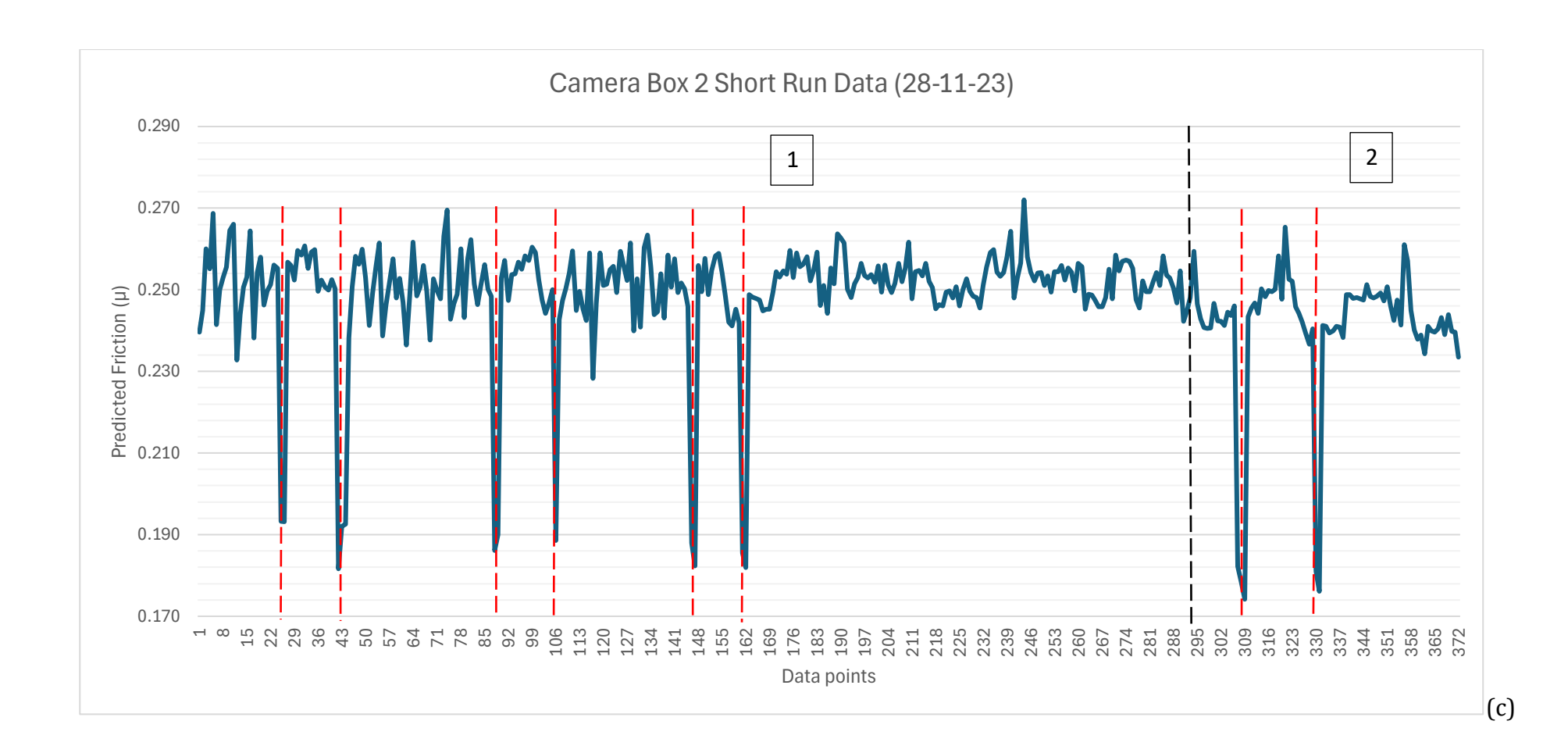


Figure 7. 22: (a) Plot of environmental data and the PTV against data points for camera box 1 short run; (b) Plot of environmental data and the PTV against data points data points for camera box 1 long run; (c) COF against data points camera box 1 short run; (d) COF against data points camera box 1 long run







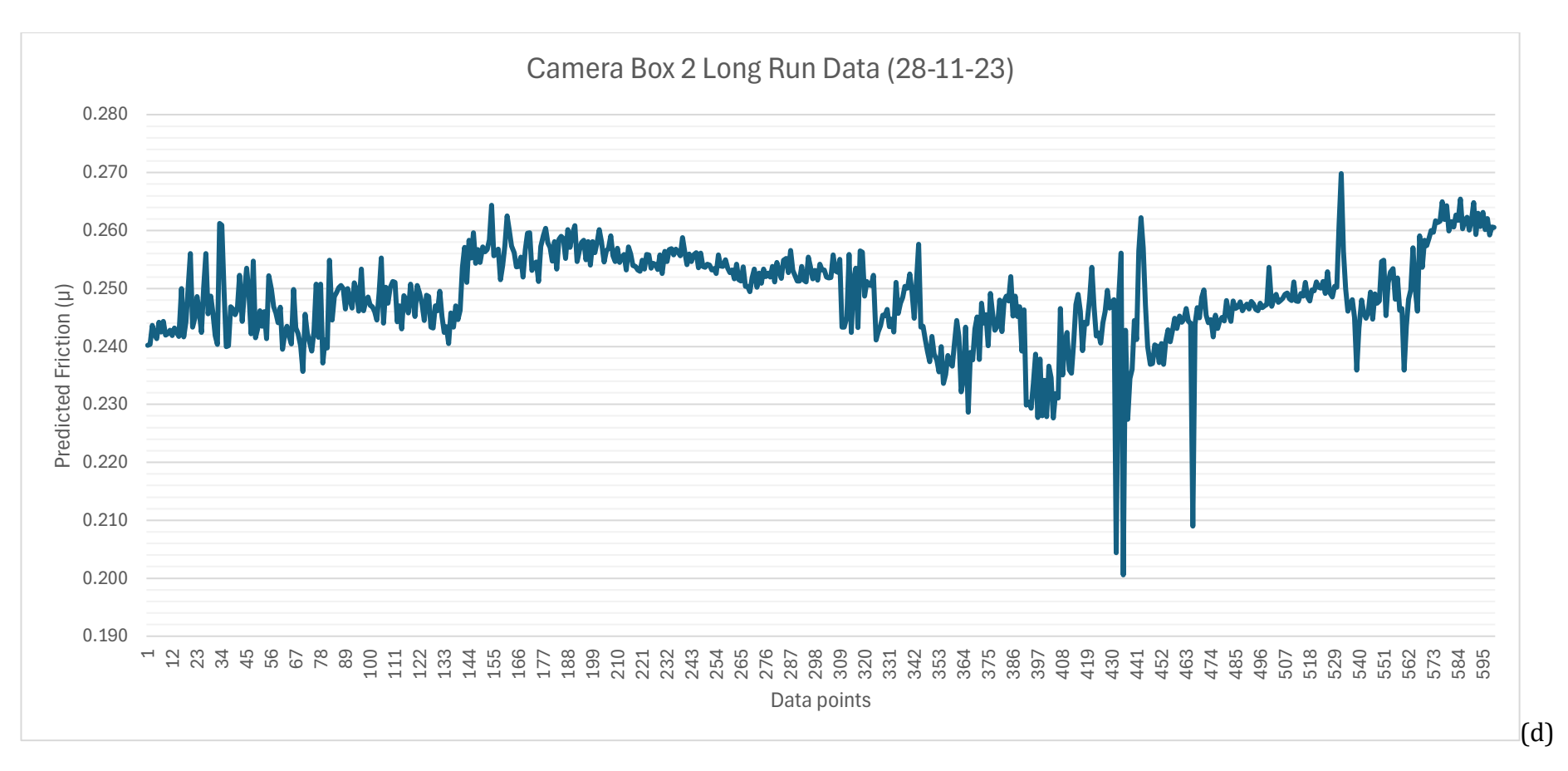


Figure 7. 23: (a) Plot of environmental data and the PTV against data points for camera box 2 short run; (b) Plot of environmental data and the PTV against data points data points for camera box 2 long run; (c) COF against data points camera box 2 short run; (d) COF against data points camera box 2 long run

Generally, both camera boxes were not expected to predict the exact same friction values in comparison to themselves, as they were capturing railhead images from 2 different rail tracks. Camera box 1 predicted a maximum CoF of 0.282 and minimum CoF of 0.166 while camera box 2 predicted a maximum CoF of 0.272 and minimum CoF of 0.174. Figure 22 and 23 (c) shows the effects of the black leaf layers created marked with the red dotted line on the railhead. The leaf layer was created on two separate occasions which has been sectioned into two on the plot using the black dotted line. Camera box 2 captured the full testing period shown in Figure 23 (c) (which also matches the leaf layer sections laid out in the schematics in Figure 7.11) while there was some operational cut out on camera box 1 which reduced the data collected. Friction coefficients of between 0.166 and 0.197 were predicted for leaf layer section recorded on camera box 1 while value between 0.174 and 0.193 was predicted for camera box 2. The friction predicted was seen to reduce at the leaf layer developed on the railhead.

7.5 DISCUSSIONS 7.5.1 WHR 14-03-23

This was the first successful test carried out on a moving train, although it was a brief test in the WHR depot on a Class 142 train. The images (3 &4) in Table 7.2 look blurry as they were captured while the train was moving. The faster the train moved blurrier the images get, the maximum speed on this test was about 10mph. That level of blurriness does not affect the prediction tool's ability to process the images and make predictions, because it can still identify the colours on the image. Obviously, this will be become a problem when the camera box is deployed on a high-speed train, where the images will be captured at a faster speed.

Predictions for static and dynamic railhead images from a separate test on the same railway track with similar conditions, were isolated and compared to confirm if there were major differences in the results and it was found (as seen in Figure 7.24) that the blurriness truly does not greatly impact the value of prediction given. As shown in Figure 7.24, images 1 and 2 are static images with friction coefficients of 0.217 while image 3 which was captured while moving and image 4 captured during the transition period of moving to coming to a halt both had friction coefficients of 0.220 and 0.215 respectively.

The forward-facing images come out fine as the vegetation and surrounding characteristics can be recognised by human eyes regardless of the train speed.

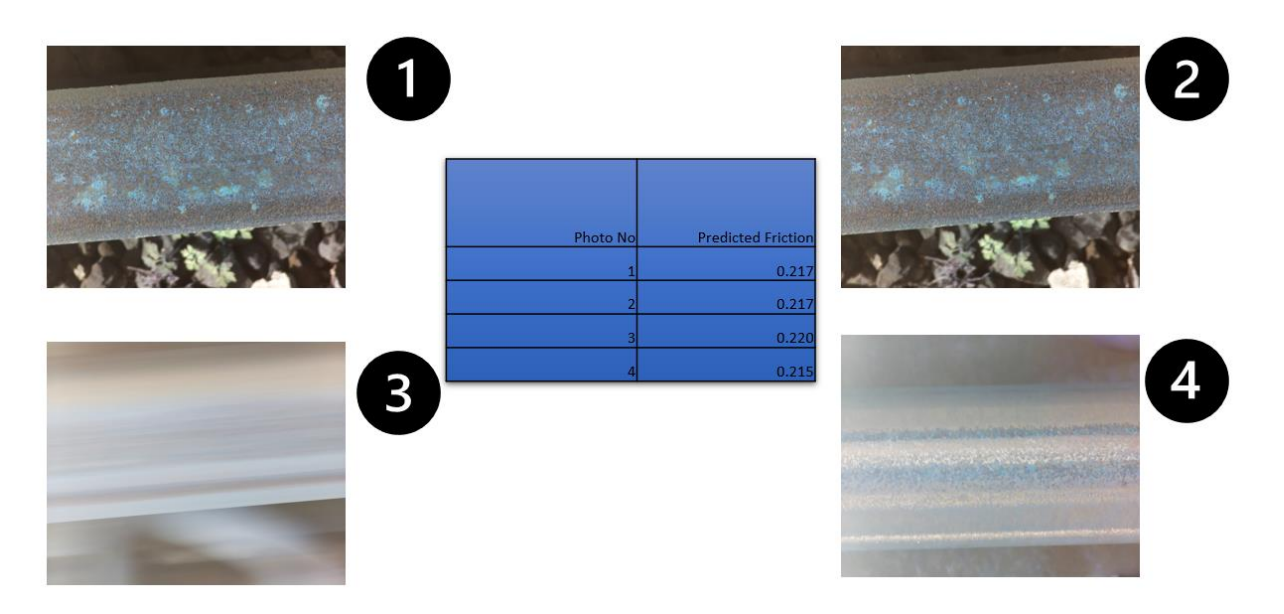


Figure 7. 24: Static vs dynamic friction prediction

Figure 7.15 (a) & (b) showed the environmental data obtained from the camera box and predicted friction from processing the data and images. The friction predicted ranged from 0.231 - 0.255 which is a normal range for the railhead conditions present in WHR. It was also noted that the air temperature recorded had a $\pm 0.3^{\circ}$ C variation for the test duration while the railhead temperature sensor recorded temperatures ranging from 4.8° C – 12.4° C. This shows the railhead temperature sensor captures the real variations occurring on the railhead as the train moves. Some parts of the railhead are shaded by surrounding trains while other parts are exposed to sunshine, the parts exposed to sunlight accounted for the peaks noticed on the railhead temperature plot in Figure 7.15a.



Figure 7. 25: Forward facing images of track sections exposed to sun (L) and a shaded sections towards the platform (R)

Figure 7.25 (L) shows the section of the track that exhibited one of the peak railhead temperatures of 11.1° C. There is no shade there. The image on the right had a railhead temperature of 6.3° C and, as can be seen from the image on the right, the track was shaded from the sun by both the platform edge and the vehicles in the siding.

Research carried out in previous work [70, 85] has also shown that shade covering the railhead (either by clouds or anything blocking the sun) brings about a decrease in

railhead temperature and the exposure to the sun would increase the railhead temperature, as seen here.

7.5.2 ScotRail 30-05-23

This trial was attempted twice, with the first attempt drawing awareness to the fact that all trains do not have their lamp bracket holders positioned in the same place. The Class 142 and 153 used earlier had lamp brackets positioned on the right side of the train and the camera box was configured to that position. A trial was attempted on a Class 170 shown in Figure 7.26, as seen in the image, the holder was positioned towards the centre of the train, therefore the railhead was not in the railhead camera's range.



Figure 7. 26: Class 170 Scotrail train showing camera box position over the railhead

A second trial was done at a different time on a Class 158 train shown in Figure 7.16 where the lamp bracket holder was placed on the left side of the train, since the camera box components were fitted in symmetrical way the 3D printed parts were mirrored and reprinted. The parts were flipped to the opposite sides, and it was close enough to the railhead. For most of the journey from Edinburgh Haymarket to Perth, the camera captured half of the railhead and ballast stones as the lamp bracket holder was about 15cm off the railhead. The forward-facing camera was tilted down (as seen in Table 7.3) in attempt to capture the railhead and analysis the railhead conditions.

Figure 7.17 (a) and (b) show results gathered on a warmer day compared to the previous test carried out at WHR in March. The railhead and air temperatures recorded was between $11.8^{\circ}\text{C} - 20.4^{\circ}\text{C}$ and $14^{\circ}\text{C} - 17^{\circ}\text{C}$ respectively, with relative humidities representative of dry environmental conditions of 47.8% to 63.7%. Given these conditions, the friction recorded is expected to be in the intermediate range and that is what the prediction model confirmed predicting frictions between 0.254 to 0.291.

In addition, the results from this trial showed that the camera box is really only useful as a temporary solution for data capture and in the longer term a more permanent, an integrated solution needs to be developed.

7.5.3 WHR 13-07 & 14-07 2023

After lessons learnt during the Scotrail trials, a third trial was conducted at WHR on a Class 142 train over 2 days. The first day involved repeated short runs of approximately

260m over the track in the depot. So, repeat results were achieved and it was also a great chance to see once again how the prediction tool reacted to slight changes in temperature as the railhead and air got warmer. The sectioned results on Figure 7.19 (a) and (b) showed similar friction ranges predicted over the same section of track for dynamic tests. An example can be seen in section 6 and 8 which had an average predicted friction of 0.229 and 0.227 respectively.

Air temperatures recorded were 19±3°C, showing the sensor was sensitive enough to record the increase/decrease due to environmental factors such as shading, cloud coverage among others, the same can be said for the sensitivity railhead sensors. Figure 7.28 shows evidence of both sensors recording high air temperature 28.7°C due to heat while the railhead sensors recorded lower temperatures of 21.1°C (as seen in Figure 29, sections 1 & 5) due to shading effects over that section of the track.



Figure 7. 27: Forward facing image of a hot spot recorded with air temperature 28.7°C with a shaded railhead section recording 21.1°C on the railhead IR sensor

The railhead temperatures recorded ranged from 20.2°C – 40.3°C , the temperature increased and decreased with exposure to sun or shade as seen in Figure 7.27. This phenomenon is very noticeable where the train is stationary at a spot with exposure to the sun for example in Section 3 and 7 on Figure 7.29 which are located on the same spot. Figure 7.28 shows the stationary position at section 3 recording between 30.1°C – 34.2°C and the right at Section 7 recording between 31.1°C – 32.6°C .



Figure 7. 28: Spots of high railhead temperature with sun exposure for section 3 (L) and section 7 (R)

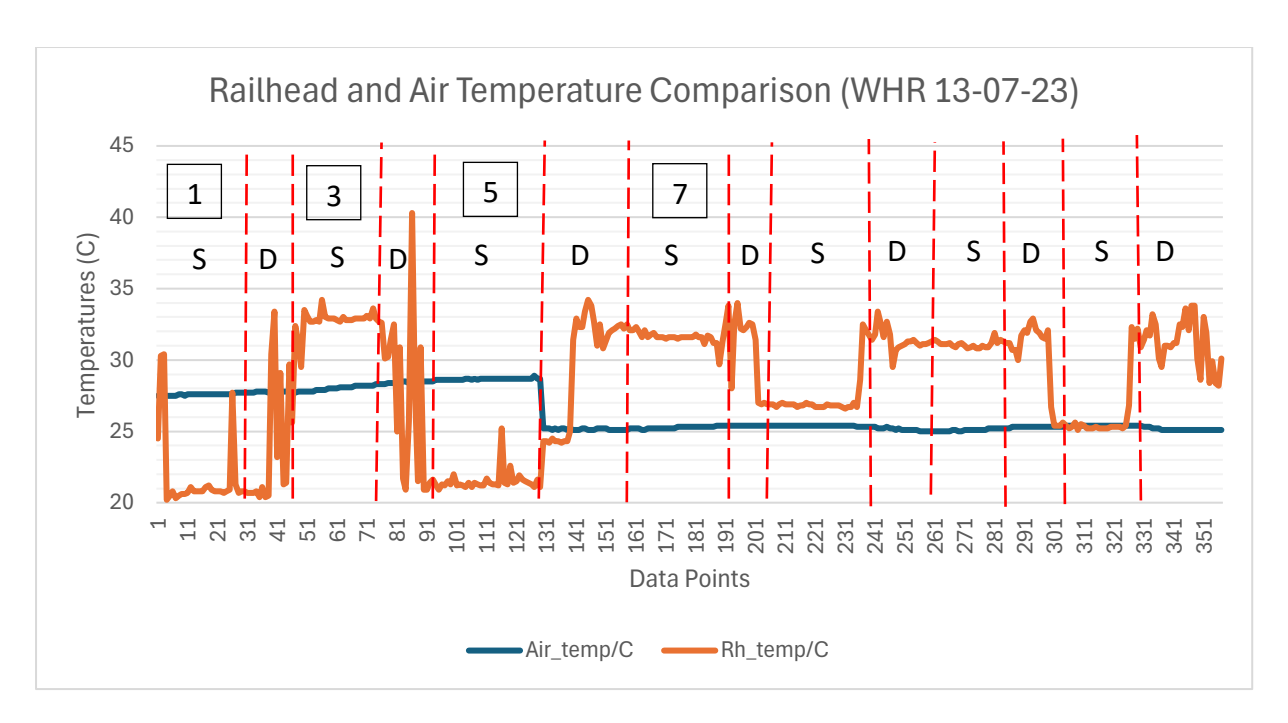


Figure 7. 29: Railhead-air temperature comparison for 13-07-23 tests in WHR

The 40.3° C railhead temperature was recorded on one occasion (the spike can be notice on Figure 7.19 (a)) with most temperatures ranging from 20.2° C – 34.2° C. The friction predicted on this test day ranged from 0.214 – 0.236 and steady friction predictions (with ± 0.001 variations) were recorded over the same section of railhead, that is, where the train was stationary, marked as 'S' in Figure 7.19 (b). Railhead temperatures recorded at stationary spots had $\pm 0.2^{\circ}$ C variations whilst the relative humidity had variations of $\pm 0.2^{\circ}$ M. This furthermore shows the prediction tool takes into account changes in the environmental conditions when making predictions, as it was found in Chapter 4 that these factors play a key role in understanding the wheel-rail adhesion. The step change noticed at the transition from section 5 to 6 was because the camera box was turned off at the end of section 5's run and then restarted at the beginning of section 6.

The trial on the second day used another Class 142 train which was travelling from Leeming Bar to Leyburn, through Bedale and Finghall Lane as a return journey. The one-way journey was an approximately 12 miles and took 42 minutes shown in Section 1 in Figure 7.20 (a) and (b) with 5-minute stop and a 2-minute stop on the return journey at Bedale station, shown in section 2 and 4 and a brief stop in Finghall lane which was not significant enough to be noted on the plot. Section 2 and 4 at Bedale station as determined with the GPS data, showed a uniform friction of 0.285±0.002 for Section 2 and 0.276±0.006 for Section 4. The data captured here was at over 20mph. This did not change the quality of the forward facing or railhead images captured.

Air temperature recorded was $20\pm3^{\circ}\text{C}$ which was similar to the previous tests and the railhead temperatures ranged from 16.9°C – 29.5°C with the majority of them being between 17°C - 24°C .

The friction predicted with all the images ranged between 0.223 – 0.292. Sections 1 and 3 of the plot presented in Figure 7.20 (b) showed a mirroring trough in the predicted friction at 0.223 and 0228 respectively. Upon further investigation it was noticed this was

recorded under a bridge just outside Leeming Bar station, as shown in Figures 7.30 (a), (b), (c) and (d). The decrease in the predicted friction can be accounted by the drop in temperatures experienced under bridge from 21.1°C to 17.1°C and 21.1°C to 17.3°C in Sections 1 and 3 respectively. Work done testing friction levels using the British Rail Research Tribometer train through Saxelby and Asfordby tunnels [86] showed friction levels decreased at the entrance into the tunnels as seen in Figure 7.31. It showed the effects tunnels have on the moisture level, shading and temperature of the railhead.

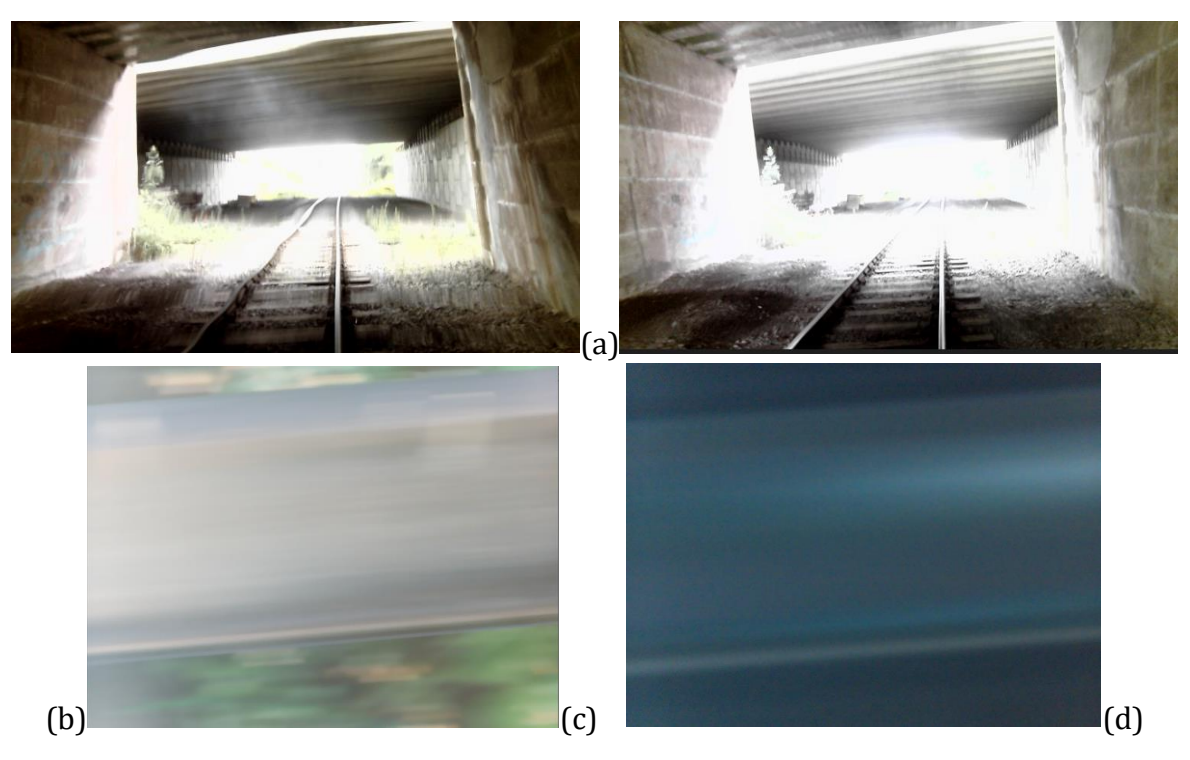


Figure 7. 30: (a) Forward facing image in the tunnel exiting Leeming Bar; (b) Forward facing image in the tunnel approaching Leeming Bar; (c) Corresponding railhead image for 'a'; (d) Corresponding railhead image for 'b'

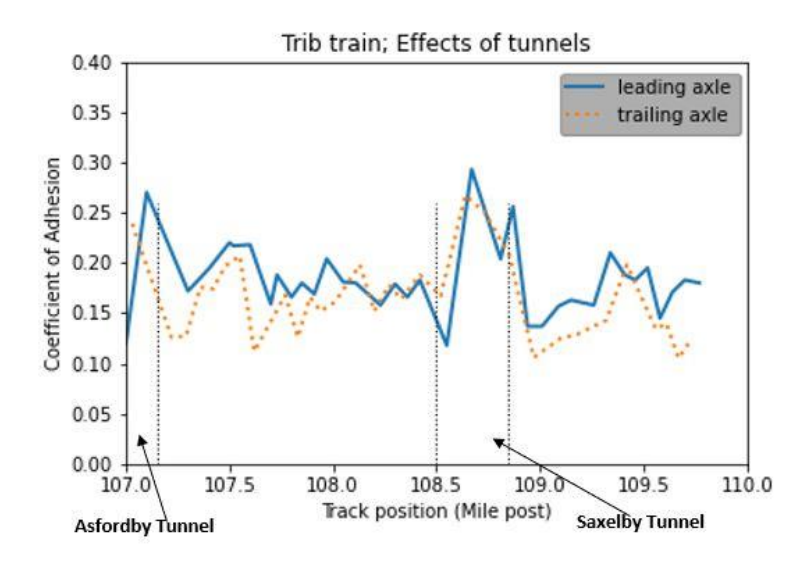


Figure 7. 31: Effects of tunnels on railhead friction measured on a Tribometer train (adapted from [86] by author)

All the images collected at WHR at this point had been under dry railhead conditions and the predictions showed consistency from the first trial to these ones, as the railhead state has not changed. This shows the predictions are not random, but a function of the railhead state and environmental data.

7.5.4 WHR 28-11-23

For the final camera box trial in this work, 2 camera boxes were used. Both camera boxes recorded similar air temperatures in the range of $8\pm2^{\circ}$ C, which shows the temperature sensors have a good tolerance and measure similar data at the same location. The railhead temperatures on the other hand had a temperature range from -1.6°C to 6.2°C for camera box 1 with -1.6 recorded on one instance and majority of low temperature was from 0.8°C. While railhead temperature recorded on camera box 2 ranged from -5.1°C to 15°C with both -5.1 and 15 occurring on one occasion (commonly when the command thread was restarted) and majority of the temperature measured was between 1.9°C – 7.9°C. Camera box 1 measured colder temperatures than box 2 because it was installed at the front of the train which is the leading part, therefore the railhead has cooler temperatures because it has not been run over by the train wheels. While box 2 sensor measured slightly higher temperature as it was on the back of the train which was the trailing side, which had railhead that was already passed over by the wheel.

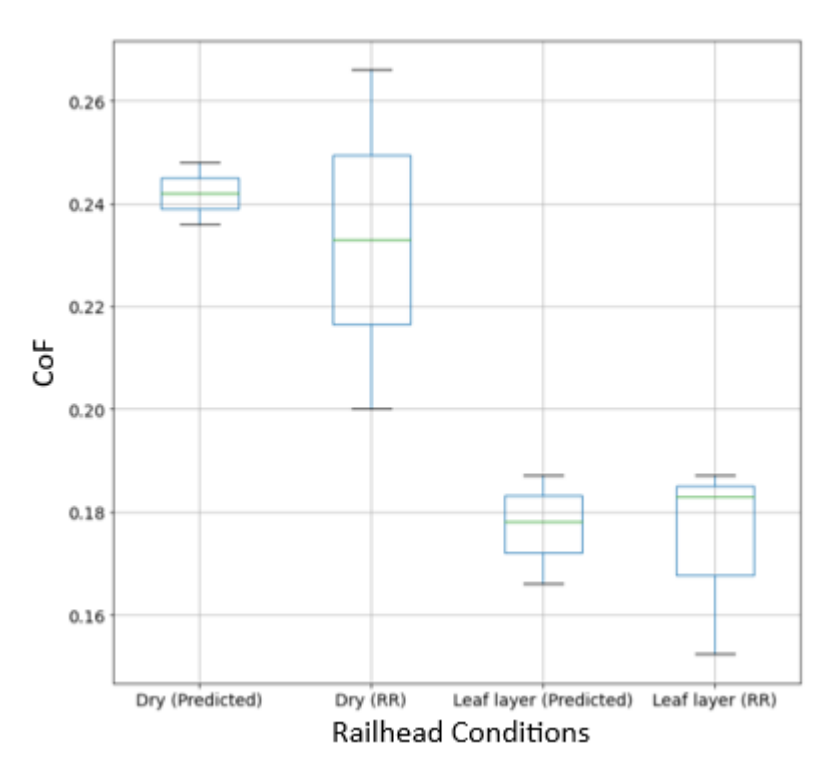


Figure 7. 32: Comparison of Prediction tool and Rivelin Rail (RR) Tribometer Friction for WHR 28-11-23

These tests offered an avenue to compare the friction predictions to friction measured by a tribometer, which in the case was the Rivelin Rail tribometer, as shown in Figure 7.32. The data presented in Figures 7.22 and 7.23 (a) & (c) were recorded during the short runs and during the leaf layer creation. The leaf layer was created on a small section of the railhead as shown in Figure 7.12 and it was represented on the plots with the red dotted

lines. Camera box 1 captures the leaf layer before the trailing camera box 2 which why it has a shorter lead shown on the plot. The predicted friction is seen to reduce at the sections where the leaf layer was being created, emphasised with the red lines. The predicted friction gets progressively lower as the train continues to pass over the leaf layer creating the black layer. The leaf layer was run over six times (3 return movements) represented by the first 6 troughs in Figure 7.23 (c). The final friction predicted of the black leaf layer section was 0.187 for box 1 and 0.182 for box 2 compared to the measured friction of 0.152 on the left side corresponding to the camera box 2 position. Although the prediction tool has not received extensive black leaf layer data training, this result shows that with more data it will accurately prediction friction comparable to a friction measurement device. Cryogenic cleaning was applied to the black layer created after sixth run and the friction predicted at that section significantly increased to around 0.25 on the left track and 0.26 on the right track.

The leaf layer was reapplied a second time on a different section of the track (seen on the second side of the black line labelled 2) and a similar trend was noticed. The model predicted a friction of 0.174 and 0.176 (return) for the leaf layer created after 2 passes while the measured friction was 0.187 on the left track. The right side of the track had a predicted friction of 0.184 compared to 0.183 measured by the tribometer.

The predictions obtained from the long run test from Leeming Bar to Bedale shown in Figure 22 and 23 (b) & (d) have a similar trend to Sections 1 and 3 of the data collected between Leeming Bar, Bedale and return seen in Figure 7.20 (b). The deep trough in the predicted friction was also noticed here at the same location of the under bridge giving a prediction of 0.210 and 0.211 from camera box 1 exiting and entering Leeming Bar respectively. On the hand Camera Box 2 encountered a software error which restarted the thread when exiting Leeming Bar while under the bridge of interest but captured it on the return journey showing the trough in Figure 7.23 (d) predicting 0.201. A second trough which predicted a friction of 0.209 was noticed where a sudden drop in railhead temperature from 3.9°C to -5.1°C where the friction reduces from 0.244 to 0.209. The drop in the temperature definitely caused by an error either from vibrations causing the IR sensor to briefly shift hence a random reading or sensor restarting. The railhead temperature returned to 4°C after the one -5.1°C reading which in turn returned the predicted friction to 0.244.

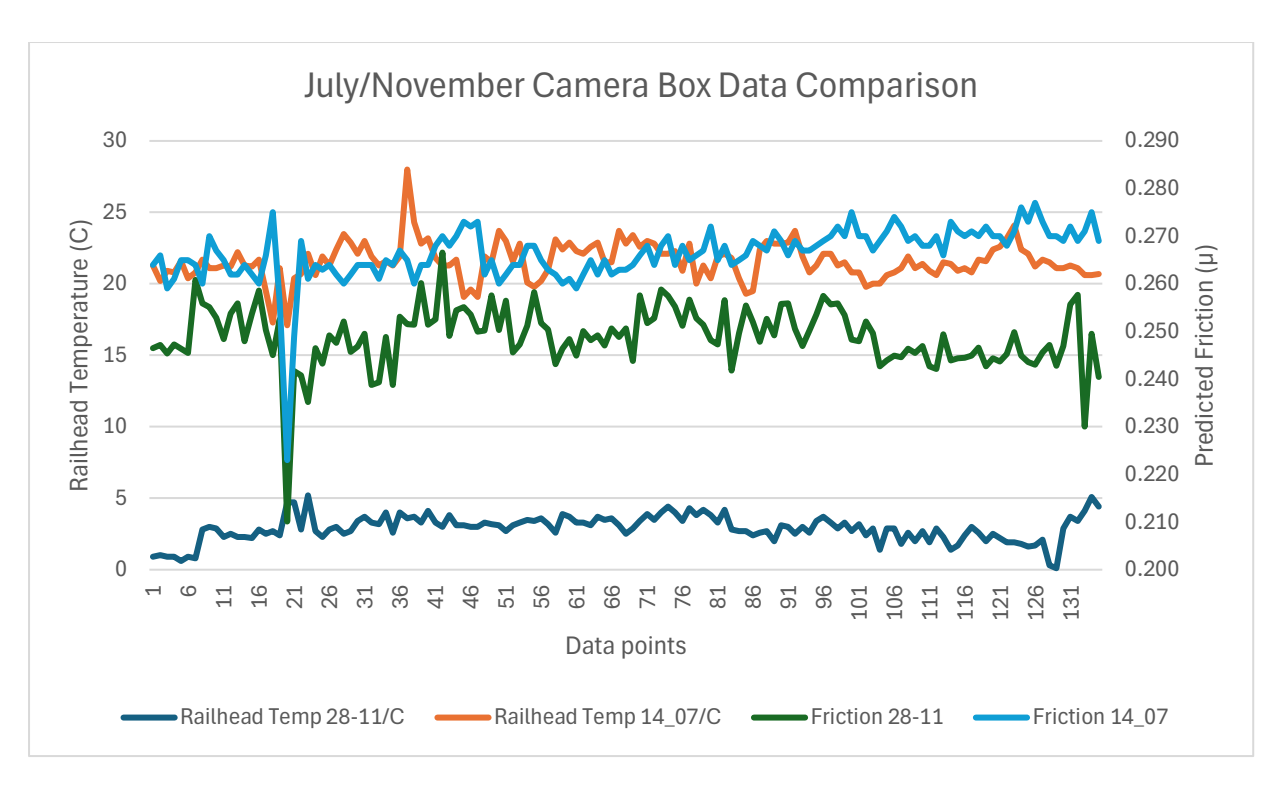


Figure 7. 33: Comparison of data collected from the camera in the summer 14-07-23 to winter 28-11-23

The predicted friction for the long run ranged between 0.227 to 0.282 and 0.227 to 0.270 with exclusion of the tunnel effects and railhead temperature anomaly for camera box 1 and 2 respectively. These predictions are slightly lower than the predictions made by model during the summer period on the same route. Figure 7.33 shows data extracted from the same route which was Leeming Bar to Bedale for 14th July where the railhead temperature was warmer than 28th November 2023. The predicted friction during the summer period was higher by an average of 0.016 than the predicted friction during winter. This correlates with findings made in Chapter 4 that railhead temperature does affect the friction levels, it may not be a big difference, but it does make a difference.

7.6 CONCLUSIONS

- The final set-up using the camera box showed that the concept of an on-train data collection and friction prediction system is feasible.
- The camera box predictions showed consistency over the same area of data collection furthermore proving the output of the prediction tool is not random.
 The prediction tool is also very sensitive to the railhead state such as wet and dry as it is expected to be. Predicting lower friction with the appearance of moisture on the railhead with lower prediction expected if the relative humidity matches.
- From Figure 7.32, it shows the friction prediction model has compared well against the Rivelin Rail tribometer measurements.
- The camera box setup done cannot be a permanent solution as the lamp bracket holder is not fitted on all rolling stock with some having them located in different positions.

- It was proven that the camera works but an integrated data capture system on the train either close to or the wheel boogie will be beneficial for collecting clearer railhead images.
- The camera box designed for this work can be used by the railway industry for other purposes other friction prediction. It can be used for accurate railhead and air temperature with relative humidity which will inform train drivers of the driving conditions. The forward-facing images can be used for monitoring the track surrounding and vegetation management. The GPS data can also aid in narrowing down locations of events recorded.

CHAPTER EIGHT

8. DISCUSSION

8.1 INTRODUCTION

The main aim of this research was to enhance the understanding of wheel/rail low adhesion and subsequently improve adhesion forecasting and validation approaches. In pursuit of this aim, a multifaceted approach was adopted, encompassing a thorough literature review, real-world railhead condition analysis, and the development of the predictive friction model along with hardware for capturing data from the railhead on train.

8.2 OBJECTIVE 1: LITERATURE REVIEW

The initial objective aimed to establish a comprehensive understanding of low adhesion through an exhaustive review of academic literature and operational insights from industry reports, such as those produced by British Rail Research. Key areas of focus encompassed the characteristics of wheel/rail interface, the role played by leaf layers and the wet-rail phenomenon on wheel/rail adhesion. Concurrently, the investigation explored existing approaches for low adhesion measurements and forecasting.

The in-depth literature review laid the foundation for the project, providing crucial insights into the existing knowledge landscape of low adhesion. Unveiling the significance of leaf layers and the wet-rail phenomenon contributed to a significant understanding of the complexities involved. The measurement techniques explored showed the most suitable method for railhead friction data collected, a pivotal aspect for accurate adhesion forecasting.

Gaps were also identified that new technology was needed to fill in terms on adhesion forecasting.

8.3 OBJECTIVE 2: RAILHEAD DATA ANALYSIS

The second objective sought to analyse rail head conditions across various locations and timeframes, offering an ample understanding of how temperatures and relative humidity vary over said time frames and their corresponding impact on railhead friction. Real-world data collection emerged as a critical aspect in achieving a complete understanding of low adhesion. This was also necessary for building a new prediction tool.

The work done in understanding the effects of temperature and relative humidity on the railhead friction showed the importance of the environmental properties in relation to railhead friction. Relative humidity is an important factor in understanding low adhesion on the railhead as seen from the data presented in Chapter 4. The variation in the relative humidity and temperature data makes the results unique, which is usually not considered in in-laboratory or controlled environment testing. A similar study done by Ishida [87] on different rail tracks In Japan, opined that relative humidity had a closer relationship to CoF than rail temperature. That is, high relative humidity brought about a decrease in CoF. Whereas this work has identified the joint effects of rail temperatures and relative humidity changes on railhead CoF, which were discussed in chapter 4.

Further work should be considered for including variations of RH levels for in-laboratory friction tests. A variation of the RH was achieved for in-laboratory data collected in Chapter 6 where the sensitivity of the friction prediction model was discussed, see Figure 6.37. Although this was done for only the wet railhead condition, this variation showed that model reacted to changes in environmental factors, RH in this case.

Air temperature was recorded during the field visits, but was not included in the analysis done, as no independent trend was identified. This was partly because an increase or decrease in the air temperature brought the same effects on the railhead temperature, therefore producing similar trends [85]. On the other hand, where some part of the rail was shaded from the sun the railhead recorded a lower temperature compared to sections exposed to the sun, as seen in Figure 4.11a, 4.13a, 7.26, 7.28 & 7.29. Further into this work in Chapter 7, where air temperature and railhead temperature were recorded using the camera box sensors, the sun exposure effect was noticed more where the railhead temperatures registered higher than air temperature for the area because the railhead exposed absorbed heat rays from the sun. While shading effects were noted where there was a drop in the railhead temperature with the air temperature being stable, Figure 7.30 being a good example.

In addition, the Pendulum tribometer used to measure the railhead friction the model was trained on found it hard to maintain the original moisture or contaminants levels present on the railhead. Due to the sweeping motion of the pendulum arm wiping off the moisture or contamination on the first measurement, thereby altering the subsequent friction levels measured for repeat readings. It will be beneficial to retrain the prediction model using a tribometer with better repeatability like the Rivelin Rail tribometer, which has only recently been developed.

8.4 OBJECTIVE 3: PREDICTION MODEL DEVELOPMENT

The third objective aimed at creating and enhancing a model for friction prediction, using Artificial Intelligence. This involved the incorporation of railhead images and environmental parameters using the Gaussian Process discussed in Chapter 5 to expand of the datasets used within the model. This was needed to cover more railhead conditions and in particular those leading to low adhesion, for example leaf layers. Leaf layer data is very hard to come by as clearly infrastructure owners do not want leaf layers to form and will plan mitigation to avoid this.

The integration of advanced technologies, exemplified by Artificial Intelligence, showcased this research's commitment to leveraging cutting-edge methodologies for improved predictions. The incorporation of visual data, such as railhead images was pivotal in elevating the model's accuracy and reliability. The iterative process of building up datasets within the model underscored the dynamic and evolving nature of the research, ensuring a robust foundation for future predictions.

8.4.1 PREDICTION MODEL LIMITATIONS

While the development of a Neural Network (NN) model for friction prediction is a promising endeavour, it is important to acknowledge potential limitations that may impact its effectiveness. Below are summaries of some considerations:

- **Data Limitations:** The NN model's performance heavily relies on the quality and quantity of available data. Insufficient or biased datasets may hinder its ability to generalize well to diverse rail conditions (this is explained further in the next paragraph).
- **Dynamic Environmental Factors:** Rail environments are subject to dynamic changes in weather, temperature, and other external conditions. The NN model may struggle to adapt to unforeseen variations that are not adequately represented in the training data.
- Complexity of Rail Systems: Railway systems are inherently complex with various interconnected components. The prediction model may oversimplify certain aspects, potentially neglecting obscure interactions that contribute to low adhesion conditions.
- Transferability to Other Rail Networks: Conditions and characteristics of rail
 networks can differ significantly. The model's effectiveness is contingent on the
 similarity of conditions between the training dataset and the target rail network,
 limiting its transferability. Therefore, retraining must be done for applications on
 different rail networks outside of the Scope of this research, that is UK.
- Ethical and Regulatory Considerations: The use of AI models in safety-critical applications such as in the Rail industry raises ethical and regulatory concerns. Ensuring compliance with standards and addressing potential biases is crucial to maintain public trust and safety.

As stated previously in Chapters 5 and 6, the prediction model can only forecast information it is familiar with (that is, previously trained data). Currently the prediction model is limited to information obtained from the Heritage rail tracks and the leaf layer data from the Salisbury incident. This is insufficient data for the model to predict friction accurately on all railhead conditions across the UK. In order to increase the robustness of the prediction tool, it needs to be trained o data collected from as many rail track locations as possible and during operational times and seasons. This is to aid the prediction model's ability to identify and forecast a wide range of railhead conditions that system may encounter on the field. All these being said, access to these rail tracks remain the greatest obstacle in training data collection encountered during this project.

In addition to this, the Salisbury data collected in Chapter 4 showed that pendulum tribometer is not suitable for railhead contamination friction measurement, when the BS 7976-2:2002+A1:2013 [63] measurement repeatability standard (8 repeat measurements) is being followed. Ideally, for contaminated railhead measurements using the pendulum, only 2 readings will be appropriate to capture the friction values before the railhead condition becomes altered by the swiping motion of the rubber pad.

Unfortunately, this variation in measurement method (2 measurements for contaminated railhead conditions) was not included in the model training as it is important to have a consistent form of data collection for the prediction model in order not to introduce bias into the model.

A very recent alternative to the pendulum tribometer is the Rivelin Rail tribometer used in comparing the camera box predictions (Chapter 7). The Rivelin Rail tribometer collects an estimated 300 data points per reading (which is averaged in the final/displayed friction measured) over a wheel running band length of 300mm, showing good repeatability. The Rivelin Rail tribometer employs a free rotating steel wheel, which can produce a similar contact stress experience in the wheel/rail contact. Therefore, there will not be an issue with the contamination or moisture being swept off the railhead. The box plot in Figure 7.32 shows the extent of measurement spread recorded by the Rivelin Rail tribometer (for example leaf layer friction ranged between 0.15 to 0.18) which is low compared to that seen in the Salisbury data time series plot shown on Figure 4.15 (a-c) (for example a measured friction ranging from 0.02-0.14 on Figure 4.15b).

8.5 OBJECTIVE 4: DATA CAPTURE TOOL DEVELOPMENT AND TESTING

The final objective encompassed the development of a simple tool for capturing railhead images, forward facing images and environmental data on a railway vehicle. Tests were conducted on a train in conjunction with the friction prediction tool to validate the output.

The successful development of the Camera box (which was the data capture tool designed) and its integration with the friction prediction model marks a pivotal milestone. Testing the camera box on rolling stock not only validates its feasibility, but also ensures the reliability of the overall prediction model in real-world, dynamic scenarios. The camera box sensors also present a unique insight into the local environmental data around the rail tracks, improving the industry's knowledge on the environment related trends and how it affects the track system. The collective achievement of these objectives has significantly advanced the understanding of low adhesion in the wheel/rail interface low adhesion. The friction prediction model, coupled with real-world data and data capture capabilities, positions this research to make substantial contributions to the improvement of adhesion forecasting in the railway industry.

8.5.1 CAMERA BOX LIMITATIONS

Although the camera box has numerous benefits and has shown great potential for enabling data collection from onboard rolling stock, it has some shortcomings which are listed below.

Unsuitable Lamb Bracket Position on Some Trains: The Camera box has been found to be unsuitable for some types of rolling stock, as discussed in Chapter 7.
 The lamp bracket holder position (which holds the camera box on the train) of different trains is not same which means the railhead camera will not be facing over the railhead sometimes and therefore it will not capture railhead images. In

fact, some trains do not have provision for a lamp bracket holder which implies that the Camera box cannot be the final design for railhead image capture.

- Railhead Image Quality: The railhead images captured from the Camera box as seen in Tables 7.2 through 7.7 emerge looking blurry due to motion of the train. Although, from comparison done in Figure 7.23 it was established that that level of blurriness does not negatively affect the friction prediction, as the model can still identify the colours in the image. The extent of blurriness required to produce inaccurate predictions is currently unknown, but it is safe to assume that as long as the colours are visible in the image, the prediction tool will be able to process the image. An alternative location and means of railhead image capture needs to be created, especially when the prediction model is employed on a train that goes on higher speed than 30mph done in WHR.
- **Remote Control of the Camera Box:** Control of the Camera box is yet to be done remotely. That is, data download is done manually by taking off the Camera box from the train and moving the data from the micro controllers to a flash drive/USB stick. An ideal system where the Camera box data can be uploaded remotely onto a cloud storage, which can then be downloaded for processing by the prediction. This will help automate and speed up the process.

8.6 HOW DOES THE VALIDATED FRICTION PREDICTION MODEL COMPARE TO EXISTING ADHESION FORCAST METHODS?

The developed prediction model holds significant potential to outperform or work alongside existing adhesion forecasting methods in the UK due to several key advancements introduced through this research project. It also has higher confidence when compared to the other methods as it uses real-time data, and the confidence will keep improving as the model training increases (see Table 8.1 for summarised comparison updated from Table 2.4). Listed below are some key characteristics considered when compared.

- Incorporation of Railhead Images: Unlike traditional methods that heavily rely
 on weather and/or train performance data, the prediction tool developed in this
 project incorporates visual and sensor data. These data set provides a holistic and
 real-world representation of the rail conditions, allowing for a more accurate
 assessment of low adhesion scenarios.
- **Comprehensive Data Sets:** The prediction model's development involved the enhancement of traditional programming technique by incorporating more diverse data sets. This includes information gathered through the literature reviewed in this work, railhead data analysis, and the integration of parameters beyond those traditionally considered. The comprehensive data sets contribute to a more robust and adaptable prediction model.
- **Dynamic Friction Understanding:** The focus on understanding adhesion mechanism in the wheel/rail interface makes this model unique. By analysing railhead conditions dynamically and considering the impact of contaminants such

- as leaf layers, the tool is better equipped to predict changes in friction levels, adapting to real-time variations and ensuring more accurate forecasting.
- Validation through Image Sensitivity Tests: The incorporation of a simple imaging tool and its validation through the sensitivity tests adds an extra layer of reliability to the prediction tool. This validation ensures that the tool's output is not only theoretically sound, but also practical and applicable in the dynamic environments typical of railway operations.
- **Potential for Industry Impact:** The overarching aim of positively impacting the railway industry is at the core of this research. The tool's potential to improve adhesion forecasting and validation approaches aligns with the industry's need for enhanced safety, operational efficiency, and cost-effectiveness.

Table 8. 1: Updated adhesion "forecasting" matrix

Туре	Tool	Spatial Resolution			Temporal R	Resolution	1	Confidence	Use		
		Metres	Stations	Routes	Real time	Hours	Days				
Rail/lineside information based	UoS Railhead Friction Prediction Tool (Camera Box)	X	X	X	X			Medium-High	Validated on WHR and ScotRail routes. Validation continues with further training		
	UoS Railhead Friction Prediction Tool (Manual data collection)	X	X		X			Low-Medium	Validation in process		
	Rail eye Sensor	X			X			Low-Medium	Only used at test phase (not on a real train)		
Weather forecast + train performance based	Met Office Adhesion Index	X	X	X		X	X	High – used over many years, verification process in place	Widespread use in UK		
	Swedish Tool		X				X	Low	Still in design phase		
	Operational data based forecast tool by University of Huddersfield and Met Office			X			X	In process	Validated on the Birmingham cross city line		

Train performance	ADS App by (3Squared)		X		X			Information unavailable	Information unavailable
based	Porterbrook			X			X	TBC	Validation in process
Rail/lineside information based + weather based	ACCAT	X		X		X		Medium-High	Used by London Underground on the central line and metropolitan line

Table 8.1 summarises the capabilities of the friction prediction model both for use in the camera box and with manual data capture (that is with a mobile phone, IR sensors or weather station data). The camera box set-up yields very good results with validation and higher confidence when further trained with relevant datasets for train routes. It has spatial resolution in metres, stations, and routes because of the GPS module whereas the manual data capture is based on the user's location and there is a limit to the amount of data a user can collect manually. In addition, the camera box set-up has in-built temperature sensors which collect environmental data at the same time as the images are taken. This increases the reliability and sensitivity of the data set when compared to manual data collection where the user may not have correct tools for environmental data collection.

The advancements made in this project suggest that it has the potential to offer a more sophisticated, accurate, and practical solution for adhesion forecasting in the UK's railway industry. The integration of novel technologies and a focus on real-world conditions positions this tool as a valuable asset in addressing the challenges associated with low adhesion.

CHAPTER NINE

9. CONCLUSIONS AND RECOMMENDATIONS

9.1 CONCLUSIONS

This research has improved the understanding of low adhesion mechanisms in the wheel/rail interface using data collected in the field and proven that Artificial Intelligence can be used by the railway industry to predict railhead friction. The Camera box set-up resulting from this work will play a key role in the future of low adhesion mitigation and also in recording environmental data that could be useful for other issues such as track buckling due to high temperatures. The Camera box temperature sensor will work independently without railhead image capture, if necessary to obtain environmental data and in conjunction with the GPS module, the location of the data collection can be obtained. The set-up has turned out to be a versatile tool, which with proper usage and/or training will increase the usefulness.

The important conclusions that can be drawn from this thesis that is novel are:

- The real-world environmental data (relative humidity, temperature) was important in understanding low adhesion mechanisms and should be considered in friction prediction models as used here. High relative humidity (>75%) with moisture is very likely to propagate low friction levels on the railhead. In addition, this work confirmed that railhead temperature is not fully dependent on air temperature. The railhead temperature is usually independent of the air temperature when external factors are in play such as shading from trees, buildings among others; cloud coverage on a warm day; a section of the railhead is in the direct line of sun exposure in a cold day.
- The Gaussian model is ideal for the type of data determined to key in understanding and predicting railhead friction (which are numerical and non-numerical data). The development and enhancement of this Neural Network model represent a leap forward in railhead friction prediction capabilities. The incorporation of visual and environmental data has refined the model's accuracy and adaptability, making it a powerful tool for friction prediction. The current model presents good precision for the data it has been trained, evident in the increase in log-likelihood when retrained. The model robustness increases with continuous training on diverse and good quality set of data, hence improving the precision for wider area of application.
- The prediction model used in this research currently conforms to real-world data, especially in terms of environmental information as drawn from the in-lab sensitivity tests. This shows the tool fully takes into account the temperatures and relative humidity when making the predictions, therefore the friction prediction is informed and not random.
- The successful integration of the prediction model and versatile data collection system created in this research, namely the camera box showed these results from this work can be employed by the Rail industry. The tool's validation (using the Rivelin Rail tribometer and Met Office data) not only assures its theoretical and

experimental reliability, but also positions it as a viable solution for railhead friction prediction in the near future and lineside environmental data collection.

In conclusion, this research represents a significant step in the right direction in addressing the challenges associated with low adhesion in the Rail industry. The achievements and contributions made during this study set the stage for industry advancements and ongoing research endeavours. The impact of this work is expected to positively impact the railway industry, contributing to a safer, more efficient, and cost-effective rail operations.

9.2 RECOMMENDATIONS FOR FUTURE WORK

As the work concludes, below are some avenues for future exploration split into general and industry recommendations:

GENERAL RECOMMENDATIONS

- The prediction model should be retrained with friction measurements from a tribometer other than the Pendulum tribometer due to its poor repeatability on contaminated railheads. The Rivelin Rail tribometer will be a good alternative as it has better repeatability and shares the portable characteristics of the Pendulum.
- Ongoing refinement of the prediction model should be pursued. This includes incorporating feedback from real-world applications to enhance accuracy and adaptability. Continuous training of the model is also required, especially with regularly used routes with help the predictions conform with these routes.
- The design of the prediction model does not consider any wheel characteristics such as the roughness or contamination presence on the wheel. In situations where a clean wheel with rough, returned surface runs on a contaminated rail, it has the ability cut through contamination on the railhead. Whereas low adhesion may occur in the contact of a clean railhead and contaminated wheel. Development of a new measurement technique looking at the wheel/rail contact in different surface conditions is required. This may be done using the linear full-scale-wheel-on-rail-rig or HAROLD, to build up new friction relationships for training a future prediction model.
- Further testing should be carried out to consider the usage of alternative or additional railhead cameras that can capture some railhead properties better than a regular camera. An example of such is an Ultra-Violet or an Infra-Red camera, which have shown to aid identification of railhead contamination [56].

INDUSTRY RECOMMENDATIONS

• The next step involves integrating the developed tools and approaches with existing industry practices. This includes creating a specialised data collection (eliminating sensor noise and blurry images) and integrating with a rolling stock, it will also push for automation of the data processing. Collaboration with rail operators and relevant stakeholders will be crucial for seamless adoption.

- In line with integrating the tool with industry existing practices, One Big Circle has a railhead camera set-up attached to the cowcatcher/rail guard of some rolling stock. The images captured are in black and white format in addition they are high resolution. They have stated friction levels can be estimated by inspecting at these railhead images, although this method has not been validated yet. It is suggested that further work can be done in capturing, analysis and classifying black and white railhead images under as many conditions as possible. This will inform us of the feasibility of this method in identifying the railhead state and determine if this can be translated to a similar prediction model as that of this research. If this yields a positive outcome, the new prediction model can be integrated into the existing railhead image capture system.
- The success of this research in the UK suggests the potential for adaptation to other railway networks globally. Assessment of applicability in different environments and climates could further extend the impact of these findings.

9.3 PUBLICATIONS ARISING FROM THIS WORK IOURNAL PUBLICATIONS

M. O. Folorunso, R. Lewis, and J. L. Lanigan, "Effects of temperature and humidity on railhead friction levels," Proceedings of the Institution of Mechanical Engineers, Part F: Journal of Rail and Rapid Transit, vol. 237, no. 8, pp. 1009-1024, 2023.

M. O. Folorunso, M. Watson, A. Martin, J. W. Whittle, G. Sutherland, and R. Lewis, "A Machine Learning Approach for Real-Time Wheel-Rail Interface Friction Estimation," Journal of Tribology, vol. 145, no. 9, p. 091102, 2023.

CONFERENCES AND SEMINAR PRESENTATIONS

Michael Watson, Morinoye Folorunso, Alan Martin, Jacob Whittle, Graham Sutherland, Roger Lewis. "A Machine Learning Approach for Real Time Wheel/Rail Interface Friction Estimation," Presented at the 13th World Congress for Railway Research, held in Birmingham, UK on 9 June 2022.

Morinoye Folorunso, "Predicting Railhead Friction Levels Using Artificial Intelligence (AI)" Presented at the knowledge exchange seminar between UNAL Medellin Colombia and The University of Sheffield, held in Medellin, Colombia on 1 November 2022.

Morinoye Folorunso, Roger Lewis, Joseph Liam Lanigan, "The Effects of Relative Humidity and Temperature on Railhead Friction" Presented at the 9th International Tribology Conference, held in Fukuoka, Japan on 30 September 2023.

Roger Lewis & Morinoye Folorunso. "A Machine Learning Tool for On-Train Adhesion Estimation" Presented at the IMechE Tribo-sensing and Condition Monitoring – The Journey to Net Zero, held in London, UK on 25 October 2023.

10. REFERENCES

- [1] Department of Transport, "Transport Statistics Great Britain," London:Crown, 2019.

 Accessed: 8 March 2021. [Online]. Available:

 https://assets.publishing.service.gov.uk/government/uploads/system/uploads/attachment

 data/file/870647/tsgb-2019.pdf
- [2] H. Ritchie. Which form of transport has the smallest carbon footprint? [Online] Available: https://ourworldindata.org/travel-carbon-footprint
- [3] RSSB. "Adhesion." Rail Safety and Standard Board. https://www.rssb.co.uk/what-we-do/key-industry-topics/adhesion (accessed 07 January 2021, 2021).
- [4] K. Ishizaka, S. R. Lewis, and R. Lewis, "The low adhesion problem due to leaf contamination in the wheel/rail contact: Bonding and low adhesion mechanisms," *Wear*, vol. 378, pp. 183-197, 2017.
- [5] M. Harmon and R. Lewis, "Review of top of rail friction modifier tribology," *Tribology Materials, Surfaces & Interfaces*, vol. 10, no. 3, pp. 150-162, 2016/07/02 2016, doi: 10.1080/17515831.2016.1216265.
- [6] R. Lewis and U. Olofsson, Wheel-rail interface handbook. Elsevier, 2009.
- [7] C. Jones, W. Tyfour, J. Beynon, and A. Kapoor, "The effect of strain hardening on shakedown limits of a pearlitic rail steel," *Proceedings of the Institution of Mechanical Engineers, Part F: Journal of Rail and Rapid Transit,* vol. 211, no. 2, pp. 131-140, 1997.
- [8] H. Hertz, "Über das Gleichgewicht schwimmender elastischer Platten," *Annalen der Physik,* vol. 258, no. 7, pp. 449-455, 1884.
- [9] K. L. Johnson, *Contact Mechanics*. Cambridge: Cambridge University Press, 1985.
- [10] J. Srivastava, P. Sarkar, and V. Ranjan, "Contact stress analysis in wheel-rail by Hertzian method and finite element method," *Journal of The Institution of Engineers (India): Series C,* vol. 95, pp. 319-325, 2014.
- [11] R. Zong and M. Dhanasekar, "Analysis of rail ends under wheel contact loading,"

 International Journal of Mechanical and Aerospace Engineering, vol. 6, pp. 452-460, 2012.
- [12] V. Garg, Dynamics of railway vehicle systems. Elsevier, 2012.
- [13] L. Huang, Z. Li, L. Li, and Q. An, "Methods to calculate accurate wheel/rail contact positions and static contact stress levels," *Proceedings of the Institution of Mechanical Engineers, Part F: Journal of Rail and Rapid Transit*, vol. 230, no. 1, pp. 138-150, 2016.
- [14] D. T. Eadie, H. Harrison, R. Kempka, R. Lewis, A. Keylin, and N. Wilson, "Field assessment of friction and creepage with a new tribometer," in *Proceedings of the 11th International Conference on Contact Mechanics and Wear of Rail/wheel Systems, CM*, 2018, pp. 208-217.
- [15] S. Bhardawaj, R. C. Sharma, and S. K. Sharma, "Development and advancement in the wheel-rail rolling contact mechanics," in *IOP Conference Series: Materials Science and Engineering*, 2019, vol. 691, no. 1: IOP Publishing, p. 012034.
- [16] J. Liu, L. Liu, J. He, C. Zhang, and K. Zhao, "Wheel/rail adhesion state identification of heavy-haul locomotive based on particle swarm optimization and kernel extreme learning machine," *Journal of advanced transportation*, vol. 2020, 2020.
- [17] A. Monk-Steel, D. Thompson, F. De Beer, and M. Janssens, "An investigation into the influence of longitudinal creepage on railway squeal noise due to lateral creepage," *Journal of Sound and Vibration*, vol. 293, no. 3-5, pp. 766-776, 2006.
- [18] G. Trummer, L. Buckley-Johnstone, P. Voltr, A. Meierhofer, R. Lewis, and K. Six, "Wheel-rail creep force model for predicting water induced low adhesion phenomena," *Tribology International*, vol. 109, pp. 409-415, 2017.
- [19] E. A. Gallardo-Hernandez and R. Lewis, "Twin disc assessment of wheel/rail adhesion," *Wear*, vol. 265, no. 9-10, pp. 1309-1316, 2008.
- [20] R. Stock, L. Stanlake, C. Hardwick, M. Yu, D. Eadie, and R. Lewis, "Material concepts for top of rail friction management-Classification, characterisation and application," *Wear*, vol. 366, pp. 225-232, 2016.

- [21] C. Fulford, "Characteristics of railhead leaf contamination: Review of low adhesion research," *Rail Safety and Standards Board Rep,* vol. 354, p. 181, 2004.
- [22] L. Buckley-Johnstone, "Wheel/Rail Contact Tribology: Characterising Low Adhesion Mechanisms and Friction Management Products," Doctor of Philosophy, Department of Mechanical Engineering, The University of Sheffield, 2017.
- [23] A. W. G. (AWG), "Managing Low Adhesion", doi: https://www.raildeliverygroup.com/media-centre-docman/121-2018-01-managing-low-adhesion-ed6-0/file.html.
- [24] Rail Safety & Standard Board (RSSB), "T1042: Investigation into the effect of moisture on rail adhesion," London, 2014.
- [25] B. White, Z. S. Lee, and R. Lewis, "Towards a Standard Approach for the Twin Disc Testing of Top-Of Rail Friction Management Products," *Lubricants*, vol. 10, no. 6, p. 124, 2022.
- [26] R. The University of Sheffield, Met Office, "Deliverable 2.1 WP2- Existing Low Adhesion Monitoring Techniques: Short report that details merits and limitations of existing low adhesion monitoring techniques (direct and proxy)." in "Setting the Verification Standard for Adhesion Forecasting," London, 2019.
- [27] G. I. Crabb, Brown, S., Sanders, P. D., Wright, D., McRobbie, S., Viner, H., "Investigation of novel systems for monitoring rail adhesion.," 2013, vol. PPR678.
- [28] R. Lewis, R. Dwyer-Joyce, S. Lewis, C. Hardwick, and E. Gallardo-Hernandez, "Tribology of the wheel-rail contact: the effect of third body materials," *International Journal of Railway Technology*, vol. 1, no. 1, pp. 167-194, 2012.
- [29] L. Buckley-Johnstone, R. Lewis, K. Six, G. Trummer, J. Stow, and H. Alturbeh, "T1149: Extension of WILAC Low Adhesion Mode," RSSB Project Report, 2020.
- [30] B. White *et al.*, "Effect of the presence of moisture at the wheel-rail interface during dew and damp conditions," *Proceedings of the Institution of Mechanical Engineers, Part F: Journal of Rail and Rapid Transit*, vol. 232, no. 4, pp. 979-989, 2018.
- [31] U. Olofsson, "A multi-layer model of low adhesion between railway wheel and rail," *Proceedings of the Institution of Mechanical Engineers, Part F: Journal of Rail and Rapid Transit,* vol. 221, no. 3, pp. 385-389, 2007.
- [32] B. White and R. Lewis, "Simulation and understanding the wet-rail phenomenon using twin disc testing," *Tribology International*, vol. 136, pp. 475-486, 2019.
- [33] Y. Zhu, U. Olofsson, and H. Chen, "Friction between wheel and rail: a pin-on-disc study of environmental conditions and iron oxides," *Tribology letters*, vol. 52, no. 2, pp. 327-339, 2013.
- [34] RSSB, "Guidance on Wheel / Rail Low Adhesion Measurement.," 160 Euston Road, London NW1 2DX, 2008. [Online]. Available: https://www.rssb.co.uk/standards-catalogue/CatalogueItem/GMGN2642-Iss-1
- [35] H. Harrison, T. McCanney, and J. Cotter, "Recent developments in coefficient of friction measurements at the rail/wheel interface," *Wear*, vol. 253, no. 1-2, pp. 114-123, 2002.
- [36] R. Lewis, S. R. Lewis, Y. Zhu, S. Abbasi, and U. Olofsson, "The modification of a slip resistance meter for measurement of railhead adhesion," *Proceedings of the Institution of Mechanical Engineers, Part F: Journal of rail and rapid transit,* vol. 227, no. 2, pp. 196-200, 2013.
- [37] S. Lewis, R. Lewis, and U. Olofsson, "An alternative method for the assessment of railhead traction," *Wear*, vol. 271, no. 1-2, pp. 62-70, 2011.
- [38] M. Pálinkó, "Estimation of wheel-rail friction at vehicle certication measurements," ed, 2016.
- [39] J. Lundberg, M. Rantatalo, C. Wanhainen, and J. Casselgren, "Measurements of friction coefficients between rails lubricated with a friction modifier and the wheels of an IORE locomotive during real working conditions," *Wear*, vol. 324, pp. 109-117, 2015.
- [40] Tribonet. "Pin on Disk Test." https://www.tribonet.org/wiki/pin-on-disk-test/ (accessed 12 November 2020, 2020).

- [41] J. Sundh, U. Olofsson, and K. Sundvall, "Seizure and wear rate testing of wheel-rail contacts under lubricated conditions using pin-on-disc methodology," *Wear*, vol. 265, no. 9-10, pp. 1425-1430, 2008.
- [42] R. Lewis *et al.*, "Full-scale Investigation of Friction Effects of Leaf Layers in the HAROLD Full-Scale Test-Rig," 1 The University of Sheffield, Department of Mechanical Engineering, UK; 2 Virtual Vehicle Research Center, Graz, Austria; 3 Institute of Railway Research, University of Huddersfield, UK., 2020.
- [43] Traintesting. "The Tribometer train." http://www.traintesting.com/tribometer train.html (accessed 30 April 2021, 2021).
- [44] Y. Zhu, U. Olofsson, and A. Söderberg, "Adhesion modeling in the wheel-rail contact under dry and lubricated conditions using measured 3D surfaces," *Tribology International*, vol. 61, pp. 1-10, 2013.
- [45] Y. Zhu and U. Olofsson, "An adhesion model for wheel-rail contact at the micro level using measured 3d surfaces," *Wear*, vol. 314, no. 1-2, pp. 162-170, 2014.
- [46] MetOffice. "Rail- Weather and climate services." https://www.metoffice.gov.uk/services/transport/rail (accessed 12 October 2020, 2020).
- [47] V. Chapman, "Understanding Adhesion Forecasting [Video & PowerPoint presentation]." 2018.
- [48] MetOffice. "Weather data for business "
 https://www.metoffice.gov.uk/services/data/business-data (accessed 12 October 2020, 2020).
- [49] R. El Rashidy, J. Stow, V. Chapman, L. Fawcett, and E. Dyer, "Feasibility of Integrating Operational Data with Adhesion Forecasts," in "ADHEsion REsearch challenge (ADHERE): Forecasting Adhesion," Institute of Railway Research; University of Huddersfield; The Met Office, COF-FCA-03, 29-07-2020 2020. [Online]. Available: https://www.sparkrail.org/Lists/Records/DispForm.aspx?ID=26857
- [50] R. Lewis, V. Chapman, L. Fawcett, E. Brock, and M. Harmon, "Setting Verification Guidance for Adhesion Forecasting-Feasibility COF-FCA-02," 2020, vol. COF-FCA-02.
- [51] G. Rowe, "The Autumn challenge-The leaves on the line saga," in " A report of the LURS meeting at All Souls clubhouse," 2008. [Online]. Available:

 https://www.lurs.org.uk/articles10 htm files/meeting%20reports.pdf
- [52] DB. "DB ESG awarded London Underground Contract."

 https://dbesg.deutschebahn.com/esg/news/press releases/press release esg awarded lo

 ndon-underground-511538 (accessed 2020).
- [53] L. Chapman, E. Warren, and V. Chapman, "Using the internet of things to monitor low adhesion on railways," in *Proceedings of the Institution of Civil Engineers-Transport*, 2016, vol. 169, no. 5: Thomas Telford Ltd, pp. 321-329.
- [54] 3Squared. "RailSmart ADS." https://3squared.com/railsmart/adhesion-digital-solution/ (accessed 2020).
- [55] R. Nilsson, "Practical experiences and research in the area of low adhesion at Stockholm Public Transport," 2013.
- [56] U. Olofsson, Y. Zhu, S. Löfving, J. Casselgren, L. Mayer, and R. Nilsson, "An Optical Sensor for the Identification of Low Adhesion in the Wheel-Rail Contact," in 9th International Conference on Contact Mechanics and Wear of Rail/Wheel Systems, CM 2012, 27 August 2012 through 30 August 2012, Chengdu, China, 2012: Southwest Jiaotong University, pp. 318-323.
- [57] Porterbrook, "Targeted Adhesion Management Using On-Train Data [PowerPoint presentation]," 2021.
- [58] J. Kocijan, Banko, B., Likar, B., Girard, A., Murray-Smith, R., & Rasmussen, C., " A case based comparison of identification with neural network and Gaussian process models.," presented at the Intelligent Control Systems and Signal Processing: ICONS, Algarve, Portugal, 2003.

- [Online]. Available: chrome-extension://efaidnbmnnnibpcajpcglclefindmkaj/https://pure.mpg.de/pubman/item/item_1 792471 2/component/file 3185562/pdf2314.pdf.
- [59] GoogleEarth, "Midland Railway, Butterley Station, 1:30," ed, 2021.
- [60] GoogleEarth, "Ecclesbourne Valley Railway, Wirksworth Station, 1:50," ed, 2021.
- [61] GoogleEarth, "Peak Rail, Darley dale Station, 1:30," ed, 2021.
- [62] S. Lewis, R. Lewis, P. Richards, and L. Buckley-Johnstone, "Investigation of the isolation and frictional properties of hydrophobic products on the rail head, when used to combat low adhesion," *Wear*, vol. 314, no. 1-2, pp. 213-219, 2014.
- [63] *Pendulum testers*, B. S. Institution, April 2013 2013.
- [64] R. Galas *et al.*, "The low adhesion problem: The effect of environmental conditions on adhesion in rolling-sliding contact," *Tribology International*, vol. 151, p. 106521, 2020.
- [65] A. Meierhofer, G. Trummer, C. Bernsteiner, and K. Six, "Vehicle tests showing how the weather in autumn influences the wheel-rail traction characteristics," *Proceedings of the Institution of Mechanical Engineers, Part F: Journal of Rail and Rapid Transit,* vol. 234, no. 4, pp. 426-435, 2020.
- [66] Y. Lyu, E. Bergseth, and U. Olofsson, "Open system tribology and influence of weather condition," *Scientific reports*, vol. 6, no. 1, pp. 1-11, 2016.
- [67] R. Hui, "MBTA-Green Line Influence of Temperature and Humidity on Coefficient of Friction," Kelsan Technologies Corp, 2004.
- [68] Y. Zhu, U. Olofsson, and K. Persson, "Investigation of factors influencing wheel-rail adhesion using a mini-traction machine," *Wear*, vol. 292, pp. 218-231, 2012.
- [69] NationalGeographic. "Dew."

 https://education.nationalgeographic.org/resource/dew/#:~:text=Moisture%20changes%20

 from%20water%20vapor,collect%20as%20a%20water%20source. (accessed 15 December 2021, 2021).
- [70] L. Chapman, J. Thornes, and S. White, "Thermal imaging of railways to identify track sections prone to buckling," *Proceedings of the Institution of Mechanical Engineers, Part F: Journal of Rail and Rapid Transit,* vol. 220, no. 3, pp. 317-327, 2006.
- [71] RAIB, "Collision between passenger trains at Salisbury Tunnel Junction, Wiltshire, 31 October 2021," Derby UK, 2023. [Online]. Available:

 https://assets.publishing.service.gov.uk/media/655b8d4a046ed4000d8b9c95/R122023_231

 024 Salisbury.pdf
- [72] J. M. Chambers and T. J. Hastie, "Statistical models," in *Statistical models in S.* UK: Routledge, 2017, pp. 13-44.
- [73] S. Brahim-Belhouari and A. Bermak, "Gaussian process for nonstationary time series prediction," *Computational Statistics & Data Analysis*, vol. 47, no. 4, pp. 705-712, 2004.
- [74] C. M. Bishop and N. M. Nasrabadi, *Pattern recognition and machine learning* (no. 4). Springer, 2006.
- [75] A. George and A. Vidyapeetham, "Anomaly detection based on machine learning: dimensionality reduction using PCA and classification using SVM," *International Journal of Computer Applications*, vol. 47, no. 21, pp. 5-8, 2012.
- [76] S. Van der Walt *et al.*, "scikit-image: image processing in Python," *PeerJ*, vol. 2, p. e453, 2014.
- [77] J. Lee, Y. Bahri, R. Novak, S. S. Schoenholz, J. Pennington, and J. Sohl-Dickstein, "Deep neural networks as gaussian processes," *arXiv preprint arXiv:1711.00165*, 2017.
- [78] Met Office. "Weather Observations Website WOW." https://wow.metoffice.gov.uk/observations/details/20240301bx1trfqzzhe67kyhyyguiqfawh (accessed 01 March, 2024).
- [79] Google Maps, "Royston Railway Sports Club," ed, 2024.
- [80] Google Maps, "Wensleydale Railway (Leeming Bar Station)," ed, 2024.

- [81] P. Krier, J. Lanigan, P. Ferriday, and R. Lewis, "Development and implementation of novel cryogenic railhead cleaning technology," *Permanent Way Institution Journal*, vol. 138, pp. 35-39, 2020.
- [82] J. Jaffe, B. White, J. Lanigan, and R. Lewis, " "A novel methodology for developing ultra-low adhesion leaf layers on a full-scale wheel/rail rig", "*Proceedings of the Institution of Mechanical Engineers, Part F: Journal of Rail and Rapid Transit,* vol. 0, no. 0, p. 09544097231216521, doi: 10.1177/09544097231216521.
- [83] Rivelin Rail. "Friction Management through Friction Measurement." https://rivelinrail.com/tribometer (accessed 1 March, 2024).
- [84] Earth Point. "Convert Coordinates Calculate a position in a variety of formats." https://www.earthpoint.us/convert.aspx (accessed 23 February.
- [85] L. Chapman, J. Thornes, Y. Huang, X. Cai, V. Sanderson, and S. White, "Modelling of rail surface temperatures: a preliminary study," *Theoretical and Applied Climatology*, vol. 92, no. 1, pp. 121-131, 2008.
- [86] D. J. Watkins, "Exploring adhesion with British Rail's tribometer train," *Railway Engineering Journal*, vol. 4, no. 4, 1975.
- [87] M. Ishida, "Managing the wheel-rail interface: the Japanese experience," in *Wheel-Rail Interface Handbook*: Elsevier, 2009, pp. 701-758.

11. APPENDICES

APPENDIX A:

A-1 SAMPLE DATA SHEET AND SPREAD SHEET USED IN COLLATING FIELD DATA

TITLE: NN Based Regression for LA Estimation Autumn data collection dates available ORIGIN UoS ISSUE 4.3DATE 03/12/2019

Track Measurement Record Sheet

Date of measurements	Person taking Measurements	Sheet no.
	Tay.	
Site	Site	
Mileage	Mileage	
Time, hh:mm	Time, hh:mm	
RH photo file names	RH photo file names	
Air temperature, *C	Air temperature, °C	
Relative humidity, %	Relative humidity, %	
Dew point, °C	Dew point, °C	
RH temperature, °C	RH temperature, °C	
Eddy current probe, μm	Eddy current probe, μι	rn
5-10 Pendulum values	5-10 Pendulum values	
Swab ID	Swab ID	
Weather (wind, clouds, sun, rain? etc.)	Weather (wind, clou sun, rain? etc.)	ds,
Spray mark location	Spray mark location	

Figure 1: Data collection sheet

	Α	В	С	D	Е	F	G	Н	1	J	K	L	M	N	0	Р	Q
1	Date of measurements	Person taking measurements	Sheet	site	mileage	time	end time	photo	air_temp		dew_poi	rh_temp	layer_thick	friction	Swab ID	Weather (wind, clouds, sun, rain? etc.)	
				Wirksworth													
2	01/12/2020	JW, MOF, TB	103	Station		11:42:00		GOPR3064.JPG	14	48.3	3.66	0.6	3.4	65		Sun	False
3	01/12/2020	JW, MOF, TB	103	Wirksworth South Station		11:50:00		GOPR3065.JPG	12.8	50.4	2.88	-3.1	1.8	63.25		Sun	False
4	01/12/2020	JW, MOF, TB	103	Wirksworth South Bridge		11:54:00		GOPR3066.JPG	12	52	2.4	-1	0	64.375		Sun	False
5	01/12/2020	JW, MOF, TB	103	Wirksworth Out building pole		11:57:00		GOPR3067.JPG	12.4	54.4	3.28	2.4	0	45.75		Sun	False
6	01/12/2020	JW, MOF, TB	104	Wirksworth 10 MPH sign		12:00:00		GOPR3068.JPG	12.1	51.7	2.44	1.3	3.6	71.75		Sun	False
7	01/12/2020	JW, MOF, TB	104	Wirksworth Points		12:05:00		GOPR3069.JPG	12.5	55.2	3.54	2.4	4.6	70.125		Sun	False
8	01/12/2020	JW, MOF, TB	104	Wirksworth Miniature Railway Gate		12:09:00		GOPR3070.JPG	12.5	53.5	3.2	2.4	12.6	63.625		Sun	False
9	01/12/2020	JW, MOF, TB	104	Wirksworth 1/4 Mile Marker		12:12:00		GOPR3071.JPG	11.5	58.9	3.28	1.6	8	35.75		Sun	False
10	01/12/2020	JW, MOF, TB	105	Wirksworth Crossing Sign		12:17:00		GOPR3072.JPG	11.3	55.8	2.46	3.5	8.4	58.25		Sun	False
11	01/12/2020	JW, MOF, TB	105	Wirksworth Clearing		12:20:00		GOPR3073.JPG	10.8	56.7	2.14	0.3	7.4	56.375		Sun	False
12	01/12/2020	JW, MOF, TB	105	Wirksworth 15 MPH sign		12:24:00		GOPR3074.JPG	10.4	60.2	2.44	0	9.2	52.75		Sun	False
13	01/12/2020	JW, MOF, TB	105	Wirksworth Ground channel		12:29:00		GOPR3075.JPG	10.2	61.7	2.54	-0.6	7	55.75		Sun	False
14	01/12/2020	JW, MOF, TB	106	Wirksworth Stop sign		12:34:00		GOPR3076.JPG	10.3	62.2	2.74	0.6	10	59		Sun	False
15	01/12/2020	MOF, TB	106	Idridgehay North Platform		13:05:00		GOPR3077.JPG	12	52.7	2.54	4.2	2.6	56.625		Sun	False

Figure 2: Data spreadsheet sample.

A-2 ADDITIONAL RESULTS FROM ENVIRONMENTAL EFFECTS ANALYSIS IN CHAPTER 4.

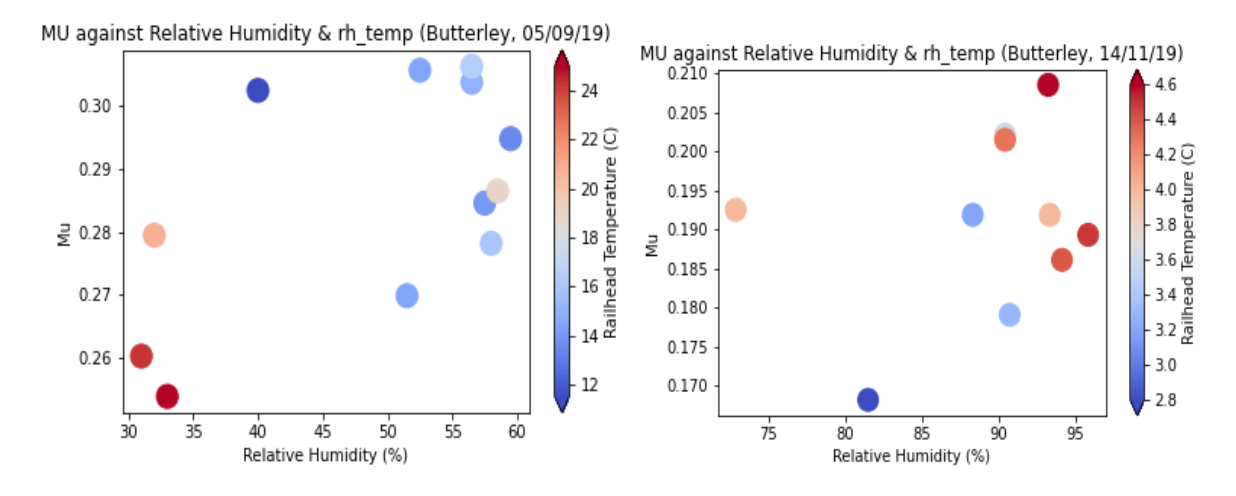


Figure 3: μ against relative humidity with a colour map representing railhead temperature for Butterley

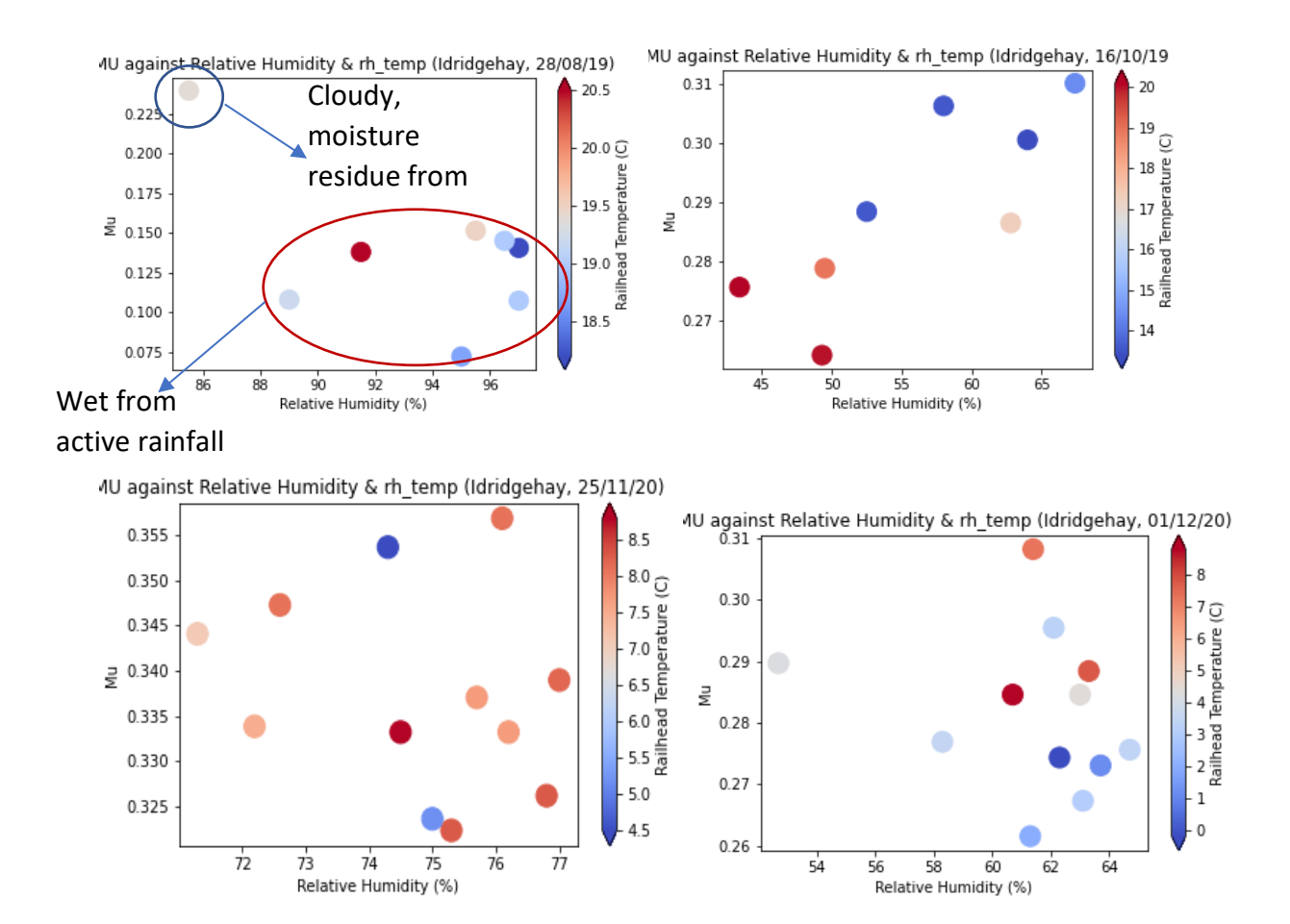
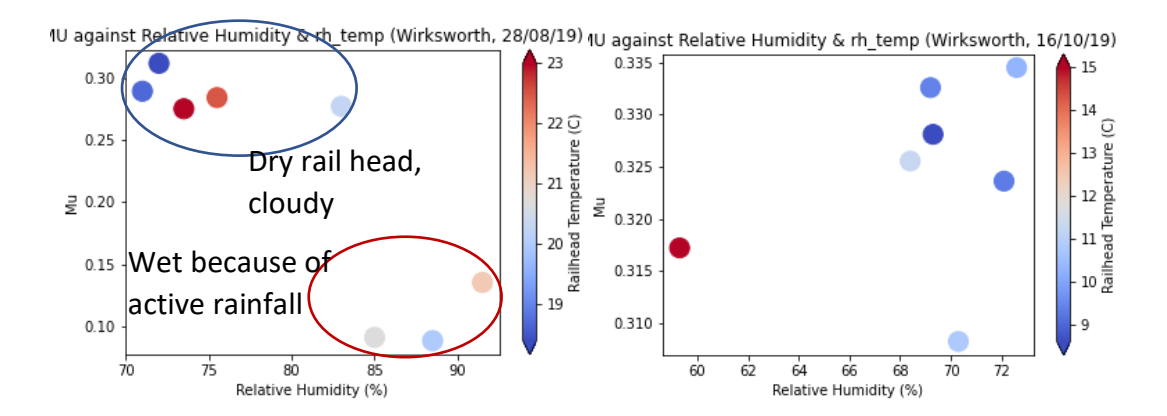


Figure 4: μ against relative humidity with a colour map representing railhead temperature for Idridgehay



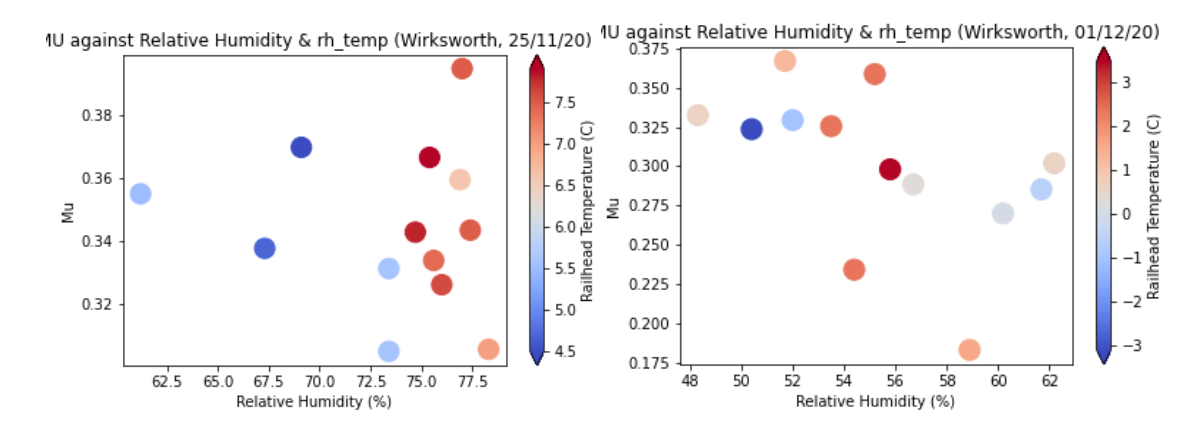


Figure 5: μ against relative humidity with a colour map representing railhead temperature for Wirksworth

APPENDIX B: PREDICTION MODEL CODES

B-1 GAUSSIAN PROCESS import pickle as pkl import pathlib import pandas as pd _this_path = pathlib.Path(__file__).parent.absolute() _all_ = ['GPModel'] class GPModel: def __init__(self): models_path = pathlib.PurePath(_this_path, 'gp_models.pkl') models = pkl.load(open(models_path, 'rb')) self.x_scaler = models['x_scaler'] self.f_scaler = models['f_scaler'] self.x_col = models['x_col'] self.gp_model = models['fitted_process'] def __call__(self, x): data = pd.DataFrame(x)for col1, col2 in zip(data.columns, self.x_col): assert col1 == col2 data_norm = pd.DataFrame(self.x_scaler.transform(data), columns=data.columns) prediction_norm, std = self.gp_model.predict(data_norm, return_std=True) cov = std/prediction_norm prediction = self.f_scaler.inverse_transform(prediction_norm) return prediction, cov

B-2 FORWARD FACING IMAGES

```
import cv2 # opencv image library
import pandas as pd # data manipulation library
import numpy as np # numeric python library
import minisom # self organising maps library
import tensorflow_hub as hub # database of pretrained models
from sklearn.preprocessing import StandardScaler
from sklearn.decomposition import PCA
import pickle as pkl
import pathlib
_this_path = pathlib.Path(__file__).parent.absolute()
_all_ = ['ImageMapper']
class ImageMapper:
 def __init__(self):
    models_path = pathlib.PurePath(_this_path, 'ffi.pkl')
   models = pkl.load(open(models_path, 'rb'))
    # do all checks here
    self.scaler = models['scaler']
   assert isinstance(self.scaler, StandardScaler)
    self.pc_analyser = models['pca']
    assert isinstance(self.pc_analyser, PCA)
    self.som = models['som']
```

```
assert isinstance(self.som, minisom.MiniSom)
    extractor path
                                            pathlib.PurePath(_this_path,
                                                                                    'tf2-
preview_mobilenet_v2_feature_vector_2')
    self.extractor = hub.KerasLayer(str(extractor_path), input_shape=(224, 224, 3))
 def get_map_point(self, paths_to_ff_image: str) -> dict:
   x = \prod
   y = \prod
   for path in paths_to_ff_image:
      if path is None:
        x.append(None)
        y.append(None)
        continue
      images = _read_trim_resize_image(path)
      features = self.extractor(images)
      data = pd.DataFrame(features)
      data_norm = pd.DataFrame(self.scaler.transform(data))
      pc = pd.DataFrame(self.pc_analyser.transform(data_norm))
      this_x, this_y = self.som.winner(pc[0])
      x.append(this_x)
    rtn_dict = {'ffi_x': x, 'ffi_y': y}
    return rtn_dict
def _read_trim_resize_image(file_name: str):
  """Reads trims and resizes the front facing rail view images
 Parameters
  -----
```

```
file_name: str
```

The full path of the image file including the extension

```
Returns
 im_1, im_2: np.arrays
  .....
 image_size = (224, 224, 3)
 image = cv2.imread(file_name)
 if image.shape != (343, 609, 3):
    original_shape = (343, 609)
    times_too_big = [i / o for i, o in zip(image.shape, original_shape)]
    cropped_shape = [int(o * np.min(times_too_big)) for o in original_shape]
    starts = [(i - c) // 2 \text{ for } i, c \text{ in } zip(image.shape, cropped_shape)]
    cropped = image[starts[0]:starts[0] + cropped_shape[0],
            starts[1]:starts[1] + cropped_shape[1]]
    resized = cv2.resize(cropped, (original_shape[1], original_shape[0]))
    image = resized
 im_1 = image[10:10 + image_size[0], 50:(image_size[1] + 50)]
 im_2 = image[10:10 + image_size[0], -1 * (image_size[1] + 50):-50]
 return np.array([im_1, im_2], dtype=np.float32) / 255
def _extract_features(images):
  extractor_path
                                            pathlib.PurePath(_this_path,
                                                                                      'tf2-
preview_mobilenet_v2_feature_vector_2')
```

```
extractor = hub.KerasLayer(str(extractor_path), input_shape=(224, 224, 3))
  return extractor(images)
B-2 RAILHEAD IMAGES
import datetime
import pandas as pd
import numpy as np
import os
import skimage.io as io
import skimage.filters as filt
import skimage.color as color
__all__ = ['get_features']
def get_features(rail_head_file_names: str):
  black = []
  orange = []
  edge_v = []
  colors = []
  mean_brightness = []
  for file_name in rail_head_file_names:
    print (file_name)
    sub_im = _read_and_localise(file_name)
    black.append(find_black(sub_im))
    orange.append(find_orange(sub_im))
    edge_v.append(sobel_v(sub_im))
```

```
colors.append(mean_color(sub_im))
    mean_brightness.append(mean_bright(sub_im))
  rtn_dict = {'mean_brightness': mean_brightness,
        'black': black,
        'orange': orange,
        'edge_v': edge_v,
        'color': colors}
  return rtn_dict
def mean_bright(image):
  return np.mean(image.flatten())
def sobel_h(image):
  gray = color.rgb2gray(image)
  return np.mean(np.abs(filt.sobel_h(gray)))
def sobel_v(image):
  gray = color.rgb2gray(image)
  return np.mean(np.abs(filt.sobel_v(gray)))
def mean_color(image):
  hsv = color.rgb2hsv(image)
  return np.mean(hsv[:,:,0] * hsv[:,:,1])
```

```
def find_orange(image):
 hsv = color.rgb2hsv(image[200:600, :, :])
 orange = np.clip(np.abs(hsv[:, :, 0] - 1 / 12), 0, 1 / 12) * -12 + 1
 o_adjust = orange * hsv[:, :, 1] * hsv[:, :, 2]
 return np.mean(o_adjust)
def find_black(image):
 hsv = color.rgb2hsv(image[200:600, :, :])
 thresh = 0.3
 black = np.clip(thresh - hsv[:, :, 2], 0, thresh) / thresh
 black_sat = np.clip(thresh - hsv[:, :, 1], 0, thresh) / thresh
 return np.mean(black_sat * black)
def _read_and_localise(file_name):
 if not os.path.exists(file_name):
    raise ValueError("Rail head image not found")
 im = io.imread(file_name)
  #resolution of image aka image size
 #sub_im = im[500:2500, 1500:2500, 2]
 sub_im = im[250:1200, 250:1250, 2]
 filt_im = filt.gaussian(sub_im, sigma=10)
 sobel_im = filt.sobel_v(filt_im)
 rail = np.std(filt_im, 1) / np.mean(filt_im, 1) ** 3 * np.mean(np.abs(sobel_im), 1)
 window size = 500
```

```
rail_starts = [sum(rail[i:i + window_size]) for i in range(len(sobel_im) - window_size)]
 start = np.argmin(rail_starts)
  #final_sub_im = im[500 + start:500 + start + window_size, 1500:2000, :]
  #(windowsize height:width)
 final_sub_im = im[250 + start:250 + start + window_size, 750:1000, :]
 return final_sub_im
B-3 PREDICTOR PROCESS
from .forward_facing_images import ImageMapper
from .rail_head_images import get_features
from .gausian_process import GPModel
import numpy as np
_all_ = ['Predictor']
class Predictor:
 def __init__(self):
    self.mapper = ImageMapper()
    self.gp_model = GPModel()
  def predict(self, air_temp, humidity, rail_temp, layer_thickness,
        is_raining, rail_head_file_name, forward_facing_file_name=None):
   n = \frac{(np.log(humidity/100) + (17.27*air_temp)}{(273.3+air_temp))}/17.27
    dew_point = 237.3*n/(1-n)
   x = {'air_temp': air_temp, 'humidity': humidity,
      'dew_point': dew_point, 'rh_temp': rail_temp,
```

'layer_thick': layer_thickness,

'is_raining': is_raining}

x.update(get_features(rail_head_file_name))

if forward_facing_file_name is not None:

x.update(self.mapper.get_map_point(forward_facing_file_name))

return self.gp_model(x)

init process

from .forward_facing_images import ImageMapper

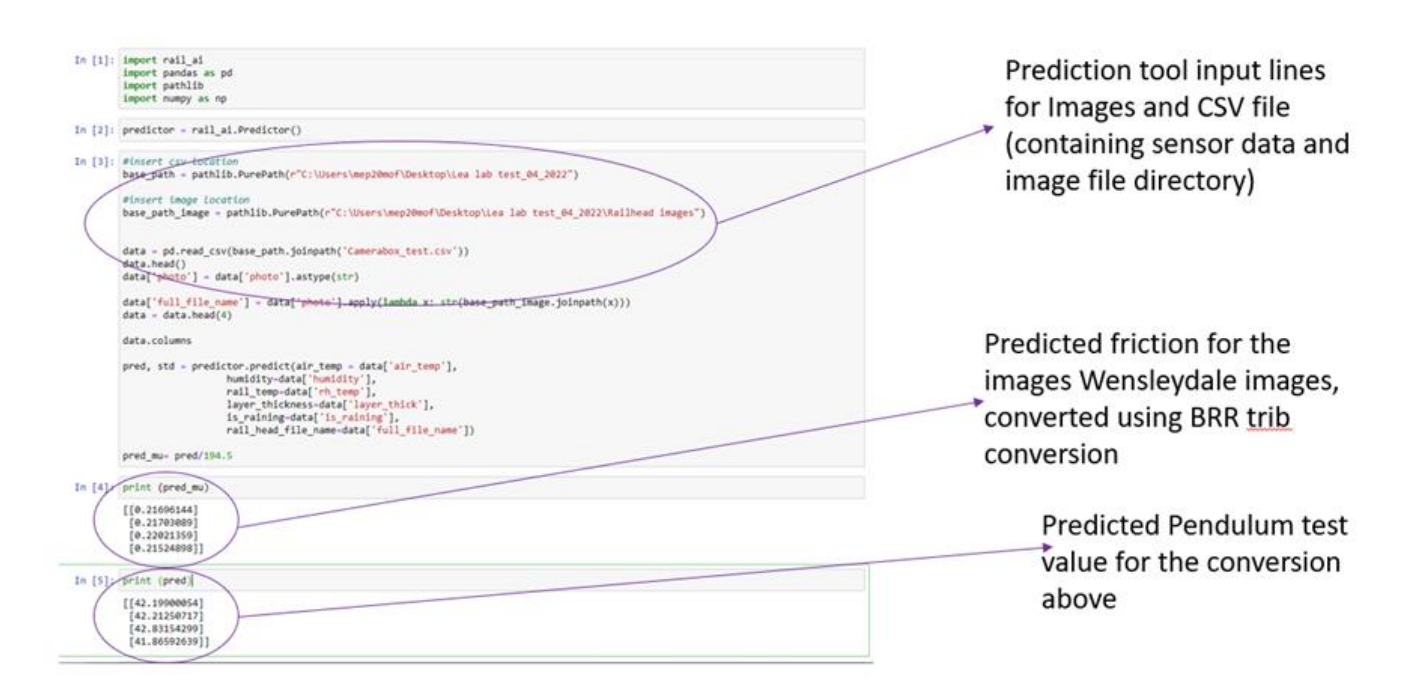
from .rail_head_images import get_features

from .gausian_process import GPModel

from .predictor import Predictor

all = ['Predictor', 'GPModel', 'get_features', 'ImageMapper']

B-4 PREDICTION MODEL INTERFACE



```
In [1]: import rail_ai
        import pandas as pd
        import pathlib
       import numpy as np
In [2]: predictor = rail_ai.Predictor()
In [3]: #insert csv location
        base_path = pathlib.PurePath(r"C:\Users\mep20mof\Desktop\WHR_NOV")
        #insert image location
        base_path_image = pathlib.PurePath(r"C:\Users\mep20mof\Desktop\WHR_NOV\Railhead_images_28_11")
        data = pd.read_csv(base_path.joinpath('whr_nov1.csv'))
        data.head()
        data['photo'] = data['photo'].astype(str)
        data = data.head(991)
        #data [:,400:1000]
        data.columns
        pred, std = predictor.predict(air_temp = data['air_temp'],
                        humidity=data['humidity'],
                        rail_temp=data['rh_temp'],
                        layer_thickness=data['layer_thick'],
                        is_raining=data['is_raining'],
rail_head_file_name=data['full_file_name'])
        pred mu= pred/195.45
```

B-5 IMAGE FEATURES

```
import rail_ai
```

import os

import numpy as np

import pathlib

import pandas as pd

data = pd.read_csv(r"C:\Users\mep20mof\Documents\Mep20mof doc\data_update.csv")

base_path = pathlib.PurePath(r"G:\My Drive\AI project-Roger Lewis\WP0 D0 Data
collection")

photo_path = data['photo'].apply(lambda x: str(base_path.joinpath(x)))

features = rail_ai.get_features(photo_path)

data['mean_brightness'] = pd.DataFrame(features['mean_brightness'])

```
data['black'] = pd.DataFrame(features['black'])
data['orange'] = pd.DataFrame(features['orange'])
data['edge_v'] = pd.DataFrame(features['edge_v'])
data['color'] = pd.DataFrame(features['color'])
data.to csv(r"C:\Users\mep20mof\Documents\Mep20mof
doc\data_update_withImganalysis_March22.csv")
B-6 GP FITTING_MO
import sklearn.gaussian process as gp
from sklearn.preprocessing import MinMaxScaler
import seaborn as sns
import pandas as pd
import matplotlib.pyplot as plt
import numpy as np
from scipy.optimize import minimize_scalar
from scipy import stats
import statsmodels.formula.api as smf
from sklearn.model_selection import KFold as KF, RepeatedKFold as RKF
from sklearn.gaussian_process.kernels import RBF, Matern, RationalQuadratic,
ConstantKernel as C, WhiteKernel as WK
data
                           pd.read_csv(r'C:\Users\mep20mof\Documents\Mep20mof
doc\data_update_withImganalysis_March22.csv')
data_small = data.drop(columns = ['people', 'location', 'photo','Unnamed: 0', 'Unnamed:
0.1', 'weather', 'site'])
models = \{\}
X = data_small.drop(columns = ['date','time', 'friction', 'edge_h'])
y = data['friction']
x_scaler = MinMaxScaler()
X_scaled = pd.DataFrame(x_scaler.fit_transform(X), columns = X.columns)
```

```
models['x_scaler'] = x_scaler
friction_scaler = MinMaxScaler()
y_scaled = friction_scaler.fit_transform(np.array(y).reshape(-1, 1))
models['f_scaler'] = friction_scaler
kernel = 0.5 + C(1.0) * RBF(1) + WK(0.1)
process = gp.GaussianProcessRegressor(kernel=kernel, n_restarts_optimizer=9)
fitted = process.fit(X_scaled, y_scaled)
preds_gp, sigma = fitted.predict(X_scaled, return_std=True)
X_scaled.columns
models['fitted_process']=fitted
models['x_col'] = X.columns
import pickle as pkl
pkl.dump(models, open('gp_models.pkl','wb'))
preds_gp.shape
plt.figure(figsize= (5,5))
plt.scatter(preds_gp, y_scaled)
ax = plt.gca()
plt.grid(True)
plt.ylabel("Actual Friction")
plt.xlabel("Predicted Friction")
plt.plot([0,1],[0,1], 'r:')
ax.set_xlim(0,1)
ax.set_ylim(0,1)
plt.savefig("GP fitting.png", dpi=500)
```

APPENDIX C: CAMERA BOX

C-1: CAMERA BOX PART DESIGNS

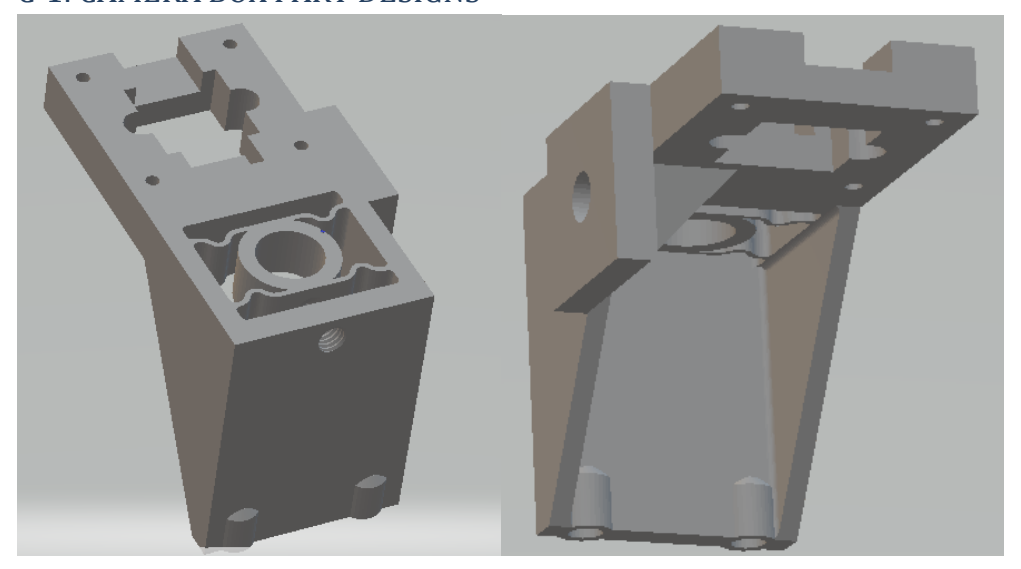


Figure 6: 3-D design of railhead camera and IR Thermometer sensor mount

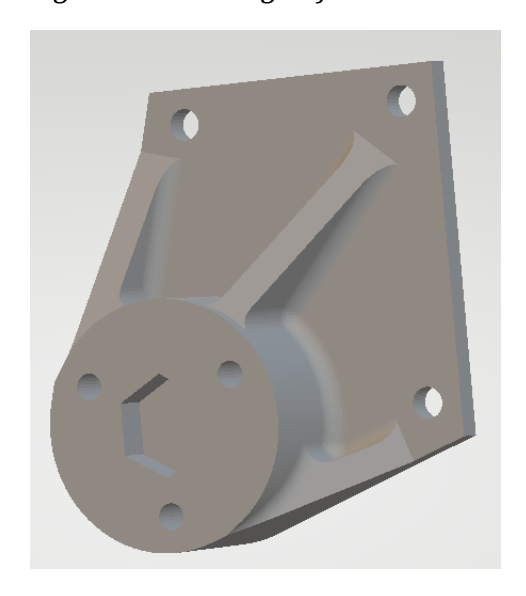


Figure 7: 3-D design of front facing camera mount



Figure 8: 3-D design of battery case bottom (L) with microcontroller mount on the cover (R)

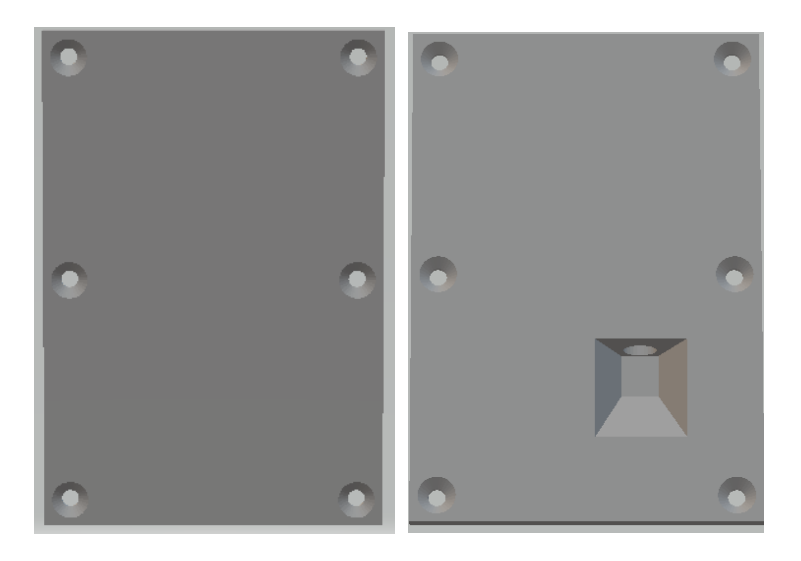


Figure 9: 3-D design for side panels for camera box with air temperature and humidity thermometer slot on the right

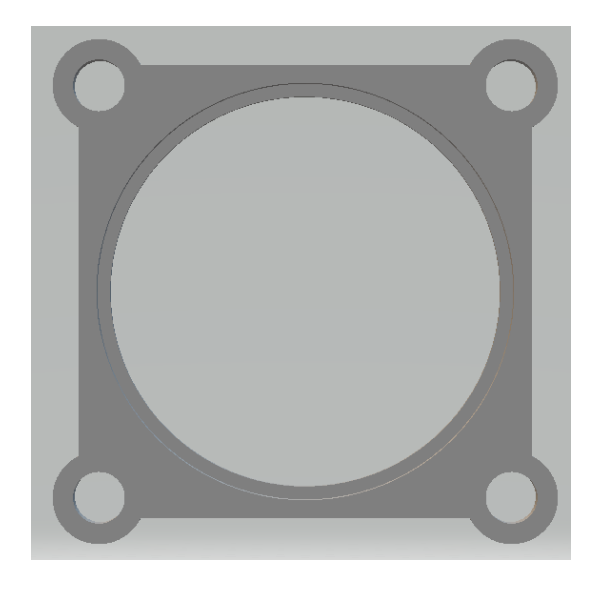


Figure 10: 3-D design for germanium window holder

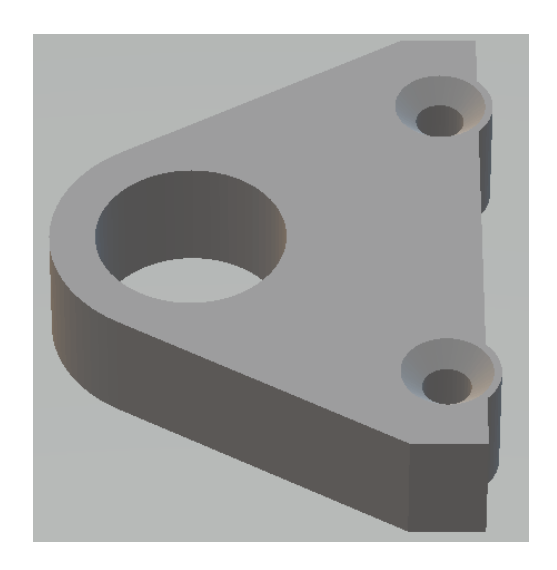


Figure 11: 3-D design for IR thermometer holder

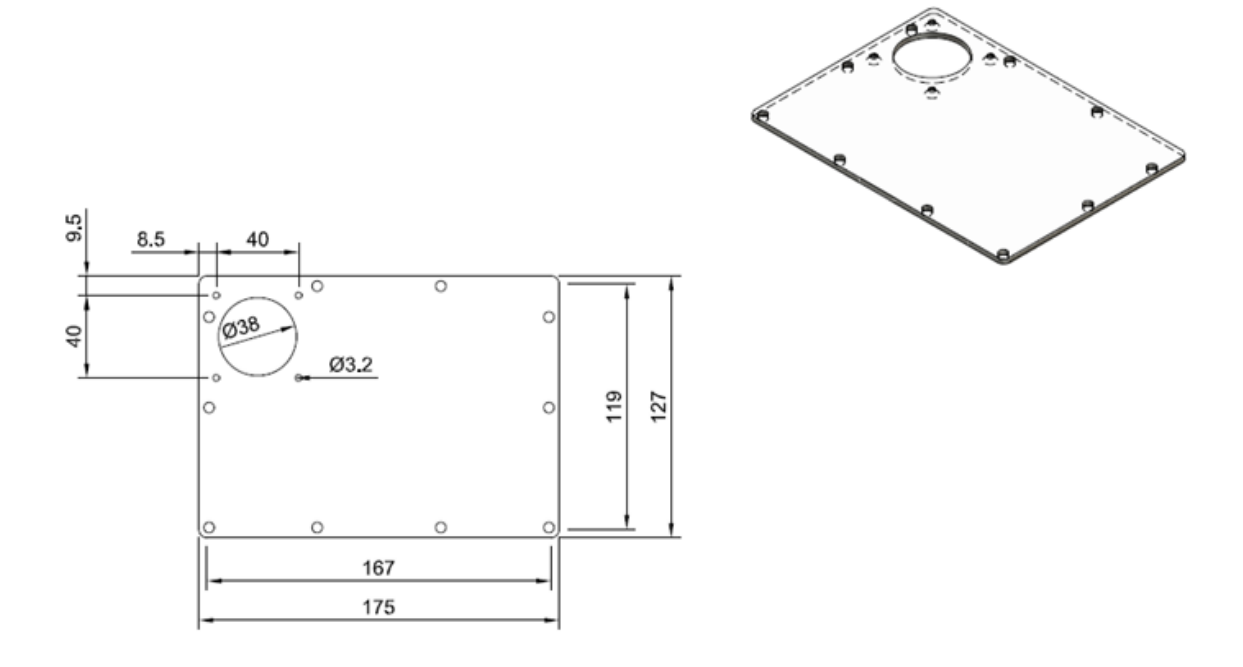


Figure 12: Engineering drawing for Perspex glass insert with Germanium window

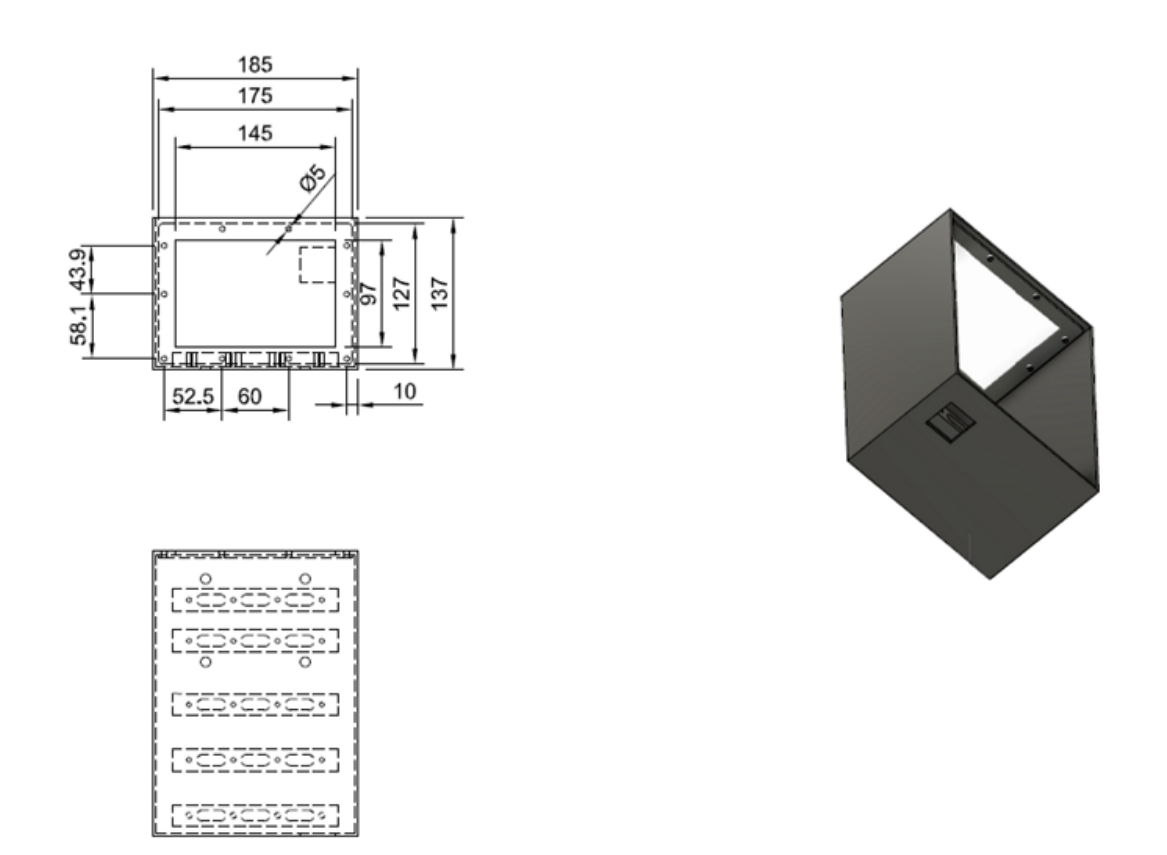


Figure 13: Engineering drawing of the modified camera box body with 3-D isometric view

C-2: CAMERA BOX DATA SAMPLE

	А	В	С	D	E	F	G	Н	1
1	forward_filename	rail_filename	rh_temp	air_temp	humidity	gps_lat	gps_lon	speed	heading
2	forward_filename	./rail_images/1701183379.7	41	97	452	54 deg 18.1892 min	001 deg 33.9124 min	0	217.18
3	./forward_images/170118	./rail_images/1701183379.78	43	98	446	54 deg 18.1892 min	001 deg 33.9124 min	0	217.18
4	./forward_images/170118	./rail_images/1701183379.7	44	98	458	54 deg 18.1892 min	001 deg 33.9124 min	0	217.18
5	./forward_images/170118	./rail_images/1701183379.7	43	98	452	54 deg 18.1892 min	001 deg 33.9124 min	0	217.18
6	./forward_images/170118	./rail_images/1701183379.78	44	98	450	54 deg 18.1892 min	001 deg 33.9124 min	0	217.18
7	./forward_images/170118	./rail_images/1701183379.78	46	98	456	54 deg 18.1892 min	001 deg 33.9124 min	0	217.18
8	./forward_images/170118	./rail_images/1701183379.78	42	98	454	54 deg 18.1892 min	001 deg 33.9124 min	0	217.18
9	./forward_images/170118	./rail_images/1701183379.78	43	98	462	54 deg 18.1892 min	001 deg 33.9124 min	0	217.18
10	./forward_images/170118	./rail_images/1701183379.78	41	98	454	54 deg 18.1892 min	001 deg 33.9124 min	0	217.18
11	./forward_images/170118	./rail_images/1701183379.78	42	98	454	54 deg 18.1892 min	001 deg 33.9124 min	0	217.18
12	./forward_images/170118	./rail_images/1701183379.78	44	98	452	54 deg 18.1892 min	001 deg 33.9124 min	0	217.18
13	./forward_images/170118	./rail_images/1701183379.78	42	98	452	54 deg 18.1892 min	001 deg 33.9124 min	0	217.18
14	./forward_images/170118	./rail_images/1701183379.78	46	98	452	54 deg 18.1892 min	001 deg 33.9124 min	0	217.18
15	./forward_images/170118	./rail_images/1701183379.78	48	98	460	54 deg 18.1892 min	001 deg 33.9124 min	0	217.18
16	./forward_images/170118	./rail_images/1701183379.78	49	99	458	54 deg 18.1892 min	001 deg 33.9124 min	0	217.18
17	./forward_images/170118	./rail_images/1701183379.78	79	98	466	54 deg 18.1892 min	001 deg 33.9124 min	0	217.18
18	./forward_images/170118	./rail_images/1701183379.78	49	98	458	54 deg 18.1892 min	001 deg 33.9124 min	0	217.18
19	./forward_images/170118	./rail_images/1701183379.78	44	99	464	54 deg 18.1892 min	001 deg 33.9124 min	0	217.18
20	./forward_images/170118	./rail_images/1701183379.78	48	98	466	54 deg 18.1892 min	001 deg 33.9124 min	0	217.18
21	./forward_images/170118	./rail_images/1701183379.78	46	98	464	54 deg 18.1892 min	001 deg 33.9124 min	0	217.18
22	./forward_images/170118	./rail_images/1701183379.78	44	97	462	54 deg 18.1892 min	001 deg 33.9124 min	0	217.18
23	./forward_images/170118	./rail_images/1701183379.78	46	98	468	54 deg 18.1892 min	001 deg 33.9124 min	0	217.18
24	./forward_images/170118	./rail_images/1701183379.78	44	98	466	54 deg 18.1892 min	001 deg 33.9124 min	0	217.18
25	./forward_images/170118	./rail_images/1701183379.78	44	98	470	54 deg 18.1892 min	001 deg 33.9124 min	0	217.18
26	./forward_images/170118	./rail_images/1701183379.78	43	98	466	54 deg 18.1892 min	001 deg 33.9124 min	0	217.18
27	./forward_images/170118	./rail_images/1701183379.78	43	98	466	54 deg 18.1892 min	001 deg 33.9124 min	0	217.18
28	./forward_images/170118	./rail_images/1701183379.78	45	98	472	54 deg 18.1892 min	001 deg 33.9124 min	0	217.18
29	./forward_images/170118	./rail_images/1701183379.78	42	98	464	54 deg 18.1892 min	001 deg 33.9124 min	0	217.18
30	./forward_images/170118	./rail_images/1701183379.78	57	97	468	54 deg 18.1892 min	001 deg 33.9124 min	0	217.18
31	./forward_images/170118	./rail_images/1701183379.78	45	98	470	54 deg 18.1892 min	001 deg 33.9124 min	0	217.18
32	./forward_images/170118	./rail_images/1701183379.78	39	98	481	54 deg 18.1892 min	001 deg 33.9124 min	0	217.18
33	./forward_images/170118	./rail_images/1701183379.78	39	97	484	54 deg 18.1892 min	001 deg 33.9124 min	0	217.18
34		./rail_images/1701183379.78	53	97	472	54 deg 18.1892 min	001 deg 33.9124 min	0	217.18
35		./rail_images/1701183379.78	51	97	472	54 deg 18.1840 min	001 deg 33.9110 min	1.35	234.8
36		./rail_images/1701183379.78	53	97		54 deg 18.1836 min	001 deg 33.9122 min	1.81	238.61
37		./rail_images/1701183379.78	57	97			001 deg 33.9133 min	2.18	237.36

Figure 14:CSV output from camera box process thread.

C-3: STANDARD OPERATING PROCEDURE FOR THE CAMERA BOX

Pre-Mounting/Test Steps:

- 1. Open either the side panel (preferably the blank one) or front panel of the camera box (using appropriate Allen keys) to access the components.
- 2. Check if battery pack is charged up if not, charge it up before use. The battery case cover can be opened up to view the battery level when it is switched on.
- 3. Turn on the battery pack with USB button switch, concurrently turning on the microcontrollers.
- 4. Check to see the GPS module light is on (lime green light under the Arduino Uno) and the IR thermometer light is on (lime green light on the sensor). If the lights are not on, check that their sensor connectors are firmly plugged into the microcontroller.
- 5. Connect the linked microcontrollers to a monitor to get familiar with the data folders located on the desktop ('rail_images' for railhead, 'forward_images' for

- forward facing images and 'CSV'). This can be done using a HDMI dongle connected to the Raspi. If prompted for username and password, use mep20mof for both.
- 6. Check Raspi memory before commencing any operation. If full, confirm current data has been backed up before deleting them, if not back them up on a USB stick and upload onto Google drive. Proceed to permanently delete backed up images from the Raspi.
- 7. To control the camera box remotely after mounting it on the train, install "RaspController" app on a mobile device. Register the Raspi's IP address on the app and install the following commands:
 - a. To run the camera box within WiFi range install, "sudo python3/home/mep20mof/Desktop/camera_box/main.py"
 - b. To run the camera box with the user away from the system for a specified length of time (although the mobile phone has to be in close proximity to start the process), install, "sudo python3/home/mep20mof/Desktop/camera_box/main.py x". Where 'x' is the time in seconds.
- 8. This directory can be saved on the app and used continuously.
- 9. The camera box can now be switched off, with the panels screwed back in position for transportation.

Mounting/Test Steps

- 1. The camera box should be mounted on the train's lamp bracket using the black slot located at the back of the box.
- 2. Ensure the camera box is sitting fully on the lamp bracket. It may need an extra push to slide it down fully.
- 3. Open the front panel of the camera box. Ensure all the components are securely mounted in the box and proceed to switch the microcontrollers on.
- 4. Access the camera and sensor feeds either through the monitor or the mobile app. Using the camera feed (USB) to view the output, adjust the forward-facing camera by moving the tripod mount to the desired position. Switch the camera feed to the railhead camera (Libcamera) to view the output, adjust the camera position and lens distance until the railhead width can be viewed with good resolution (this is all determined by the user).
- 5. Using the method described in section 7.2.2B position the IR thermometer to read the railhead temperature. The temperature feed can be accessed on the monitor or the SSH Shell command saved earlier. This should be viewed to make sure all sensors are working and record correct data. The GPS module take about 5-10 minutes to pin the first location so it will not record data while setting up, if the process takes less than 10minutes generally.
- 6. When these processes are completed, the monitor should be disconnected (if used) while the mobile can remain connected. Camera box front panel should be

- securely screwed back in place while the system is left on (because the user would not have access to the camera box while in use).
- 7. The camera box is ready for use. The camera box can either be operated remotely by the user, where the run command is set to capture data for the time corresponding to the train journey. Or the user can sit close to the train cab and control the data capture, this is very useful for repeat tests.

Post-Tests Step

- 1. After data capture completion, the microcontrollers can be shut down using the mobile app.
- 2. Unmount the camera box and turn off the system before transportation to save battery energy.
- 3. Data transfer can happen before or after transporting the camera box from the testing site. Follow the same process of connecting the microcontroller to the monitor; the images and CSV can be accessed using the folders stated in "Pre-Test Step" no. 5.
- 4. The images and CSV should be copied/moved to USB stick, saving them in separate folders.
- 5. The users can now access the data at their convenience and process it.
- 6. To carry out friction predictions, the data should be compiled into a similar spreadsheet shown in Figure 2 Appendix A-2 and save as a CSV file. Then follow the steps laid out in Appendix B-4 for the '.ipynb' file as written by user (should be similar to image in B-4). Basically, the codes displayed in B-4 can be re-used, although the base path, image base path and csv file have to be updated.